Elucidating the Important Structural Features of Aryl Glycosides and Antifreeze Glycoprotein Disaccharide Analogs for Ice Recrystallization Inhibition

Vanessa B. Musca

B.Sc. Honours Biochemistry – University of Ottawa, 2014

Thesis submitted to the
Faculty of Graduate & Postdoctoral Studies
in partial fulfillment of the requirements for the
M.Sc. degree in Chemistry

Department of Chemistry and Biomolecular Sciences
Faculty of Science
University of Ottawa

Candidate	Supervisor
_____	_____
Vanessa B. Musca	Professor Robert N. Ben

© Vanessa B. Musca, Ottawa, Canada, 2016

Dedicated to my family (who still has no idea what I do), to the cleaning staff for tolerating my late-night Justin Bieber karaoke sessions, and to anyone who has ever dared to be different

I will beat the odds
I can go the distance
I will face the world
Fearless, proud, and strong

-Disney's Hercules

All our dreams can come true,
If we have the courage to pursue them

-Walt Disney

Acknowledgments

There are not enough words to describe my gratitude to all the individuals without whom the completion of this thesis would not be possible. First and foremost, I would like to thank Dr. Robert Ben for welcoming me into your laboratory and for teaching me to come out of my comfort zone. Most importantly, thank you for allowing me to decorate the office with Disney portraits and Justin Bieber calendars. They have made the lab feel more like home. To Dr. Tony Durst, it has been both an honor and a privilege to share a lab space with you and your group. Thank you for your chemistry guidance and support over the past two years. I appreciate all the time you have devoted to our office chats and all of the invaluable life lessons you have taught me.

To past and present graduate students (Kyle McClymont, Jennie Briard, Malay Doshi, Thomas Charlton, Stephanie Abraham, Jessica Poisson, Madeleine Adam, and Julia Meyer) and undergraduate students (Danielle McCulloch and Emily Zhang) of the Ben lab, thank you for making the lab a great workplace. Thank you Jennie Briard for helping me set up my first carbohydrate reaction and for being a great friend. Car rides will not be the same without you. To Kyle McClymont, thank you for being a great role model. Your dedication and passion for chemistry has inspired me to be as good a chemist as you have already become. To Thomas Charlton (A.K.A T-Digits), I look forward to finding more bee syrup and will miss your sassy "Aurelio" side.

To past and present members of the Durst lab (Amanda Saikaley, Vik Raina, Adrien Fluet, Ariel Buchler, and Jessica Huynh), thank you for all the laughs and for being truly amazing people to share a workspace with. To Amanda Saikaley, ever since we bonded over honey ham that one night in the lab, I knew we'd be good friends. Thank you for showing me some tips and tricks along the way and for encouraging me to persevere. You are a great travel buddy and an even more extraordinary friend.

Finally, a huge thank-you to my parents Carmela and Silvano Musca for putting up with me in general, but especially for these past two years. It has definitely been an

emotional journey, but I am extremely grateful to have two supportive parents that encourage me not only to achieve my goals, but also to surpass them. Even when I had trouble recognizing it myself, you have always seen my potential. Thank you for working as hard as you did/do to get me here. I love you both very much. To my sister Kristina, thank you for bringing me food and for picking me up when I've had to work late nights in the lab. You have always been there to listen to my bad days and celebrate on my good days. Thanks for being an amazing older sister and for taking care of your "Science Beebs." Finally, to my little furry Pujito, thank you for keeping me company during this writing process. Even though I envied you for sleeping as I worked, your silent support was appreciated.

Abstract

Cryopreservation of human red blood cells (RBCs) extends the storage time from 42 days (hypothermic storage limit) to a maximum of 10 years. While this reduces the possibility of RBC shortages in emergency situations, this preservation method is currently limited to individuals with rare blood phenotypes, patients who require autologous blood transfusions, and military applications. Furthermore, cryopreservation is associated with a high degree of cellular damage, which can subsequently reduce the viability of cells post-thaw. The cellular damage incurred upon cryopreservation is primarily attributed to the process of ice recrystallization. To reduce the degree of cellular damage, cryoprotective agents (CPAs) are used. Currently, 10 % dimethyl sulphoxide (DMSO) and 40 % glycerol are used for the cryopreservation of hematopoietic stem cells (HSCs) and human RBCs respectively. Unfortunately, these CPAs do not provide protection against ice recrystallization.

The biological antifreezes (BAs) consisting of antifreeze proteins (AFPs) and antifreeze glycoproteins (AFGPs) were identified as the first inhibitors of ice recrystallization. Consequently, the Ben laboratory is interested in synthesizing small molecule carbohydrate-based inhibitors of ice recrystallization that can be used as an alternative to glycerol or DMSO for the cryopreservation of various cell types. Therefore, this thesis focuses on elucidating important structural features of carbohydrate-based derivatives that are responsible for IRI activity. The first part of this study examines the importance of the anomeric oxygen atom of aryl glycosides for IRI activity. Our laboratory previously demonstrated that the *O*-linked aryl glycosides are effective inhibitors of ice recrystallization. However, the influence of stereoelectronic effects at the C_1 position of aryl glycosides on IRI activity has not been investigated. As a result, *N*- and *S*-linked aryl glycosides were synthesized in this study and their IRI activities were compared to that of the *O*-linked aryl glycosides. These results suggest that a stronger *exo*-anomeric effect exhibited by the C_1 nitrogen derivatives reduces the IRI activity of aryl glycosides.

The second part of this study focuses on the synthesis of AFGP disaccharide analogs. While the β-(1,3) glycosidic linkage found in native AFGP-8 was previously assessed for its influence on IRI activity, an extensive structure-function analysis of

AFGP disaccharide analogs has not yet been performed. As a result, an AFGP disaccharide analog was designed whereby a *para*-methoxyphenyl (PMP) substituent was incorporated. This was done to assess whether the PMP substituent could enhance the lack of IRI activity exhibited previously with AFGP disaccharide analogs. Although the synthesis of this disaccharide target was not completed, a number of advantageous developments have been made regarding the glycosylation of *N*-acetyl-D-glycosamine derivatives. In addition, the PMP-GlcNAc intermediate encountered in disaccharide synthesis was assessed for its IRI activity, confirming that the acetamido (NHAc) function is not required for IRI activity.

Table of Contents

List of Figures

Chapter 1:

Chapter 2:

Chapter 3:

Chapter 4:

List of Tables

Chapter 3:

Chapter 4:

List of Schemes

Chapter 3:

Chapter 4:

List of Abbreviations

α	Alpha
β	Beta
ε	Epsilon
^{13}C	Carbon
^{1}H	Proton
AABB	American Association of Blood Banks
AFGP(s)	Antifreeze glycoprotein(s)
AFP(s)	Antifreeze protein(s)
Ala-Ala-Thr	Alanine-alanine-threonine
ATP	Adenosine triphosphate
BA(s)	Biological antifreeze(s)
$BF_3{\cdot}OEt_2$	Boron trifluoride diethyl etherate
$Bi(OTf)_3$	Bismuth (III) trifluoromethanesulfonate
CPA(s)	Cryoprotective agent(s)
CPD	Citrate-phosphate-dextrose
CPD/SAGM	Citrate-phosphate-dextrose/saline-adenine-glucose-mannitol
$Cu(OTf)_2$	Copper (II) triflate
DCPhth	Dichlorophthalimide
DMSO	Dimethyl sulphoxide
$Et_3N^+Br^-$	Tetrabutylammonium bromide
Gal	Galactose
GalNAc	*N*-acetyl-D-galactosamine
Glc	Glucose
GlcNAc	*N*-acetyl-D-glucosamine
HSC(s)	Hematopoietic stem cell(s)
HSL	Hypothermic storage lesion
I_c	Cubic ice
IC_{50}	Half maximal inhibitory concentration
I_h	Hexagonal ice
IIF	Intracellular ice formation
IRI	Ice recrystallization inhibition
IRIs	Ice recrystallization inhibitors
Man	Mannose
MGS	Mean grain size
NHAc	*N*-acetyl
O-Ph-Glc	*O*-linked phenyl glucoside
OGG	Ornithine-glycine-glycine
OMe	Methoxy
Orn-Gly-Gly	Ornithine-glycine-glycine
p-OCF_3	*Para*-trifluoromethoxy
p-OCF_3-Ph-Glc	*Para*-(trifluoromethoxy)phenyl glucose
p-OCF_3-Ph-Glc	*Para*-(trifluoromethoxy)phenyl galactose
p-OMe	*Para*-methoxy

PBS	Phosphate-buffered saline
Phth	Phthalimide
PMP	*Para*-methoxyphenyl
PMP-Glc	*Para*-methoxyphenyl glucose
PMP-GlcNAc	*Para*-methoxyphenyl-*N*-acetyl-D-glucosamine
PTC	Phase-transfer catalysis
QLL	Quasi-liquid layer
RBC(s)	Red blood cells(s)
rt	Room temperature
SAGM	Saline-adenine-glucose-mannitol
t-Bu	*Tert*-butyl
Tal	Talose
TCA	Trichloroacetimidate
TCP	Tetrachlorophthalimide
TCPA	Tetrachlorophthalic anhydride
Tf_2O	Trifluoromethanesulfonic anhydride
TH	Thermal hysteresis
TMSOTf	Trimethylsilyl trifluoromethanesulfonate

Chapter 1: Introduction – Cryopreservation and Small Molecule Carbohydrate Ice Recrystallization Inhibitors

1.1 Biopreservation of Human Red Blood Cells

The long-term storage of various cell types is particularly important for clinical applications such as tissue engineering, tissue transplantation, and red blood cell (RBC) transfusion. Biopreservation is a process that preserves the integrity and functionality of cells that have been isolated from their native environment for extended storage periods.[1] There are typically three different categories of biopreservation, which differ by their technique and cell type that is being stored. These include hypothermic storage, cryopreservation, and vitrification.[1,2] Of these strategies, hypothermic storage is the most widely used method of storage for human red blood cells (RBCs).[3]

1.1.1 Hypothermic Storage

For patients with low oxygen-carrying capacity resulting from increased RBC loss, reduced bone marrow production, defective hemoglobin, or decreased RBC survival, RBC transfusion is a life-saving procedure.[2] While millions of RBC units are transfused each year, successful biopreservation of human RBCs requires extensive understanding of the biochemical changes that take place in RBCs *ex vivo*. Hypothermic storage of human RBCs is a procedure that is based on the principle that a reduction in temperature can suppress biochemical processes and molecular reactions.[1,2,4] This procedure consists of storing RBC concentrates at a temperature that is lower than the normal physiological temperature, but higher than the freezing point of the storage solution (typically between 4 and 10 ^{o}C).[2,5] RBC concentrates are stored in a solution that is designed to provide nutrient supplementation and maintain the quality of RBCs during storage.[2,6] Numerous solutions have been investigated, each differing in permissible storage length of RBCs and post-transfusion RBC recovery.[7] In Canada, the current method employed involves storing leukoreduced RBCs in a citrate-phosphate-dextrose/saline-adenine-glucose-mannitol (CPD/SAGM) preservative solution.[6] During extended storage, nutrient

depletion and accumulation of wastes result in biochemical and morphological RBC changes referred to as hypothermic storage lesion (HSL).[8] This HSL results in adenosine triphosphate (ATP) depletion (required to maintain electrolyte balance) and RBC membrane injury resulting from lipid loss (microvesiculation) and reduced surface area to volume ratio.[2,6,8,9] The presence of citrate-phosphate-dextrose (CPD) serves as an anticoagulant solution, while the saline-adenine-glucose-mannitol (SAGM) additive solution maintains ATP levels, nutrient supplementation, and membrane integrity.[10–13] This enables a hypothermic storage limit of up to 42 days.[2,3] Within this storage period, 75 % red blood cell recovery can be attained *in vivo* 24 hours post-transfusion with a maximum of 1 % hemolysis, criteria stipulated by the American Association of Blood Banks (AABB).[14] While hypothermic storage of RBC concentrates addresses the immediate need for RBC transfusions, this hypothermic storage limit is problematic for patients who require extended RBC storage or for emergency situations where RBC units are in high demand. As a result, alternative methods for the long-term preservation of various cell types including human RBCs is required to accommodate these unique circumstances.

1.1.2 Cryopreservation and Cryoinjury

Cryopreservation is a process that enables the long-term preservation of cells, tissues, and embryos by cooling them to -196 ^{o}C, thus enabling medical applications such as fertility treatment, bone marrow transplantation, and regenerative therapies.[15,16] Unlike hypothermic storage, cryopreservation enables the storage of human RBCs up to 10 years since very few biochemical and metabolic reactions can occur at cryopreservation temperatures (typically -80 ^{o}C or -196 ^{o}C).[4,15,17] As a result, RBC physiology is generally unaffected by extended storage.[2] While cryopreservation is a routine procedure, it is associated with a high degree of cellular damage, which results in reduced cell viability post-thaw. Although cells can endure storage at low temperatures, the cellular damage associated with cryopreservation is prominent during the freezing and thawing processes.[16,18]

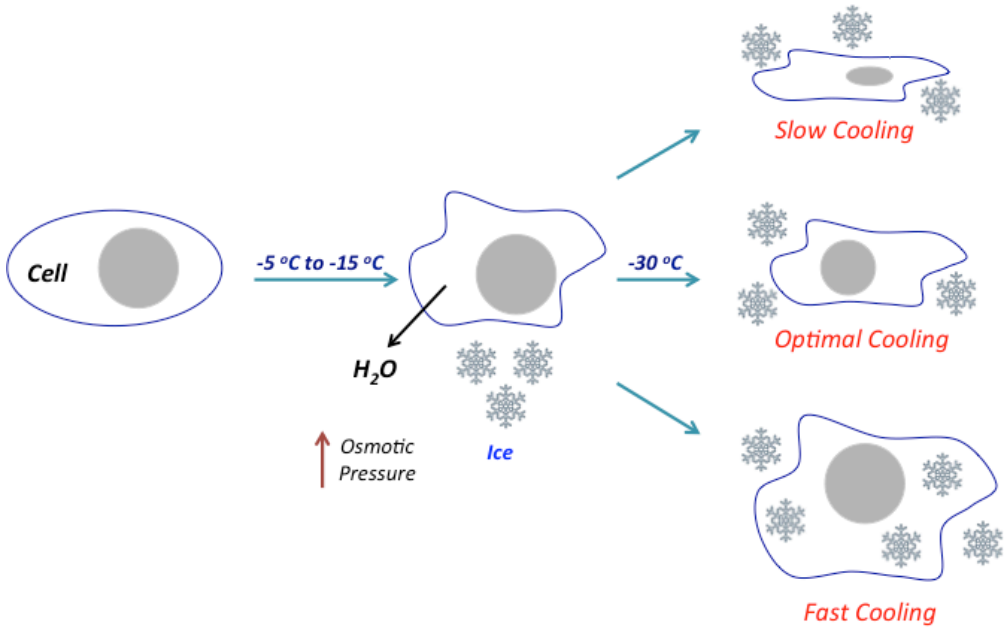

Figure 1.1 Schematic representation of Mazur's two-factor hypothesis of freezing injury. This figure was adapted from Gao, D. and Critser, J. K. in *Mechanisms of Cryoinjury in Living Cells*.[16,19]

The mechanism of cryoinjury during freezing can be summarized by Mazur's two-factor hypothesis of freezing injury (**Figure 1.1**).[19] As the temperature decreases, ice begins to form between -5 °C and -15 °C in the medium surrounding the cell.[16,19] However, the contents of the cell remain supercooled and unfrozen due to the plasma membrane, which blocks the growth of ice crystals in the cytoplasm.[16,17] Since solutes are excluded from the ice lattice, the solute concentration increases in the unfrozen fractions outside the cell, leading to an increase in osmotic pressure across the cell membrane.[2,16,17] As a result, the supercooled water inside the cell has a greater chemical potential than the unfrozen solution in the external medium, causing water to flow out of the cell.[2,16,18] According to Mazur's two-factor hypothesis, the fate of cells depends on the rate at which they are cooled.[19] If cells are cooled too rapidly, the formation of extracellular ice occurs much faster than the efflux of water.[18] As a result, water remains trapped inside the cell, resulting in intracellular ice formation (IIF).[17,20] Although the mechanism by which IIF occurs is not quite understood, the conditions leading to this phenomenon are associated with lethal cell injury.[20,21] For instance, cell injury can occur as a result of the formation, recrystallization, or melting of intracellular ice acquired during rapid cooling.[20] On the other hand, if cells are cooled too slowly, water will continue to flow

out of the cell in an attempt to balance the solute concentration in the external medium.[16] Although this eliminates the possibility of IIF, excessive loss of water results in the concentration of intracellular solutes.[2,16] If cooling is sufficiently slow, cells will experience a reduction in volume (resulting from cell dehydration)[22] and exposure to high solute concentrations (solution effects)[23–25] which is lethal to cells. Thus, optimal cooling rates for cell survival (which vary amongst different cell types) should be slow enough to avoid cell injury by IIF, yet fast enough to minimize solution effects and cell dehydration.

During the thawing process, the rate of warming can also compromise the viability of cryopreserved cells. However, the fate of cells during slow or rapid thaw depends on whether the rate of freezing has induced IIF or cell dehydration.[16] For instance, if cells have undergone IIF as a result of rapid freezing, slow thawing results in intracellular ice recrystallization (**Section 1.2**).[19,20,26] However, rapid thawing is capable of "rescuing" these cells by preventing this lethal process.[16,17] Contrarily, if cells have undergone dehydration as a result of slow freezing, the thawing process will induce osmotic shock.[27] As cells are rapidly thawed, there is insufficient time for excess additive to diffuse out of the cell during thawing. As a result, extracellular water will flow into the cell, ultimately resulting in cell lysis.[17] However, slow warming is optimal for dehydrated cells since it reduces the incidence of osmotic shock.[16] As a result, the major challenge associated with cryopreservation is not the ability of cells to withstand low temperatures during prolonged storage, but rather the lethality of the freezing and thawing processes.

1.1.3 Cryoprotective Agents

Additives that enhance the post-thaw survival of cells are known as cryoprotective agents (CPAs) and are typically provided to cells before freezing. These CPAs are classified into two categories (membrane-permeating and non-membrane-permeating), depending on the cooling rate employed.[28] Non-membrane-permeating CPAs (such as sugars, starches, and polymers) remain outside the cell and prevent against rapid freezing injury by dehydrating the cell and reducing the incidence of IIF.[17,29] In addition, non-membrane permeating CPAs have also been shown to stabilize cell membranes by

protecting the structure and function of cellular macromolecules.[30,31] Contrarily, membrane-permeating CPAs (such as glycerol and dimethyl sulphoxide) readily penetrate the cell membrane and protect cells against slow freezing injury by preventing cell dehydration and lethal solute concentrations.[28,29,32] This category of cryoprotectants is utilized more frequently for clinical cryopreservation.

In 1949, Christopher Polge and his colleagues introduced glycerol as the first CPA to preserve fowl spermatozoa at subzero temperatures.[33] The protective action of glycerol is attributed to its ability to penetrate cells and prevent the concentration of intracellular solutes that would otherwise occur during cryopreservation.[34] By 1959, Lovelock and Bishop were the first to report that dimethyl sulphoxide (DMSO) was superior to glycerol in cryopreserving human/bovine red blood cells and bull spermatozoa.[34] This is due to increased membrane permeability of DMSO compared to that of glycerol.[34] To date, DMSO remains one of the most versatile cryoprotective agents available due to its ability to preserve a wider variety of cells compared to glycerol.[34–36] Despite this advantage, membrane-permeating CPAs such as DMSO are significantly cytotoxic since their ability to cross cell membranes disrupts many cellular processes, ultimately inducing apoptosis.[37–39] In addition, membrane-permeating CPAs such as glycerol and DMSO are colligative in nature.[29,40] As such, higher concentrations of these CPAs are required to further elicit protection against cryoinjury. Unfortunately, increasing the concentration of membrane-permeating CPAs increases the degree of cytotoxicity as well as the incidence of posthypertonic hemolysis during the thawing process.[40–42] Thus, the development of an ideal cryoprotective agent capable of protecting cells against cryoinjury without being cytotoxic presents a major challenge to the field of cryobiology.

1.1.4 Long-term Storage of Human Red Blood Cells

The development of new methods for the long-term storage of various cells types such as human red blood cells (RBCs) and hematopoietic stem cells (HSCs) has made tremendous advancements in transfusion medicine and regenerative therapies. While hypothermic storage addresses the immediate need for red blood cell transfusions, the

hypothermic storage limit of 42 days is problematic. Specifically, this storage period is limiting for emergency situations where a high volume of RBC units is required. Fortunately, cryopreservation has enabled the storage of cells and some tissues for several years by cooling them to subzero temperatures.[15] Although cryopreservation can extend the storage of RBC units up to 10 years,[5,14] current cryopreservation protocols do not permit the direct transfusion of RBCs post-thaw.[5,43,44] As a result, this method of human RBC preservation is currently limited to military applications, individuals with rare blood phenotypes, and autologous RBC storage.[5,43,44]

In 1950, Smith was the first to report a method for freezing whole blood at -79 ^{o}C using glycerol as a CPA, which resulted in only a slight degree of hemolysis.[2,45] Since then, different methods for human RBC cryopreservation have been developed. These methods differ by the type and concentration of CPA used, storage temperature, and cooling/thawing rates. There are currently two methods that have been approved for the clinical cryopreservation of human RBCs: 1) low glycerol concentration with rapid freezing and 2) high glycerol concentration with slow freezing. The low glycerol concentration and rapid freezing procedure for the clinical cryopreservation of human RBCs is routinely used in Europe.[2,46] This procedure involves the use of low glycerol concentrations (15-20 % *v/v*) and rapid freezing of RBC units (>65 ^{o}C/min) by submerging them in liquid nitrogen (-196 ^{o}C) for approximately 2-3 minutes.[2,47,48] RBC units are then thawed in a 42-45 ^{o}C water bath.[2,47,48] In Canada and the United States, however, the high glycerol concentration with slow freezing procedure is employed. This method utilizes high glycerol concentrations (40 % *v/v*) in conjunction with slow freezing rates (1 ^{o}C/min) for storage at -80 ^{o}C.[2,5,14] While these methods enable long-term storage of RBC concentrates and high recoveries post-thaw, there are two main drawbacks concerning clinical cryopreservation. First, these methods are expensive due to the cost of specialized equipment as well as the cost of liquid nitrogen tanks or -80 ^{o}C freezers.[43] In addition, cryopreservation protocols require post-thaw RBC processing to reduce glycerol concentrations to less than 1 % prior to transfusion.[2,14] These deglycerolization procedures are required to prevent post-transfusion intravascular hemolysis and to minimize recipient exposure to glycerol.[2,14] Unfortunately, these procedures can take up

to 1 hour of processing per unit of RBCs.[49] Regardless of the cryopreservation procedure used, both procedures must meet the standards put forth by the American Association of Blood Banks (AABB). Specifically, a minimum of 80 % RBC recovery must be achieved following deglycerolization procedures.[2,5] Furthermore, deglycerolized RBCs must be transfused within 24 hours of processing to prevent bacterial contamination.[3,4,14] In addition to high costs, deglycerolization is time-consuming and may result in a reduction of up to 20 % RBC volume following this procedure.[2] Aside from necessitating post-thaw cell processing, the use of glycerol as a CPA does not protect against all methods of cryoinjury. Since glycerol is a membrane-permeating CPA, it is capable of protecting cells against slow freezing injury such as dehydration and lethal solute concentrations (**Section 1.1.2**). However, glycerol does not provide protection against intracellular ice recrystallization (**Section 1.2.2**), a lethal phenomenon that is responsible for reduced RBC recovery post-thaw.[19,20,26] As a result, minimizing RBC processing procedures and protecting cells against cryoinjury by inhibiting intracellular ice recrystallization are characteristics that can improve the development of an ideal CPA.

1.2 Ice Recrystallization

Recrystallization of ice is a phenomenon that frequently occurs in metallurgy and frozen foods as a result of temperature fluctuations or long-term storage.[50–52] This phenomenon is problematic for food stability, structure, and texture which ultimately alters the quality of frozen foods.[52] Ice recrystallization is a process whereby larger ice crystals are formed at the expense of smaller ones. There are three main types of ice recrystallization: isomass recrystallization (or rounding), migratory recrystallization (or Ostwald ripening), and accretion recrystallization.[51,53] Temperature fluctuations favour migratory recrystallization, a process whereby larger ice crystals are formed at the expense of smaller ones.[52,54] Following a temperature fluctuation, unfrozen water from smaller ice crystals will refreeze onto the surface of larger ice crystals and increase their size.[50,52] Regardless of the mechanism, ice recrystallization reduces the quality and shelf life of frozen foods, presenting a problem for long-term storage and food transportation.

In addition to frozen foods, ice recrystallization is a phenomenon that also occurs during cryopreservation and compromises the viability of stored cells.

1.2.1 Structure of Ice

The mechanism by which water freezes into ice plays a significant role in the field of clinical science and in nature. Almost all ice found in nature is crystalline, comprised of water molecules arranged either in repeating hexagonal or cubic patterns.[55,56] The predominant structure of crystalline ice depends on the ambient temperature and pressure.[57] For instance, metastable cubic ice (denoted I_c) is predominantly formed in regions of the Earth's atmosphere where temperatures range between -130 ^{o}C and -160 ^{o}C.[56,58,59] In addition, cubic ice has also been found in biological tissues that have undergone cryopreservation.[56,59,60] However, the presence of cubic ice is relatively benign to cells.[60,61] Rather, the transition from cubic ice into hexagonal ice leads to cellular damage of cryopreserved cells since I_h can undergo recrystallization.[60–62] Specifically, studies have shown that the transition of cubic ice into hexagonal ice in cryopreserved cells precedes damage to embryos and human RBCs.[60–62]

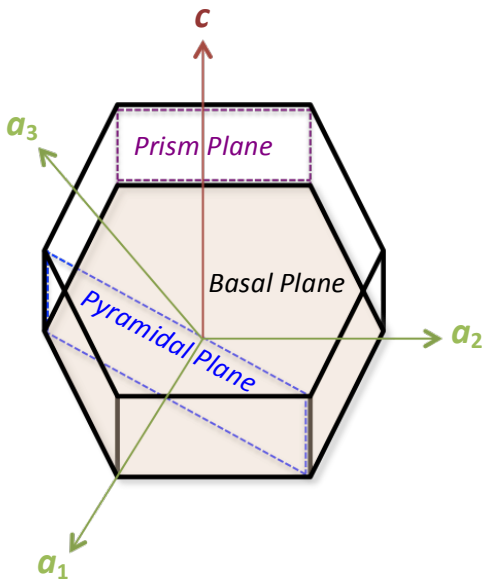

Figure 1.2 Schematic representation of a single unit of hexagonal ice (I_h). Each unit consists of a prism plane, a basal plane, and a pyramidal plane as well as four axes: a_1, a_2, a_3, and c.

In contrast, hexagonal ice (denoted I_h) exists predominantly between -90 °C and -100 °C and is more stable than cubic ice.[56,63] The structure of hexagonal and cubic ice consists of six water molecules arranged in hexagonal rings that assume a chair-like conformation.[56,57] Each unit consists of four axes (a_1,a_2,a_3, and c) and eight faces, two basal faces and six prism faces (**Figure 1.2**).[64] These hexagonal ice lattice units are held together by hydrogen bonds between oxygen and hydrogen atoms, forming a single layer.[57] Similarly, each layer is also held together by hydrogen bonds.[57] Unlike cubic ice, each layer of hydrogen-bonded water molecules that constitute hexagonal ice is a mirror image of the previous layer, resulting in hexagonal symmetry (**Figure 1.3**). When viewed from the basal plane, hexagonal ice units adopt a chair-like conformation. However, these units adopt a boat-like conformation when viewed from the prism plane.

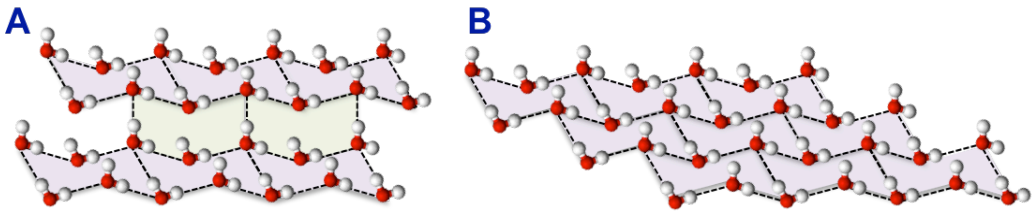

Figure 1.3 (**A**) Schematic representation of hexagonal ice (I_h) whereby water molecules assume a chair-like conformation along the basal plane (purple) and a boat-like conformation along the prism plane (green). (**B**) Schematic representation of cubic ice (I_c) whereby water molecules are arranged only in a chair-like conformation.

Despite its rigidity, ice is made up of multiple layers. More than 150 years ago, Faraday was the first to propose the existence of a thin, liquid-like layer that covers the surface of ice at temperatures slightly below its melting point.[65,66] However, it wasn't until the 1980s when this semi-ordered quasi-liquid layer (QLL) surrounding ice crystals could be measured experimentally.[65] Although the thickness of the QLL is temperature-dependent, it is approximately 10-15 Å wide and is located between the highly-ordered ice layer and the disordered bulk phase of water (**Figure 1.4**).[67–69] Although the nature of the QLL is still a topic of debate, its influence on thundercloud electrification, changes in snow crystal morphology, and ice recrystallization is highly recognized.[65]

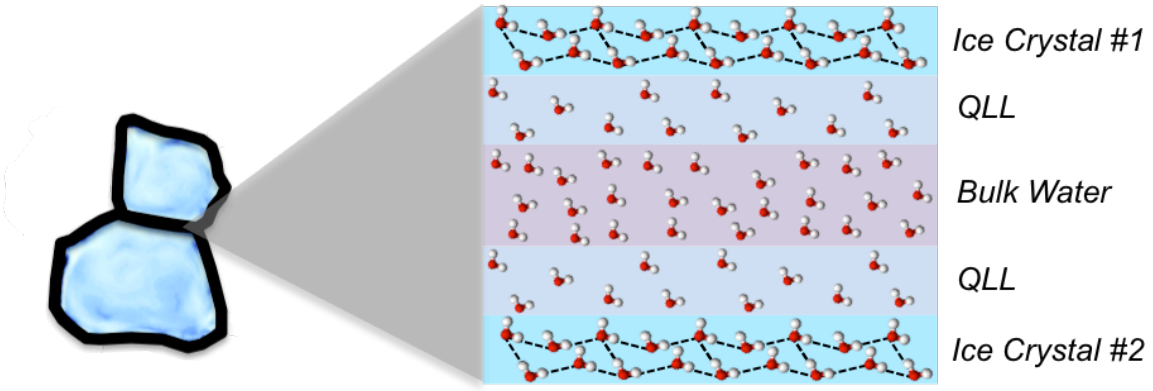

Figure 1.4 Schematic representation of the quasi-liquid layer (QLL) within the boundary between two ice crystals. The QLL is located between the highly ordered ice crystal lattice and disordered bulk water.

1.2.2 Mechanism of Ice Recrystallization

As previously mentioned, the process of ice recrystallization that occurs with hexagonal ice (I_h) is the leading cause of cellular damage in cryopreserved cells. Although cubic ice (I_c) has been detected in cryopreserved biological tissues, it is benign to cells compared to the needle-like crystals that can be formed from hexagonal ice.[56,61,62,70] At temperatures above −100 °C, the transition from cubic ice into hexagonal ice is thermodynamically favoured.[57,70] As a result, hexagonal ice is the only crystalline structure that exists above −100 °C.[63] Following this transition, hexagonal ice undergoes ice recrystallization resulting in cellular damage.[62]

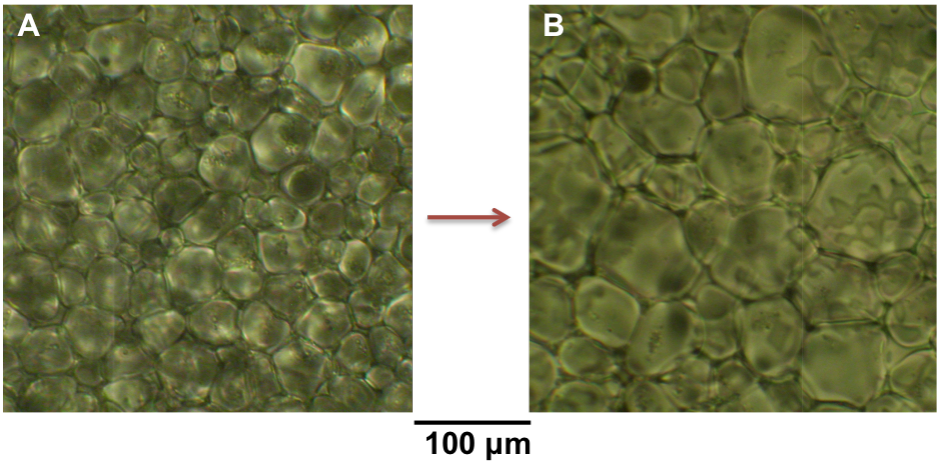

Figure 1.5 Microscopic images of (**A**) small ice crystals undergoing ice recrystallization via Ostwald ripening to form (**B**) larger ice crystals.

The process of ice recrystallization is believed to occur through grain boundary migration (or Ostwald ripening) of polycrystalline ice.[71,72] This process was first described by Ostwald in 1896 and is characterized by the formation of larger ice crystals at the expense of smaller ones (**Figure 1.5**).[71,72] This thermodynamically driven phenomenon occurs because larger ice crystals are more energetically favoured compared to smaller ice crystals due to their large volume to surface area ratio.[73,74] Although smaller ice crystals are kinetically favoured (i.e. can nucleate more easily), they are unstable due to their large surface area to volume ratio.[73,74] Consequently, smaller ice crystals have a higher surface free energy compared to larger ice crystals. Since water molecules on the surface are less stable than water molecules within ice crystals, water molecules will transfer from the surface of smaller ice crystals to the surface of larger ice crystals. This process is driven by a decrease in total surface free energy, which can be achieved by a reduction in interfacial area.[75] This occurs via diffusional mass transfer, whereby water molecules from regions of high interfacial curvature (small ice crystals) are first transferred to bulk water, then to regions of low interfacial curvature (large ice crystals).[75] Thus, the overall result of Ostwald ripening is a decrease in the number of ice crystals (with constant ice volume) and a reduction in free energy of the system.[70,73–75]

1.3 Biological Antifreezes

The blood serum of marine teleost fish typically freezes between -0.5 ^{o}C and -0.9 ^{o}C.[76] However, in 1957 Scholander and colleagues were the first to observe that these deep water fish were able to withstand seawater temperatures as low as -1.8 ^{o}C.[76,77] While the survival of marine teleost fish was initially attributed to temperature-induced osmoadaptation and metastability, their survival was later attributed to the presence of biological antifreezes.[76,78] These biological antifreezes (BAs) were first discovered by DeVries and Wohlschlag in 1969 and classified as either antifreeze proteins (AFPs) or antifreeze glycoproteins (AFGPs).[79,80]

1.3.1 Structure of Antifreeze Glycoproteins

The antifreeze glycoproteins (AFGPs) constitute the major protein component in the blood serum of Arctic and Antarctic fish.[80,81] Each AFGP consists of an alanine-alanine-threonine (Ala-Ala-Thr)$_n$ tripeptide repeat with minor sequence variations from one AFGP to the next.[80–82] The secondary hydroxyl group of the threonine residue is glycosylated to a β-D-galactosyl-(1-3)-α-*N*-acetyl-D-galactosamine disaccharide moiety (**Figure 1.6 A**).[79–82]

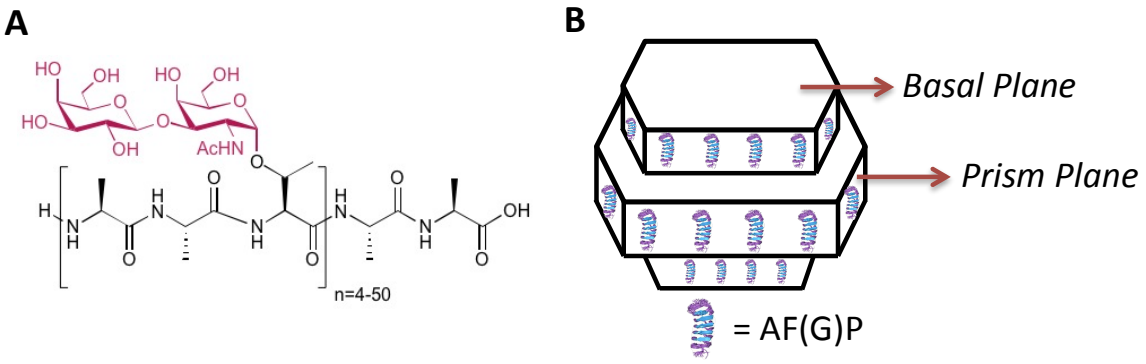

Figure 1.6 (**A**) Structure of native AFGP-8 consisting of a β-D-galactosyl-(1-3)-α-*N*-acetyl-D-galactosamine disaccharide moiety glycosylated with an Ala-Ala-Thr tripeptide repeat. (**B**) AF(G)Ps adsorbing to the surface of ice crystals to halt further growth. This figure was adapted from Haridas, V. and Naik, S. in *Natural Macromolecular Antifreeze Agents to Synthetic Antifreeze Agents*.[117]

AFGPs are divided into 8 subclasses (AFGP 1-8) depending on their molecular masses, which range from 2.6 kDa (n = 4) to 33.7 kDa (n = 50).[81,82] While smaller molecular mass AFGPs 6-8 possess only two-thirds of the antifreeze activity compared to larger molecular mass AFGPs 1-5, all classes of AFGPs in the blood serum of marine teleost fish act in a similar manner.[83–86] Specifically, these AFGPs adsorb to ice crystals on specific axes (**Figure 1.6 B**) and impede further growth and recrystallization.[81–83] Thus, a hysteresis between the equilibrium melting point and the observed freezing point is formed (i.e. thermal hysteresis).[81–83] As a result, AFGPs lower the freezing point of blood serum in a non-colligative manner and promote the survival of fish in Antarctic seawater.

1.3.2 AFGPs as Cryoprotective Agents

Since the presence of AFGPs in the blood serum of marine teleost fish promote their survival, in 1994 DeVries and colleagues investigated their use as potential cryoprotective agents as a means to preserve rat cardiomyocytes.[87,88] Previous reports suggest that AFGPs protect various mammalian cells such as animal oocytes, embryos,[89,90] and rat liver[88] against freezing injury at non-physiological temperatures. However, AFGPs did not protect rat cardiomyocytes against freezing damage.[87,88] Rather, the presence of AFGPs enhanced cardiac damage after freezing.[87,88] Although the presence of AFGPs in plants and insects confers protection against ice recrystallization incurred upon warming,[84,91,92] AFGPs promote changes in ice crystal morphology.[87] As a consequence of thermal hysteresis (TH), a morphological change from hexagonal plates to dendritic, needle-like structures causes ice crystals to penetrate cell membranes resulting in cellular damage.[87] Thus, while AFGPs possess the desirable property of ice recrystallization inhibition (IRI), their ability to exhibit TH is detrimental to cells at cryopreservation temperatures (-80 ^{o}C or -196 ^{o}C) since they are well below the thermal hysteresis gap.[93] However, AFGP analogs possessing IRI activity without the detrimental effects of TH ("custom-tailored AFGP analogs) may be suitable cryoprotective agents.

1.4 Small Molecule Ice Recrystallization Inhibitors

Since AFGPs possess antifreeze activity, early work by the Ben laboratory involved the synthesis of *C*-linked AFGP analogs as a suitable alternative to the isolation of natural antifreezes.[94,95] These analogs possess "custom-tailored" antifreeze activity since they inhibit ice recrystallization without the detrimental effects of thermal hysteresis.[94,95] In comparison to native AFGPs, these *C*-linked AFGP analogs consist of a *C*-linked α-pyranose moiety conjugated to the ε-amine of an ornithine residue in an ornithine-glycine-glycine (Orn-Gly-Gly) tripeptide unit (**Figure 1.7**).[96] Once synthesized, these *C*-linked AFGP analogs were assessed for their ability to inhibit ice recrystallization using a splat-cooling assay. In the splat-cooling assay, a 10 μl droplet of the sample solution is dropped onto an aluminum block precooled to -80 ^{o}C. The droplet freezes upon impact

and the resulting ice wafer is then transferred to a cryostage and annealed at -6.4 ^{o}C for 30 minutes. After this time, microscopic images of ice crystals are obtained. From these images, ice crystal areas are measured and IRI activity is reported as a percent mean grain size (% MGS) relative to that of a phosphate-buffered saline (PBS) solution. In the absence of inhibitor, the PBS solution serves as a positive control for ice recrystallization.

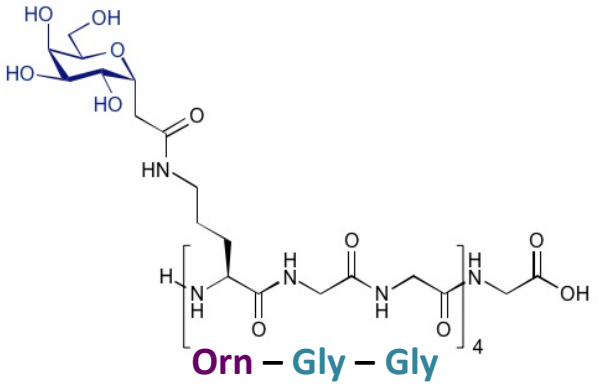

Figure 1.7 Structure of *C*-linked AFGP analog OGG-Gal.

A series of *C*-linked AFGP analogs were synthesized incorporating D-galactose, D-glucose, D-mannose, and D-talose to the same Orn-Gly-Gly tripeptide backbone.[96] While OGG-Man, OGG-Tal, and OGG-Glc exhibit weak to moderate IRI activity, OGG-Gal was able to inhibit ice recrystallization to the same extent as native AFGP-8.[96] This was evident from the smaller mean grain size of ice crystals in the presence of this *C*-linked AFGP analog compared to that in the presence of PBS.[96] In addition to possessing "custom-tailored" antifreeze activity, a 0.5-0.8 mM concentration of OGG-Gal is as effective as a 2.5% DMSO solution at protecting human embryonic liver cells against cryoinjury.[97] Despite their ability to mitigate cellular damage, these *C*-linked AFGP analogs are not amenable to scale-up that is required for *in vitro* studies.

1.4.1 Natural Monosaccharides as Ice Recrystallization Inhibitors

The OGG-Gal derivative inhibited ice recrystallization more effectively compared to the remaining *C*-linked AFGP analogs. These results suggested the importance of the carbohydrate moiety of these glycoprotein analogs for antifreeze activity.[96] Specifically, these results suggest that carbohydrate configuration is important for IRI activity.[96] As a

result, the Ben laboratory assessed monosaccharides individually as reducing sugars for their ability to inhibit ice recrystallization. When assessed at 22 mM, compounds producing a % MGS of 20 % or lower relative to PBS were considered effective inhibitors of ice recrystallization. However, compounds producing a % MGS above 80 % exhibited little to no IRI activity. Similar to their corresponding *C*-linked AFGP analogs, D-talose, D-mannose, and D-glucose displayed little to no IRI activity with a % MGS between 70 % and 90 %.[98,99] Despite being moderately IRI active, D-galactose was the most effective inhibitor of all the monosaccharides assessed with a % MGS slightly higher than 60 %.[98,99]

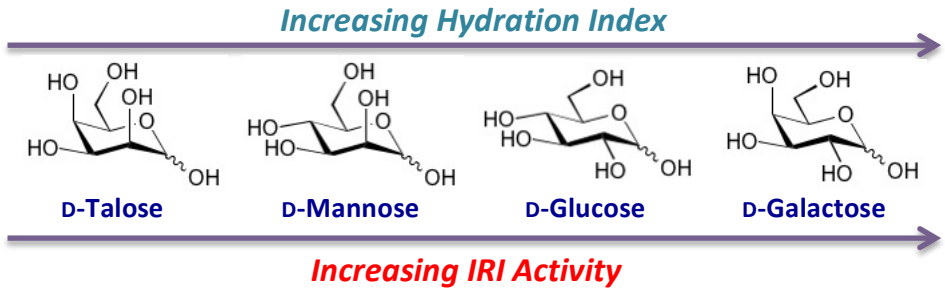

Figure 1.8 Proportionality between hydration index and IRI activity of monosaccharides.

While native AFPs and AFGPs act by being adsorbed on the surface of nucleated ice crystals, which prevents further growth and recrystallization, the Ben laboratory has proposed a different mechanism by which monosaccharides inhibit ice recrystallization. Galema and colleagues have performed extensive studies regarding the hydration of various monosaccharides.[100–102] In these studies, hydration refers to the number of water molecules that interact closely with various carbohydrates.[100–102] Specifically, these studies indicate that the relative stereochemistry at the C_2 and C_4 positions in addition to hydrogen bond cooperativity (Dashnau *et al*.) modulate the magnitude of hydration.[96,100–103] The Ben laboratory has since developed a *hydration index*, which is the value corresponding to the hydration number divided by the molar volume of the carbohydrate.[98] Following the assessment of monosaccharides for their IRI activity, these experiments suggest that IRI activity is maximized when the C_4 hydroxyl substituent is axial while all remaining hydroxyl groups are equatorial, as with D-galactose.[96,98] Thus, hydration index and IRI activity are proportional. For instance, D-galactose (possessing

the highest hydration index) exhibited the most IRI activity of all the monosaccharides assessed (**Figure 1.8**).[96] From these experiments, the Ben laboratory has proposed a mechanism by which monosaccharides inhibit ice recrystallization. As a consequence of stereochemistry, highly hydrated monosaccharides such as D-galactose reduce their compatibility within the three-dimensional hydrogen-bonded network of water.[96,98] As a result, the semi-ordered quasi-liquid layer becomes more disordered and the addition of water molecules from the QLL to the highly ordered ice crystal lattice is entropically unfavourable. Thus, the Ben laboratory has hypothesized that highly hydrated monosaccharides such as D-galactose result in greater disorder of the QLL, which ultimately increases their IRI activity. In contrast, marginally hydrated monosaccharides such as D-talose are more compatible with bulk water. Thus, they cause little disruption to the QLL and possess little to no IRI activity.

1.4.2 Aryl Glycosides as Effective Inhibitors of Ice Recrystallization

While D-galactose was the most effective inhibitor of ice recrystallization of all the monosaccharides assessed, it exhibited only moderate IRI activity (% MGS approximately 60 %).[98,99] Thus, structure-function analyses were performed on monosaccharides to elucidate important structural features that further enhance their IRI activity. While *C*-linked AFGP analogs were effective inhibitors of ice recrystallization, these analogs were large peptide-based molecules whose synthesis was not amenable to scale-up. Subsequent research by the Ben laboratory involved the synthesis of low molecular weight carbohydrate-based derivatives as effective inhibitors of ice recrystallization. In accordance with the proposed mechanism of action, the Ben laboratory sought to investigate small molecule ice recrystallization inhibitors (IRIs) whose functional groups cause further disorder in bulk water.[104] Such molecules include surfactants, organogelators, and hydrogelators. These amphiphilic molecules possess a hydrophilic head and a hydrophobic tail allowing them to self-assemble and form micelles/hydrogels in solution.[105,106] While carbohydrate surfactants (specifically *n*-Octyl-β-D-glycosides) have been extensively studied for crystallization and solubilization of membrane proteins, their ability to inhibit ice recrystallization had not been previously

explored.[107,108] As a result, prior work by our laboratory involved the synthesis of these *n*-Octyl-β-D-glycosides followed by their assessment for IRI activity using a splat-cooling assay.[104] When tested at 22 mM, β-Octyl-Glc (**101**) performed similarly to its parent carbohydrate D-glucose. These results were consistent with previous hypotheses suggesting that the substituent and stereochemistry at the C_1 position has little influence on hydration, thus, little to no influence on IRI activity.[98,104] However, when tested at 22 mM, β-Octyl-Gal (**102**) performed significantly better than its parent carbohydrate D-galactose.[104] These results suggest the importance of hydrophobic moieties (specifically long alkyl chains) at the C_1 position of monosaccharides for IRI activity.[109,110]

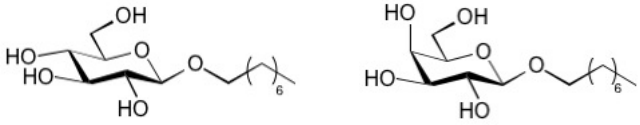

101 **102**

Figure 1.9 Structure of β-Octyl-Glc (**101**) and β-Octyl-Gal (**102**).

Despite the efficiency of long alkyl chains to inhibit ice recrystallization, these derivatives are surfactants. As such, alkyl glycoside derivatives such as β-Octyl-Gal are not suitable cryoprotective agents since their ability to solubilize cell membranes is detrimental to cells.[107,108,111–113] However, the IRI activity of β-Octyl-Gal suggests the importance of hydrophobic moieties at the C_1 position of monosaccharides for ice recrystallization inhibition. As a result, the Ben laboratory sought to explore other hydrophobic substituents that could result in another class of small molecule carbohydrate-based inhibitors of ice recrystallization. Specifically, hydrophobic aryl ring substituents were employed at the C_1 position of monosaccharides in place of long alkyl chains.

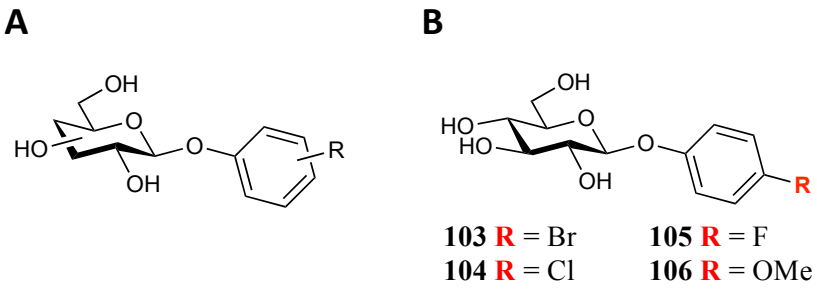

Figure 1.10 (**A**) Structure of various *ortho*-, *meta*-, and *para*- substituted *O*-linked aryl glycosides. (**B**) Most effective *O*-linked aryl glucoside inhibitors of ice recrystallization.

A PhD graduate of the Ben laboratory (Chantelle Capicciotti) synthesized various *O*-linked aryl glycosides with different substituents at the *ortho*-, *meta*-, and *para*-positions of the aromatic ring (**Figure 1.10 A**). Once synthesized, these derivatives were tested for their IRI activity once again using the splat-cooling assay. These results indicated that the *ortho*- and *meta*- substituted *O*-linked aryl glycosides were not very effective inhibitors of ice recrystallization.[114] However, when substituents were placed at the *para*- position of the aromatic ring, the IRI activity of these *O*-linked aryl glycosides was significantly increased.[114] Despite the IRI activity of β-Octyl-Gal, most of the *O*-linked aryl galactosides tested at 22mM were not effective inhibitors of ice recrystallization exhibiting a % MGS of approximately 80 %.[114] However, when assessed at similar concentrations, the *O*-linked aryl glucosides performed significantly better than their corresponding galactose counterparts exhibiting a % MGS of roughly 60 %.[114] Of these *O*-linked aryl glucosides, the *para* -Br, -Cl, -F, and -OMe derivatives **103-106** (**Figure 1.10 B**) were the most effective inhibitors of ice recrystallization. These results are particularly interesting since D-galactose possessed greater IRI activity compared to D-glucose when both parent carbohydrates were assessed as reducing sugars. The Ben laboratory previously correlated carbohydrate hydration with IRI activity.[96,98] Since D-galactose is more hydrated than D-glucose, the greater IRI activity of β-Octyl-Gal (**102**) compared to that of β-Octyl-Glc (**101**) was not surprising. However, the opposite is true for the *O*-linked aryl glycosides. For instance, the aryl glucosides possessing a D-glucose moiety resulted in more effective inhibitors of ice recrystallization compared to the aryl galactosides possessing a moiety of D-galactose (**Section 3.1**). Since the hydration of aryl

glycosides could not be measured, it is uncertain as to whether the aryl glucosides are more hydrated than their corresponding aryl galactosides. Despite these unexpected results, the *O*-linked aryl glucosides remain some of the most effective inhibitors of ice recrystallization that the Ben laboratory has encountered to date.

1.4.3 Aryl Glycosides as Cryopreservatives for Human RBCs

Ice recrystallization that occurs during freezing and thawing of cryopreserved cells contributes significantly to cellular damage and reduced cell viability post-thaw.[17] Due to the IRI activity of the *O*-linked aryl glucosides, the Ben laboratory previously assessed the ability of these carbohydrate-based derivatives to protect human RBCs against freezing injury. The current procedure utilized in North America for human RBC cryopreservation involves high glycerol concentrations (40% *v/v*) in conjunction with slow freezing rates (1 ^{o}C/min) for storage at -80^{o}C.[2,5,14] Thus, post-thaw RBC integrity was assessed in the presence of 15 % glycerol and either *p*-Br-Ph-Glc (**103**) or PMP-Glc (**106**), two of our laboratory's most effective inhibitors of ice recrystallization.[115,116] In the absence of inhibitor, post-thaw RBC integrity ranges from 20-30 % with a solution of 15 % glycerol.[115] However, upon addition of 110 mM PMP-Glc, the post-thaw RBC integrity nearly doubled (approximately 50 % intact RBCs).[115] Furthermore, RBC integrity increased to 70-80 % when 30 mM of *p*-Br-Ph-Glc was added to a solution of 15 % glycerol.[115] These results previously demonstrated that effective small molecule inhibitors of ice recrystallization could be used in conjunction with reduced glycerol concentrations to successfully protect human RBCs against freezing injury. Thus, structure-function analyses of carbohydrate derivatives may result in the elucidation of key structural features that further enhance their IRI activity and increase their ability to confer protection against cryoinjury.

1.5 References

(1) Acker, J. P. *Adv. Biochem. Engin./Biotechnol.* **2006**, *103*, 157–187.

(2) Scott, K. K.; Lecak, J.; Acker, J. P. *Transfus. Med. Rev.* **2005**, *19* (2), 127–142.

(3) D'Alessandro, A.; Liumbruno, G.; Grazzini, G.; Zolla, L. *Blood Transfus.* **2010**, *8*, 82–88.

(4) Holovati, J. L.; Hannon, J. L.; Gyongyossy-Issa, M. I. C.; Acker, J. P. *Transfus. Med. Rev.* **2009**, *23*, 25–41.

(5) Lecak, J.; Scott, K.; Young, C.; Hannon, J.; Acker, J. P. *Transfusion* **2004**, *44* (9), 1306–1313.

(6) Kurach, J. D. R.; Almizraq, R.; Bicalho, B.; Acker, J. P.; Holovati, J. L. *Transfusion* **2014**, *54*, 1595–1603.

(7) Högman, C. F. *Vox Sang.* **1998**, *74*, 177–187.

(8) Kanias, T.; Gladwin, M. T. *Transfusion* **2013**, *52*, 1388–1392.

(9) Hysi, E.; Strohm, E. M.; Berndl, E. S. L.; Kolios, M. C.; Acker, J. P. *IEEE Int. Ultrason. Symp. Proc.* **2014**, 1662–1665.

(10) Sparrow, R. L. *Blood Transfus.* **2012**, *10*, s7–s11.

(11) Högman, C. F.; Hedlund, K.; Zetterström, H. *N. Engl. J. Med.* **1978**, *299*, 1377–1382.

(12) Högman, C. F.; Hedlund, K.; Sahleström, Y. *Vox Sang.* **1981**, *41*, 274–281.

(13) Gibson, J. G.; Rees, S. B.; McManus, T. J.; Scheitlin, W. A. *Am. J. Clin. Path.* **1957**, *28*, 569–578.

(14) Kanias, T.; Acker, J. P. *FEBS J.* **2010**, *277*, 343–356.

(15) Baust, J. M. *Cell Preserv. Technol.* **2002**, *1*, 17–31.

(16) Gao, D.; Critser, J. K. *ILAR J.* **2000**, *41* (4), 187–196.

(17) Mazur, p. *Am. J. Physiol.* **1984**, *247* (19), C125–C142.

(18) Mazur, P. *J. Gen. Physiol.* **1963**, *47*, 347–369.

(19) Mazur, P.; Leibo, S. P.; Chu, E. H. Y. *Exp. Cell Res.* **1972**, *71*, 345–355.

(20) Muldrew, K.; McGann, L. E. *Biophys. J.* **1990**, *57*, 525–532.

(21) Toner, M.; Cravalho, E. G.; Karel, M. *J. Appl. Phys.* **1990**, *67*, 1582–1593.

(22) Zade-Oppen, A. M. M. *Acta. Phsiol. Scand.* **1968**, *73*, 341–364.

(23) Pegg, D. E.; Diaper, M. P. *Cryobiology* **1991**, *28*, 18–35.
(24) Pegg, D. E.; Diaper, M. P. *Biophys. J.* **1988**, *54*, 471–488.
(25) Lovelock, J. E. *Proc. R. Soc. London* **1957**, *147*, 427–433.
(26) Mazur, P. *J. Bacteriol.* **1961**, *82*, 662–672.
(27) Klossner, D. P.; Robilotto, A. T.; Clarke, D. M.; Vanbuskirk, R. G.; Baust, J. M.; Gage, A. A.; Baust, J. G. *Cryobiology* **2007**, *55*, 189–199.
(28) McGann, L. E. *Cryobiology* **1978**, *15*, 382–390.
(29) Meryman, H. T. *Cryobiology* **1971**, *8*, 173–183.
(30) Crowe, J. H.; Crowe, L. M.; Carpenter, J. F.; Rudolph, A. S.; Wistrom, C. A.; Spargo, B. J.; Anchordoguy, T. J. *Biochim. Biophys. Acta* **1988**, *947*, 367–384.
(31) Rapatz, G.; Sullivan, J. J.; Luyet, B. *Cryobiology* **1968**, *5*, 18–25.
(32) Lovelock, J. E. *Biochim. Biophys. Acta* **1953**, *11*, 28–36.
(33) Polge, C.; Smith, A. U.; Parkes, A. S. *Nature* **1949**, *164*, 666.
(34) Lovelock, J. E.; Bishop, M. W. H. *Nature* **1959**, *183*, 1394–1395.
(35) Snedeker, W. H.; Gaunya, W. S. *J. Anim. Sci.* **1970**, *30*, 953-956.
(36) Karow, A. M. *J. Pharm. Pharmac.* **1969**, *21*, 209–223.
(37) Malinin, Theodore, I.; Perry, V. P. *Cryobiology* **1967**, *4*, 90–96.
(38) Galvao, J.; Davis, B.; Tilley, M.; Normando, E.; Duchen, M. R.; Cordeiro, M. F. *FASEB J.* **2013**, *28*, 1317–1330.
(39) Hanslick, J. L.; Lau, K.; Noguchi, K. K.; Olney, J. W.; Zorumski, C. F.; Mennerick, S.; Farber, N. B. *Neurobiol. Dis.* **2009**, *34* (1), 1–10.
(40) Fahy, G. M. *Cryobiology* **1986**, *23*, 1–13.
(41) Fahy, G. M.; Karow, A. M. *Cryobiology* **1977**, *14*, 418–427.
(42) Lovelock, J. E. *Biochim. Biophys. Acta* **1953**, *10*, 414–426.
(43) Hess, J. R. *Transfus. Med. Rev.* **2004**, *14*, 1–8.
(44) Hess, J. R.; Greenwalt, T. G. *Transfus. Med. Rev.* **2002**, *16* (4), 283–295.
(45) Smith, A. u. *Lancet* **1950**, *256*, 910–911.
(46) Asghar, W.; El Assal, R.; Shafiee, H.; Anchan, R. M.; Demirci, U. *Biotechnol J.* **2015**, *9*, 895–903.
(47) Rowe, A. W.; Eyster, E.; Kellner, A. *Cryobiology* **1968**, *5*, 119–128.
(48) Krijnen, H. W.; De Wit, J. J.; Kuivenhoven, A. C. J.; Loos, J. A.; Prins, H. K. *Vox*

Sang. **1964**, *9*, 559–572.

(49) Lusianti, R. E.; Higgins, A. Z. *Biomocrofluidics* **2014**, *8*, 54124.

(50) Adapa, S.; Schmidt, K. A.; Jeon, I. J.; Herald, T. J.; Flores, R. A. *Food Rev. Int.* **2000**, *16*, 259–271.

(51) Flores, A. A.; Goff, H. D. *J. Dairy Sci.* **1999**, *82*, 1408–1415.

(52) Ndoye, F. T.; Alvarez, G. *J. Food Eng.* **2015**, *148*, 24–34.

(53) Cook, K. L. .; Hartel, R. W. *Compr. Rev. Food Sci. Food Saf.* **2010**, *9*, 213–222.

(54) Donhowe, D. P.; Hartel, R. W. *Int. Dairy J.* **1996**, *6*, 1191–1208.

(55) Owston, P. G.; Lonsdale, K. *J. Glaciol.* **1948**, *1*, 118–123.

(56) Malkin, T. L.; Murray, B. J.; Brukhno, A. V.; Anwar, J.; Salzmann, C. G.; Malkin, T. L.; Murray, B. J.; Brukhno, A. V; Anwar, J.; Salzmann, C. G. *Proc. Natl. Acad. Sci. U. S. A.* **2012**, *109*, 1041–1045.

(57) Thürmer, K.; Nie, S. *Proc. Natl. Acad. Sci. U. S. A.* **2013**, *110*, 11757–11762.

(58) Murray, B. J.; Knopf, D. A.; Bertram, A. K. *Nature* **2005**, *434*, 202–205.

(59) Murray, B. J.; Bertram, A. K. *Phys. Chem. Chem. Phys.* **2006**, *8*, 186–192.

(60) Dubochet, J.; Adrian, M.; Chang, J.-J.; Homo, J.-C.; Lepault, J.; McDowall, A. W.; Schultz, P. *Q. Rev. Biophys.* **1988**, *21*, 129–228.

(61) Mehl, P.; Boutron, P. *Cryobiology* **1988**, *25*, 44–54.

(62) Boutron, P.; Arnaud, F. *Cryobiology* **1984**, *21*, 348–358.

(63) Kumai, M. *J. Glaciol.* **1968**, *7*, 95–108.

(64) Harding, M. M.; Ward, L. G.; Haymet, A. D. J. *Eur. J. Biochem.* **1999**, *264*, 653–665.

(65) Sazaki, G.; Zepeda, S.; Nakatsubo, S.; Yokomine, M.; Furukawa, Y. *Proc. Natl. Acad. Sci. U. S. A.* **2012**, *109*, 1052–1055.

(66) Fletcher, N. H. *Philos. Mag.* **1968**, *18*, 1287–1300.

(67) Furukawa, Y.; Yamamoto, M.; Kuroda, T. *J. Cryst. Growth* **1987**, *82*, 665–677.

(68) KARIM, omar A.; Haymet, A. D. J. *Chem. Phys. Lett.* **1987**, *138*, 531–534.

(69) Beaglehole, D.; Nason, D. *Surf. Sci.* **1980**, *96*, 357–363.

(70) Budke, C.; Koop, T. *Chem. Phys. Chem.* **2006**, *7*, 2601–2606.

(71) Budke, C.; Heggemann, C.; Koch, M.; Sewald, N.; Koop, T. *J. Phys. Chem.* **2009**, *113*, 2865–2873.

(72) Nagel, L.; Budke, C.; Dreyer, A.; Koop, T.; Sewald, N. *Beilstein J. Org. Chem.* **2012**, *8*, 1657–1667.

(73) Ng, J. D.; Lorber, B.; Witz, J.; Theobald-Dietrich, A.; Kern, D.; Giege, R. *J. Cryst. Growth* **1996**, *168*, 50–62.

(74) Boistelle, R.; Astier, J. P. *J. Cryst. Growth* **1988**, *90*, 14–30.

(75) Baldan, A. *J. Mater. Sci.* **2002**, *37*, 2171–2202.

(76) Scholander, P. F.; Van Dam, L.; Kanwisher, J. W.; Hammel, H. T.; Gordon, M. S. *J. Cell. Physiol.* **1957**, *49*, 5–24.

(77) Gordon, M. S.; Amdur, B. H.; Scholander, P. F. *Biol. Bull.* **1962**, *122*, 52–62.

(78) DeVries, A. L.; Wohlschlag, D. E. *Science* **1969**, *163*, 1073–1075.

(79) DeVries, A. L.; Komatsu, S. K.; Feeney, R. E. *J. Biol. Chem.* **1970**, *245*, 2901–2908.

(80) DeVries, A. L. *Comp. Biochem. Physiol.* **1982**, *73*, 627–640.

(81) Harding, M. M.; Anderberg, P. I.; Haymet, A. D. J. *Eur. J. Biochem.* **2003**, *270*, 1381–1392.

(82) Garner, J.; Harding, M. M. *ChemBioChem.* **2010**, *11*, 2489–2498.

(83) Wu, Y.; Banoub, J.; Goddard, S. V; Kao, M. H.; Fletcher, G. L. *Comp. Biochem. Physiol. Part B* **2001**, *128*, 265–273.

(84) Knight, C. A.; DeVries, A. L.; Oolman, L. D. *Nature* **1984**, *308*, 295–296.

(85) Burcham, T. S.; Osuga, D. T.; Chino, H.; Feeney, R. E. *Anal. Biochem.* **1984**, *139*, 197–204.

(86) Ahlgren, J. A.; Cheng, C.-H. C.; Schrag, J. D.; DeVries, A. L. *J. Exp. Biol.* **1988**, *137*, 549–563.

(87) Mugnano, J. A.; Wang, T.; Layne, J. R.; DeVries, A. L.; Lee JR., R. E. *Am. J. Physiol.* **1995**, 474–479.

(88) Wang, T.; Zhu, Q.; Yang, X.; Layne, J. R.; DeVries, A. L. *Cryobiology* **1994**, *31*, 184–192.

(89) Rubinsky, B.; Arav, A.; Mattioli, M.; Devries, A. L. *Biochem. Biophys. Res. Commun.* **1990**, *173*, 1369–1374.

(90) Rubinsky, B.; Arav, A.; Fletcher, G. L. *Biochem. Biophys. Res. Commun.* **1991**, *180*, 566–571.

(91) Knight, C. A.; Duman, J. G. *Cryobiology* **1986**, *23*, 256–262.

(92) Urrutia, M. E.; Duman, J. G.; Knight, C. A. *Biochim. Biophys. Acta* **1992**, *1121*, 199–206.

(93) Bar-dolev, M.; Celik, Y.; Wettlaufer, J. S.; Davies, P. L.; Braslavsky, I. *J. R. Soc. Interface* **2012**, *9*, 3249–3259.

(94) Eniade, A.; Purushotham, M.; Ben, R. N.; Wang, J. B.; Horwath, K. *Cell Biochem. Biophys.* **2003**, *38*, 115–124.

(95) Liu, S.; Ben, R. N. *Org. Lett.* **2005**, *7*, 2385–2388.

(96) Czechura, P.; Tam, R. Y.; Dimitrijevic, E.; Murphy, A. V; Ben, R. N. *J. Am. Chem. Soc.* **2008**, *130*, 2928–2929.

(97) Leclere, M.; Kwok, B. K.; Wu, L. K.; Allan, D. S.; Ben, R. N. *Bioconjug. Chem.* **2011**, *22*, 1804–1810.

(98) Tam, R. Y.; Ferreira, S. S.; Czechura, P.; Chaytor, J. L.; Ben, R. N. *J. Am. Chem. Soc.* **2008**, *130*, 17494–17501.

(99) Chaytor, J. L.; Tokarew, J. M.; Wu, L. K.; Leclère, M.; Tam, R. Y.; Capicciotti, J.; Guolla, L.; von Moos, E.; Findlay, C. S.; Allan, D. S.; Ben, R. N. *Glycobiology* **2012**, *22* (1), 123–133.

(100) Galema, S. A.; Engberts, J. B. F. .; Hoiland, H.; Forland, G. M. *J. Phys. Chem.* **1993**, *97*, 6885–6889.

(101) Galema, S. A.; Hoiland, H. *J. Phys. Chem.* **1991**, *95* (22), 5321–5326.

(102) Galema, S. A.; Howard, E.; Engberts, J. B. F. N.; Grigera, J. R. *Carbohydr. Res.* **1994**, *265*, 215–225.

(103) Dashnau, J. L.; Sharp, K. A.; Vanderkooi, J. M. *J. Phys. Chem.* **2005**, *109*, 24152–24159.

(104) Capicciotti, C. J.; Leclere, M.; Perras, F. A.; Bryce, D. L.; Paulin, H.; Harden, J.; Liu, Y.; Ben, R. N. *Chem. Sci.* **2012**, *3*, 1345–1716.

(105) Loos, M. De; Feringa, B. L.; Esch, J. H. Van. *Eur. J. Org. Chem.* **2005**, *2005*, 3615–3631.

(106) Estroff, L. A.; Hamilton, A. D. *Chem. Rev.* **2004**, *104*, 1201–1218.

(107) Michel, H.; Oesterhelt, D. *Proc. Natl. Acad. Sci. USA* **1980**, *77*, 1283–1285.

(108) Lorber, B.; Bishop, J. B.; DeLucas, L. J. *Biochim. Biophys. Acta.* **1990**, *1023*, 254–

265.

(109) Capicciotti, C. J.; Leclere, M.; Perras, F. A.; Bryce, D. L.; Paulin, H.; Harden, J.; Liu, Y.; Ben, R. N. *Chem. Sci.* **2012**, *3*, 1408–1416.

(110) Balcerzak, A. K.; Febbraro, M.; Ben, R. N. *RSC Adv.* **2013**, *3*, 3232–3236.

(111) Hildreth, J. E. K. *Biochem. J.* **1982**, *207*, 363–366.

(112) Rosevear, P.; VanAken, T.; Baxter, J.; Ferguson-miller, S. *Biochemistry* **1980**, *19*, 4108–4115.

(113) Corma, A.; Iborra, S.; Miquel, S.; Primo, J. *J. Catal.* **1998**, *180*, 218–224.

(114) Capicciotti, C. The Rational Design of Potent Ice Recrystallization Inhibitors for Use as Novel Cryoprotectants, University of Ottawa, 2014.

(115) Capicciotti, C. J.; Kurach, J. D. R.; Turner, T. R.; Mancini, R. S.; Acker, J. P.; Ben, R. N. *Sci. Rep.* **2015**, *5*, 9692–9715.

(116) Briard, J. G.; Poisson, J. S.; Turner, T. R.; Capicciotti, C. J.; Acker, J. P.; Ben, R. N. *Sci. Rep.* **2016**, *6*, 23619.

(117) Haridas, V.; Naik, S. *RSC Adv.* **2013**, *3*, 14199–14218.

Chapter 2: Goals and Objectives

2.1 Introduction

In North America, the currently accepted protocol for the clinical cryopreservation of human red blood cells (RBCs) involves the use of high glycerol concentrations (40% *v/v*) and slow cooling rates (1 ^{o}C/min) for storage at -80 ^{o}C.[1–3] Glycerol is a membrane-permeating cryoprotective agent that provides protection against freezing injury by preventing cell dehydration and the concentration of intracellular solutes.[4–6] Glycerol and dimethyl sulphoxide (DMSO) are two of the most commonly used cryoprotective agents. Unfortunately, they do not protect cells against ice recrystallization, a phenomenon that occurs as a consequence of intracellular ice formation (IIF).[7–9] As a result, the overall goal of the Ben laboratory is to develop small molecule carbohydrate-based ice recrystallization inhibitors (IRIs). Provided that these IRIs are non-toxic to cells, the ultimate goal is to use these IRIs as an alternative to glycerol and DMSO for the cryopreservation of various cell types such as human RBCs and hematopoietic stem cells (HSCs) from umbilical cord blood. Specifically, the objectives of this thesis are to perform structure-function analyses on carbohydrate-based derivatives to determine the important structural features responsible for ice recrystallization inhibition (IRI) activity.

2.2 Objective 1 –Determining the Importance of the C_1 Heteroatom of Aryl Glycosides for Ice Recrystallization Inhibition

Our laboratory has previously demonstrated that the *O*-linked aryl glycosides are an effective class of small molecule inhibitors of ice recrystallization.[10] Structure-function analyses were performed whereby the parent carbohydrate, the type of glycosidic bond, and various aryl substituents were assessed for their influence on IRI activity. Conclusions from this study suggest that a moiety of D-glucose, a β-glycosidic bond, and either a halogen or –methoxy substituent at the *para*- position of the aromatic ring are all features that further enhance the IRI activity of *O*-linked aryl glycosides.[10] However, the

anomeric oxygen atom of aryl glycosides has not yet been investigated for its influence on ice recrystallization inhibition. Thus, the objective of this study was to synthesize a variety of *N*- and *S*-linked aryl glycosides and assess the importance of the C_1 heteroatom of aryl glycosides for IRI activity. Three *para*-substituted *O*-linked aryl glycosides exhibiting different IRI activities were selected for investigation. The corresponding C_1 nitrogen and sulphur derivatives were synthesized and assessed for their IRI activity (**Figure 2.1**). Specifically, we sought to explore whether a change in stereoelectronic effects at the anomeric position of aryl glycosides could improve the overall activity of aryl glycosides and confer activity to inactive *O*-linked aryl derivatives.

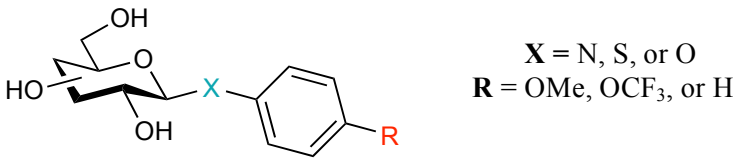

Figure 2.1 Structure of *O*-, *N*-, and *S*-linked aryl glycoside targets synthesized and assessed for their IRI activity using the improved splat-cooling assay.

The IRI activity of *O*-linked aryl glycosides was previously reported as a percent mean grain size (% MGS) of ice crystals relative to that of a phosphate-buffered saline (PBS) solution. Thus, these derivatives were previously assessed at a single concentration (typically 22 mM) and time point (30 minutes), an approach that neglects both the effects of time and concentration on IRI activity. As a result, another objective of this study was to assess the *O*-, *N*-, and *S*-linked aryl glycosides for their IRI activity using the improved splat-cooling assay. By assessing the rate of ice crystal growth, dose-response curves were constructed and IC_{50} values were calculated. The IC_{50} value represents the concentration at which our ice recrystallization inhibitors have obtained half of their maximum inhibitory capability.[11] Compared to the % MGS formerly used, the IC_{50} value provides a more quantifiable measure of IRI activity. In addition, this enables direct comparisons of IRI activity between *O*-, *N*-, and *S*-linked aryl glycosides.

2.3 Objective 2 –Determining the Importance of the *p*-methoxyphenyl substituent for Ice Recrystallization Inhibition by AFGP Disaccharide Analogs

A variety of *C*-linked AFGP analogs were previously synthesized by our laboratory and assessed for their IRI activity. From this study, our laboratory demonstrated that the carbohydrate moiety of these glycoprotein analogs determines the extent of ice recrystallization inhibition.[12] Conclusions from this study also suggest that compounds are capable of exhibiting IRI activity without the detrimental effects of thermal hysteresis (i.e. "custom-tailored" antifreeze activity).[13,14] Thus, truncated AFGP disaccharide analogs were previously synthesized and assessed for their IRI activity. Specifically, the importance of the β-(1,3) glycosidic linkage for ice recrystallization inhibition was assessed (**Figure 2.2 B**).[15–17] While native AFGP-8 possesses a β-(1,3) glycosidic linkage (**Figure 2.2 A**), the AFGP disaccharide analog possessing a β-(1,4) glycosidic linkage was the most IRI active exhibiting a percent mean grain size (% MGS) of approximately 50 %.[17]

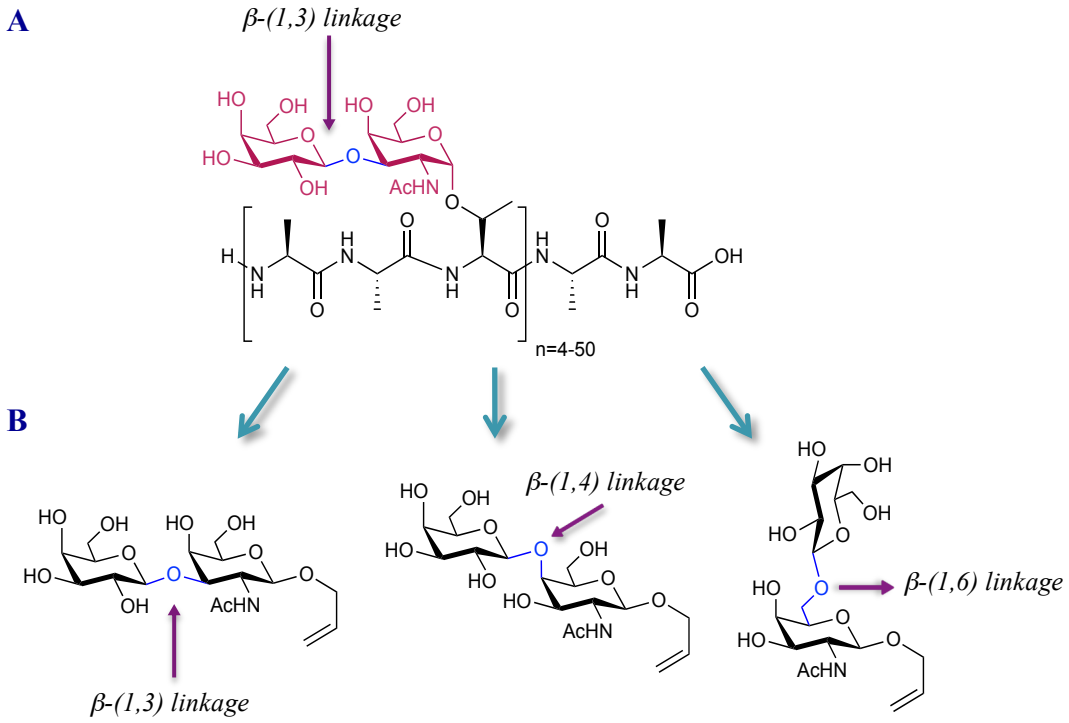

Figure 2.2 Structure of (**A**) native AFGP-8 whereby the disaccharide moiety and β-(1,3) glycosidic linkage have been highlighted and (**B**) AFGP disaccharide analogs highlighting the different glycosidic linkages.

In addition to elucidating the importance of the β-(1,3) glycosidic linkage for IRI activity, the acetamido (NHAc) function present in AFGP disaccharide analogs was also assessed. Tachibana and colleagues previously demonstrated that the acetamido function is important for thermal hysteresis.[18] However, when the acetamido function was replaced with a hydroxyl substituent, both AFGP disaccharide analogs in **Figure 2.3** exhibited a % MGS of approximately 70 %.[17,19] As a result, our laboratory previously demonstrated that the acetamido function is not required for IRI activity.

Figure 2.3 Structure of AFGP disaccharide analogs assessed for their IRI activity to elucidate the importance of the acetamido (NHAc) function for ice recrystallization inhibition.

Despite these developments, an extensive structure-function analysis of AFGP disaccharide analogs has not yet been performed. Thus, the objective of this study was to synthesize an AFGP disaccharide analog whereby the β-allyl ether substituent is replaced with a *p*-methoxyphenyl (PMP) substituent (**Figure 2.4 A**). The *p*-methoxy substituted *O*-linked aryl glucoside (PMP-Glc) was one of the most effective inhibitors of ice recrystallization. As a result, our laboratory sought to incorporate the *p*-methoxyphenyl (PMP) substituent into AFGP disaccharide analogs and assess whether this substituent could increase the IRI activity of these analogs.

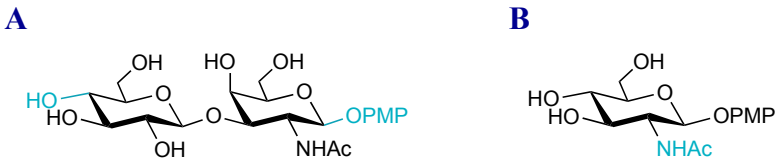

Figure 2.4 Structure of (**A**) AFGP disaccharide target and (**B**) the PMP-GlcNAc intermediate assessed for IRI activity.

Furthermore, the PMP-GlcNAc derivative was an intermediate encountered in disaccharide synthesis (**Figure 2.4 B**). This intermediate was also assessed for its IRI activity to confirm previous work by our laboratory, suggesting that the acetamido (NHAc) function present in AFGP disaccharide analogs is not required for ice recrystallization inhibition.[17,19]

2.4 References

(1) Scott, K. K.; Lecak, J.; Acker, J. P. *Transfus. Med. Rev.* **2005**, *19* (2), 127–142.

(2) Lecak, J.; Scott, K.; Young, C.; Hannon, J.; Acker, J. P. *Transfusion* **2004**, *44* (9), 1306–1313.

(3) Kanias, T.; Acker, J. P. *FEBS J.* **2010**, *277*, 343–356.

(4) McGann, L. E. *Cryobiology* **1978**, *15*, 382–390.

(5) Meryman, H. T. *Cryobiology* **1971**, *8*, 173–183.

(6) Lovelock, J. E.; Bishop, M. W. H. *Nature* **1959**, *183*, 1394–1395.

(7) Mazur, P.; Leibo, S. P.; Chu, E. H. Y. *Exp. Cell Res.* **1972**, *71*, 345–355.

(8) Muldrew, K.; McGann, L. E. *Biophys. J.* **1990**, *57*, 525–532.

(9) Mazur, P. *J. Bacteriol.* **1961**, *82*, 662–672.

(10) Capicciotti, C. The Rational Design of Potent Ice Recrystallization Inhibitors for Use as Novel Cryoprotectants, University of Ottawa, 2014.

(11) Abraham, S.; Keillor, K.; Capicciotti, C. J.; Perley-Robertson, G. E.; Keillor, J. W.; Ben, R. N. *Cryst. Growth Des.* **2015**, *15*, 5034–5039.

(12) Czechura, P.; Tam, R. Y.; Dimitrijevic, E.; Murphy, A. V; Ben, R. N. *J. Am. Chem. Soc.* **2008**, *130*, 2928–2929.

(13) Eniade, A.; Purushotham, M.; Ben, R. N.; Wang, J. B.; Horwath, K. *Cell Biochem. Biophys.* **2003**, *38*, 115–124.

(14) Liu, S.; Ben, R. N. *Org. Lett.* **2005**, *7*, 2385–2388.

(15) Balcerzak, A. K. Elucidating the Key Structural Features of Carbohydrates and Surfactants Necessary for Inhibiting Ice Recrystallization, University of Ottawa, 2014.

(16) Ferreira, S. S. Improving the Rational Design of Antifreeze Glycoproteins Through Identification of the Parameters that Influence Ice Recrystallization Inhibition, University of Ottawa, 2014.

(17) Balcerzak, A. K.; Ferreira, S. S.; Trant, J. F.; Ben, R. N. *Bioorg. Med. Chem. Lett.* **2012**, *22* (4), 1719–1721.

(18) Tachibana, Y.; Fletcher, G. L.; Fujitani, N.; Tsuda, S.; Monde, K.; Nishimura, S. *Angew. Chem. Int. Ed.* **2004**, *116*, 874–880.

(19) Trant, J. F. Importance of the structural components of C-linked glycopeptides to specific antifreeze activity : from glycopeptides to small molecule inhibitors of ice recrystallization, University of Ottawa, 2012.

Chapter 3: Investigating the Importance of the C_1 Heteroatom of Aryl Glycosides for Ice Recrystallization Inhibition

3.1 Introduction

Prior work by the Ben laboratory involved the assessment of monosaccharides as reducing sugars for their IRI activity. While these monosaccharides were moderate inhibitors of ice recrystallization (i.e. 80 % > mean grain size > 10 %), our laboratory hypothesized that their inhibitory activity is attributed to their ability to disorder the structure of bulk water.[1,2] As a result, carbohydrate-based surfactants that are known to disrupt the structure of bulk water were assessed for their IRI activity.[3] In addition to β-Octyl-Gal, the previously discussed *C*-linked AFGP analog OGG-Gal is also an effective inhibitor of ice recrystallization encountered by our laboratory. Thus, truncated derivatives ranging from one to sixteen carbons in length were subsequently investigated to determine the smallest subunit that can exhibit IRI activity similar to that of OGG-Gal (**Figure 3.1**).[4] Conclusions from this study previously suggested that long alkyl chains are beneficial for IRI activity since octyl, nonyl, and decyl derivatives were effective inhibitors of ice recrystallization at 5.5 mM (i.e. % MGS = 30-40 %).[4] Despite their IRI activity, the surfactant nature of β-Octyl-Gal and long alkyl chain derivatives is detrimental to cells due to their ability to solubilize cell membranes.[5–9] This prevents the use of these derivatives as cryo-additives for cell preservation.

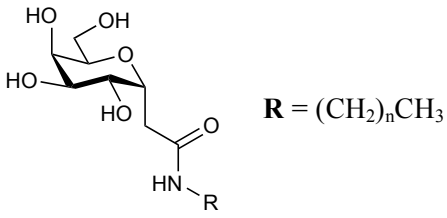

Figure 3.1 Structure of *C*-linked D-galactose derivatives with long alkyl chains ranging from one (n = 0) to sixteen (n = 15) carbons in length.

Although carbohydrate-based surfactants solubilize cell membranes, their IRI activities suggest the importance of hydrophobic substituents at the C_1 position of

monosaccharides for ice recrystallization inhibition. As a result, the Ben laboratory sought to employ hydrophobic aryl ring substituents at the C_1 position of various monosaccharides in place of long alkyl chains. Specifically, Chantelle Capicciotti (a former PhD student of the Ben laboratory) previously synthesized a variety of β-*O*-linked aryl glycosides with substituents at the *para*- position of the aromatic ring.[10] These aryl glycosides were then assessed for their IRI activity using the splat-cooling assay. While the *ortho*- and *meta*-substituted aryl glycosides were previously investigated (**Section 1.4.2**), these derivatives were excluded from this study for comparative purposes.

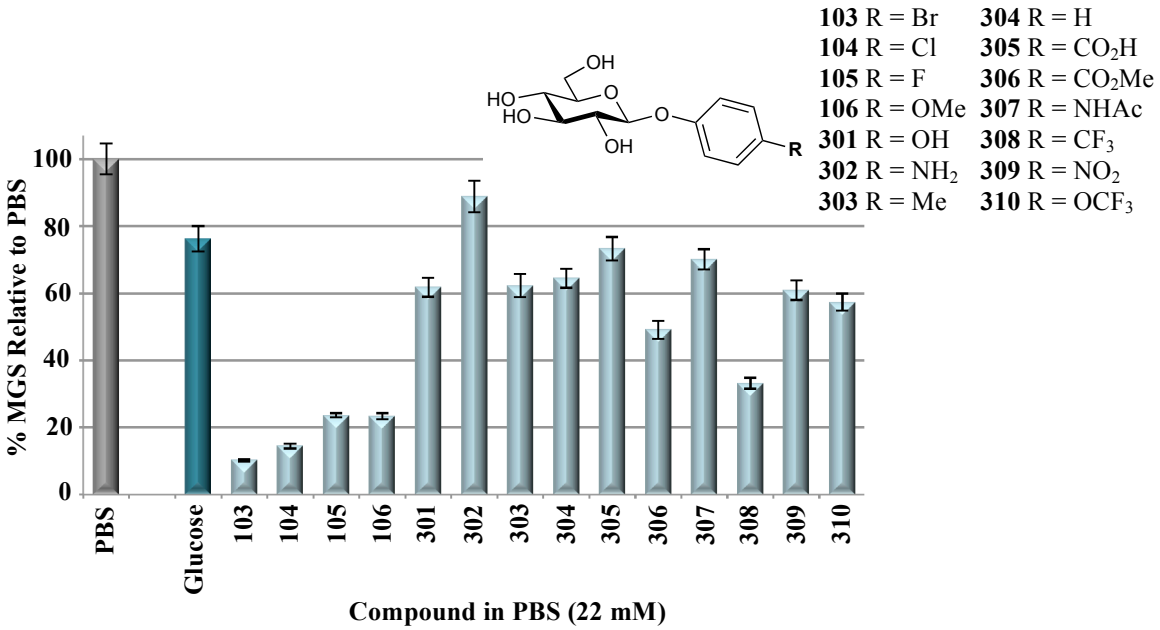

Figure 3.2 IRI activity of 22 mM *p*-substituted *O*-linked aryl glucosides indicated by % mean grain size (% MGS) of ice crystals relative to that of PBS, a positive control for ice recrystallization. Error bars represent the standard error of the mean (SEM). This figure was reproduced from Chantelle Capicciotti's PhD dissertation (University of Ottawa, 2009).[10]

When assessed at 22 mM, the *para*-bromo (**103**), *para*-chloro (**104**), *p*-fluoro (**105**), and *para*-methoxy (**106**) *O*-linked aryl glucosides were the most effective inhibitors of ice recrystallization exhibiting a % MGS between 8 % and 23 % (**Figure 3.2**). These results suggest that the nature of the aryl substituent (i.e. electron donating vs. electron withdrawing) has no effect on IRI activity.[10] Furthermore, the majority of these aryl glucosides were more IRI active than their parent carbohydrate D-glucose (i.e. %

MGS < 80 %). In contrast, the *O*-linked aryl galactosides displayed significantly different IRI activities.

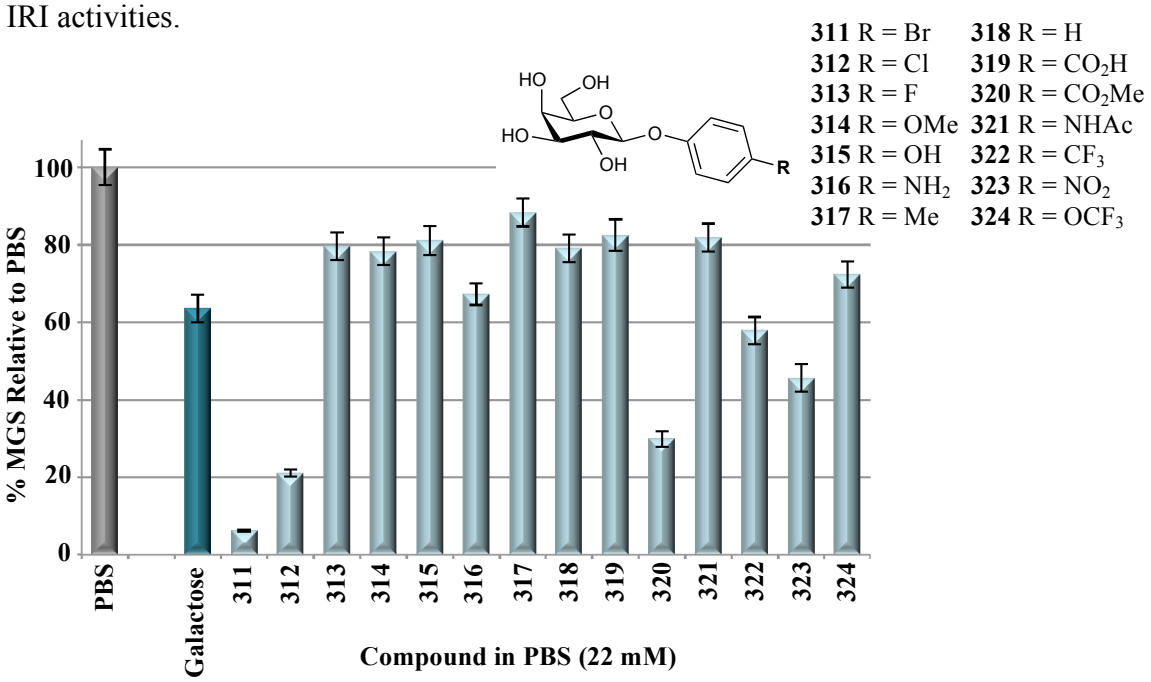

Figure 3.3 IRI activity of 22 mM *p*-substituted *O*-linked aryl galactosides indicated by % mean grain size (% MGS) of ice crystals relative to that of PBS, a positive control for ice recrystallization. Error bars represent the standard error of the mean (SEM). This figure was reproduced from Chantelle Capicciotti's PhD dissertation (University of Ottawa, 2009).[10]

Compared to the *O*-linked aryl glucosides, substituting the parent carbohydrate from glucose to galactose exacerbated the IRI activity of aryl glycosides (**Figure 3.3**). Specifically, the majority of the *O*-linked aryl galactosides exhibited little to no IRI activity with a % MGS larger than that of D-galactose (i.e. % MGS > 60 %). Of the *O*-linked aryl galactosides assessed, the *para*-bromo (**311**) and *para*-chloro (**312**) derivatives were the most IRI active exhibiting a % MGS of 20 % or below.

The Ben laboratory previously hypothesized that the mechanism of carbohydrate ice recrystallization inhibition is correlated to carbohydrate hydration.[11,12] As with β-Octyl-Gal, the derivative possessing the more hydrated carbohydrate moiety (i.e. galactose) resulted in the highest IRI activity since it further disrupts the structure of bulk water.[11,12] However, unexpected results were obtained with the *O*-linked aryl glycosides since the glucose derivatives gave rise to more effective inhibitors of ice recrystallization

compared to their corresponding galactose derivatives.[10] Since the hydration number of aryl glycosides could not be measured, the improved IRI activity of these derivatives cannot be directly correlated to an increase in carbohydrate hydration relative to that of glucose or galactose. However, these results suggest that the identity of the carbohydrate moiety has a significant impact on the IRI activity of aryl glycosides.

The *O*-linked aryl glycosides represent the second class of carbohydrate-based small molecule inhibitors of ice recrystallization encountered by our laboratory. In addition, the influence of functional group, regiochemistry of aryl substituents, and stereochemistry of the glycosidic bond on IRI activity were all previously investigated. Conclusions from this study suggest that a glucose moiety, a β-glycosidic bond, and either a halogen or -methoxy substituent at the *para*- position of the aromatic ring are all features that enhance the IRI activity of aryl glycosides.[10] However, the C_1 heteroatom of aryl glycosides has not yet been investigated for its influence on ice recrystallization inhibition. Thus, the objectives for this chapter are as follows:

1. *N*- and *S*-linked aryl glycosides were synthesized and assessed for their ability to inhibit ice recrystallization. Specifically, C_1 nitrogen and sulphur derivatives of the previously assessed *O*-linked aryl glycosides were synthesized to determine the influence of the C_1 heteroatom of aryl glycosides on IRI activity. Specifically, we sought to explore whether a change in stereoelectronic effects at the anomeric position could improve the overall activity of aryl glycosides and restore activity for inactive *O*-linked derivatives.

2. *O*-, *N*-, and *S*-linked aryl glycosides were assessed using the ameliorated splat-cooling assay in order to obtain IC_{50} values for each inhibitor from their corresponding dose-response curves. This IC_{50} value provides a more quantifiable measure of IRI activity compared to the % MGS formerly used with our previous assay.

3.2 Influence of *O*-linked Aryl Glycosides on the Kinetics of Ice Crystal Growth

Shortly following investigations into the effect of various *O*-linked aryl glycosides on IRI activity, Stephanie Abraham (a recent Master's graduate of the Ben laboratory) addressed limitations with the splat-cooling assay used to assess ice recrystallization inhibition. Our previous splat-cooling assay was adapted from that first demonstrated by Knight *et al*.[13] In this assay, ice recrystallization was monitored by a change in ice crystal size, whereby smaller ice crystals indicate a greater degree of IRI activity.[13,14] Ice recrystallization inhibitors were measured in triplicate by first dissolving them in a phosphate-buffered saline (PBS) solution. A 10 μL droplet of the sample solution was then released from a micropipette onto a precooled aluminum block (-80 ^{o}C) from a distance of roughly 2 m. The ice wafer was then transferred to a precooled glass coverslip and annealed on a cryostage at -6.4 ^{o}C for 30 minutes.[14] After this time, microscopic images of ice crystal wafers were obtained. Using a domain recognition software program, the cross-sectional area of 12 randomly selected ice crystals was measured. From these measurements, IRI activity was quantified by calculating a percent mean grain size (% MGS) of ice crystals relative to PBS, a positive control for ice recrystallization.[14] While the % MGS provides a general indication for the degree in which ice recrystallization has been inhibited, the previously employed splat-cooling assay is only semi-quantifiable due to several limitations. First, the analysis of 12 randomly selected ice crystals neglects the heterogeneity of ice crystal size within a population.[15] In addition, most of our carbohydrate-based inhibitors were assessed at a single time point (30 minutes) and concentration (typically 22 mM), an approach that neglects both the effects of time and concentration on IRI activity.[15] As a result, the Ben laboratory has ameliorated the existing splat-cooling assay to account for these limitations.

The current method for measuring IRI activity involves assessing the kinetics of ice recrystallization inhibition. In contrast to the previously employed splat-cooling assay, the new method involves assessing each carbohydrate-based inhibitor at a range of different concentrations.[15,16] In addition, early investigations by our laboratory indicate

that ice recrystallization primarily occurs within the first 5-10 minutes of annealing.[15,16] As a result, ice wafers are annealed at -6.4 ^{o}C for five minutes instead of the thirty-minute annealing period employed in our previous assay. The improved splat-cooling assay uses ImageJ software to measure the area of each individual ice crystal within the field of view. Ice crystal areas are then "binned" according to their size, whereby the proportionate area is measured as a function of time.[15] The rate of depletion of ice crystals in the bin with the smallest area is then used to represent the initial rate of ice crystal growth. From these initial rates, dose-response curves were constructed. From these dose-response curves, IC_{50} values were calculated providing a more quantifiable measure of IRI activity.

Prior to analyzing the effect of the C_1 heteroatom on ice recrystallization inhibition (IRI) activity, dose-response curves for selected *O*-linked aryl glycosides were required in order to make direct comparisons with their corresponding nitrogen and sulphur isosteres. As such, three aryl glycoside derivatives exhibiting different IRI activities (i.e. % MGS) were reassessed using the improved splat-cooling assay. Specifically, dose-response curves for the *p*-methoxy, *p*-trifluoromethoxy, and unsubstituted glucose (**Figure 3.2**, compounds **106**, **310**, **304**) and galactose (**Figure 3.3**, compounds **314**, **324**, **318**) aryl derivatives were constructed. The PMP-Glc derivative **106** was one of the most effective inhibitors of ice recrystallization of all the aryl glycosides assessed exhibiting a % MGS of 23 % (**Figure 3.2**). However, the corresponding aryl galactoside PMP-Gal (**314**) exhibited little to no IRI activity (**Figure 3.2**). As a result, the *p*-OMe derivative was selected to investigate whether a change in stereoelectronic effects at the anomeric position could further enhance the IRI activity of the aryl glucoside in an attempt to restore activity in the corresponding aryl galactoside. In addition, the unsubstituted and *p*-OCF_3 aryl glucosides (**Figure 3.2** compounds **304** and **310**) and corresponding aryl galactosides (**Figure 3.3** compounds **318** and **324**) were not very effective inhibitors of ice recrystallization. As a result, these derivatives were selected to investigate whether a change in anomeric stereoelectronic effects could improve their IRI activity.

3.2.1 Synthesis of O-linked Aryl Glycosides

Controlling the stereoselectivity of the glycosidic bond remains one of the most challenging aspects of carbohydrate synthesis.[17–19] However, the nature of the protecting group at the C_2 position of the glycosyl donor influences anomeric stereoselectivity.[17–19] For instance, glycosyl donors with a participating protecting group at the C_2 position (i.e. esters or amides) exert an anchimeric effect favouring 1,2-*trans* glycosides.[18–20] This approach was first exemplified by the Helferich reaction whereby glycosylation of fully acetylated sugars with phenols was mediated by the presence of *p*-toluenesulfonic acid, forming β-aryl glycosides.[21] In these reactions, a Lewis acid promoter facilitates the departure of the anomeric leaving group forming an oxo-carbenium ion.[18,20,22–24] An anchimeric effect exerted by the acyl protecting group at C_2 forms a stable five-membered dioxolenium intermediate as a 1,2-*cis* fused ring system.[18,20,22–24] The corresponding phenol glycosylates the anomeric center of the dioxolenium intermediate from the less hindered β-face, resulting in the 1,2-*trans* glycoside.[18–20]

The *O*-linked aryl glycosides were synthesized in the same manner as previously described by Chantelle Capicciotti (**Scheme 3.1**). From commercially available D-glucose or D-galactose, the reducing sugars were acetylated in the presence of sodium acetate and acetic anhydride to afford the corresponding fully acetylated gluco- and galacto-pyranoses **325** and **326** in 94 % and 58 % respectively. Using boron trifluoride diethyl etherate ($BF_3{\cdot}OEt_2$) as the Lewis acid promoter, glycosylation of the acetylated pyranose sugars with the designated phenol produced the corresponding acetate protected aryl glycosides **327** to **332** in moderate yields. Finally, Zemplén deacetylation afforded the desired *O*-linked aryl glycosides in high yield (**Scheme 3.1**).

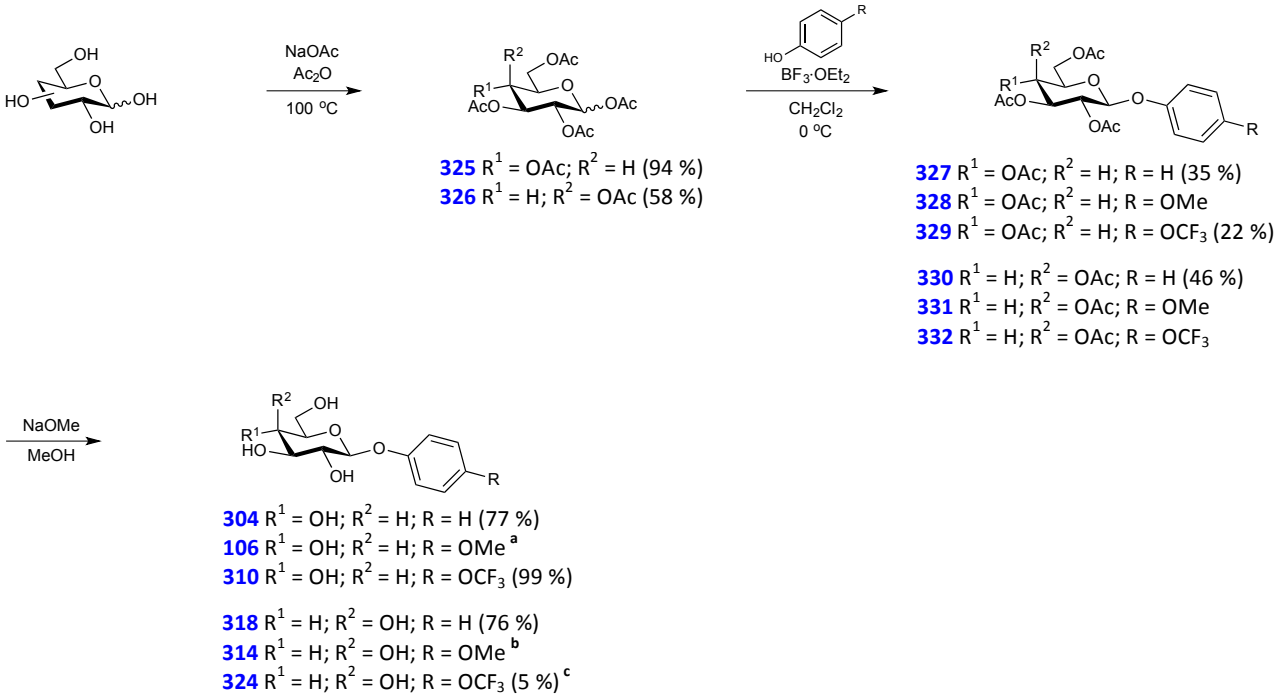

Scheme 3.1 Synthesis of *O*-linked aryl glycosides. [a] Compound was previously synthesized by Chantelle Capicciotti. [b] Compound was previously synthesized by Thomas Charlton. [c] Indicates yield over two steps.

With the exception of the PMP-Glc derivative **106** that was previously assessed for its IRI activity by Stephanie Abraham (a former student of the Ben laboratory), all derivatives in **Scheme 3.1** were synthesized and assessed for their IRI activity using the improved splat-cooling assay. In addition, the PMP-Gal derivative **314** was previously synthesized by a current PhD candidate of the Ben laboratory, Thomas Charlton, and was generously donated for IRI analysis.

3.2.2 IRI Activity of O-linked Aryl Glycosides

The dose-response curves for the *O*-linked aryl glycosides are presented in **Figure 3.4**. All compounds were assessed at various concentrations by measuring the area of individual ice crystals in the presence of aryl glycosides. As the overall area of ice crystals increases with decreasing concentration, the initial rate of ice crystal growth was calculated and normalized to that of a PBS control. The normalized rates of ice crystal

growth were then plotted against the log concentration, from which dose-response curves were constructed. From these dose-response curves an IC_{50} value was calculated, which is the concentration at which our ice recrystallization inhibitors have achieved half of their maximum inhibitory capability.[16] This IC_{50} value provides a quantifiable measure of IRI activity for the *O*-linked aryl glycosides in place of the % MGS formerly used.

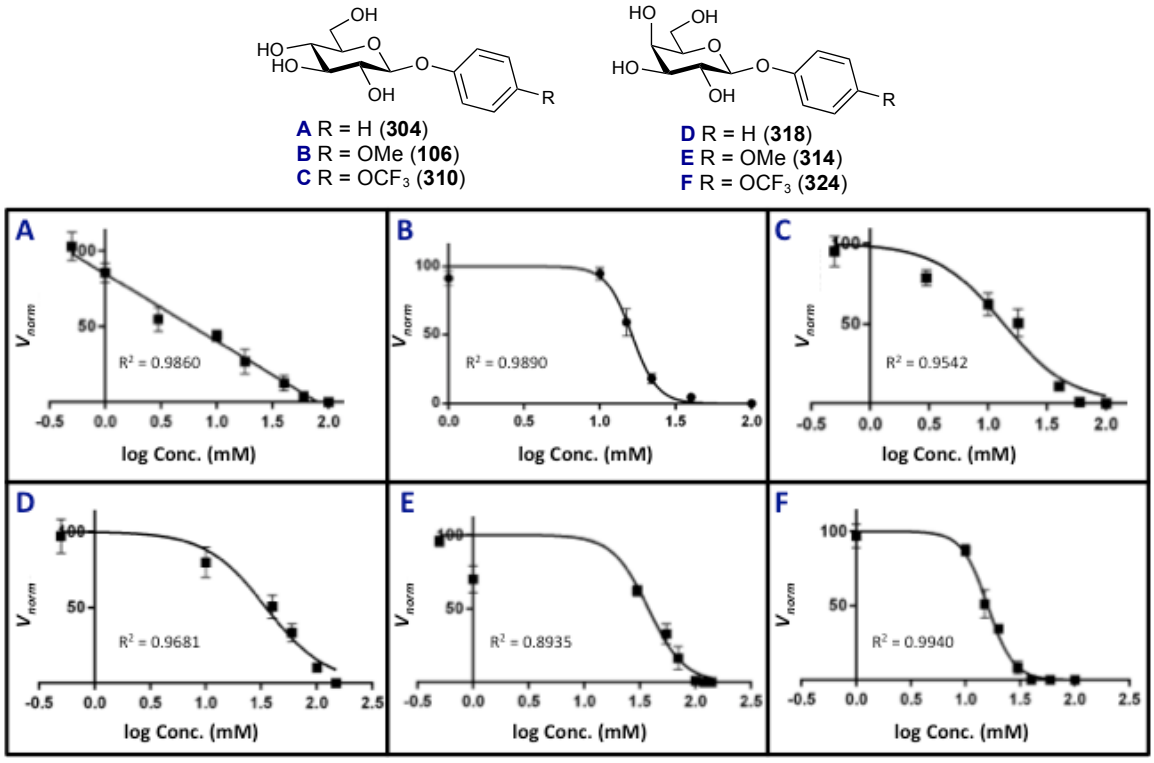

Figure 3.4 Initial rates of ice crystal growth normalized to PBS (V_{norm}) and plotted against the log concentration (mM) of *O*-linked aryl glycosides. Error bars represent the standard error of the mean (SEM). Equation of fit for **A**: y = –44.56x + 84.77. Equation of fit for **B-F**: y = 100/(1 + 10^((LogIC$_{50}$-x)(Hill slope))).

Figure 3.4 suggests that all of the *O*-linked aryl glycosides are effective inhibitors of ice recrystallization since they are able to achieve full inhibition at their highest solubility (i.e. V_{norm} = 0 %). Although the *O*-Ph-Glc derivative **304** achieves full inhibition of ice recrystallization at 100 mM, this derivative displays a colligative relationship as opposed to the characteristic sigmoidal curve that is typically observed with our inhibitors (**Figure 3.4; A**). As a result, the *O*-Ph-Glc derivative **304** is not biologically relevant for cryopreservation purposes despite its inhibitory capability. In

contrast, the remaining *O*-linked aryl glycosides exhibit a characteristic sigmoidal dose-response curve, thus enabling the calculation of an IC_{50} value from their inflection points (**Figure 3.4; B-F**).

Table 3.1 IC_{50} values for *O*-linked aryl glycosides

Compound	IC_{50} Value (mM)
304	N/A
106	16.3 ± 1.0
310	13.6 ± 1.2
318	35.0 ± 1.2
314	37.8 ± 1.2
324	15.9 ± 1.0

In addition to being an effective inhibitor of ice recrystallization, the PMP-Glc derivative **106** is also an efficacious inhibitor since it is capable of achieving inhibition at minimal concentrations, indicated by its corresponding IC_{50} value of 16.3 ± 1.0 mM (**Table 3.1**). When previously assessed for its IRI activity, the *p*-OCF_3-Ph-Glc derivative **310** was deemed an ineffective inhibitor of ice recrystallization possessing a % MGS of roughly 60 % (**Figure 3.1**). However, when assessed for the kinetics of ice recrystallization inhibition, these results suggest that this is not the case (**Figure 3.4; C**). As previously mentioned, the *O*-linked aryl glycosides were formerly assessed after a thirty-minute annealing period, which is well beyond the crucial interval where ice crystals primarily undergo recrystallization.[15] Thus, in addition to being an effective inhibitor of ice recrystallization, the *p*-OCF_3-Ph-Glc derivative **310** is also an efficacious inhibitor exhibiting an IC_{50} value of 13.6 ± 1.2 mM, similar to that of PMP-Glc (**Table 3.1**). Similarly, the *p*-OCF_3-Ph-Gal derivative **324** is also an efficacious inhibitor since it corresponds to an IC_{50} value of 15.9 ± 1.0 mM. While both the unsubstituted and *p*-OMe substituted aryl galactosides **318** and **314** are effective inhibitors of ice recrystallization (i.e. V_{norm} = 0 %), they are not very efficacious inhibitors since they require higher concentrations to elicit an effective inhibitory response (IC_{50} = 35.0 ± 1.2 mM and 37.8 ± 1.2 mM respectively). However, as previously suggested by the % MGS, the dose-

response curves in conjunction with the corresponding IC_{50} values indicate that the *O*-linked aryl glucosides are more efficient inhibitors of ice recrystallization compared to their corresponding aryl galactosides.

3.3 Influence of *S*-linked Aryl Glycosides on the Kinetics of Ice Crystal Growth

Chantelle Capicciotti previously demonstrated that changing the nature of the substituent on the aromatic ring does not influence the IRI activity of aryl glycosides. Specifically, the results presented in **Figures 3.2** and **3.3** were inconclusive since electron donating and electron withdrawing substituents gave rise to aryl glycosides with an array of different IRI activities. While the nature of the aromatic substituent had little influence on IRI activity, the nature of the glycosidic bond has not yet been investigated. Although the influence of anomeric stereoelectronic effects on IRI activity is difficult to quantify for solvated compounds, the oxygen atom of the glycosidic bond of aryl glycosides was replaced with a sulphur atom to assess any differences in IRI activity. Thus, the unsubstituted, *p*-OMe, and *p*-OCF_3 substituted *S*-linked aryl glycosides were synthesized and assess for their IRI activity.

3.3.1 Synthesis of S-linked Aryl Glycosides

The *S*-linked aryl glycosides were synthesized in a similar manner as their corresponding oxygen isosteres (**Scheme 3.2**).

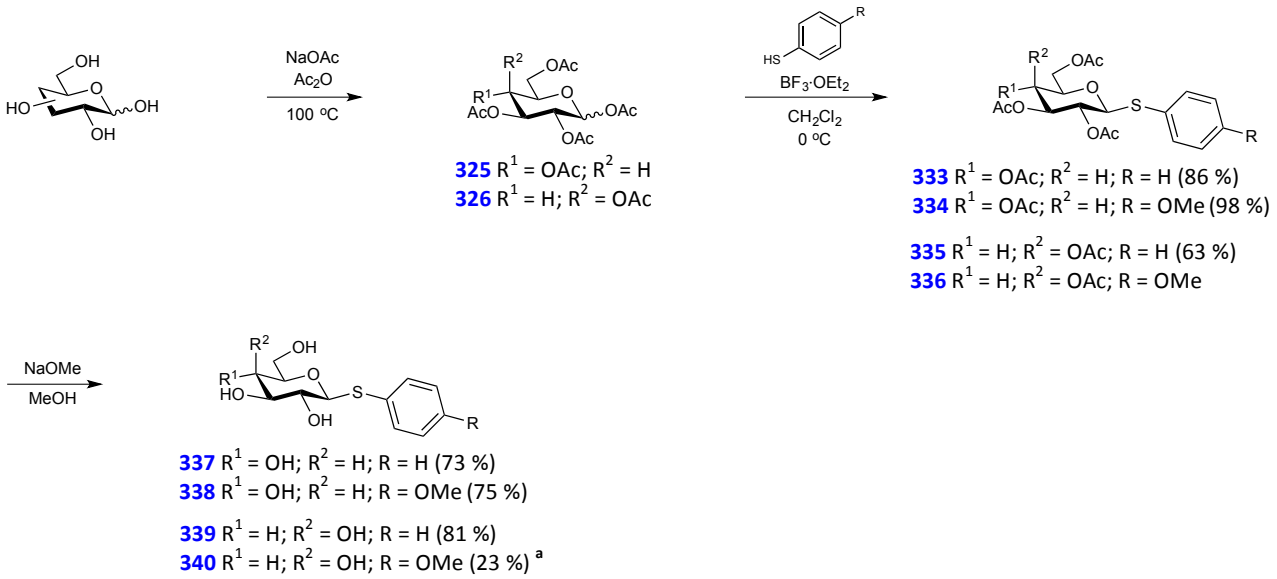

Scheme 3.2 Synthesis of *S*-linked aryl glycosides. [a] Indicates yield over two steps.

Once again using $BF_3{\cdot}OEt_2$ as the promoter, the fully acetylated gluco- and galacto-pyranoses **325** and **326** were reacted with the appropriate thiophenol, forming the corresponding acetate protected glycosylation products **333** to **336** in high yield. Finally, the *S*-linked aryl glycosides **337** to **340** were obtained in moderate to high yields following Zemplém deactylation.

3.3.2 IRI Activity of S-linked Aryl Glycosides

Similar to the *O*-linked aryl glycosides, the corresponding *S*-linked aryl glycosides **337** to **340** are all effective inhibitors of ice recrystallization achieving full inhibition (i.e. V_{norm} = 0 %) at higher concentrations (**Figure 3.5; A-D**). However, the dose-response curves for the unsubstituted thiophenyl glucose (**337**) and galactose (**339**) derivatives do not possess identifiable inflection points (**Figure 3.5; A, C**). Thus, IC_{50} values could only be calculated for the *p*-OMe substituted thiophenyl derivatives **338** and **340**.

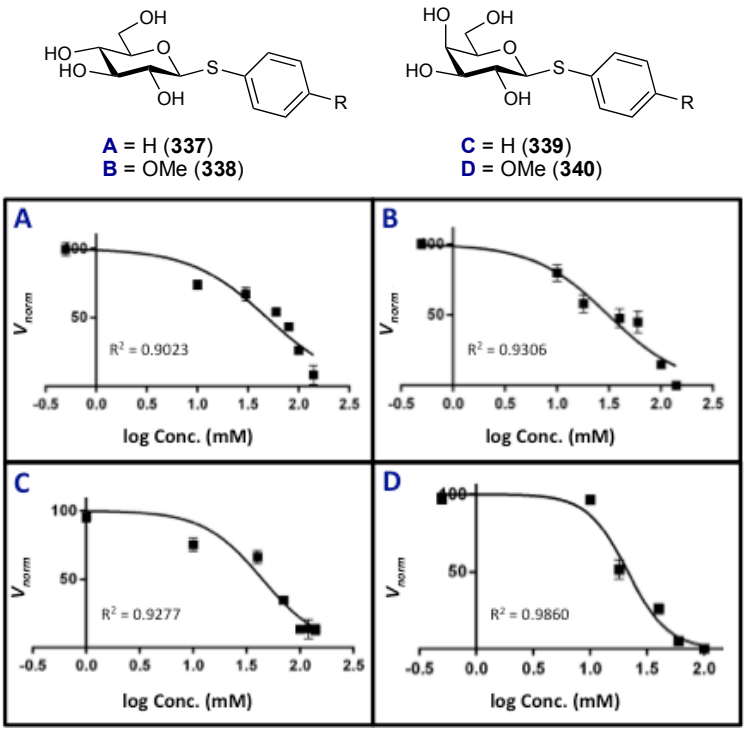

Figure 3.5 Initial rates of ice crystal growth normalized to PBS (V_{norm}) and plotted against the log concentration (mM) of *S*-linked aryl glycosides. Error bars represent the standard error of the mean (SEM). Equation of fit: y = 100/(1 + 10^((LogIC$_{50}$-x)(Hill slope))).

These results were consistent with those observed with the *O*-linked aryl glycosides, suggesting that the *p*-OMe aryl substituent enhances the inhibition of ice recrystallization. However, while the *O*-PMP-Glc derivative **106** is a more efficacious inhibitor than its corresponding *O*-PMP-Gal derivative **314** (IC$_{50}$ of 16.3 ± 1.0 mM versus 37.8 ± 1.2 mM), the opposite trend is observed with the corresponding *S*-linked aryl glycosides. For instance, the *p*-OMe thiophenyl galactose derivative **340** corresponds to an IC$_{50}$ value of 21.4 ± 1.1 mM whereas the *p*-OMe thiophenyl glucose derivative **338** corresponds to an IC$_{50}$ value of 31.0 ± 1.2 mM (**Table 3.2**). Thus, the *p*-OMe substituted glucose derivative **338** possesses only two-thirds the activity of the *p*-OMe substituted galactose derivative **340**. Furthermore, the *S*-linked aryl galactoside **340** exhibits an IC$_{50}$ value of 21.4 ± 1.1 mM, which is similar to that of the PMP-Glc derivative **106** (IC$_{50}$ = 16.3 ± 1.0 mM). These results suggest that the *S*-linked aryl galactoside **340** is also an efficacious inhibitor of ice recrystallization.

Table 3.2 IC_{50} values for *S*-linked aryl glycosides

Compound	IC_{50} Value (mM)
337	N/A
338	31.0 ± 1.2
339	N/A
340	21.4 ± 1.1

Overall, the *S*-linked aryl glycosides were effective inhibitors of ice recrystallization. However, substituting the anomeric oxygen for a sulphur atom reverses the behavior of the glucose and galactose derivatives compared to that observed with the *O*-linked aryl glycosides. For instance, while the *p*-OMe substituted *S*-linked aryl galactoside **340** was a more efficacious inhibitor compared to the corresponding aryl glucoside **338**, the opposite trend is observed with the *p*-OMe substituted *O*-linked aryl glycosides.

Oxygen and sulphur both possess two lone pairs of electrons and are found in the same column of the periodic table. However, they exert different influences on IRI activity when employed at the anomeric position of aryl glycosides. Despite their similarities, the stereoelectronic effects exhibited by both atoms are quite different. As a consequence of increased C-S bond lengths and poor orbital overlap, the anomeric sulphur atom is a weak donor for the *exo*-anomeric effect.[25,26] As a result, the *S*-linked aryl glycosides exhibit a smaller *exo*-anomeric effect compared to that of the *O*-linked aryl glycosides.[25–27] These changes in stereoelectronic effects exhibited by sulphur may alter the preferred conformation of the *S*-linked aryl glycosides in solution, thus altering their ability to inhibit ice recrystallization. Specifically, the difference in anomeric stereoelectronic effects exhibited by the *S*-linked aryl glycosides may account for the opposite trend in IRI activity that is observed with the *O*-linked aryl glycosides.[28] However, conformational analyses should be performed to substantiate whether a change in anomeric stereoelectronic effects alters the preferred conformation of aryl glycosides in solution.

3.4 Influence of *N*-linked Aryl Glycosides on the Kinetics of Ice Crystal Growth

To accurately assess the influence of stereoelectronic effects at the C_1 position of aryl glycosides on IRI activity, various *N*-linked aryl glycosides were also synthesized and assessed for their ability to inhibit ice recrystallization.

3.4.1 Synthesis of N-linked Aryl Glycosides

In solution, reducing sugars exist in various forms at different temperatures. For instance, at 31 ^{o}C D-glucose exists as 38 % α-pyranose, 62 % β-pyranose, 1 % furanose, and 0.002 % as an open-chain.[29] At the same temperature, D-galactose exists as 30 % α-pyranose, 64 % β-pyranose, 6 % furanose, and 0.02 % as an open-chain.[29] Despite the small proportion of open-chain reducing sugars in solution, these aldoses participate in a large number of reactions due to the reactivity of aldehydes. As a result, the *N*-linked aryl glycosides were synthesized without the use of protecting groups unlike their corresponding *O*- and *S*-linked aryl glycosides. The synthesis of *N*-alkylaldosylamines has been well documented and can be obtained by reacting aldoses with primary or secondary aliphatic amines.[30–33] Similarly, *N*-arylpyranosylamines have been previously synthesized by heating reducing sugars with the corresponding substituted aniline in hot methanol or ethanol.[30,34,35] As a result, this methodology was used for the synthesis of the *N*-linked aryl glycosides in **Scheme 3.3**. Either D-glucose or D-galactose was heated with the desired substituted aniline in the presence of ethanol to form the corresponding *N*-arylpyranosylamines **341** to **346** in moderate to high yields.

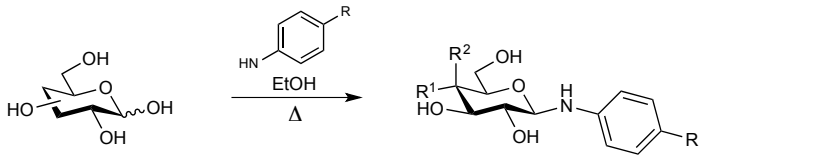

341 R^1 = OH; R^2 = H; R = H (85 %)
342 R^1 = OH; R^2 = H; R = OMe (40 %)
343 R^1 = OH; R^2 = H; R = OCF_3 (54 %)

344 R^1 = H; R^2 = OH; R = H (76 %)
345 R^1 = H; R^2 = OH; R = OMe (56 %)
346 R^1 = H; R^2 = OH; R = OCF_3 (60 %)

Scheme 3.3 Synthesis of *N*-linked aryl glycosides.

Depending on the proton-accepting ability of the solvent, the monosaccharide used, and the strength of the base, these reactions can either result in the formation of the open-chain Schiff base or the cyclic glycosylamine.[34] Despite the equilibrium that exists between various forms in solution, the form that ultimately crystallizes is difficult to predict and may not be the predominant form that exists in solution.[34,36] However, spectroscopic and X-ray crystallographic evidence has since supported the accumulation of the cyclic form of *N*-arylglycosylamines in the crystalline state over the open-chain Schiff base.[34,37,38] Furthermore, X-ray crystallographic studies by Ojala *et al*. confirm that the nature of the aromatic substituent (i.e. electron donating vs. electron withdrawing) has no influence on the crystalline structure of *N*-arylglycosylamines.[34] Thus, the cyclic *N*-aryl-glycopyranosylamine is the predominant crystalline form for all monosaccharides reacted with primary aromatic amines. As a result, recrystallization from EtOH afforded the desired *N*-linked aryl glycosides in moderate to high yields. Once synthesized, the *N*-linked aryl glycosides were then assessed for their IRI activity.

3.4.2 IRI Activity of N-linked Aryl Glycosides

The normalized rate of ice crystal growth in the presence of various *N*-linked aryl glycosides was plotted against log concentration and the results are presented in **Figure 3.6**. Unlike their corresponding oxygen isosteres, the majority of the *N*-linked aryl glycosides are not effective inhibitors of ice recrystallization. With the exception of the *p*-

OMe substituted glucose derivative **342**, all of the *N*-linked aryl glycosides fail to achieve full inhibition of ice recrystallization (i.e $V_{norm} \neq 0$ %) when assessed at their highest solubility (**Figure 3.6; A, C-F**). For instance, the unsubstituted aryl glucoside **341** and galactoside **344** are only able to reduce V_{norm} to 46.3 % and 24.3 % respectively (**Figure 3.6; A, D**). While the *p*-OCF_3 substituted aryl glucoside **343** could only be assessed at a maximum solubility of 30 mM, its corresponding aryl galactoside **346** is only able to reduce V_{norm} to 20.9 % when assessed at its maximum solubility of 100 mM (**Figure 3.6; C, F**). Although the *p*-OCF_3 aryl substituent gave rise to *O*-linked aryl glycosides that are both efficient and efficacious inhibitors of ice recrystallization (IC_{50} = 13.6 ± 1.2 mM and 15.9 ± 1.0 mM for derivatives **310** and **324** respectively), replacing the anomeric oxygen for a nitrogen atom decreases the inhibitory activity of the *p*-OCF_3 aryl substituent.

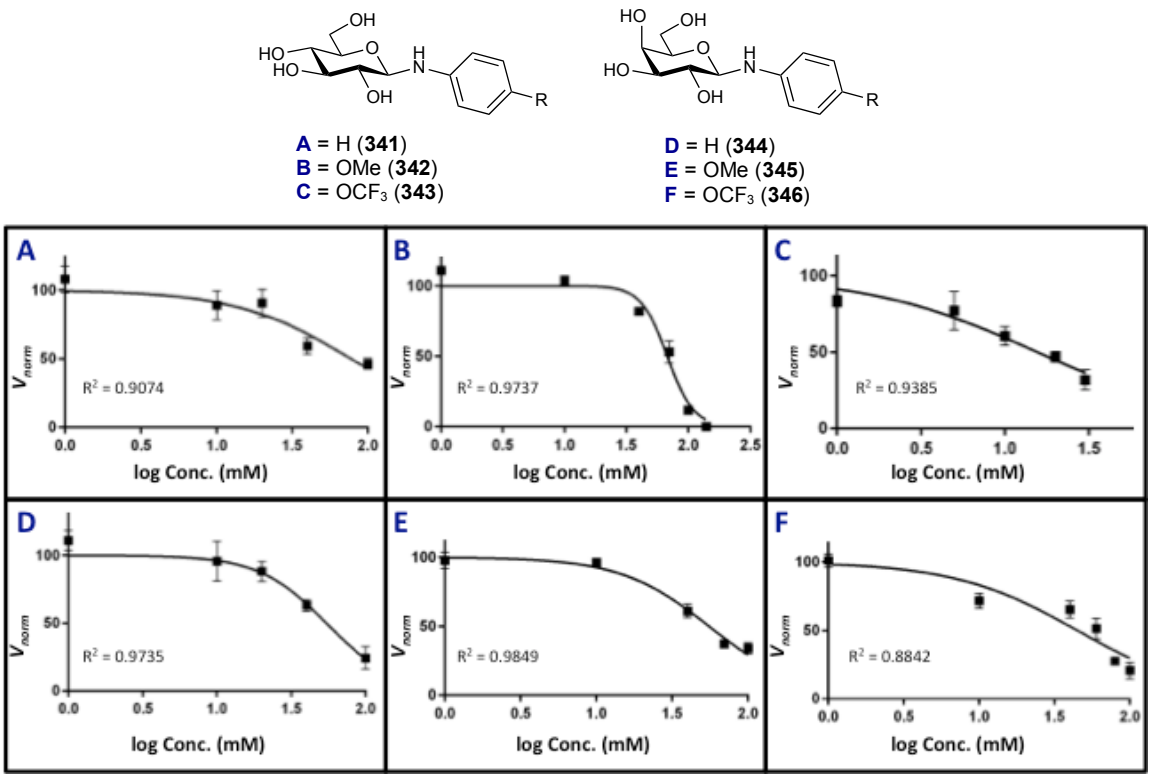

Figure 3.6 Initial rates of ice crystal growth normalized to PBS (V_{norm}) and plotted against the log concentration (mM) of *N*-linked aryl glycosides. Error bars represent the standard error of the mean (SEM). Equation of fit: y = 100/(1 + 10^((LogIC_{50}-x)(Hill slope))).

Despite the lack of efficiency exhibited by the *p*-OMe substituted aryl galactoside **345** (i.e V_{norm} = 34.1 % at 100 mM), the corresponding aryl glucoside **342** is an effective

inhibitor of ice recrystallization achieving full inhibition at 140 mM (**Figure 3.6; B, E**). However, the *p*-OMe substituted glucose derivative **342** is not a very efficacious inhibitor of ice recrystallization since it exhibits an IC_{50} value of 67.6 ± 1.1 mM. While these results suggest the importance of the *p*-OMe aryl substituent for inhibiting ice recrystallization, replacing the anomeric oxygen for a nitrogen atom decreases the inhibitory activity of *p*-OMe substituted aryl glycosides as previously observed with the *p*-OCF_3 substituted *N*-linked aryl derivatives.

Due to solubility constraints, full inhibition of ice recrystallization (i.e. V_{norm} = 0 %) could not be observed at higher concentrations for the majority of the *N*-linked aryl glycosides assessed. Thus, a characteristic sigmoidal dose-response curve could not be properly constructed for these derivatives (**Figure 3.6; A, C-F**). However, if these *N*-linked aryl glycosides were capable of achieving full inhibition of ice recrystallization at higher concentrations, they would not be efficacious inhibitors since their IC_{50} values would be quite large. Thus, unlike the *S*-linked aryl glycosides, substituting the anomeric oxygen atom for a nitrogen atom exacerbates the efficiency of ice recrystallization inhibition by aryl glycosides.

While nitrogen and oxygen are both isosteres and possess a similar van der Waal's radius, these atoms exert different influences on IRI activity when employed at the anomeric position of aryl glycosides. As the electronegativity of the anomeric substituent (X) increases, the strength of the *endo*-anomeric effect also increases.[39] This is due to increased acceptor ability of the $\sigma^*_{C\text{-}X}$ orbital for the delocalized electrons of the endocyclic oxygen atom.[39] However, the reverse is true for the *exo*-anomeric effect. In this case, the electrons of the anomeric heteroatom are delocalized into the $\sigma^*_{C\text{-}O}$ orbital of the endocyclic oxygen.[25,40] Since nitrogen is less electronegative than oxygen, it is a better donor for delocalizing electrons into the $\sigma^*_{C\text{-}O}$ orbital.[30,41] Thus, the *N*-linked aryl glycosides exhibit a stronger *exo*-anomeric effect compared to that of the *O*-linked aryl glycosides. As seen previously with the *S*-linked aryl glycosides, this change in stereoelectronic effects exhibited by the *N*-linked aryl glycosides may alter their ability to inhibit ice recrystallization. Specifically, aryl glycosides that exhibit a stronger *exo*-

anomeric effect are less effective inhibitors of ice recrystallization. These results suggest the importance of the anomeric oxygen atom of aryl glycosides for ice recrystallization inhibition.

3.5 Conclusion

By assessing the kinetics of ice recrystallization inhibition, dose-response curves were constructed and IC_{50} values were calculated. This IC_{50} value represents the concentration at which our ice recrystallization inhibitors have achieved half of their maximum inhibitory capability.[16] Three aryl substituents were chosen and the corresponding *O*-, *S*-, and *N*-linked aryl glycosides were synthesized and assessed for their IRI activity using the improved splat-cooling assay. The aryl glycosides were then compared in terms of their efficiency (ability to achieve full inhibition of ice recrystallization) and their efficacy (ability to inhibit ice recrystallization at minimal concentrations) and the results are presented in **Table 3.3**.

Table 3.3 IRI activity of *O*-, *S*-, and *N*-linked aryl glycosides

Compound	Efficiency (min. V_{norm})	Efficacy (IC_{50})
***O*-linked Aryl Glycosides**		
Ph-Glc (**304**)	0 %	N/A
PMP-Glc (**106**)	0 %	16.3 ± 1.0 mM
p-OCF_3-Ph-Glc (**310**)	0 %	13.6 ± 1.2 mM
Ph-Gal (**318**)	0 %	35.0 ± 1.2 mM
PMP-Gal (**314**)	0 %	37.8 ± 1.2 mM
p-OCF_3-ph-Gal (**324**)	0 %	15.9 ± 1.0 mM
***S*-linked Aryl Glycosides**		
Ph-Glc (**337**)	8.2 %	N/A
p-OMe-Ph-Glc (**338**)	0 %	31.0 ± 1.2 mM
Ph-Gal (**339**)	13.2 %	N/A
p-OMe-Ph-Gal (**340**)	0 %	21.4 ± 1.1 mM
***N*-linked Aryl Glycosides**		
Ph-Glc (**341**)	46.3 %	N/A
p-OMe-Ph-Glc (**342**)	0 %	67.6 ± 1.1 mM
p-OCF_3-Ph-Glc (**343**)	31.8 %	N/A
Ph-Gal (**344**)	24.3 %	N/A
p-OMe-Ph-Gal (**345**)	34.1 %	N/A
p-OCF_3-Ph-Gal (**346**)	20.9 %	N/A

The efficiency of ice recrystallization inhibition was assessed by the ability of various aryl glycosides to fully inhibit the normalized rate of ice crystal growth at higher concentrations (i.e. V_{norm} = 0 %). Thus, **Table 3.3** suggests that the *O*-linked aryl glycosides are the most effective inhibitors since all derivatives are able to achieve full inhibition of ice recrystallization at their maximum solubility. Substituting the anomeric oxygen for a sulphur atom preserves the inhibitory efficiency of the *p*-OMe aryl substituent. However, this change in stereoelectronic effects at the C_1 position of aryl glycosides reduces the efficiency of the unsubstituted derivatives **337** and **339** (i.e. V_{norm} = 8.2 % and 13.2 % respectively). Finally, replacing the anomeric oxygen for a nitrogen atom exacerbates the IRI efficiency of aryl glycosides since all derivatives are incapable of achieving full inhibition of ice recrystallization (i.e. $V_{norm} \neq 0$ %) with the exception of the *p*-OMe aryl glucoside **342**. Thus, substituting the anomeric oxygen for either sulphur or nitrogen reduces the overall efficiency of aryl glycosides to inhibit ice recrystallization.

In addition to the efficiency of IRI activity, all derivatives were also assessed for their efficacy of ice recrystallization inhibition. Ideally, our carbohydrate-based derivatives should be effective inhibitors of ice recrystallization at minimal concentrations to limit the amount of IRI that could potentially be used to cryopreserve various cell types. Thus, the IC_{50} values of aryl glycosides were compared to assess the efficacy of ice recrystallization inhibition. In addition to producing the most effective inhibitors of ice recrystallization, the *O*-linked aryl glycosides also gave rise to some of the most efficacious inhibitors exhibiting IC_{50} values of 16.3 ± 1.0 mM, 13.6 ± 1.2 mM, and 15.9 ± 1.0 mM for derivatives **106**, **310**, and **324** respectively. However, the unsubstituted (**318**) and *p*-OMe substituted (**314**) galactose derivatives are not as efficacious (i.e. IC_{50} values of 35.0 ± 1.2 mM and 37.8 ± 1.2 mM respectively) as their corresponding glucose derivatives. These results support previous hypotheses by our laboratory, which suggest that *O*-linked aryl glucosides are more effective inhibitors of ice recrystallization compared to their corresponding aryl galactosides. Substituting the anomeric oxygen for a sulphur atom results in two *S*-linked aryl glycosides for which

IC_{50} values were calculated. While the *p*-OMe thiophenyl glucose derivative **338** is not as efficacious at inhibiting ice recrystallization (IC_{50} = 31.0 ± 1.2 mM), the efficacy of the corresponding galactose derivative **340** is similar to that of *O*-PMP-Glc (IC_{50} = 21.4 ± 1.1 mM versus 16.3 ± 1.0 mM respectively). These results suggest that the change in anomeric stereoelectronic effects exhibited by the *S*-linked aryl glycosides opposes the trend observed with the *O*-linked aryl glycosides. Specifically, the *O*-linked aryl glucosides are more effective inhibitors of ice recrystallization compared to their corresponding aryl galactosides, whereas the reverse is true for the *S*-linked aryl glycosides. Finally, substituting the anomeric oxygen for a nitrogen atom results in only one efficient inhibitor of ice recrystallization. However, the *p*-OMe aryl glucoside **342** is not a very efficacious inhibitor exhibiting an IC_{50} value of 67.6 ± 1.1 mM, which is four times greater than its corresponding oxygen isostere *O*-PMP-Glc (**106**).

Thus, these results suggest the importance of the anomeric oxygen atom of aryl glycosides for ice recrystallization inhibition. Specifically, replacing the anomeric oxygen for a nitrogen atom significantly reduces the IRI activity of aryl glycosides. While the *S*-linked aryl glycosides reverse the behavior of the *O*-linked aryl glucosides and galactosides, these changes in stereoelectronic effects preserve the efficiency of ice recrystallization inhibition. Despite their efficiency, the weaker *exo*-anomeric effect exhibited by the *S*-linked aryl glycosides results in slightly less efficacious inhibitors of ice recrystallization. Due to different stereoelectronic effects exhibited by sulphur and nitrogen compared to that of oxygen, substituting the C_1 heteroatom of aryl glycosides alters both the efficiency and efficacy of IRI activity. Our laboratory previously hypothesized that the inhibitory activity of *O*-linked aryl glycosides is attributed to their ability to alter the structure of bulk water, thus disfavouring the ordering of water molecules into the highly structured ice lattice.[11,12] However, altering the stereoelectronic effects at the anomeric position of aryl glycosides may alter the preferred orientation of these aryl glycosides in solution. Thus, *N*- and *S*-linked aryl glycosides may not impede the structure of bulk water to the same extent as the *O*-linked aryl glycosides resulting in less effective inhibitors of ice recrystallization. Furthermore, our laboratory previously correlated IRI activity to carbohydrate hydration and reported that highly hydrated

monosaccharides (such as D-galactose) were more IRI active than less hydrated monosaccharides such as D-glucose.[11,12,42–44] By substituting the anomeric oxygen atom for either nitrogen or sulphur, this may alter the hydration of these aryl glycosides resulting in less efficient and efficacious inhibitors of ice recrystallization. However, since the hydration of *O*-, *N*-, and *S*-linked aryl glycosides has not been reported, a correlation cannot explicitly be made.

3.6 *S*-linked Aryl Glycosides as Cryopreservatives for Human Red Blood Cells

Previous work by the Ben laboratory involved the assessment of *O*-linked aryl glycosides for their ability to protect human red blood cells (RBCs) against freezing injury. Post-thaw RBC integrity was previously assessed in the presence of PMP-Glc (**106**) in conjunction with 15 % glycerol.[45,46] In the absence of inhibitor, the post-thaw RBC integrity ranged from 20-30 %.[45] However, RBC integrity increased to roughly 50 % upon addition of 110 mM of PMP-Glc (**106**).[45] These results previously demonstrated that effective small molecule inhibitors of ice recrystallization could be successfully utilized in conjunction with reduced glycerol concentrations for the cryopreservation of human RBCs.

The *S*-linked aryl glycosides were previously assessed for their IRI activity. While the *p*-OMe substituted derivatives **338** and **340** were the most effective inhibitors of ice recrystallization, all derivatives were assessed for their ability to protect human RBCs against freezing injury. All samples were cooled at a rate of 1 ^{o}C/min until frozen at -40 ^{o}C, conditions closely resembling the clinical protocols utilized in North America for RBC cryopreservation.[45–49] Following storage, cryopreserved RBCs were rapidly thawed in a 37 ^{o}C water bath and RBC integrities were determined using Drabkin's assay.[45,46] The resulting RBC integrities are presented in **Figure 3.7**.

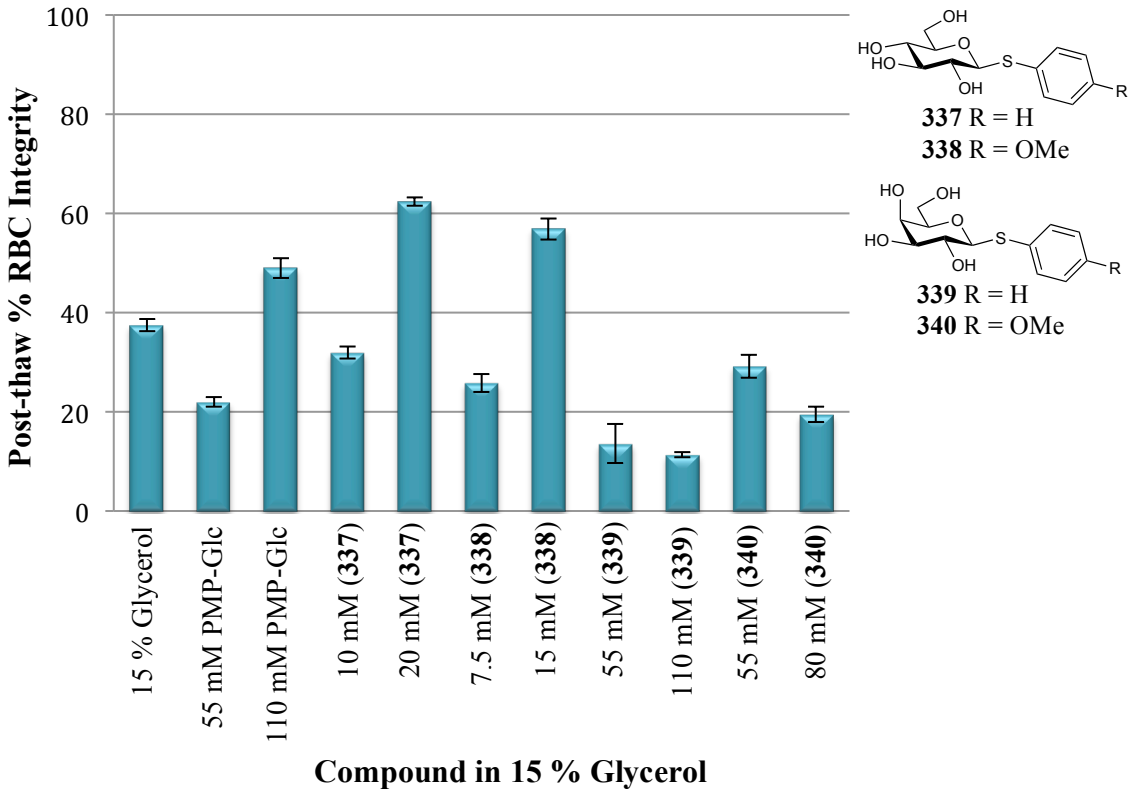

Figure 3.7 Post-thaw recoveries of human red blood cells frozen at -40 °C in the presence of various *S*-linked aryl glycosides. RBCs were cooled to -40 °C at a rate of 1 °C/min followed by rapid-thaw at 37 °C. All derivatives were assessed in the presence of 15 % glycerol. Error bars represent the standard error of the mean (SEM).

The *S*-linked aryl glycosides were assessed in the same manner as the *O*-linked aryl glycosides utilizing the rate-controlled freezing procedure.[45,46] Following rapid thaw, the % hemolysis of RBCs was determined using Drabkin's assay.[45] From the % hemolysis, the post-thaw RBC integrity was determined and the results are presented in **Figure 3.7**. The unsubstituted glucose derivative **337** and galactose derivative **339** were not effective inhibitors of ice recrystallization. Agreeably, the unsubstituted galactose derivative **339** reduces the post-thaw RBC integrity approximately by half when assessed at 55 mM and 110 mM compared to that of 15 % glycerol. Since ice recrystallization is a major factor contributing to cellular damage during cryopreservation, these results were not surprising since this derivative was not an effective inhibitor of ice recrystallization. Similarly, the unsubstituted glucose derivative **337** results in a post-thaw RBC recovery similar to that of 15 % glycerol when assessed at 10 mM. However, when assessed at 20 mM, the RBC

integrity increases to 62 %. In addition, derivative **337** provides more protection against freezing injury compared to 110 mM of PMP-Glc, which requires roughly 5 times the concentration to exhibit a RBC recovery of only 49 %. These unprecedented results are interesting since the PMP-Glc derivative **106** is a more efficient and efficacious inhibitor of ice recrystallization compared to the unsubstituted *S*-linked aryl glucoside **337**. Despite being a less effective inhibitor of ice recrystallization, these results suggest that derivative **337** may promote the post-thaw integrity of RBCs by providing protection against other lethal processes resulting in cryoinjury.

The *p*-OMe substituted glucose derivative **338** and galactose derivative **340** were both effective inhibitors of ice recrystallization. However, the galactose derivative **340** not only fails to protect RBCs against freezing injury, but also provides less protection than 15 % glycerol when assessed at 55 mM and 80 mM. In contrast, while a 7.5 mM solution of the *p*-OMe glucose derivative **338** results in a RBC recovery similar to that of 55 mM PMP-Glc, the RBC integrity increases to 57 % when this derivative is assessed at 15 mM. While PMP-Glc (**106**) is a slightly more efficacious inhibitor of ice recrystallization compared to the *p*-OMe substituted *S*-linked aryl glucoside **338** (IC_{50} of 16.3 ± 1.0 mM versus 31.0 ± 1.2 mM), derivative **338** provides the same degree of protection as 110 mM of PMP-Glc at a significantly reduced concentration. Furthermore, although the *p*-OMe aryl glucoside **338** was an efficient inhibitor of ice recrystallization, it was not as efficacious as its corresponding aryl galactoside **340** (IC_{50} of 31.0 ± 1.2 mM versus 21.4 ± 1.1 mM). Thus, the increased post-thaw RBC integrity obtained with the *p*-OMe aryl glucoside **338** over the corresponding aryl galactoside **340** was once again unprecedented. As previously observed with the unsubstituted derivatives **337** and **339**, these results suggest that these *S*-linked aryl glycosides provide protection against other lethal processes resulting in cryoinjury.

Our laboratory previously demonstrated that efficient inhibitors of ice recrystallization could be used in conjunction with reduced glycerol concentrations to protect human red blood cells against freezing injury. However, these results suggest that aryl glycosides confer protection against freezing injury by providing protection against

other lethal processes. For instance, although the *S*-linked aryl glycosides **337** and **338** were not as efficient or efficacious at inhibiting ice recrystallization compared to PMP-Glc, they exhibit post-thaw RBC integrities of 62 % and 57 % respectively. Thus, these derivatives confer more protection against freezing injury than 110 mM of PMP-Glc. As a result, the ability of these derivatives to provide protection against freezing injury cannot be fully attributed to their IRI activity. Rather, these results suggest that the *S*-linked aryl glycosides also protect human RBCs against cryoinjury by protecting against other lethal processes that induce cellular damage upon freezing. Unfortunately, the mechanism by which these *S*-linked aryl glycosides protect human RBCs against cryoinjury could not be investigated. However, prospective research by the Ben laboratory may involve further investigations into the protective mechanism of *S*-linked aryl glycosides.

3.7 Aryl Glycoside Experimental Procedures and Compound Characterizations

Splat-cooling Assay for the Kinetics of Ice Crystal Growth:

Ice recrystallization inhibition of aryl glycosides was assessed at various concentrations in a phosphate-buffered saline solution. A 10 μL droplet of the sample solution was released from a micropipette at a height of approximately 2 meters onto a precooled aluminum block (−80 ^{o}C). The droplet was immediately frozen upon impact and the resulting ice wafer (approximately 20 μm thick and 1 cm wide) was then transferred to a precooled glass cover slip and annealed at −6.4 ^{o}C on a cryostage for 5 minutes. After this time, the cryostage was placed under a microscope and the middle of the ice wafer was photographed using an LMPlanF1 20x/0.40 objective lens.

Dose-response curves:

Images of ice crystals in the absence of inhibitor (i.e. PBS only) were analyzed in triplicate. In addition, each compound was assessed in triplicate at a minimum of 5

different concentrations. The area of each individual ice crystal within the field of view was analyzed using ImageJ and corrected for the appropriate magnification factor and objective lens utilized in the splat-cooling assay. The ice crystal areas were "binned" according to their size using an Excel spreadsheet with the smallest bin occupying ice crystal areas of 0.001 mm^2 and each sequential bin increasing by increments of 0.001 mm^2. From the rate of depletion of ice crystals occupying Bin 1, the initial rates of ice crystal growth were calculated using the following equation:

$$\upsilon_t = \frac{1 - A_t^{rel}}{t}$$

where ν_t is the initial rate at 5 minutes, A_t^{rel} is the relative area of bin 1 at 5 minutes, and t is time. From the initial rates of ice crystal growth, dose-response curves were constructed whereby the normalized rate of ice crystal growth (i.e. initial rate normalized to that of PBS) was plotted against the log concentration. From the dose-response curves, IC_{50} values were calculated which is the concentration at which our ice recrystallization inhibitors have achieved half of their maximum inhibitory capability.

Freezing and Thawing of Human Red Blood Cells with Aryl Glycosides:

Human red blood cell units were obtained from the Canadian Blood Services' Network Centre for Applied Development (NetCAD) donated from healthy volunteers from which informed consent was obtained. All experimental protocols were approved by NetCAD and Canadian Blood Services (CBS), while ethics approvals were obtained from Research Ethics Board (REB) at CBS and the University of Alberta.

The *S*-linked aryl glycosides were dissolved in a cryosolution consisting of 0.2%/0.9% dextrose/saline buffer, to which an equal volume of RBCs was added (1:1 (v/v)). The RBC solution was incubated at room temperature for 10 minutes, after which the cryovials were cooled to -5 ^oC in a methanol bath for 5 minutes. After this time, ice nucleation was initiated by touching the glass cryovials with tongs that were precooled in

liquid nitrogen. Following nucleation, cryovials were held at -5 ^{o}C for an additional 5 minutes, after which they were frozen to -40 ^{o}C at a rate of 1 ^{o}C/minute. Once frozen, samples were rapidly thawed in a 37 ^{o}C water bath for approximately 1-2 minutes.

Post-thaw % RBC Integrity:

Once thawed, the post-thaw hematocrits were measured and the % hemolysis of RBCs was quantified using Drabkin's assay. From the % hemolysis, the post-thaw RBC integrity was determined as follows: post-thaw % RBC integrity = 100 % - % hemolysis. Each *S*-linked aryl glycoside was assessed twice (n = 2) for their ability to protect human RBCs against freezing injury.

General Experimental:

All anhydrous reactions were performed in flame-dried or oven-dried glassware under a positive pressure of dry argon. Air sensitive reagents were transferred using oven-dried syringes or cannulae. All flash chromatography was performed with E. Merck silica gel 60 (230-400 mesh). All solution phase reactions were monitored using thin layer chromatography (TLC) with 0.2 mm pre-coated silica gel aluminum plates 60 F254 (E. Merck). Components were visualized with short-wavelength (254 nm) ultra-violet light and/or staining (ceric ammonium molybdate or orcinol/sulphuric acid stain solution). ^{1}H-NMR (300 or 400 MHz) and ^{13}C-NMR (100 MHz) spectra were recorded on a Bruker Avance 300 or Bruker Avance 400 spectrometer. Deuterated chloroform ($CDCl_3$), water (D_2O), or dimethyl sulphoxide ($(CD_3)_2SO$) were used as NMR solvents unless otherwise stated. Chemical shifts are reported in ppm and corrected using the solvent residual peak as an internal standard. Splitting patterns are designated as follows: s, singlet; d, doublet; t, triplet; q, quartet; quint, quintet; m, multiplet; and br, broad. Low resolution mass spectrometry (LRMS) was performed on a Micromass Quatro-LC Electrospray spectrometer with a pump rate of 20 μL/min using electrospray ionization (ESI).

NMR spectra of novel compounds assessed for IRI activity and of intermediate compounds are provided. D-glucose and D-galactose are commercially available carbohydrates. Compound **106** was previously synthesized by Chantelle Capicciotti and previously assessed for its IRI activity by Stephanie Abraham using the improved splat-cooling assay. Compound **314** was previously synthesized by Thomas Charlton and generously donated for the assessment of its IRI activity.

1,2,3,4,6-Penta-*O*-acetyl-D-glucopyranose (325)

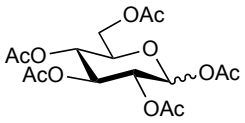

A mixture of 10.02 g (55.60 mmol) of D-glucose, 11.40 g (138.9 mmol) of NaOAc, and 35.0 mL of Ac_2O was heated to 100 ^oC and stirred under Ar for 2 hours. Once cooled to room temperature, the precipitate was dissolved in CH_2Cl_2 and the organic phase was washed with H_2O and saturated brine, followed by drying over $MgSO_4$. The solution was filtered, concentrated, and the crude solid was recrystallized from EtOAc –hexanes to afford 20.34 g of a white, powdery solid as a mixture of anomers in 94 % yield. All spectral data was consistent with that reported in the literature.[50]

1,2,3,4,6-Penta-*O*-acetyl-D-galactopyranose (326)

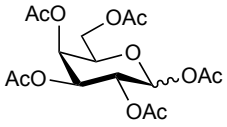

A mixture of 10.00 g (55.55 mmol) of D-galactose, 11.40 g (139.0 mmol) of NaOAc, and 32.0 mL of Ac_2O was heated to 100 ^oC and stirred under Ar for 2 hours. Once cooled to room temperature, the precipitate was dissolved in CH_2Cl_2 and the

organic phase was washed with H_2O and saturated brine, followed by drying over $MgSO_4$. The solution was filtered, concentrated, and the crude solid was recrystallized from EtOH to afford 12.61 g of an off-white, powdery solid as a mixture of anomers in 58 % yield. All spectral data was consistent with that reported in the literature.[51]

Phenyl-2,3,4,6-tetra-*O*-acetyl-β-D-glucopyranoside (327):

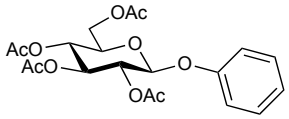

To a mixture of 1.032 g (2.644 mmol) of 1,2,3,4,6-penta-*O*-acetyl-D-glucopyranose (**325**), 740.4 mg (7.867 mmol) of phenol, and 12.0 mL of anhydrous CH_2Cl_2 at 0 ^oC, 1.5 mL (12.15 mmol) of $BF_3{\cdot}OEt_2$ was added and the reaction mixture was gradually warmed to room temperature and stirred overnight. The reaction mixture was diluted with CH_2Cl_2 and quenched with saturated $NaHCO_3$. The organic phase was washed with H_2O and saturated brine, followed by drying over $MgSO_4$. The solution was filtered, concentrated, and the crude product was purified by flash column chromatography (3:7 EtOAc –hexanes) to afford 385.4 mg of a white, powdery solid in 35 % yield. **^{1}H-NMR** (300 MHz, $CDCl_3$): δ 7.30 (dd, *J* = 8.6, 7.5 Hz, 2H), 7.10-7.05 (m, 1H), 7.01-6.97 (m, 2H), 5.31-5.27 (m, 2H), 5.20-5.14 (m, 1H), 5.10-5.07 (m, 1H), 4.29 (dd, *J* = 12.3, 5.3 Hz, 1H), 4.17 (dd, *J* = 12.2, 2.5 Hz, 1H), 3.86 (ddd, *J* = 9.9, 5.3, 2.5 Hz, 1H), 2.07 (s, 3H), 2.06 (s, 3H), 2.05 (s, 3H), 2.04 (s, 3H). **^{13}C-NMR** (100 MHz, $CDCl_3$): δ 170.72, 170.39, 169.53, 169.44, 157.01, 129.73, 123.51, 117.14, 99.29, 72.90, 72.17, 71.34, 68.49, 62.12, 20.82, 20.77, 20.77, 20.74 **ESI-MS** *m/z* calcd for $C_{20}H_{24}O_{10}$ $[M + Na]^+$: 447.13. Found 447.1.

***p*-Methoxyphenyl-2,3,4,6-tetra-*O*-acetyl-β-D-glucopyranoside (328):**

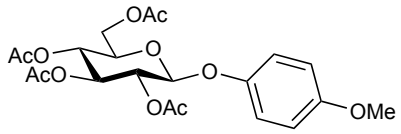

This compound was previously synthesized by Chantelle Capicciotti, a former PhD graduate of the Ben laboratory.

***p*-(Trifluoromethoxy)phenyl-2,3,4,6-tetra-*O*-acetyl-β-D-glucopyranoside (329):**

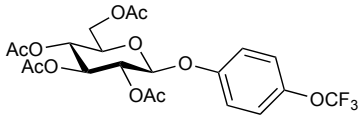

To a mixture of 0.4998 g (1.280 mmol) of 1,2,3,4,6-penta-*O*-acetyl-D-glucopyranose (**325**), 0.25 mL (1.853 mmol) of *p*-(trifluoromethoxy)phenol, and 12.0 mL of anhydrous CH_2Cl_2 at 0 ^oC, 0.8 mL (6.482 mmol) of $BF_3{\cdot}OEt_2$ was added and the reaction mixture was gradually warmed to room temperature and stirred overnight. The reaction mixture was diluted with CH_2Cl_2 and quenched with saturated $NaHCO_3$. The organic phase was washed with H_2O and saturated brine, followed by drying over $MgSO_4$. The solution was filtered, concentrated, and the crude product was purified by flash column chromatography (2:8 EtOAc –hexanes) to afford 141.6 mg of a white, powdery solid in 22 % yield. **^{1}H-NMR** (400 MHz, $CDCl_3$): δ 7.15 (d, *J* = 8.4 Hz, 2H), 7.00 (d, *J* = 9.2 Hz, 2H), 5.32-5.24 (m, 2H), 5.16 (t, *J* = 9.6 Hz, 1H), 5.06 (d, *J* = 7.5 Hz, 1H), 4.28 (dd, *J* = 12.3, 5.4 Hz, 1H), 4.17 (dd, *J* = 12.3, 2.4 Hz, 1H), 3.85 (ddd, *J* = 10.0, 5.4, 2.5 Hz, 1H), 2.07 (s, 3H), 2.07 (s, 3H), 2.05 (s, 3H), 2.04 (s, 3H). **^{13}C-NMR** (100 MHz, $CDCl_3$): δ 170.64, 170.34, 169.51, 169.38, 155.26, 144.83, 122.61, 118.27, 99.34, 72.77, 72.30, 71.26, 68.36, 62.04, 20.79, 20.77, 20.75, 20.72. **ESI-MS** *m/z* calcd for $C_{21}H_{23}F_3O_{11}$ $[M + Na]^+$: 531.11. Found 531.1.

Phenyl-2,3,4,6-tetra-*O*-acetyl-β-D-galactopyranoside (330):

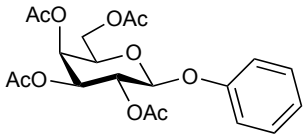

To a mixture of 1.077 g (2.758 mmol) of 1,2,3,4,6-penta-*O*-acetyl-D-galactopyranose (**326**), 761.3 mg (8.089 mmol) of phenol, and 12.0 mL of anhydrous CH_2Cl_2 at 0 ^oC, 1.5 mL (12.15 mmol) of $BF_3{\cdot}OEt_2$ was added and the reaction was gradually warmed to room temperature and stirred overnight. The reaction mixture was diluted with CH_2Cl_2 and quenched with saturated $NaHCO_3$. The organic phase was washed with H_2O and saturated brine, followed by drying over $MgSO_4$. The solution was filtered, concentrated, and the crude product was purified by flash column chromatography (3:7 EtOAc –hexanes) to afford 534.8 mg of a white, powdery solid in 46 % yield. **^{1}H-NMR** (300 MHz, $CDCl_3$): δ 7.30 (m, 2H), 7.09-6.99 (m, 3H), 5.52-5.45 (m, 2H), 5.11 (dd, *J* = 10.4, 3.4 Hz, 1H), 5.04 (d, *J* = 7.9 Hz, 1H), 4.20 (m, 2H), 4.06 (t, *J* = 6.6 Hz, 1H), 2.18 (s, 3H), 2.06 (s, 3H), 2,05 (s, 3H), 2.01 (s, 3H). **^{13}C-NMR** (100 MHz, $CDCl_3$): δ 170.46, 170.36, 170.24, 169.49, 157.09, 129.70, 123.45, 117.09, 99.84, 71.14, 71.00, 68.82, 67.03, 61.49, 20.85, 20.76, 20.76, 20.70. **ESI-MS** *m/z* calcd for $C_{20}H_{24}O_{10}$ $[M + Na]^+$: 447.13. Found 447.1.

***p*-Methoxyphenyl-2,3,4,6-tetra-*O*-acetyl-β-D-galactopyranoside (331):**

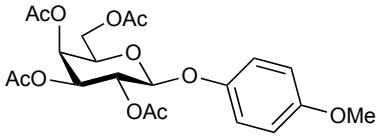

This compound was previously synthesized by Thomas Charlton, a PhD candidate of the Ben laboratory.

***p*-(Trifluoromethoxy)phenyl-2,3,4,6-tetra-*O*-acetyl-β-D-galactopyranoside (332):**

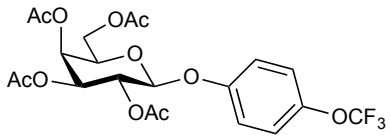

To a mixture of 0.5051 g (1.294 mmol) of 1,2,3,4,6-penta-*O*-acetyl-D-galactopyranose (**326**), 0.25 mL (1.853 mmol) of *p*-(trifluoromethoxy)phenol, and 12.0 mL of anhydrous CH_2Cl_2 at 0 ^oC, 0.8 mL (6.482 mmol) of $BF_3{\cdot}OEt_2$ was added and the reaction was gradually warmed to room temperature and stirred overnight. The reaction mixture was diluted with CH_2Cl_2 and quenched with saturated $NaHCO_3$. The organic phase was washed with H_2O and saturated brine, followed by drying over $MgSO_4$. The solution was filtered, concentrated, and the crude product was purified by flash column chromatography (2:8 EtOAc –hexanes) to afford 116.5 mg of a crude oil. Due to minor impurities, the crude product was carried directly to the next step (Compound **324**).

Phenyl-β-D-glucopyranoside (304):

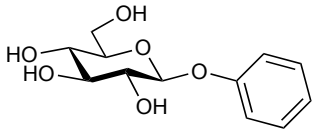

To 0.3854 g (0.9087 mmol) of phenyl-2,3,4,6-tetra-*O*-acetyl-β-D-glucopyranoside (**327**) dissolved in MeOH, a 1 M NaOMe/MeOH solution was added dropwise until a pH of approximately 10 was obtained. The reaction was stirred at room temperature until TLC analysis indicated reaction completion (~ 4 h). The reaction was neutralized with Amberlite® IR-120 (H+) ion-exchange resin, filtered, and concentrated. The crude solid was recrystallized from MeOH –ether to afford 178.6 mg of a white, powdery solid in 77 % yield. **^{1}H-NMR** (400 MHz, D_2O): δ 7.44-7.39 (m, 2H), 7.16 (m, 3H), 5.14 (d, J = 7.5 Hz, 1H), 3.93 (d, J = 12.4 Hz, 1H), 3.76 (dd, J = 12.4, 5.8 Hz, 1H), 3.66-3.55 (m, 3H), 3.50 (m, 1H). **^{13}C-NMR** (100 MHz, D_2O): δ 156.54, 129.96, 123.34, 116.58, 100.16,

76.12, 75.59, 72.97, 69.47, 60.56. **ESI-MS** *m/z* calcd for $C_{12}H_{16}O_6$ $[M + Na]^+$: 279.08. Found 279.0.

***p*-Methoxyphenyl-β-D-glucopyranoside (106):**

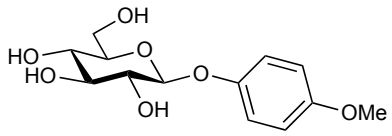

This compound was previously synthesized by Chantelle Capicciotti (PhD)[10] and assessed for its IRI activity by Stephanie Abraham (MSc),[15] former graduate students of the Ben laboratory.

***p*-(Trifluoromethoxy)phenyl-β-D-glucopyranoside (310):**

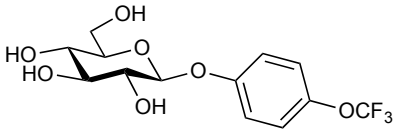

To 0.1416 g (0.2787 mmol) of *p*-(trifluoromethoxy)phenyl-2,3,4,6-tetra-*O*-acetyl-β-D-glucopyranoside (**329**) dissolved in MeOH, a 1 M NaOMe/MeOH solution was added dropwise until a pH of approximately 10 was obtained. The reaction was stirred at room temperature until TLC analysis indicated reaction completion. The reaction was neutralized with Amberlite® IR-120 (H+) ion-exchange resin, filtered, and concentrated. The crude solid was recrystallized from MeOH –ether to afford 97.8 mg of a white, powdery-solid in quantitative yield. **^{1}H-NMR** (300 MHz, D_2O): δ 7.34 (d, *J* = 9.3 Hz, 2H), 7.21 (d, *J* = 9.3 Hz, 2H), 5.14 (d, *J* = 7.6 Hz, 1H), 3.95 (dd, *J* = 12.3, 2.1 Hz, 1H), 3.78 (dd, *J* = 12.4, 5.7 Hz, 1H), 3.69-3.59 (m, 3H), 3.53 (m, 1H). **^{13}C-NMR** (100 MHz, D_2O): δ 155.10, 144.13, 122.70, 117.72, 100.36, 76.13, 75.49, 72.87, 69.38, 60.49. **ESI-MS** *m/z* calcd for $C_{13}H_{15}F_3O_7$ $[M + Na]^+$: 363.07. Found 363.1.

Phenyl-β-D-galactopyranoside (318):

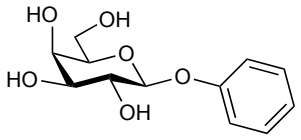

To 0.5348 g (1.261 mmol) of phenyl-2,3,4,6-tetra-*O*-acetyl-β-D-galactopyranoside (**330**) dissolved in MeOH, a 1 M NaOMe/MeOH solution was added dropwise until a pH of approximately 10 was obtained. The reaction was stirred at room temperature until TLC analysis indicated reaction completion (~ 4 h). The reaction was neutralized with Amberlite® IR-120 (H+) ion-exchange resin, filtered, and concentrated. The crude solid was recrystallized from MeOH –ether to afford 245.4 mg of a white, powdery solid in 76 %. **^{1}H-NMR** (300 MHz, D_2O): δ 7.31-7.25 (m, 2H), 7.04-7.00 (m, 3H), 4.95 (d, *J* = 7.4 Hz, 1H), 3.88 (dd, *J* = 3.0, 0.7 Hz, 1H), 3.77-3.72 (m, 1H), 3.71-3.62 (m, 4H). **^{13}C-NMR** (100 MHz, D_2O): δ 156.67, 129.93, 123.20, 116.52, 100.73, 75.40, 72.59, 70.57, 68.50, 60.75. **ESI-MS** *m/z* calcd for $C_{12}H_{16}O_6$ $[M + Na]^+$: 279.08. Found 279.0.

***p*-Methoxyphenyl-β-D-galactopyranoside (314):**

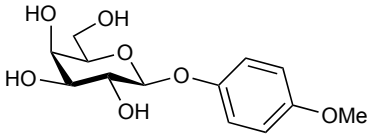

This compound was previously synthesized by Thomas Charlton, a PhD candidate of the Ben laboratory, and was generously donated for the assessment of its IRI activity.

***p*-(Trifluoromethoxy)phenyl-β-D-galactopyranoside (324):**

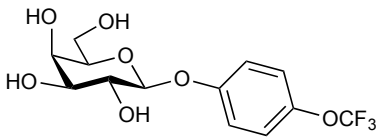

To 0.1165 g of crude *p*-(trifluoromethoxy)phenyl-2,3,4,6-tetra-*O*-acetyl-β-D-galactopyranoside (**332**) dissolved in MeOH, a 1 M NaOMe/MeOH solution was added dropwise until a pH of approximately 10 was obtained. The reaction was stirred at room temperature until TLC analysis indicated reaction completion. The reaction was neutralized with Amberlite® IR-120 (H+) ion-exchange resin, filtered, and concentrated. The crude solid was recrystallized from MeOH –ether to afford 18.8 mg of a white, powdery solid in 5 % yield over two steps. **^{1}H-NMR** (400 MHz, D_2O): δ 7.19 (d, *J* = 8.7 Hz, 2H), 7.06 (d, *J* = 9.2 Hz, 2H), 4.92 (d, *J* = 7.3 Hz, 1H), 3.87 (d, *J* = 3.0 Hz, 1H), 3.74 (t, *J* = 6.2 Hz, 1H), 3.70-3.62 (m, 4H). **^{13}C-NMR** (100 MHz, D_2O): δ 155.26, 144.08, 122.69, 117.69, 100.95, 75.46, 72.52, 70.50, 68.46, 60.73. **ESI-MS** *m/z* calcd for $C_{13}H_{15}F_3O_7$ $[M + Na]^+$: 363.05. Found 363.0.

Thiophenyl-2,3,4,6-tetra-*O*-acetyl-β-D-glucopyranoside (333):

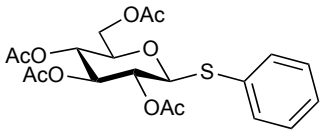

To a mixture of 5.008 g (12.89 mmol) of 1,2,3,4,6-penta-*O*-acetyl-D-glucopyranose (**325**), 2.6 mL (25.48 mmol) of thiophenol, and 25.0 mL of anhydrous CH_2Cl_2 at 0 ^{o}C, 8.0 mL (64.82 mmol) of $BF_3{\cdot}OEt_2$ was added and the reaction was gradually warmed to room temperature and stirred overnight. The reaction mixture was diluted with CH_2Cl_2 and quenched with saturated $NaHCO_3$. The organic phase was washed with H_2O and saturated brine, followed by drying over $MgSO_4$. The solution was

filtered, concentrated, and the crude solid was recrystallized from EtOAc –hexanes to afford 4.848 g of a yellow, powdery solid in 86 % yield. **^{1}H-NMR** (400 MHz, $CDCl_3$): δ 7.52-7.48 (m, 2H), 7.32 (m, 3H), 5.22 (t, *J* = 9.4 Hz, 1H), 5.04 (t, *J* = 9.8 Hz, 1H), 4.98 (t, *J* = 9.7 Hz, 1H), 4.71 (d, *J* = 10.1 Hz, 1H), 4.25-4.16 (m, 2H), 3.73 (ddd, *J* = 10.1, 5.0, 2.6 Hz, 1H), 2.09 (s, 3H), 2,08 (s, 3H), 2.02 (s, 3H), 1.99 (s, 3H). **^{13}C-NMR** (100 MHz, $CDCl_3$): δ 170.73, 170.30, 169.62, 169.42, 132.94, 131.74, 129.08, 128.05, 85.90, 75.95, 74.12, 70.09, 68.36, 62.30, 20.90, 20.88, 20.75, 20.73. **ESI-MS** *m/z* calcd for $C_{20}H_{24}O_9S$ $[M + Na]^+$: 463.10. Found 463.1.

_p_-Methoxythiophenyl-2,3,4,6-tetra-_O_-acetyl-β-D-glucopyranoside (334):

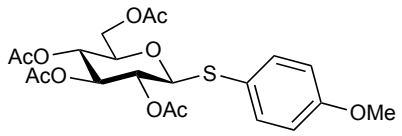

To a mixture of 4.994 g (12.79 mmol) of 1,2,3,4,6-penta-*O*-acetyl-D-glucopyranose (**325**), 1.6 mL (13.01 mmol) of *p*-methoxythiophenol, and 25.0 mL of anhydrous CH_2Cl_2 at 0 ^{o}C, 8.0 mL (64.82 mmol) of $BF_3{\cdot}OEt_2$ was added and the reaction was gradually warmed to room temperature and stirred overnight. The reaction mixture was diluted with CH_2Cl_2 and quenched with saturated $NaHCO_3$. The organic phase was washed with H_2O and saturated brine, followed by drying over $MgSO_4$. The solution was filtered, concentrated, and the crude solid was recrystallized from EtOAc –hexanes to afford 5.896 g of a yellow, powdery solid in 98 % yield. **^{1}H-NMR** (400 MHz, $CDCl_3$): δ 7.44 (d, *J* = 8.8 Hz, 2H), 6.85 (d, *J* = 8.8 Hz, 2H), 5.19 (t, *J* = 9.4 Hz, 1H), 4.99 (t, *J* = 9.8 Hz, 1H), 4.89 (t, *J* = 9.6 Hz, 1H), 4.55 (d, *J* = 10.0 Hz, 1H), 4.19-4.18 (m, 2H), 3.82 (s, 3H), 3.67 (ddd, *J* = 10.0, 4.2, 3.1 Hz, 1H), 2.10 (s, 3H), 2.07 (s, 3H), 2.01 (s, 3H), 1.98 (s, 3H). **^{13}C-NMR** (100 MHz, $CDCl_3$): δ 170.75, 170.32, 169.50, 169.35, 160.67, 136.70, 120.92, 114.54, 85.82, 75.89, 74.22, 70.03, 68.31, 62.22, 55.48, 20.96, 20.90, 20.75, 20.73. **ESI-MS** *m/z* calcd for $C_{21}H_{26}O_{10}S$ $[M + Na]^+$: 493.11. Found 493.1.

Thiophenyl-2,3,4,6-tetra-*O*-acetyl-β-D-galactopyranoside (335):

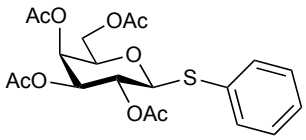

To a mixture of 5.002 g (12.81 mmol) of 1,2,3,4,6-penta-*O*-acetyl-D-galactopyranose (**326**), 2.5 mL (24.50 mmol) of thiophenol, and 25.0 mL of anhydrous CH_2Cl_2 at 0 ^oC, 8.0 mL (64.82 mmol) of $BF_3{\cdot}OEt_2$ was added and the reaction was gradually warmed to room temperature and stirred overnight. The reaction mixture was diluted with CH_2Cl_2 and quenched with saturated $NaHCO_3$. The organic phase was washed with H_2O and saturated brine, followed by drying over $MgSO_4$. The solution was filtered, concentrated, and the crude solid was recrystallized from EtOAc –hexanes to afford 3.543 g of an off-white, powdery solid in 63 % yield. **^{1}H-NMR** (300 MHz, $CDCl_3$): δ 7.54-7.49 (m, 2H), 7.34-7.29 (m, 3H), 5.42 (dd, *J* = 3.3, 1.0 Hz, 1H), 5.24 (t, *J* = 10.0 Hz, 1H), 5.05 (dd, *J* = 9.9, 3.3 Hz, 1H), 4.72 (d, *J* = 10.0 Hz, 1H), 4.20 (dd, *J* = 11.3, 7.0 Hz, 1H), 4.11 (dd, *J* = 11.3, 6.1 Hz, 1H), 3.94 (ddd, *J* = 7.1, 6.1, 1.0 Hz, 1H), 2.12 (s, 3H), 2.10 (s, 3H), 2.04 (s, 3H), 1.98 (s, 3H). **^{13}C-NMR** (100 MHz, $CDCl_3$): δ 170.50, 170.32, 170.18, 169.56, 132.71, 132.60, 129.03, 128.30, 87.77, 74.57, 72.15, 67.40, 67.36, 61.77, 20.99, 20.81, 20.78, 20.73. **ESI-MS** *m/z* calcd for $C_{20}H_{24}O_9S$ $[M + Na]^+$: 463.10. Found 463.1.

***p*-Methoxythiophenyl-2,3,4,6-tetra-*O*-acetyl-β-D-galactopyranoside (336):**

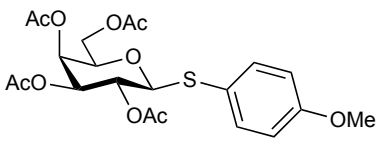

To a mixture of 5.025 g (12.87 mmol) of 1,2,3,4,6-penta-*O*-acetyl-D-galactopyranose (**326**), 1.8 mL (14.64 mmol) of *p*-methoxythiophenol, and 25.0 mL of anhydrous CH_2Cl_2 at 0 ^oC, 8.0 mL (64.82 mmol) of $BF_3{\cdot}OEt_2$ was added and the reaction

was gradually warmed to room temperature and stirred overnight. The reaction mixture was diluted with CH_2Cl_2 and quenched with saturated $NaHCO_3$. The organic phase was washed with H_2O and saturated brine, followed by drying over $MgSO_4$. The solution was filtered, concentrated, and the crude oil was purified by flash column chromatography (3:7 EtOAc –hexanes). Due to minor impurities, the crude column product was carried directly to the next step (Compound **340**).

Thiophenyl-β-D-glucopyranoside (337):

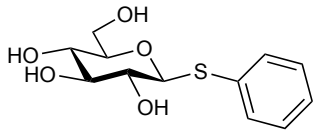

To 4.157 g (9.445 mmol) of thiophenyl-2,3,4,6-tetra-*O*-acetyl-β-D-glucopyranoside (**333**) dissolved in MeOH, a 1 M NaOMe/MeOH solution was added dropwise until a pH of approximately 10 was obtained. The reaction was stirred at room temperature until TLC analysis indicated reaction completion (~ 2 h). The reaction was neutralized with Amberlite® IR-120 (H+) ion-exchange resin, filtered, and concentrated. The crude solid was recrystallized from MeOH –ether to afford 1.883 g of a white, powdery solid in 73 % yield. **^{1}H-NMR** (300 MHz, DMSO-d_6): δ 7.47-7.44 (m, 2H), 7.33-7.28 (m, 2H), 7.24-7.19 (m, 1H), 5.27 (d, *J* = 6.1 Hz, 1H), 5.08 (d, *J* = 4.9 Hz, 1H), 4.97 (d, *J* = 5.2 Hz, 1H), 4.60 (d, *J* = 9.7 Hz, 1H), 4.55 (t, *J* = 5.7 Hz, 1H), 3.69 (ddd, *J* = 11.8, 5.3, 1.8 Hz, 1H), 3.44 (m, 1H), 3.25-3.18 (m, 2H), 3.13-3.01 (m, 2H). **^{13}C-NMR** (100 MHz, D_2O): δ 131.98, 131.62, 129.32, 128.10, 87.26, 79.89, 77.22, 71.71, 69.36, 60.79. **ESI-MS** *m/z* calcd for $C_{12}H_{16}O_5S$ $[M + Na]^+$: 295.06. Found 295.1.

***p*-Methoxythiophenyl-β-D-glucopyranoside (338):**

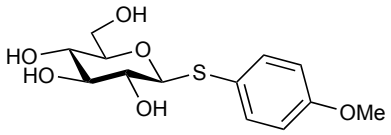

To 4.174 g (8.879 mmol) of *p*-methoxythiophenyl-2,3,4,6-tetra-*O*-acetyl-β-D-glucopyranoside (**334**) dissolved in MeOH, a 1 M NaOMe/MeOH solution was added dropwise until a pH of approximately 10 was obtained. The reaction was stirred at room temperature until TLC analysis indicated reaction completion (~ 2 h). The reaction was neutralized with Amberlite® IR-120 (H+) ion-exchange resin, filtered, and concentrated to afford 2.009 g of a yellow, powdery solid in 75 % yield. **^{1}H-NMR** (400 MHz, D_2O): δ 7.56 (d, *J* = 9.0 Hz, 2H), 7.00 (d, *J* = 9.0 Hz, 2H), 4.61 (d, *J* = 9.8 Hz, 1H), 3.88 (dd, *J* = 12.4, 2.2 Hz, 1H), 3.83 (s, 3H), 3.70 (dd, *J* = 12.4, 5.6 Hz, 1H), 3.49 (t, *J* = 8.9 Hz, 1H), 3.42 (ddd, *J* = 9.8, 5.6, 2.2 Hz, 1H), 3.35 (dd, *J* = 9.8, 8.8 Hz, 1H), 3.26 (dd, *J* = 9.8, 9.0 Hz, 1H). **^{13}C-NMR** (100 MHz, D_2O): δ 159.46, 135.18, 122.09, 114.83, 87.78, 79.88, 77.23, 71.58, 69.37, 60.83, 55.47. **ESI-MS** *m/z* calcd for $C_{13}H_{18}O_6S$ $[M + Na]^+$: 325.07. Found 325.1.

Thiophenyl-β-D-galactopyranoside (339):

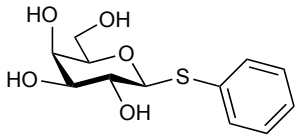

To 3.500 g (7.953 mmol) of thiophenyl-2,3,4,6-tetra-*O*-acetyl-β-D-galactopyranoside (**335)** dissolved in MeOH, a 1 M NaOMe/MeOH solution was added dropwise until a pH of approximately 10 was obtained. The reaction was stirred at room temperature until TLC analysis indicated reaction completion (~ 2 h). The reaction was neutralized with Amberlite® IR-120 (H+) ion-exchange resin, filtered, and concentrated.

The crude solid was recrystallized from MeOH –ether to afford 1.761 g of a white, powdery solid in 81 % yield. **^{1}H-NMR** (300 MHz, DMSO-d_6): δ 7.46-7.43 (m, 2H), 7.32-7.27 (m, 2H), 7.22-7.18 (m, 1H), 5.12 (d, *J* = 5.8 Hz, 1H), 4.86 (d, *J* = 5.4 Hz, 1H), 4.63 (t, *J* = 4.8 Hz, 1H), 4.58 (d, *J* = 9.4 Hz, 1H), 4.46 (d, *J* = 4.3 Hz, 1H), 3.71 (t, *J* = 3.6 Hz, 1H), 3.46 (m, 4H), 3.39-3.35 (m, 1H). **^{13}C-NMR** (100 MHz, D_2O): δ 132.70, 131.07, 129.33, 127.84, 88.04, 78.98, 73.97, 69.22, 68.69, 60.95. **ESI-MS** *m/z* calcd for $C_{12}H_{16}O_5S$ $[M + Na]^+$: 295.06. Found 295.1.

***p*-Methoxythiophenyl-β-D-galactopyranoside (340):**

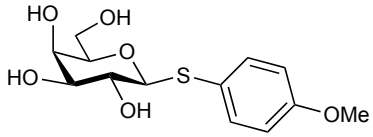

To 1.5 g of crude *p*-methoxythiophenyl-2,3,4,6-tetra-*O*-acetyl-β-D-galactopyranoside (**336**) dissolved in MeOH, a 1 M NaOMe/MeOH solution was added dropwise until a pH of approximately 10 was obtained. The reaction was stirred at room temperature until TLC analysis indicated reaction completion (~ 2 h). The reaction was neutralized with Amberlite® IR-120 (H+) ion-exchange resin, filtered, and concentrated. The crude solid was recrystallized from MeOH –ether to afford 866.9 mg of a white, powdery solid in 23 % yield over two steps. **^{1}H-NMR** (400 MHz, D_2O): δ 7.57 (d, *J* = 8.9 Hz, 2H), 7.01 (d, *J* = 8.9 Hz, 2H), 4.59 (d, *J* = 9.7 Hz, 1H), 3.96 (d, *J* = 3.2 Hz, 1H), 3.84 (s, 3H), 3.79-3.71 (m, 2H), 3.69-3.64 (m, 2H), 3.56 (t, *J* = 9.6 Hz, 1H). **^{13}C-NMR** (100 MHz, D_2O): δ 159.28, 134.68, 122.89, 114.87, 88.82, 78.96, 73.99, 69.14, 68.70, 60.94, 55.46. **ESI-MS** *m/z* calcd for $C_{13}H_{18}O_6S$ $[M + Na]^+$: 325.07. Found 325.1.

***N*-phenyl-D-glucopyranosylamine (341):**

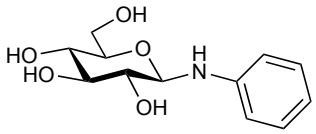

To 0.2081 g (1.155 mmol) of D-glucose dissolved in 2.0 mL EtOH, 0.30 mL (3.286 mmol) of aniline was added and the reaction was refluxed for 5 hours. The reaction mixture was gradually cooled to room temperature, concentrated, and the crude solid was recrystallized from EtOH to afford 0.2506 g of a white, powdery solid in 85 % yield. **^{1}H-NMR** (400 MHz, D_2O): δ 7.29 (m, 2H), 6.91-6.88 (m, 3H), 4.77 (d, *J* = 8.9 Hz, 1H), 3.88 (dd, *J* = 12.3, 2.3 Hz, 1H), 3.71 (dd, *J* = 12.4, 5.6 Hz, 1H), 3.62-3.54 (m, 2H), 3.46-3.42 (m, 2H). **^{13}C-NMR** (100 MHz, D_2O): δ 145.63, 129.62, 119.61, 114.40, 84.87, 76.87, 76.48, 72.70, 69.76, 60.79. **ESI-MS** *m/z* calcd for $C_{12}H_{17}NO_5$ $[M + Na]^+$: 278.10. Found 277.9.

***N*-(*p*-Methoxyphenyl)-β-D-glucopyranosylamine (342):**

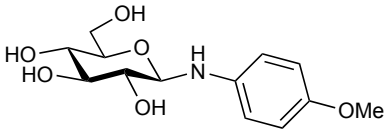

A mixture of 0.1579 g (0.8765 mmol) of D-glucose, 0.2888 g (2.345 mmol) of *p*-anisidine, and 2.0 mL of EtOH was refluxed for 5 hours. The reaction mixture was gradually cooled to room temperature, concentrated, and the crude solid was recrystallized from EtOH to afford 0.1010 g of an off-white, powdery solid in 40 % yield. **^{1}H-NMR** (300 MHz, D_2O): δ 6.94 (d, *J* = 9.1 Hz, 2H), 6.88 (d, *J* = 9.1 Hz, 2H), 4.69 (d, *J* = 8.8 Hz, 1H), 3.88 (dd, *J* = 12.3, 2.2 Hz, 1H), 3.79 (s, 3H), 3.71 (dd, *J* = 12.3, 5.5 Hz, 1H), 3.62-3.51 (m, 2H), 3.43 (m, 2H). **^{13}C-NMR** (100 MHz, D_2O): δ 152.50, 139.80,

116.02, 115.23, 85.78, 76.87, 76.49, 72.74, 69.78, 60.80, 55.89. **ESI-MS** *m/z* calcd for $C_{13}H_{19}NO_6$ $[M + Na]^+$: 308.11. Found 308.0.

***N*-(*p*-trifluoromethoxyphenyl)-β-D-glucopyranosylamine (343):**

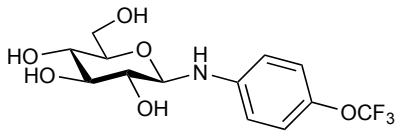

To 0.3057 g (1.697 mmol) of D-glucose dissolved in 2.0 mL EtOH, 0.67 mL (4.993 mmol) of *p*-(trifluoromethoxy)aniline was added and the reaction was refluxed for 8 hours. The reaction mixture was gradually cooled to room temperature, concentrated, and the crude solid was recrystallized from EtOH to afford 312.7 mg of a white, powdery solid in 54 % yield. **^{1}H-NMR** (400 MHz, D_2O): δ 7.21 (d, *J* = 8.2 Hz, 2H), 6.90 (d, *J* = 9.0 Hz, 2H), 4.74 (d, *J* = 8.9 Hz, 1H), 3.88 (dd, *J* = 12.4, 2.3 Hz, 1H), 3.72 (dd, *J* = 12.4, 5.5 Hz, 1H), 3.59 (q, *J* = 9.1 Hz, 1 H), 3.59-3.56 (m, 1H), 3.47-3.42 (m, 2H). **^{13}C-NMR** (100 MHz, D_2O): δ 144.64, 141.57, 122.54, 114.91, 84.86, 76.83, 76.48, 72.61, 69.69, 60.74. **ESI-MS** *m/z* calcd for $C_{13}H_{16}F_3NO_6$ $[M + Na]^+$: 362.08. Found 362.0.

***N*-phenyl-D-galactopyranosylamine (344):**

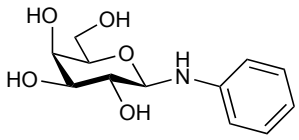

To 0.1026 g (0.5695 mmol) of D-galactose dissolved in 2.0 mL EtOH, 0.15 mL (31.64 mmol) of aniline was added and the reaction was refluxed for 5 hours. The reaction mixture was gradually cooled to room temperature, concentrated, and the crude solid was recrystallized from EtOH to afford 0.2506 g of a white, powdery solid in 76 % yield. **^{1}H-NMR** (400 MHz, D_2O): δ 7.29 (m, 2H), 6.89 (m, 3H), 4.72 (d, *J* = 8.6 Hz, 1H),

4.00 (d, J = 3.3 Hz, 1H), 3.81 (t, J = 6.2 Hz, 1H), 3.76 (dd, J = 9.6, 3.4 Hz, 1H), 3.73-3.65 (m, 3H). **^{13}C-NMR** (100 MHz, D_2O): δ 145.72, 129.60, 119.51, 114.37, 85.31, 75.51, 73.74, 70.33, 68.86, 60.91. **ESI-MS** *m/z* calcd for $C_{12}H_{17}NO_5$ $[M + Na]^+$: 278.10. Found 278.0.

***N*-(*p*-methoxyphenyl)-β-D-galactopyranosylamine (345):**

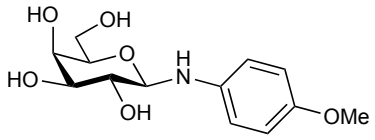

A mixture of 0.1088 g (0.6039 mmol) of D-galactose, 0.2433 g (1.976 mmol) of *p*-anisidine, and 2.0 mL of EtOH was refluxed for 5 hours. The reaction mixture was gradually cooled to room temperature, concentrated, and the crude solid was recrystallized from EtOH to afford 97.0 mg of an off-white, powdery solid in 56 % yield. **^{1}H-NMR** (400 MHz, D_2O): δ 6.94 (d, J = 9.1 Hz, 2H), 6.89 (d, J = 9.2 Hz, 2H), 4.64 (d, J = 8.7 Hz, 1H), 4.00 (d, J = 2.8 Hz, 1H), 3.81-3.71 (m, 4H), 3.79 (s, 3H), 3.65 (dd, J = 9.6, 8.7 Hz, 1H). **^{13}C-NMR** (100 MHz, D_2O): δ 152.4, 139.9, 115.9, 115.2, 86.2, 75.5, 73.7, 70.4, 68.9, 60.9, 55.9. **ESI-MS** *m/z* calcd for $C_{13}H_{19}NO_6$ $[M + Na + H]^+$: 309.10. Found 309.1.

***N*-(*p*-trifluoromethoxyphenyl)-β-D-galactopyranosylamine (346):**

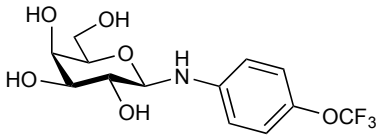

To 0.3000 g (1.665 mmol) of D-galactose dissolved in 2.0 mL EtOH, 0.67 mL (4.993 mmol) of *p*-(trifluoromethoxy)aniline was added and the reaction was refluxed for 9 hours. The reaction mixture was gradually cooled to room temperature, concentrated,

and the crude solid was recrystallized from EtOH to afford 336.9 mg of a white, powdery solid in 60 % yield. **^{1}H-NMR** (400 MHz, DMSO-d_6): δ 7.08 (d, *J* = 8.5 Hz, 2H), 6.74 (d, *J* = 9.0 Hz, 2H), 6.51 (d, *J* = 7.6 Hz, 1H), 4.77 (d, *J* = 5.5 Hz, 1H), 4.71 (d, *J* = 5.3 Hz, 1H), 4.55 (t, *J* = 5.2 Hz, 1H), 4.38 (d, *J* = 4.2 Hz, 1H), 4.30 (t, *J* = 8.0 Hz, 1H), 3.71 (t, *J* = 3.7 Hz, 1H), 3.53-3.41 (m, 4H), 3.38 (ddd, *J* = 9.2, 5.6, 3.4 Hz, 1H). **^{13}C-NMR** (100 MHz, DMSO-d_6): δ 146.70, 139.24, 121.84, 113.62, 85.39, 75.61, 74.29, 70.06, 68.40, 60.54. **ESI-MS** *m/z* calcd for $C_{13}H_{16}F_3NO_6$ $[M + Na]^+$: 362.08. Found 361.9.

3.8 NMR Spectra of Aryl Glycosides

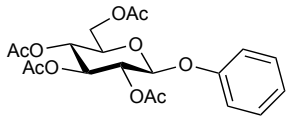

327

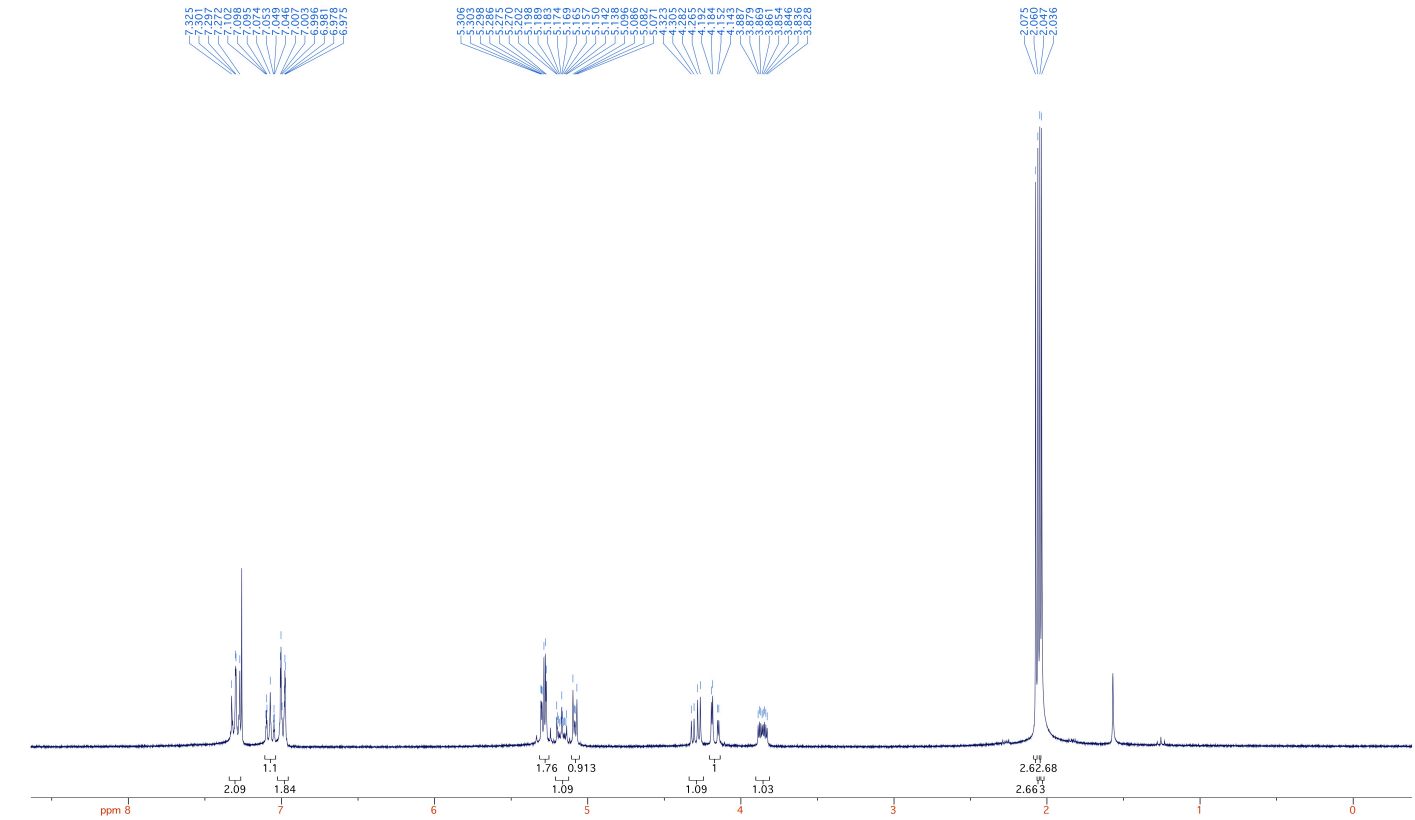

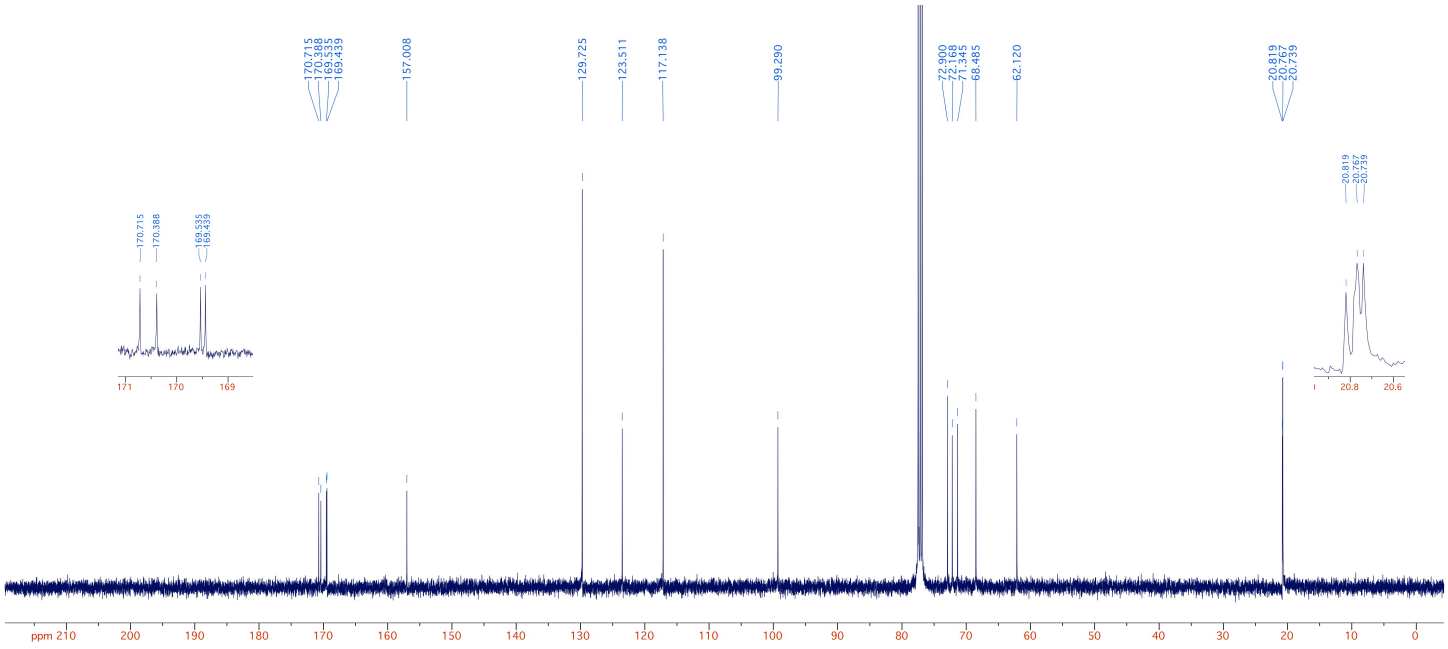

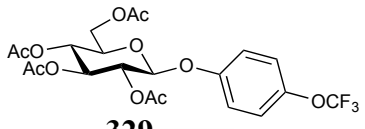
OAc
AcO
AcO
O
O
OAc
OCF3

329

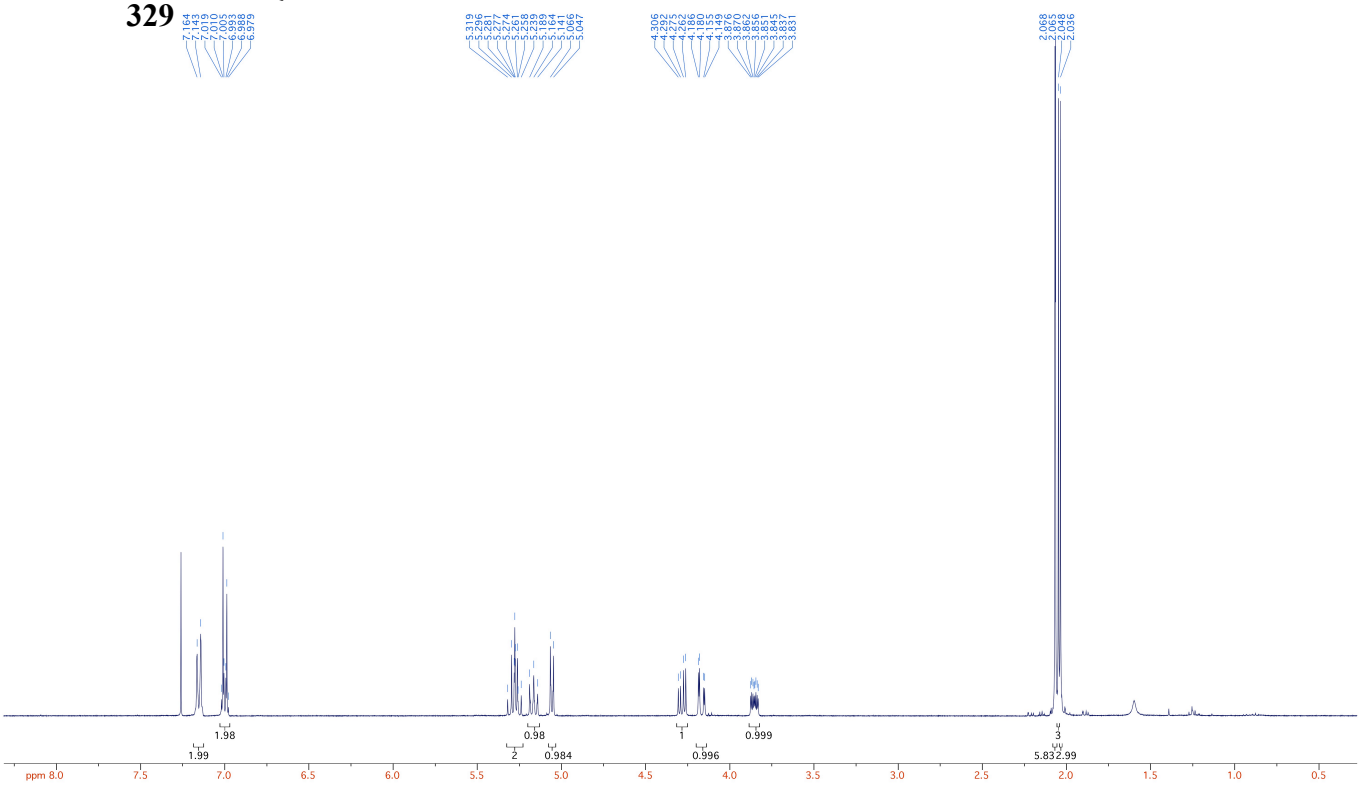
7.164
7.143
7.019
7.010
7.000
6.993
6.978
6.959
5.319
5.296
5.281
5.277
5.274
5.261
5.258
5.239
5.189
5.164
5.141
5.066
5.047
4.306
4.292
4.275
4.262
4.186
4.170
4.155
4.149
4.076
3.870
3.862
3.856
3.851
3.847
3.837
3.831
2.068
2.065
2.048
2.036
1.98
0.98
1
0.999
3
1.99
2
0.984
0.996
5.83
2.99
ppm 8.0
7.5
7.0
6.5
6.0
5.5
5.0
4.5
4.0
3.5
3.0
2.5
2.0
1.5
1.0
0.5

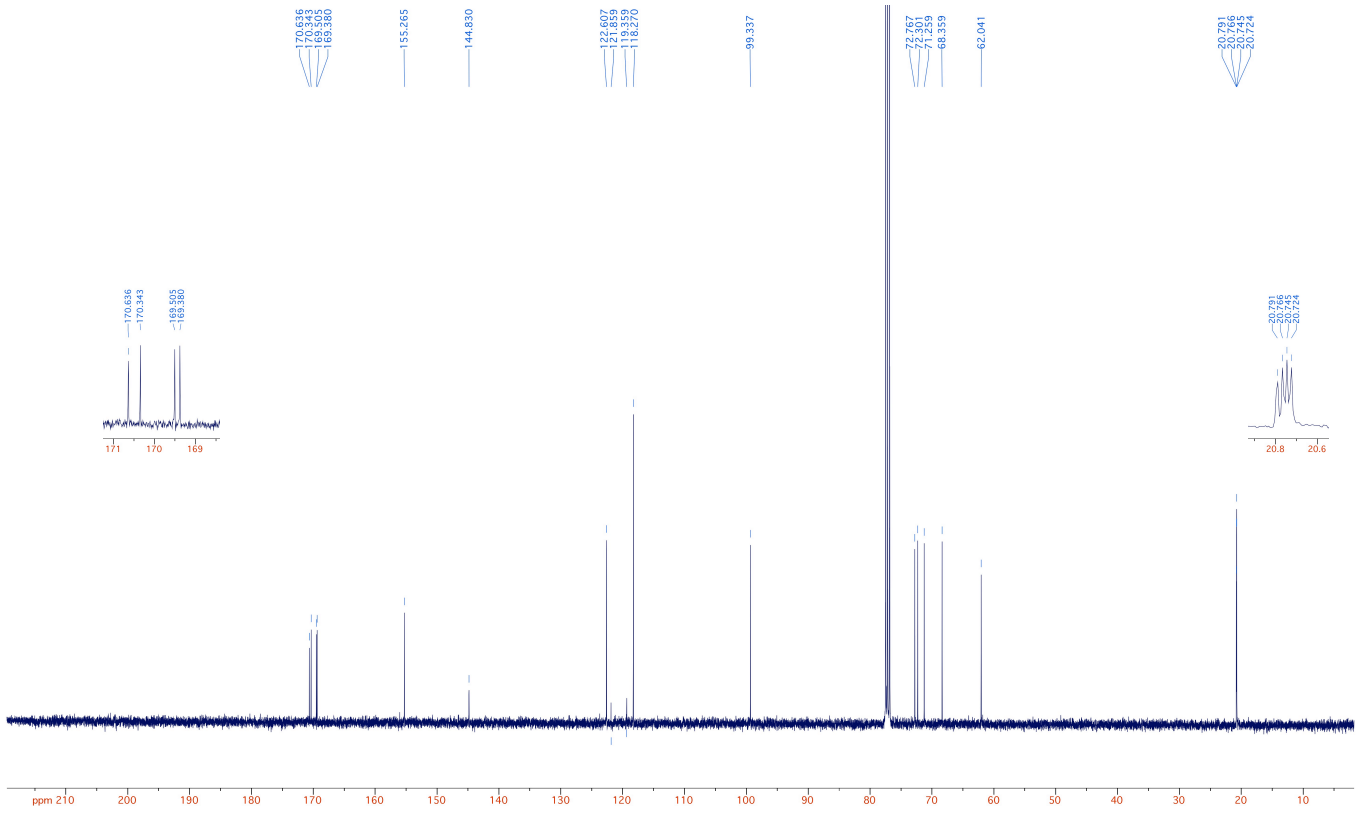
170.636
170.343
169.505
169.380
155.265
144.830
122.607
121.859
119.359
118.270
99.337
72.767
72.301
71.259
68.359
62.041
20.791
20.761
20.745
20.724
171
170
169
20.8
20.6
ppm 210
200
190
180
170
160
150
140
130
120
110
100
90
80
70
60
50
40
30
20
10

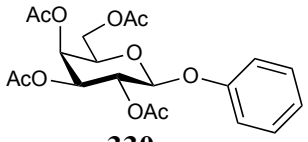
AcO
OAc
O
AcO
O
OAc

330

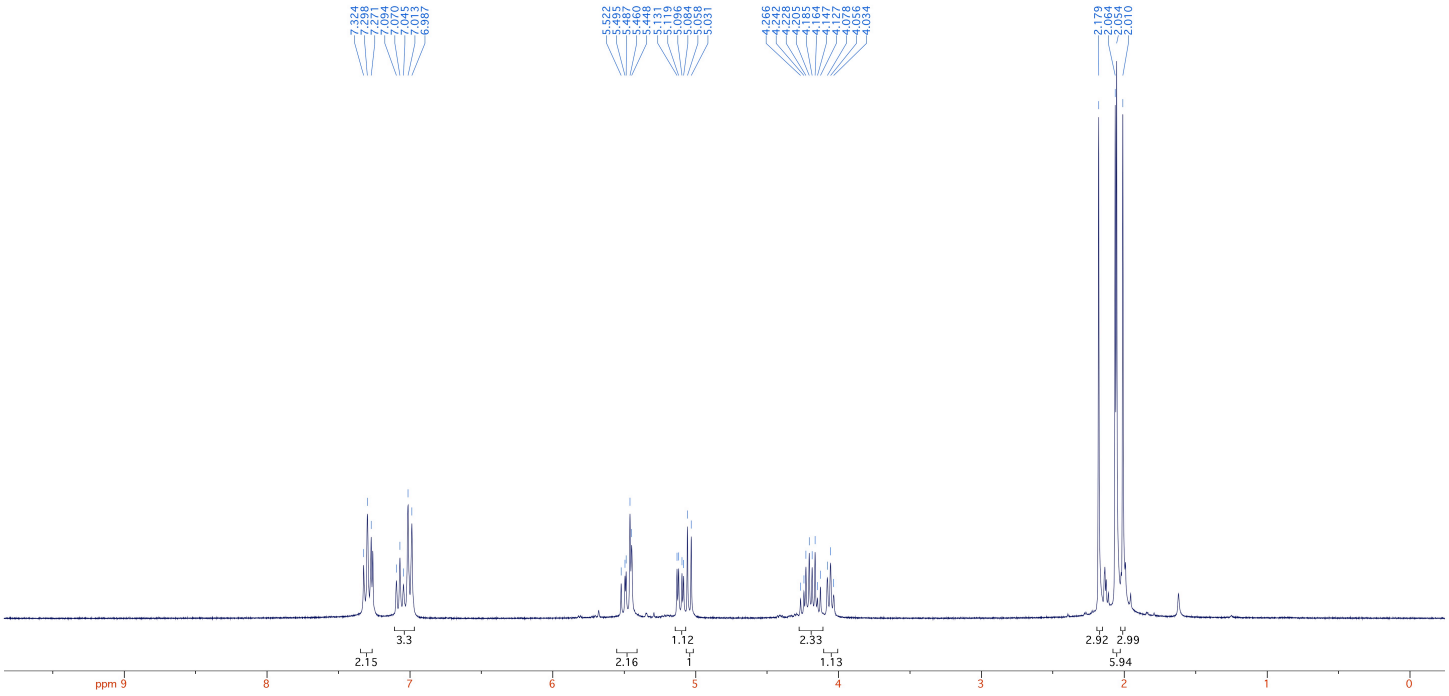
7.324
7.298
7.271
7.094
7.070
7.045
7.013
6.987
5.522
5.495
5.487
5.460
5.446
5.131
5.119
5.096
5.084
5.058
5.031
4.266
4.242
4.228
4.205
4.185
4.164
4.147
4.127
4.078
4.056
4.034
2.179
2.064
2.054
2.010
3.3
2.15
1.12
1
2.16
2.33
1.13
2.92
2.99
5.94
ppm 9
8
7
6
5
4
3
2
1
0

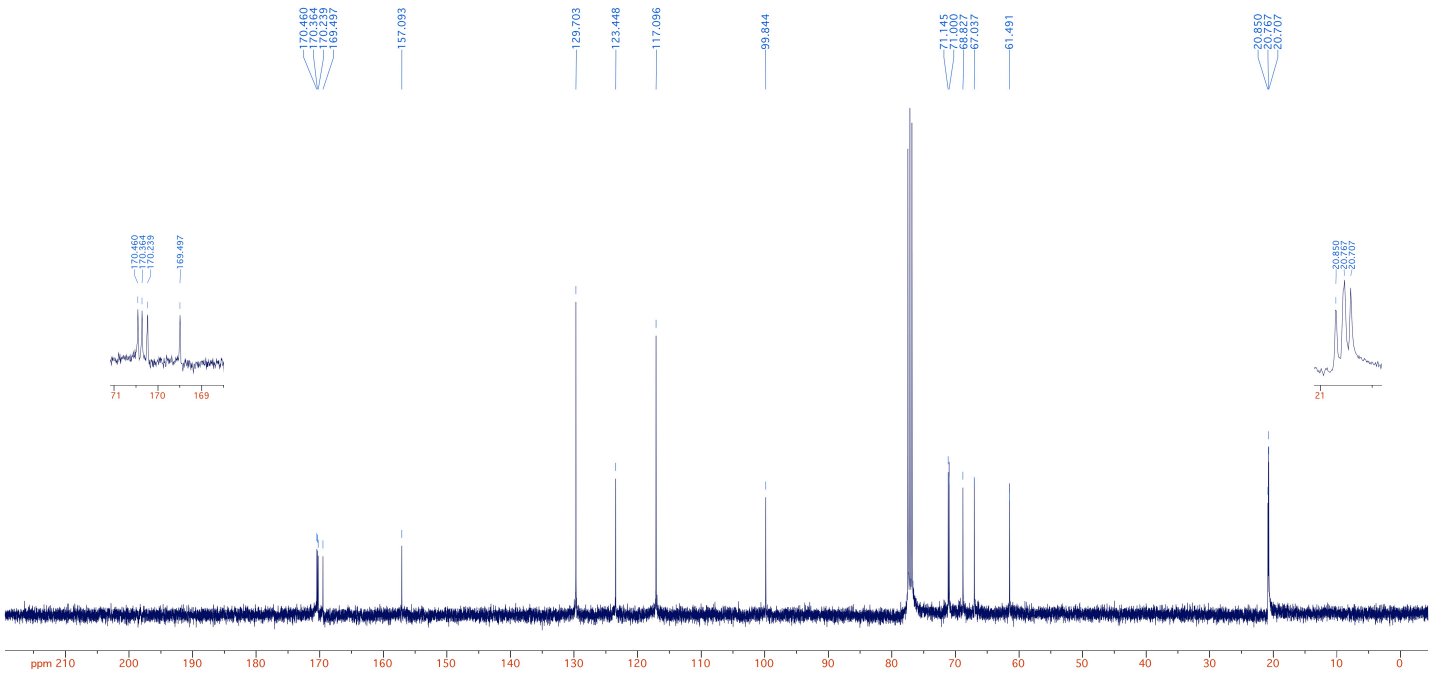
170.460
170.364
170.239
169.497
157.093
129.703
123.448
117.096
99.844
71.145
71.000
68.827
67.037
61.491
20.850
20.767
20.707
ppm 210
200
190
180
170
160
150
140
130
120
110
100
90
80
70
60
50
40
30
20
10
0

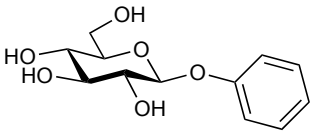
OH
HO
HO
O
O
OH

304

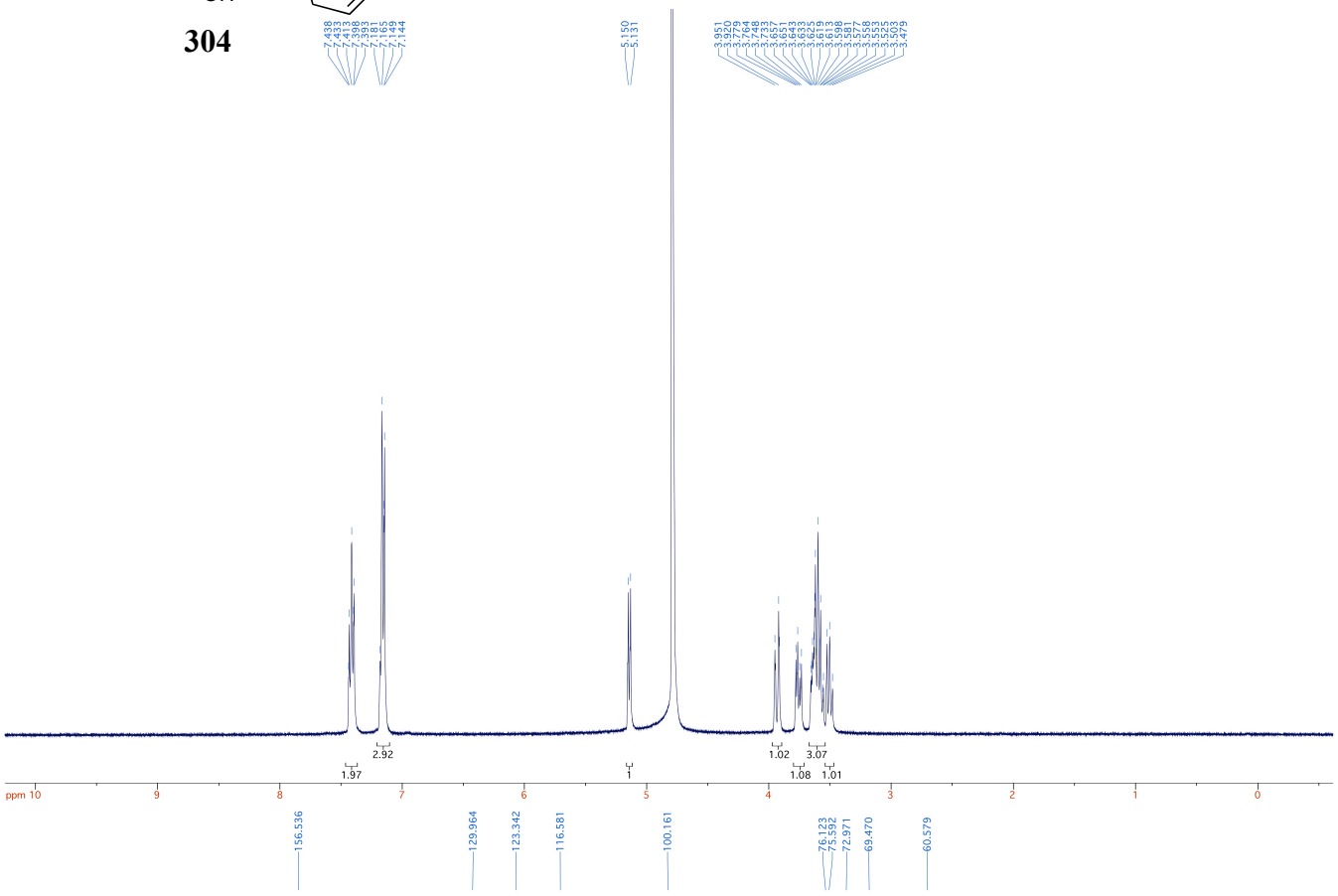
7.438
7.433
7.413
7.399
7.181
7.165
7.149
7.144
5.150
5.131
3.951
3.920
3.779
3.764
3.748
3.733
3.657
3.651
3.643
3.633
3.625
3.619
3.613
3.598
3.581
3.577
3.558
3.553
3.535
3.503
3.479
2.92
1.97
1
1.02
1.08
3.07
1.01
ppm 10
9
8
7
6
5
4
3
2
1
0
156.536
129.964
123.342
116.581
100.161
76.123
75.592
72.971
69.470
60.579

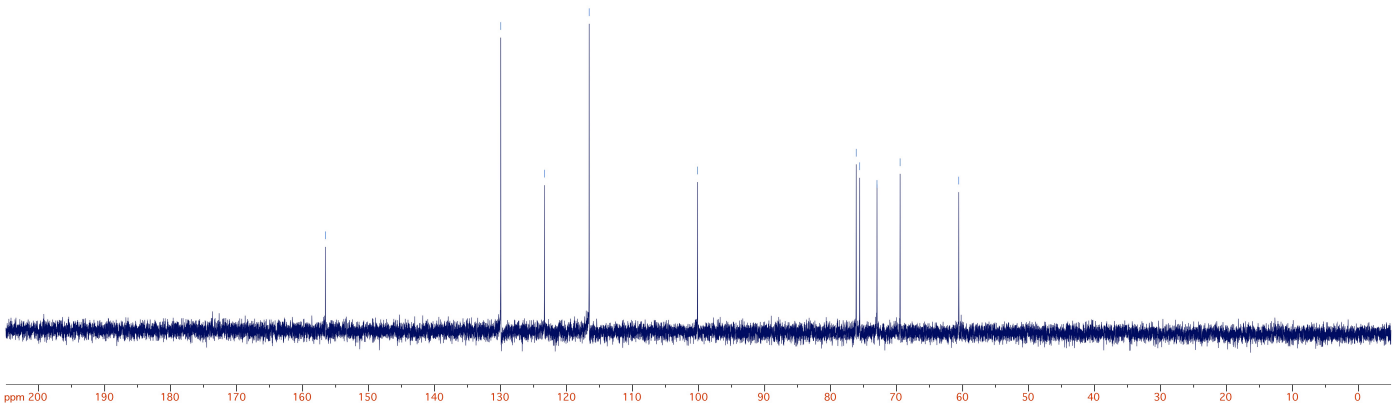
ppm 200
190
180
170
160
150
140
130
120
110
100
90
80
70
60
50
40
30
20
10
0

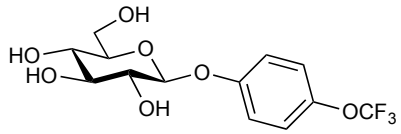
OH
HO
HO
O
O
OH
OCF3

310

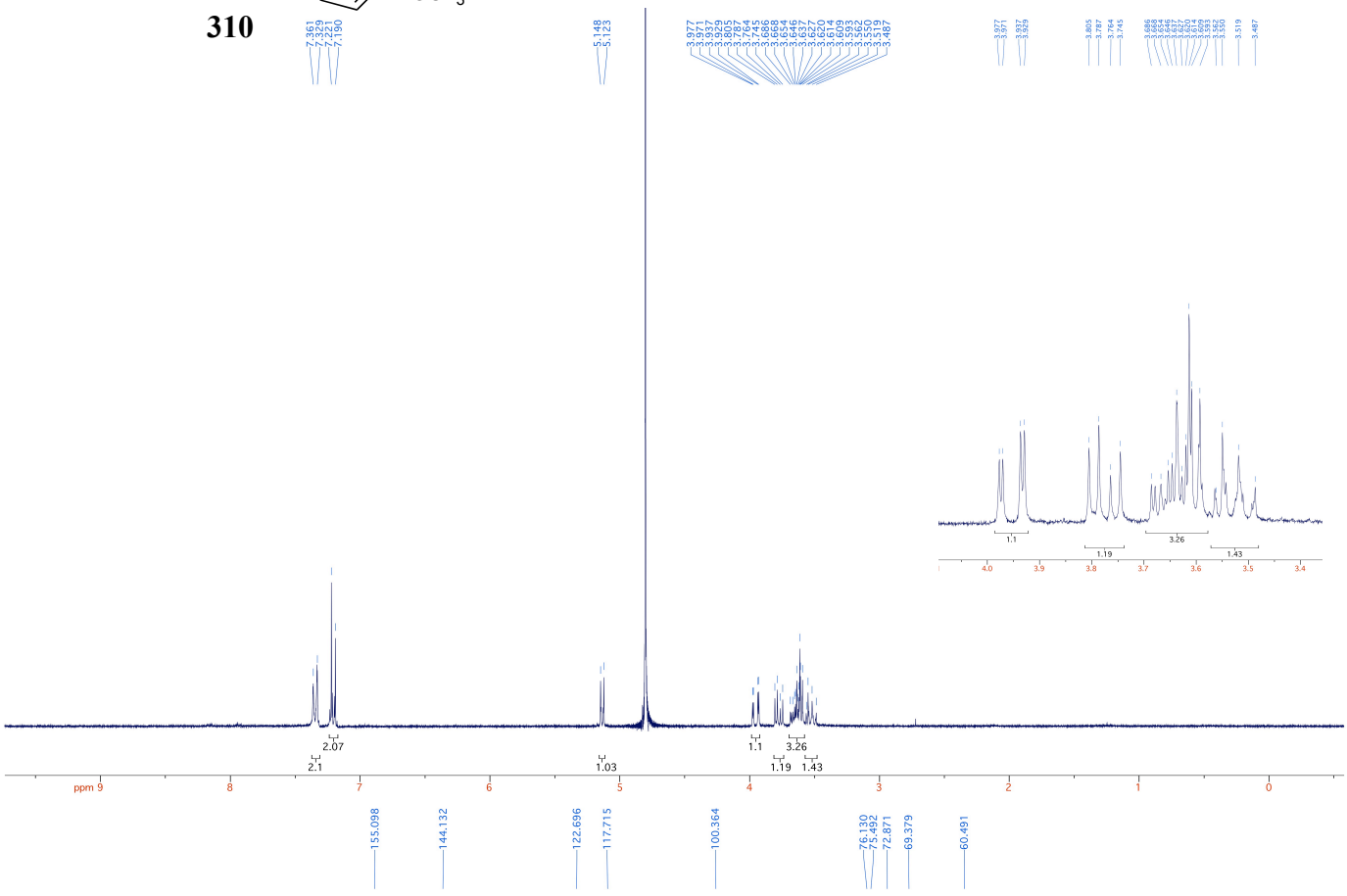
7.361
7.329
7.221
7.190
5.148
5.123
3.977
3.971
3.937
3.929
3.805
3.787
3.764
3.745
3.686
3.668
3.654
3.646
3.627
3.620
3.614
3.609
3.593
3.582
3.550
3.519
3.487
2.1
2.07
1.03
1.1
1.19
3.26
1.43
ppm 9
8
7
6
5
4
3
2
1
0

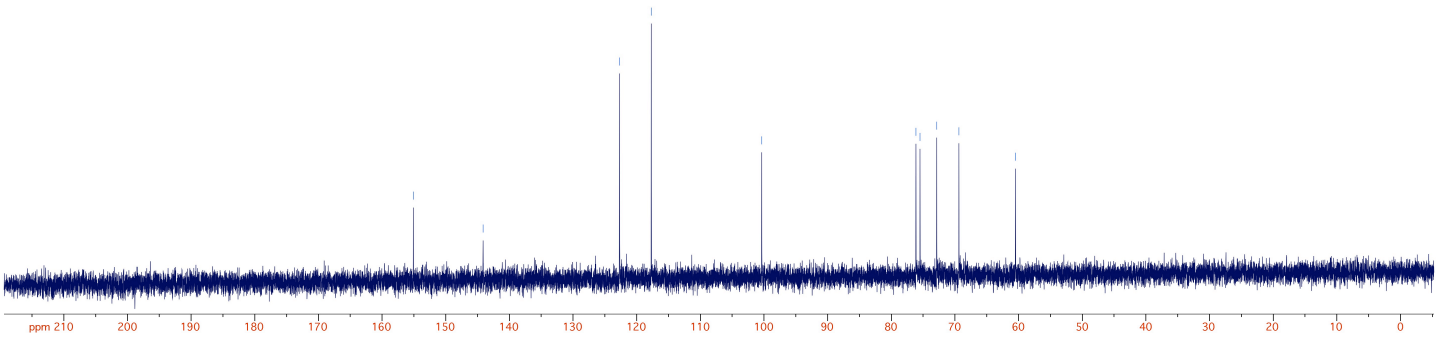
155.098
144.132
122.696
117.715
100.364
76.130
75.492
72.871
69.379
60.491
ppm 210
200
190
180
170
160
150
140
130
120
110
100
90
80
70
60
50
40
30
20
10
0

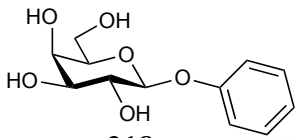
HO
OH
O
HO
O
OH

318

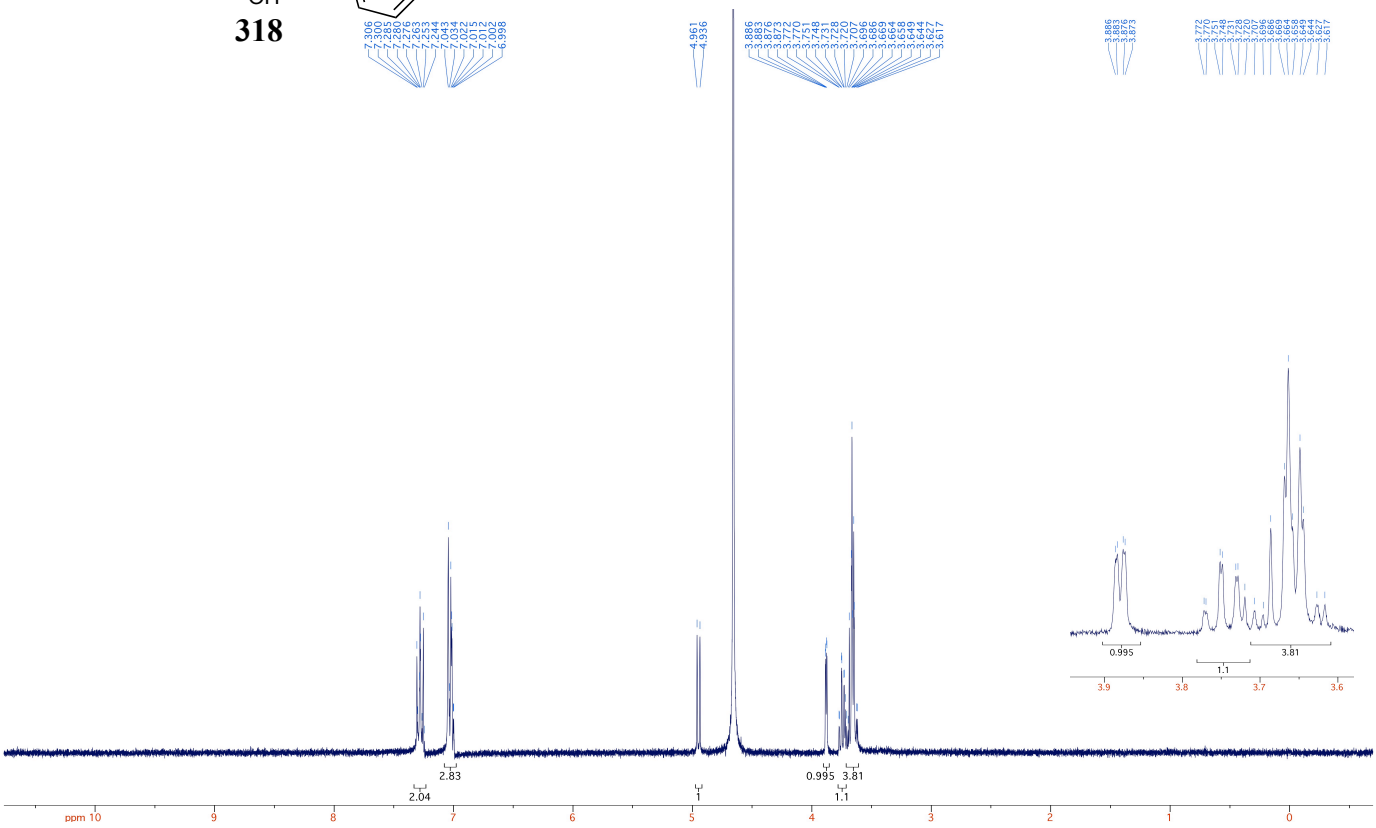
7.306
7.300
7.295
7.280
7.276
7.263
7.253
7.244
7.243
7.034
7.022
7.015
7.011
7.002
6.998
4.961
4.936
3.886
3.883
3.876
3.873
3.772
3.770
3.731
3.748
3.731
3.720
3.707
3.686
3.669
3.664
3.658
3.649
3.644
3.627
3.617
3.886
3.883
3.876
3.873
3.772
3.770
3.755
3.748
3.731
3.720
3.707
3.696
3.686
3.669
3.664
3.658
3.649
3.644
3.627
3.617
2.04
2.83
1
0.995
3.81
1.1
0.995
1.1
3.81
ppm 10
9
8
7
6
5
4
3
2
1
0
3.9
3.8
3.7
3.6

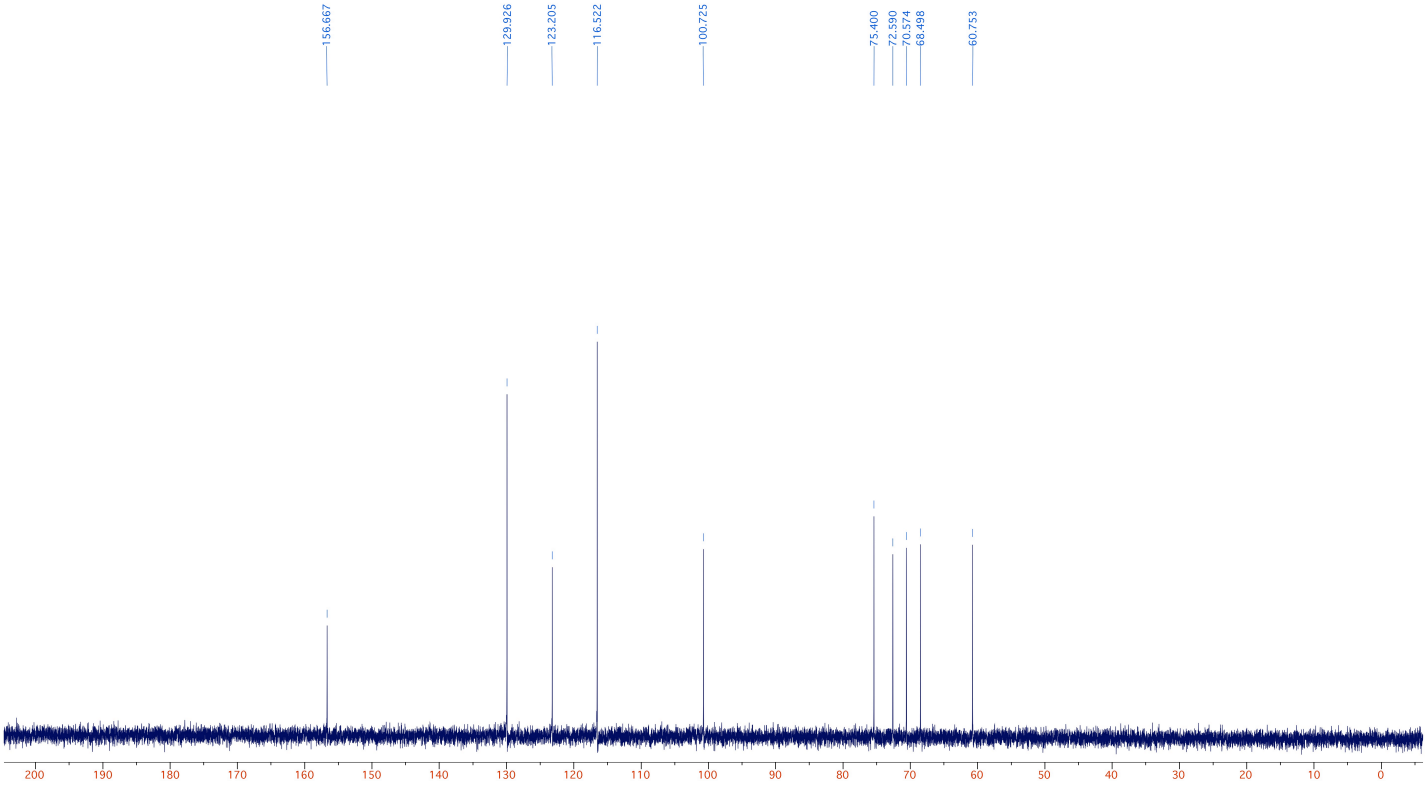
156.667
129.926
123.205
116.522
100.725
75.400
72.590
70.574
68.498
60.753
200
190
180
170
160
150
140
130
120
110
100
90
80
70
60
50
40
30
20
10
0

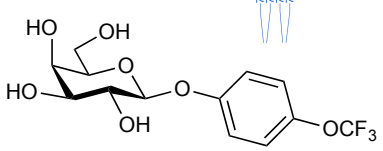
HO
OH
O
HO
O
OH
OCF3

324

7.199
7.177
7.067
7.044
4.926
4.907
3.877
3.869
3.759
3.743
3.728
3.705
3.691
3.686
3.680
3.662
3.657
3.648
3.646
3.642
3.624
3.616
1.01
4.14
1.03
3.9
3.8
3.7
3.6
2.01
2.02
1
1.01
4.14
1.03
ppm 9
8
7
6
5
4
3
2
1
0

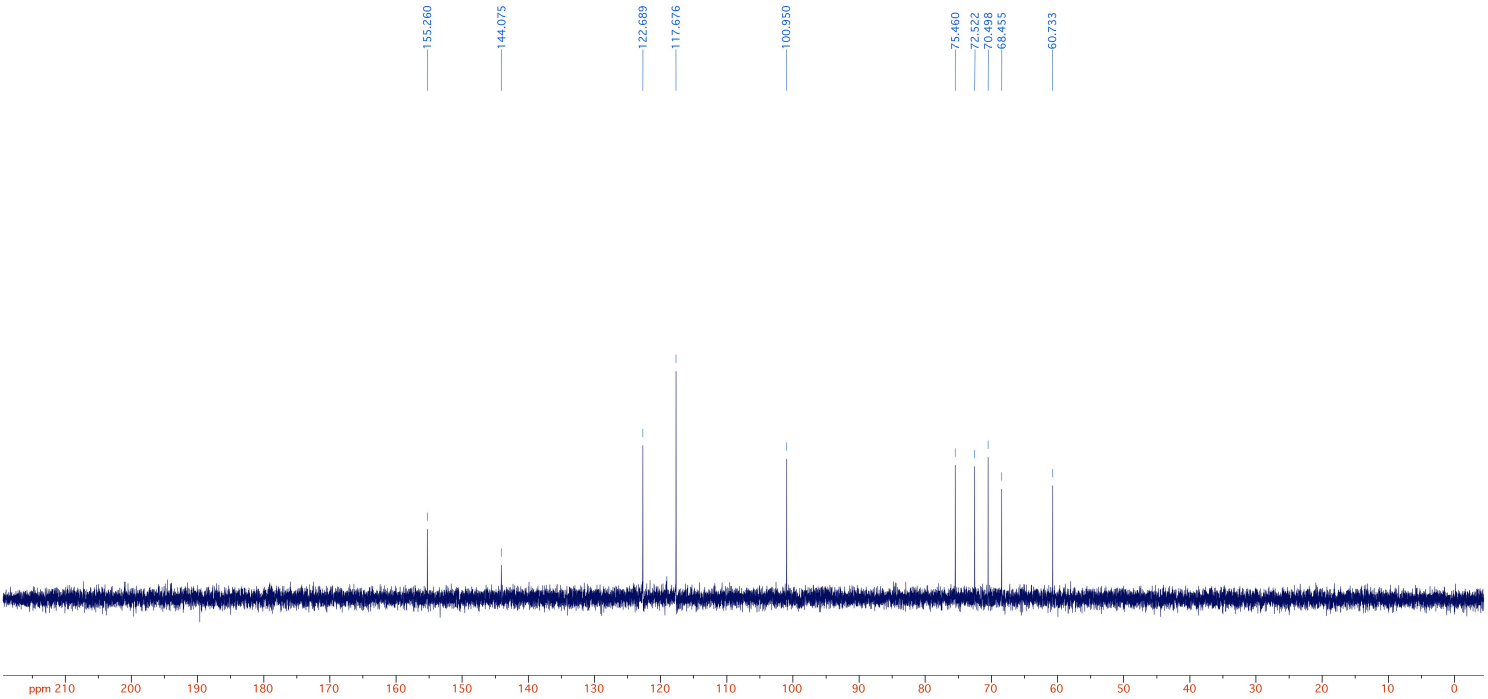
155.260
144.075
122.689
117.676
100.950
75.460
72.522
70.498
68.455
60.733
ppm 210
200
190
180
170
160
150
140
130
120
110
100
90
80
70
60
50
40
30
20
10
0

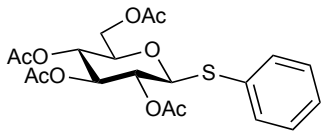
OAc
AcO
AcO
O
S
OAc

333

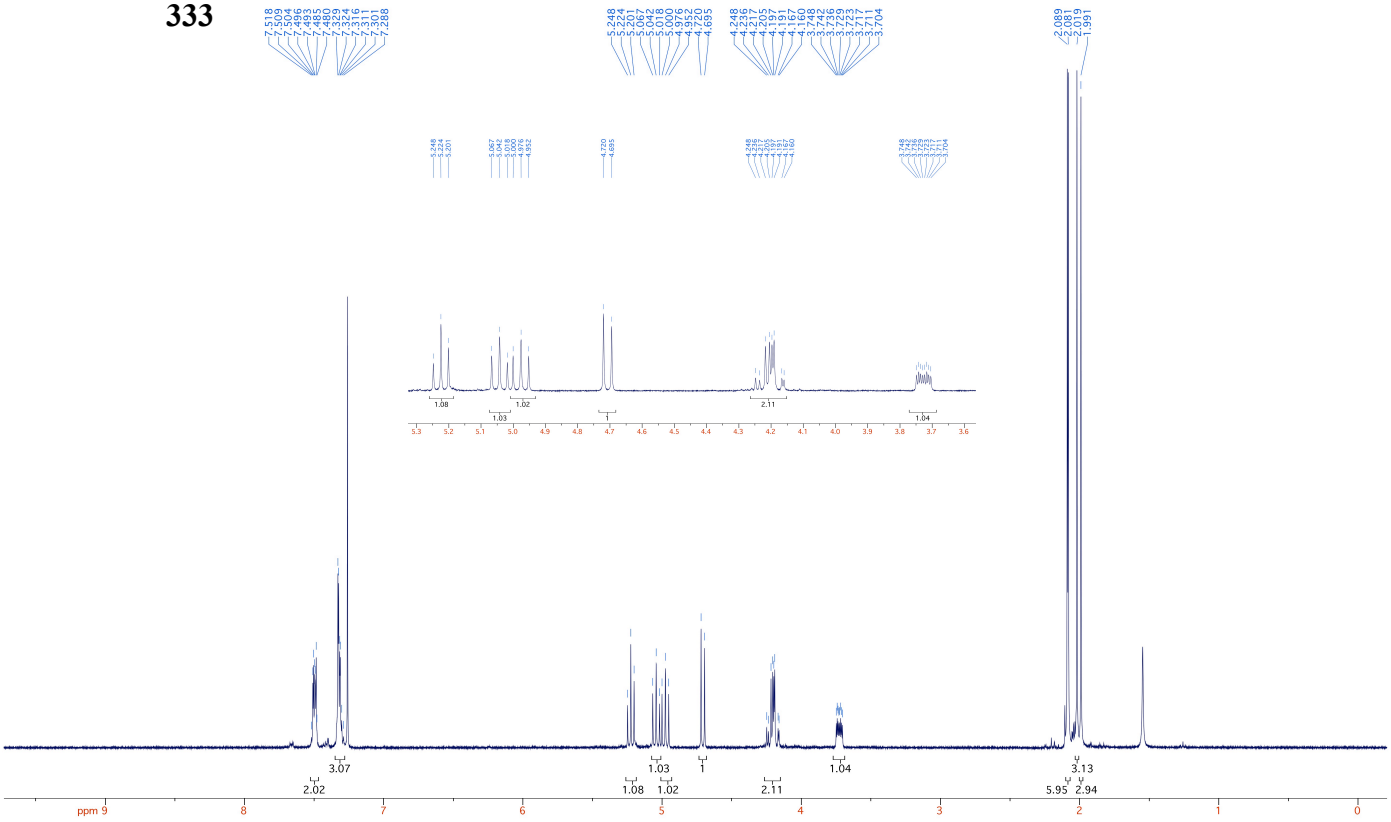
7.518
7.509
7.504
7.496
7.495
7.485
7.465
7.459
7.324
7.316
7.311
7.301
7.288
5.248
5.224
5.220
5.067
5.042
5.008
5.000
4.976
4.932
4.720
4.695
4.248
4.241
4.217
4.205
4.197
4.191
4.167
4.160
3.748
3.742
3.736
3.729
3.723
3.717
3.711
3.704
2.089
2.011
2.009
1.991
3.07
2.02
1.03
1.08
1.02
1
1.04
2.11
3.13
5.95
2.94
ppm 9
8
7
6
5
4
3
2
1
0

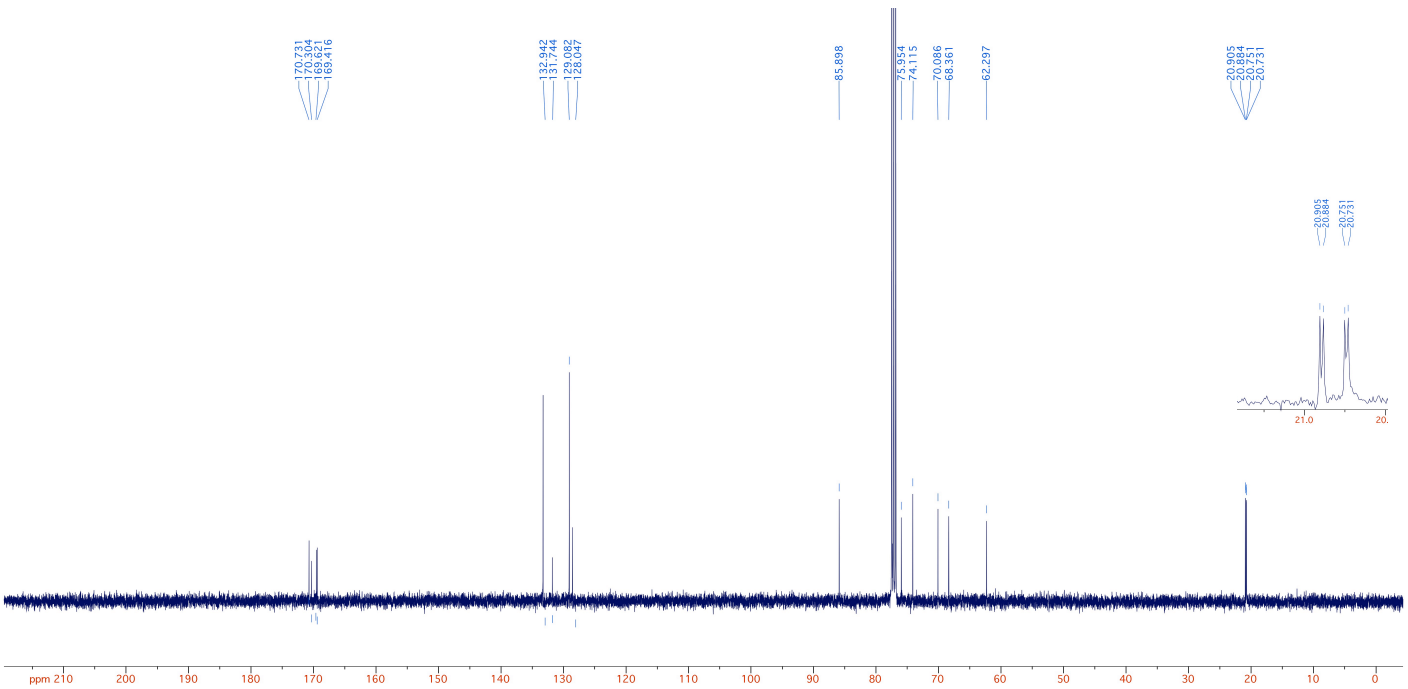
170.731
170.304
169.621
169.416
132.942
131.744
129.082
128.047
85.898
75.354
74.115
70.086
68.361
62.297
20.905
20.884
20.751
20.731
ppm 210
200
190
180
170
160
150
140
130
120
110
100
90
80
70
60
50
40
30
20
10
0

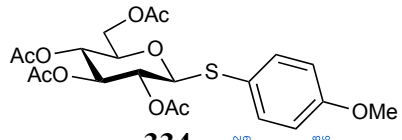
OAc
AcO
AcO
O
S
OAc
OMe

334

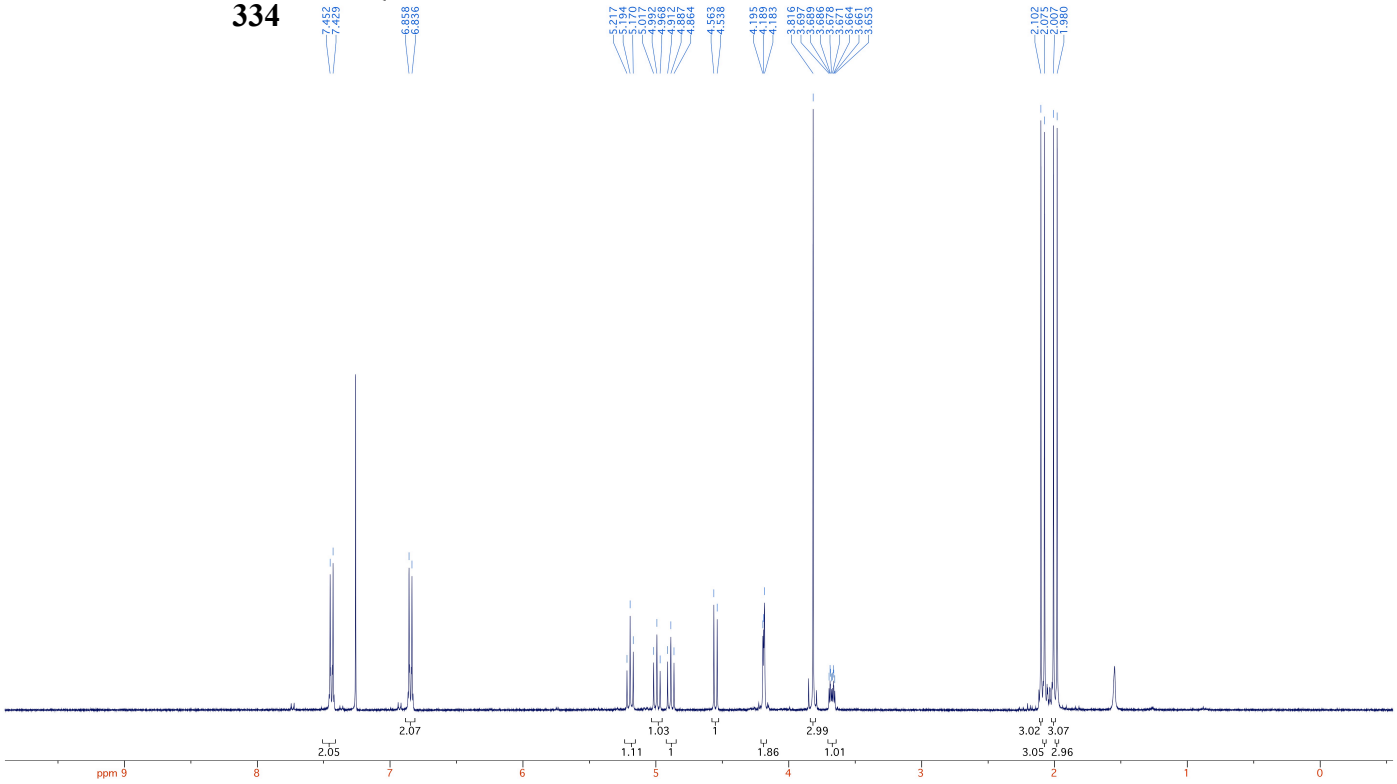
7.452
7.429
6.858
6.836
5.217
5.194
5.170
5.017
4.968
4.912
4.887
4.864
4.563
4.538
4.195
4.180
4.183
3.816
3.697
3.689
3.678
3.676
3.671
3.664
3.661
3.653
2.102
2.075
2.007
1.980
2.07
1.03
1
2.99
3.02
3.07
2.05
1.11
1
1.86
1.01
3.05
2.96
ppm 9
8
7
6
5
4
3
2
1
0

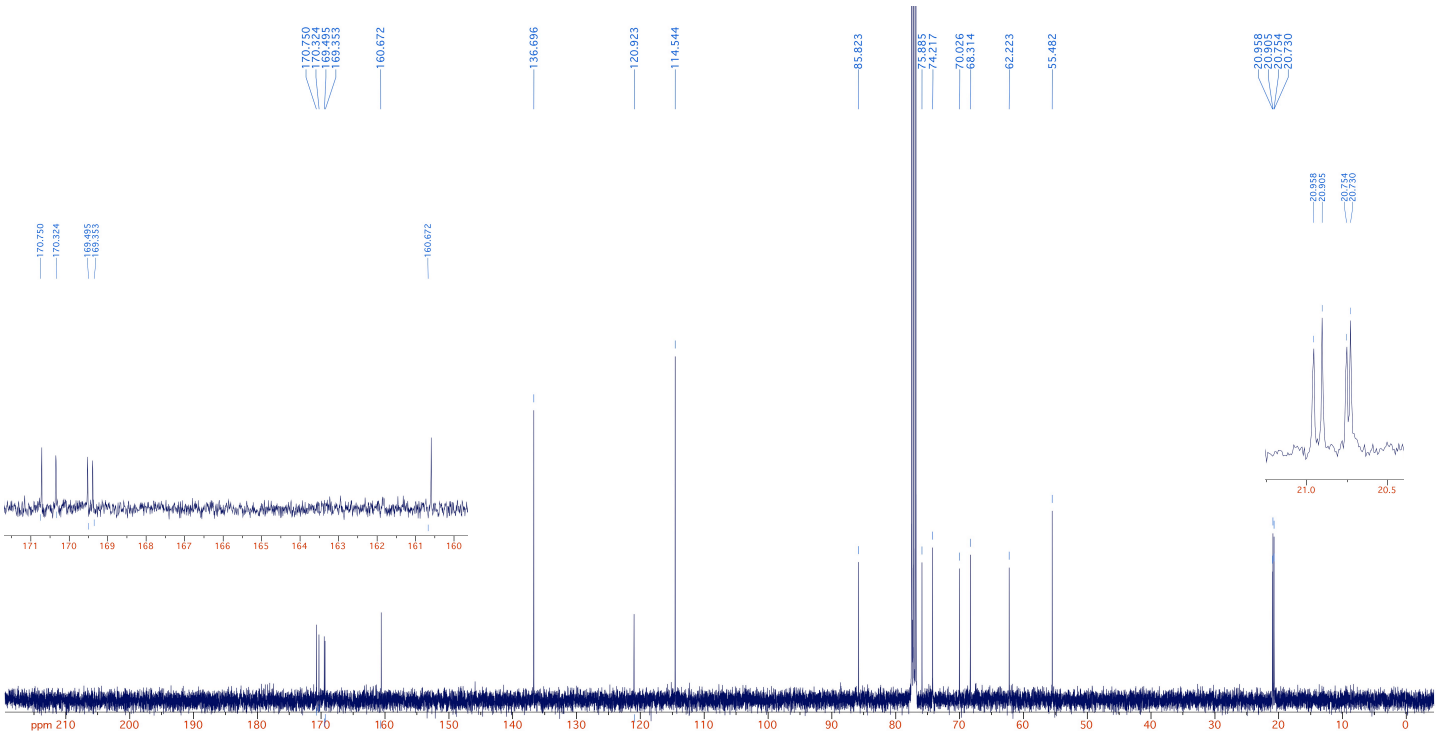
170.750
170.324
169.495
169.353
160.672
136.696
120.923
114.544
85.823
75.885
74.217
70.026
68.314
62.223
55.482
20.958
20.905
20.754
20.730
ppm 210
200
190
180
170
160
150
140
130
120
110
100
90
80
70
60
50
40
30
20
10
0

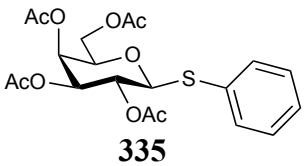

335

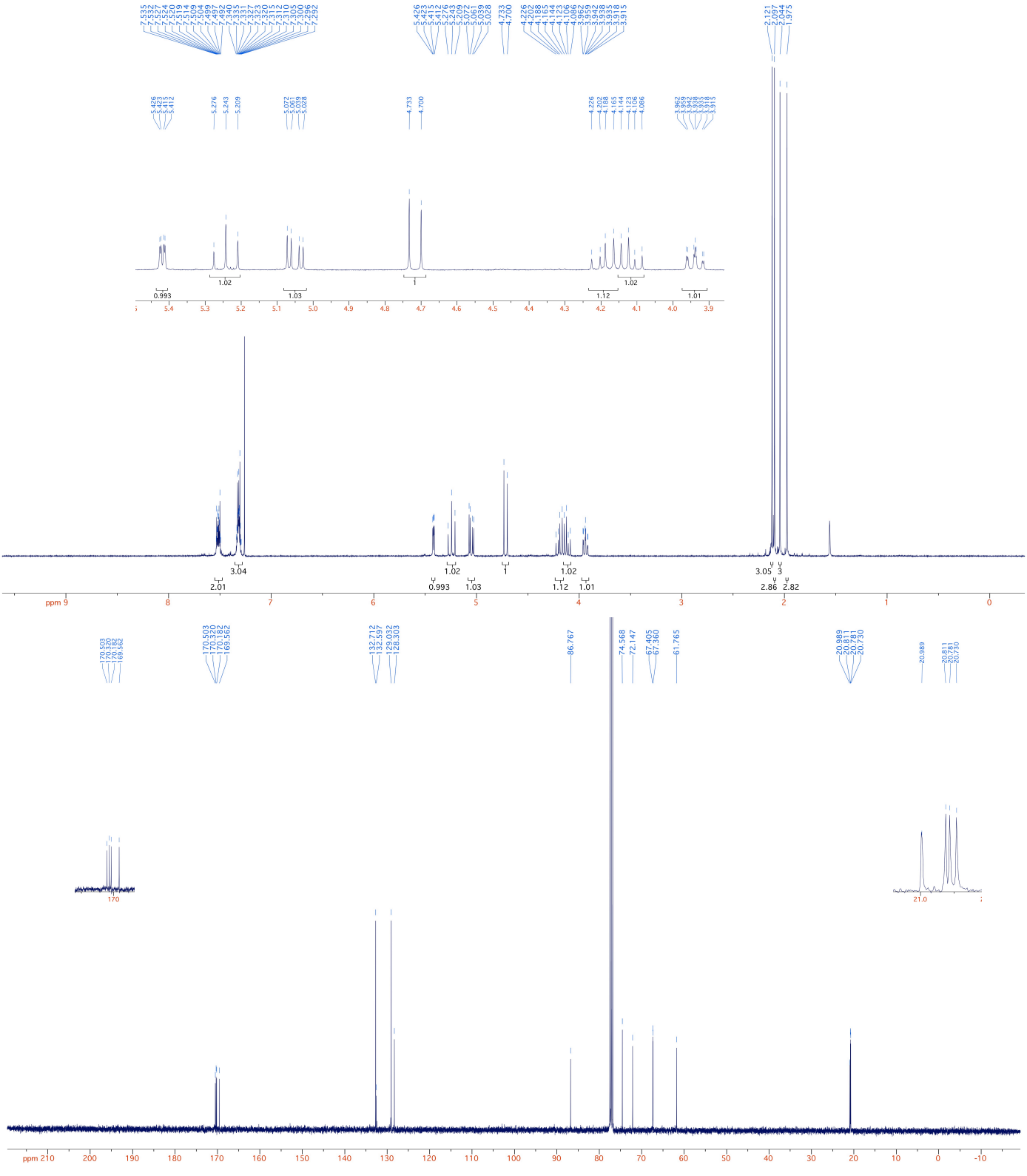

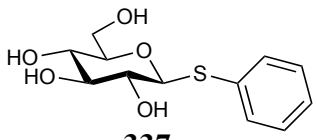
OH
HO
HO
O
S
OH

337

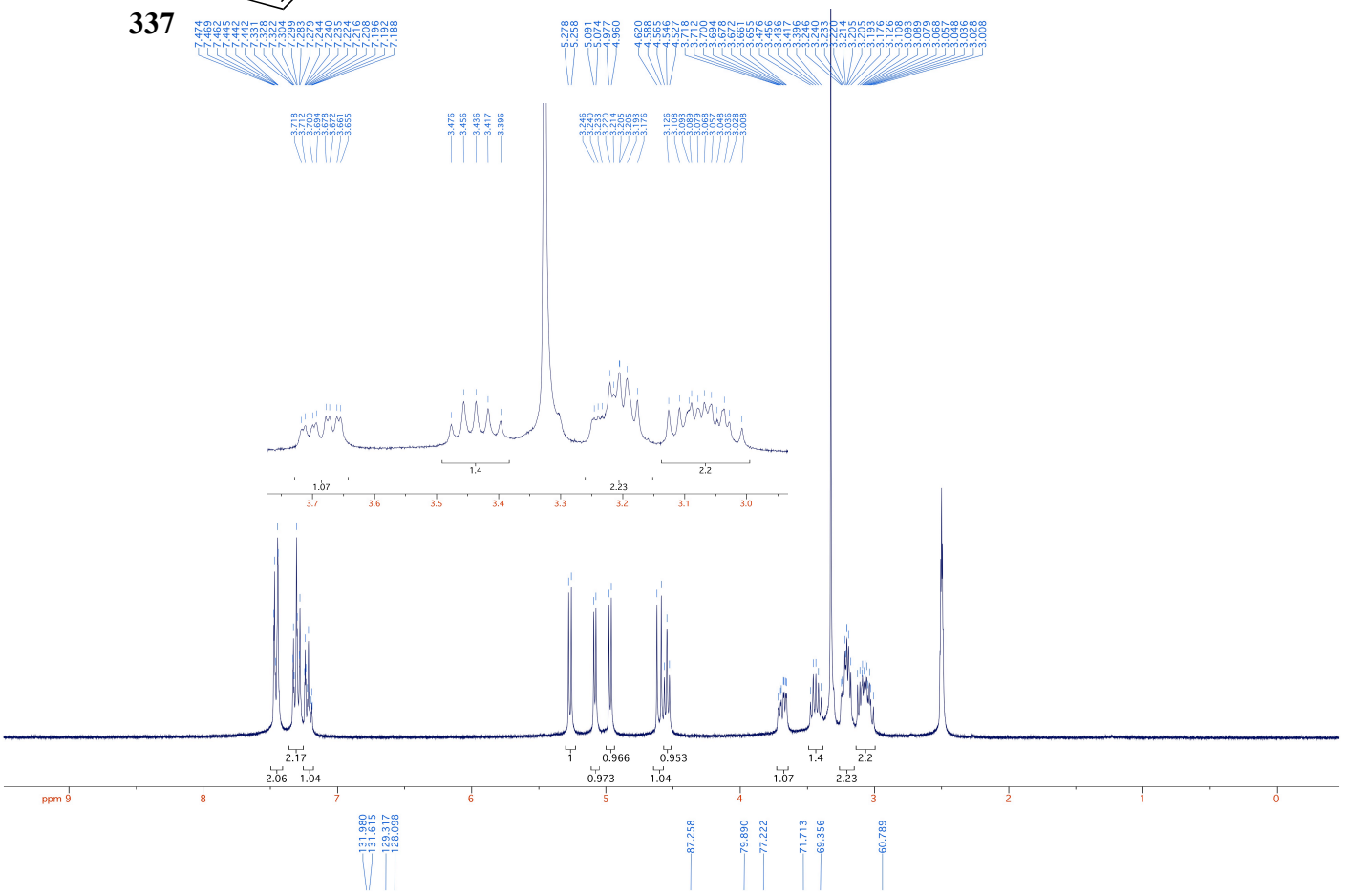
ppm 9
8
7
6
5
4
3
2
1
0

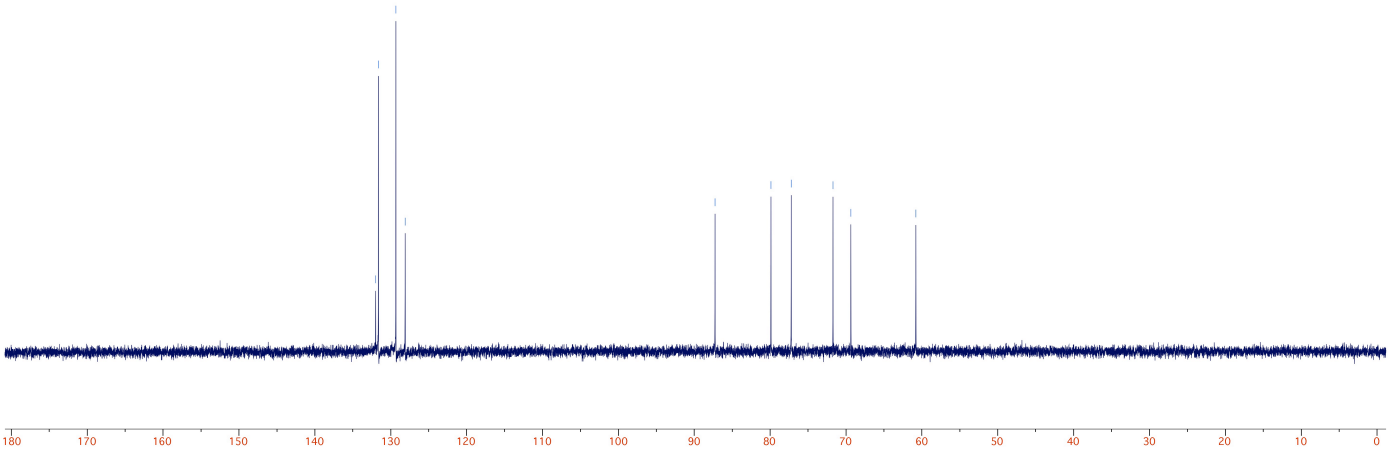
180
170
160
150
140
130
120
110
100
90
80
70
60
50
40
30
20
10
0

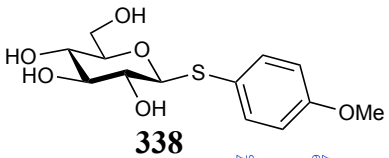
OH
HO
O
HO
S
OH
OMe

338

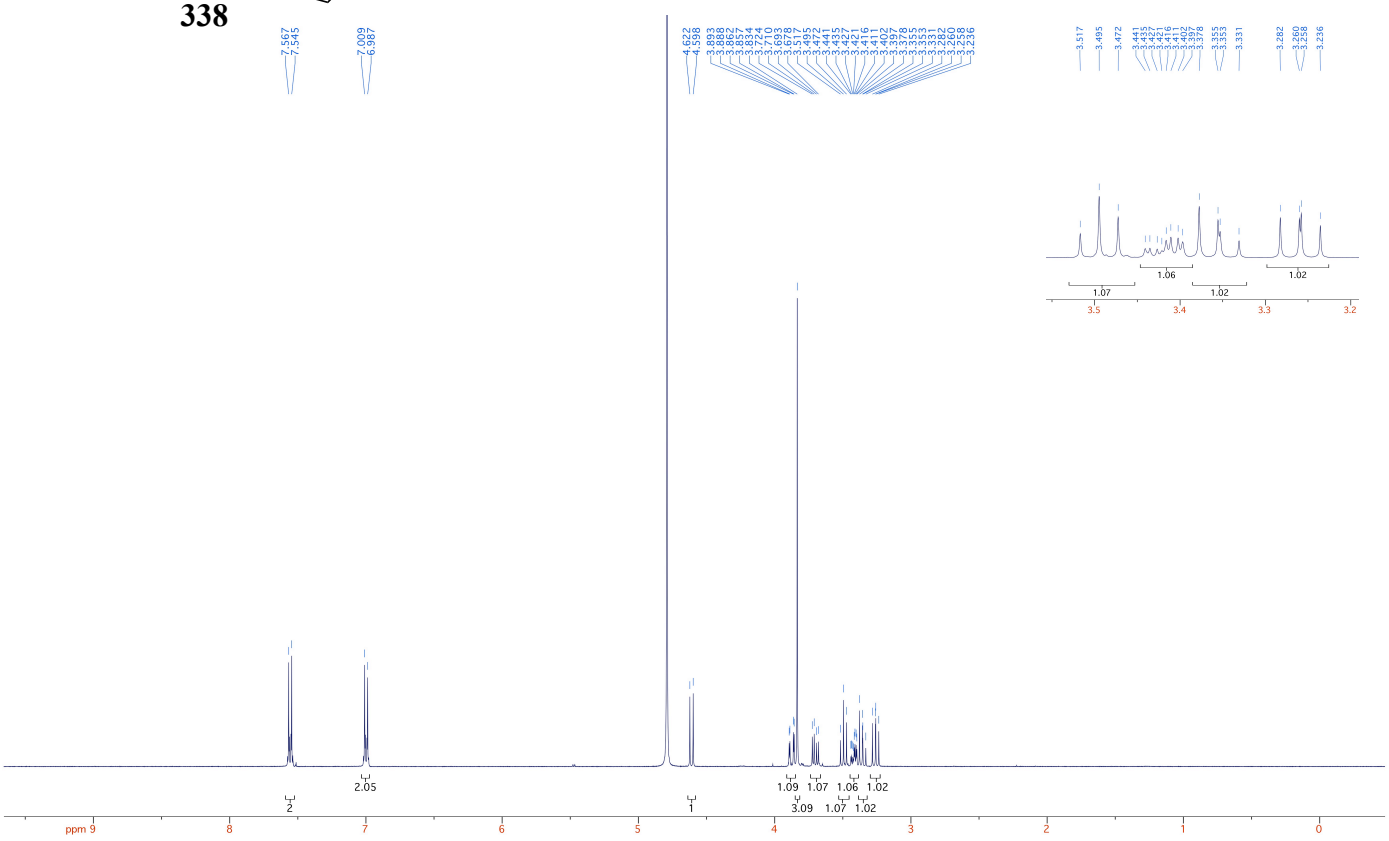
7.567
7.545
7.009
6.987
4.622
4.598
3.893
3.868
3.857
3.834
3.774
3.710
3.693
3.517
3.495
3.472
3.441
3.435
3.427
3.421
3.416
3.411
3.397
3.378
3.355
3.353
3.331
3.282
3.260
3.258
3.236
1.06
1.07
1.02
3.5
3.4
3.3
3.2
2.05
1.09
1.07
1.06
1.02
3.09
1.07
1.02
ppm 9
8
7
6
5
4
3
2
1
0

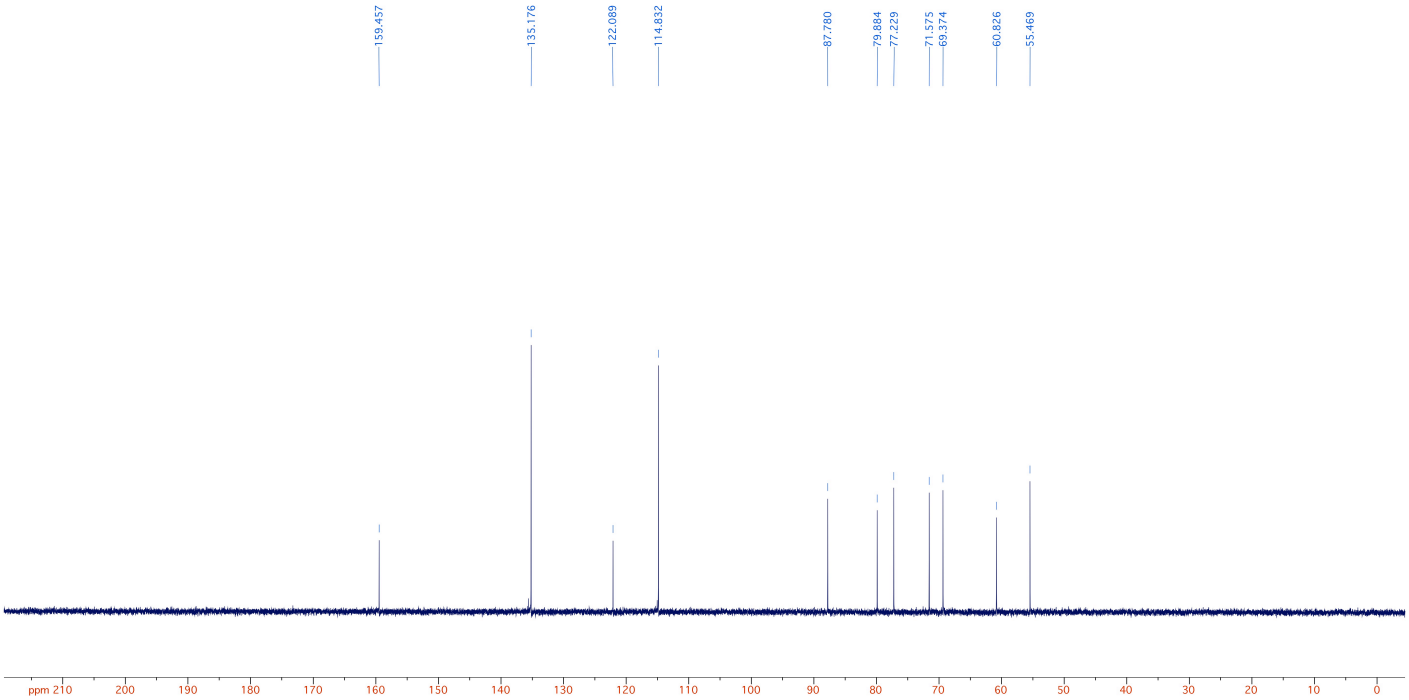
159.457
135.176
122.089
114.832
87.780
79.884
77.229
71.575
69.374
60.826
55.469
ppm 210
200
190
180
170
160
150
140
130
120
110
100
90
80
70
60
50
40
30
20
10
0

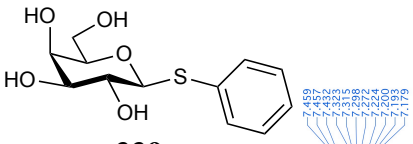
HO
OH
O
HO
S
OH

339

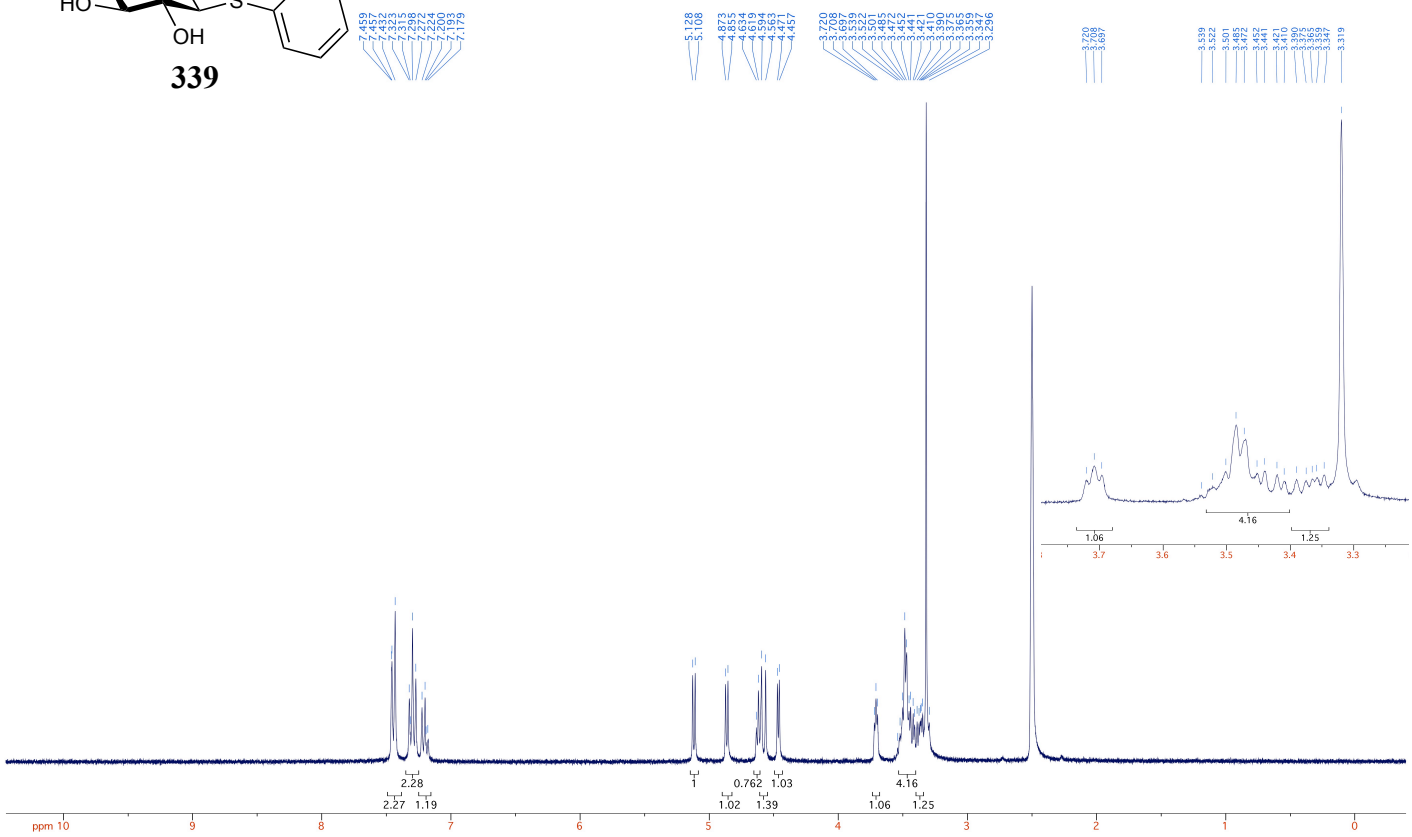
7.459
7.457
7.432
7.333
7.315
7.298
7.224
7.204
7.200
7.193
7.179
5.128
5.108
4.873
4.855
4.634
4.619
4.594
4.573
4.471
4.457
3.720
3.708
3.697
3.689
3.522
3.501
3.475
3.452
3.441
3.421
3.410
3.390
3.375
3.365
3.359
3.347
3.296
3.720
3.708
3.697
3.689
3.539
3.522
3.501
3.485
3.472
3.452
3.441
3.421
3.410
3.390
3.375
3.365
3.359
3.347
3.319
2.28
2.27
1.19
1
0.762
1.02
1.03
1.39
4.16
1.06
1.25
4.16
1.06
1.25
ppm 10
9
8
7
6
5
4
3
2
1
0
3.7
3.6
3.5
3.4
3.3

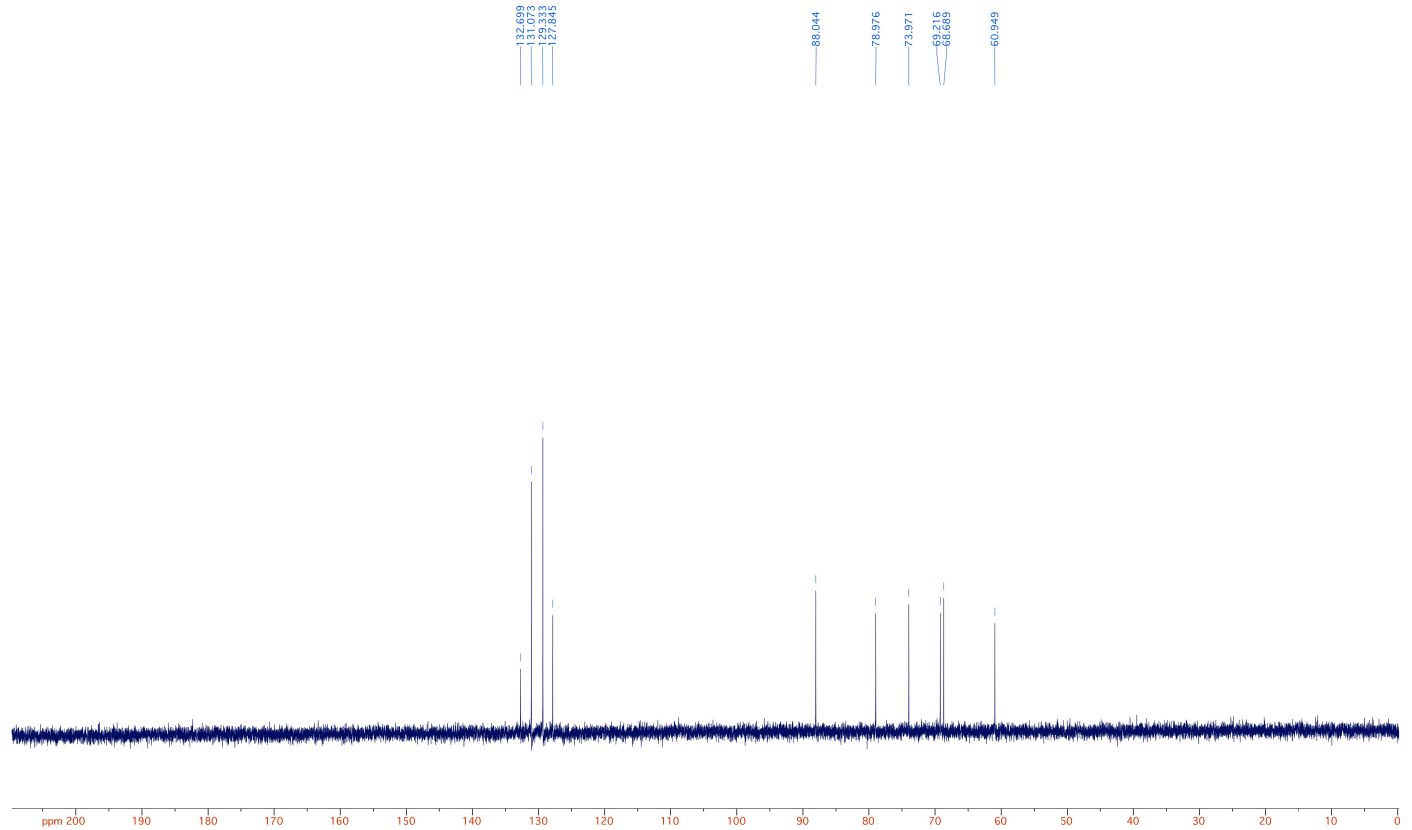
132.699
131.773
129.333
127.845
88.044
78.976
73.971
69.216
68.689
60.949
ppm 200
190
180
170
160
150
140
130
120
110
100
90
80
70
60
50
40
30
20
10
0

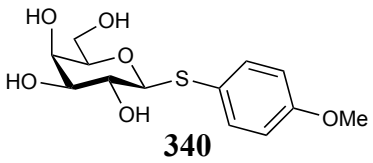
HO
OH
O
HO
S
OH
OMe

340

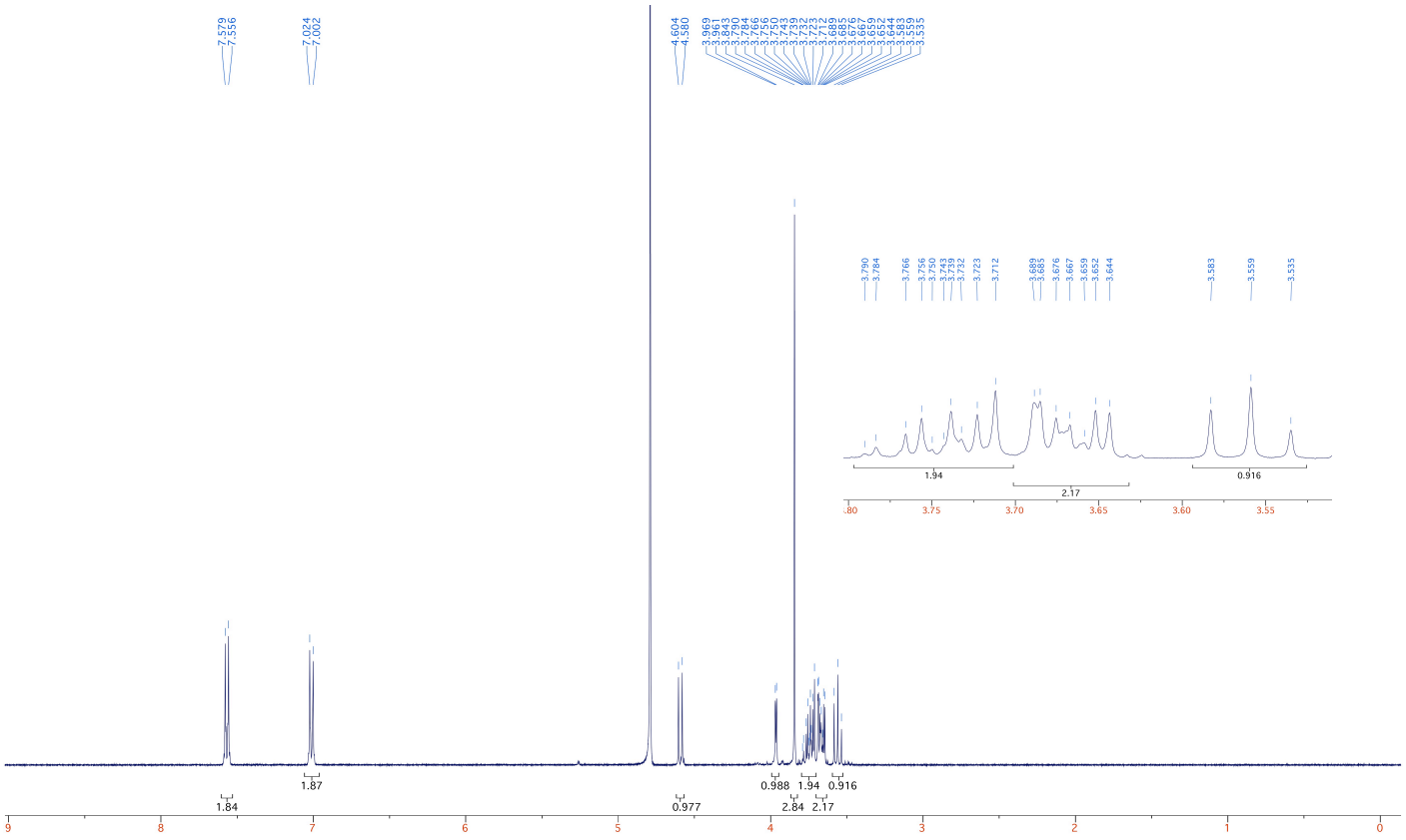
7.579
7.556
7.024
7.002
4.604
4.580
3.969
3.961
3.943
3.790
3.784
3.766
3.756
3.750
3.743
3.739
3.732
3.723
3.712
3.689
3.685
3.676
3.667
3.659
3.652
3.644
3.583
3.559
3.535
1.84
1.87
0.977
0.988
1.94
0.916
2.84
2.17
1.94
2.17
0.916

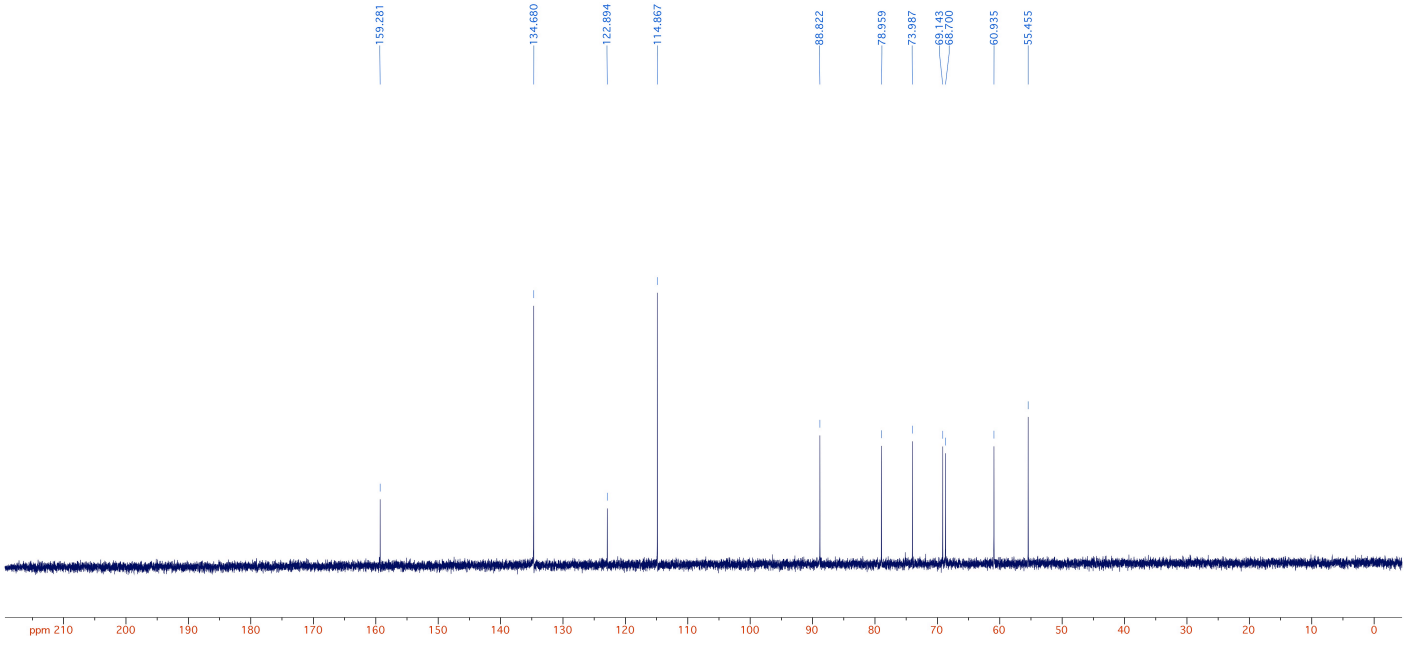
159.281
134.680
122.894
114.867
88.822
78.959
73.987
69.143
68.700
60.935
55.455

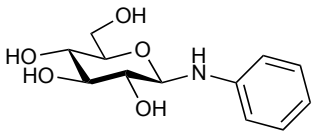

341

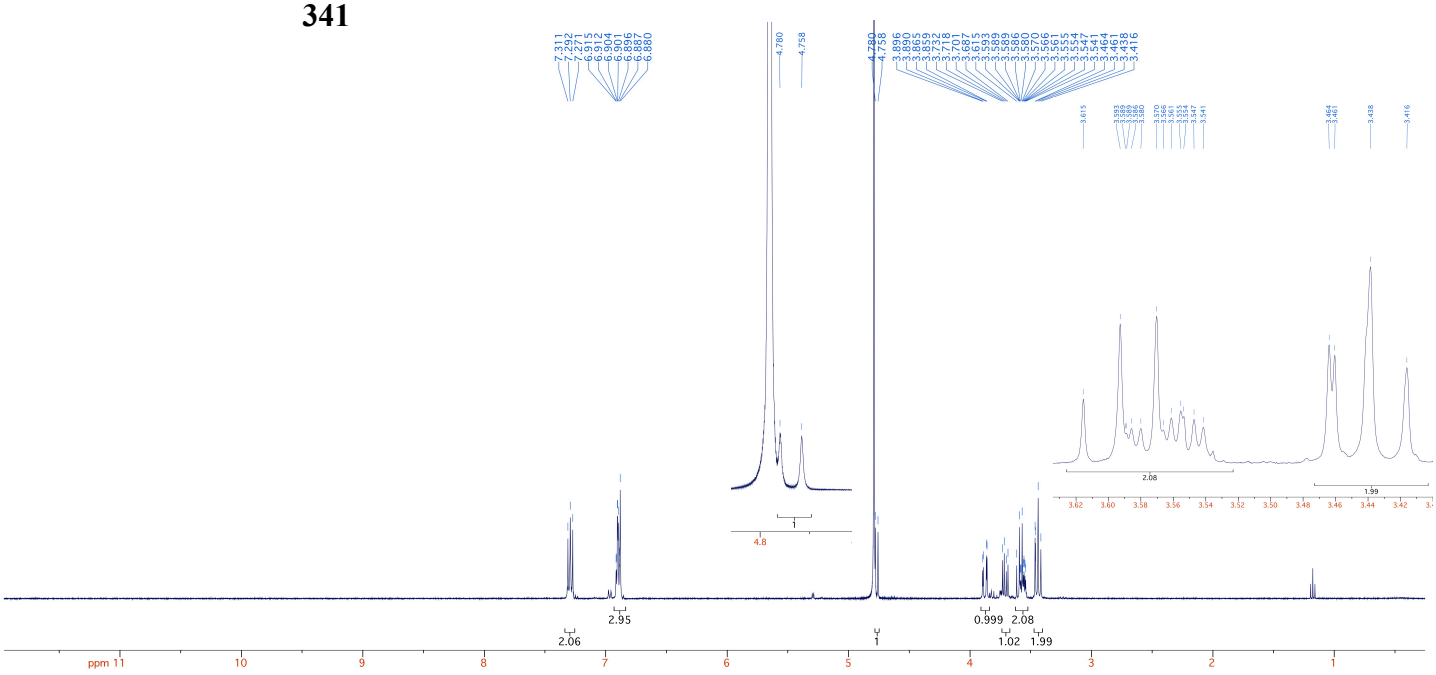

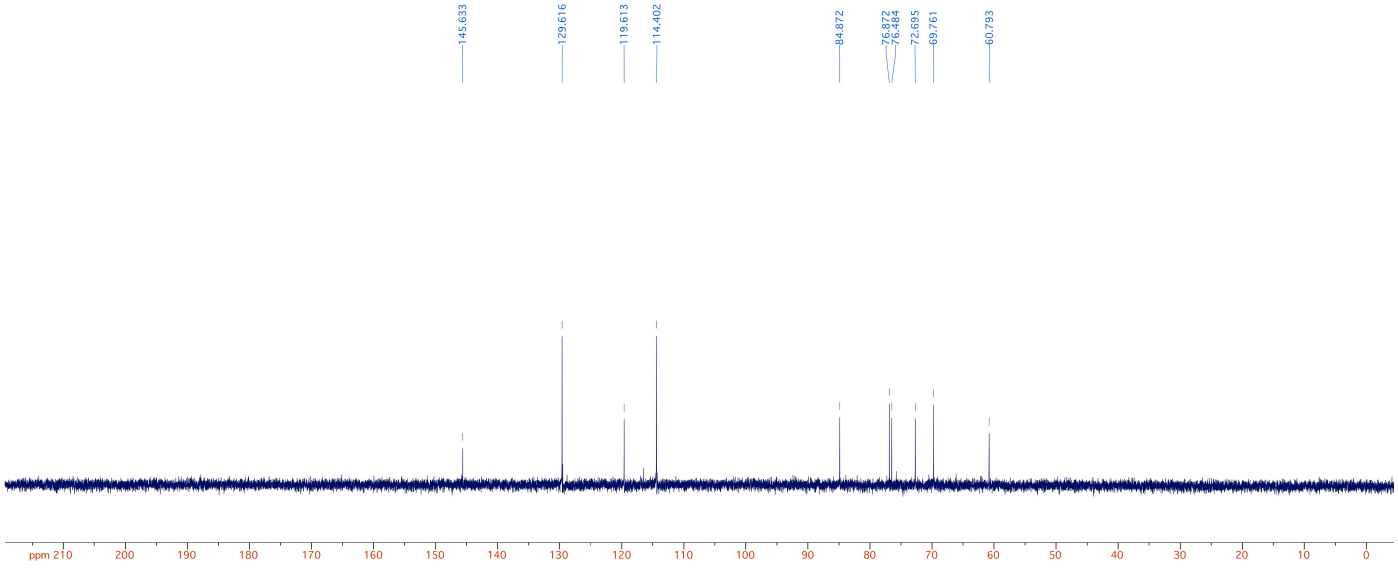

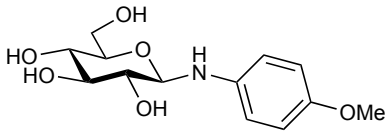
OH
HO
HO
O
H
N
OH
OMe

342

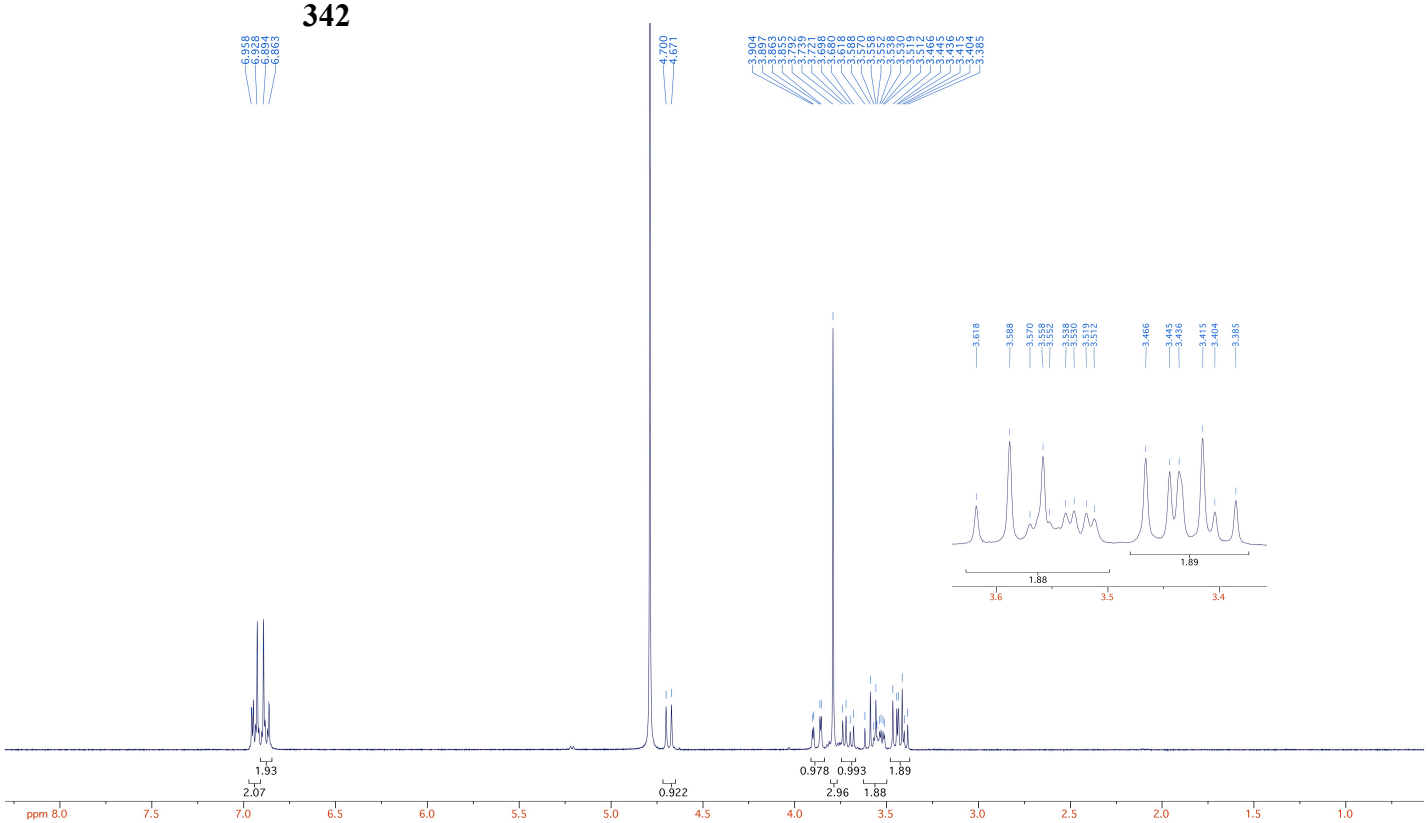
6.958
6.928
6.894
6.863
4.700
4.671
3.804
3.687
3.663
3.655
3.552
3.739
3.721
3.680
3.660
3.618
3.588
3.570
3.558
3.552
3.538
3.530
3.519
3.512
3.466
3.445
3.436
3.415
3.404
3.385
1.93
2.07
0.922
0.978
0.993
2.96
1.88
1.89
ppm 8.0
7.5
7.0
6.5
6.0
5.5
5.0
4.5
4.0
3.5
3.0
2.5
2.0
1.5
1.0

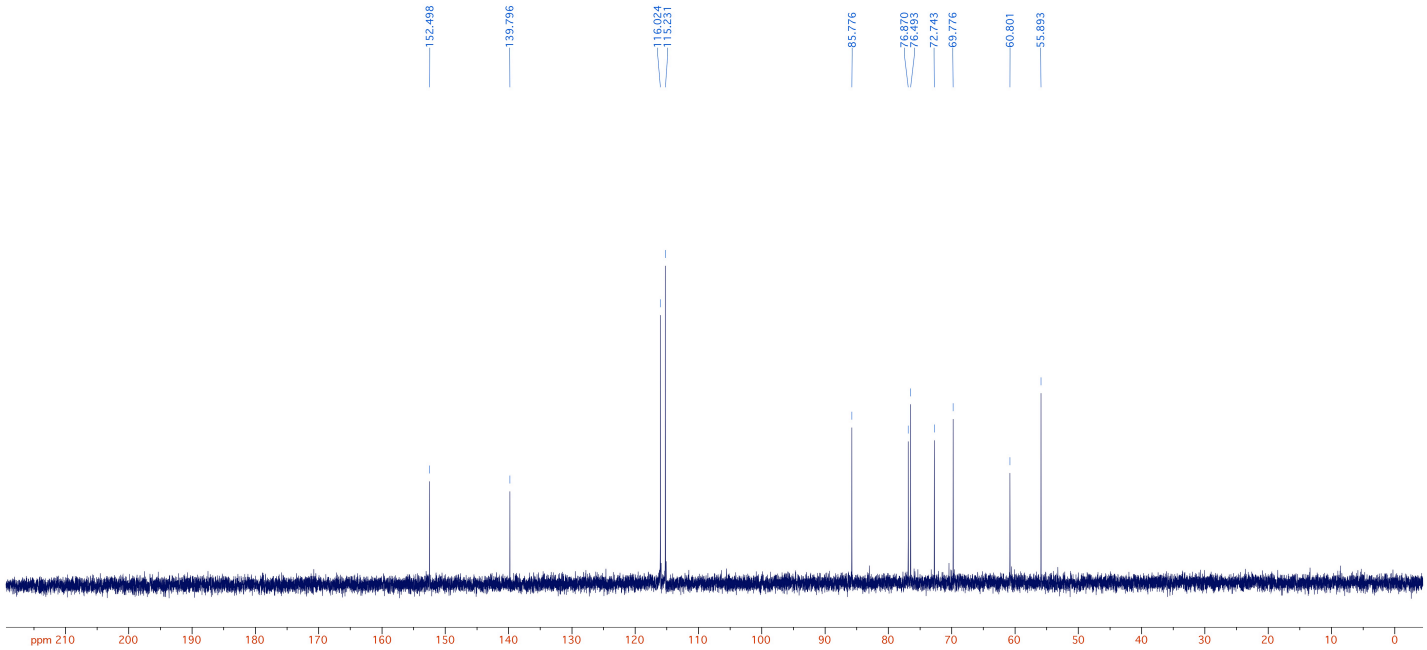
152.498
139.796
116.024
115.231
85.776
76.870
76.493
72.743
69.776
60.801
55.893
ppm 210
200
190
180
170
160
150
140
130
120
110
100
90
80
70
60
50
40
30
20
10
0

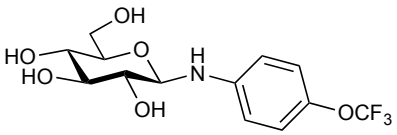
OH
HO
HO
O
H
N
OH
OCF3

343

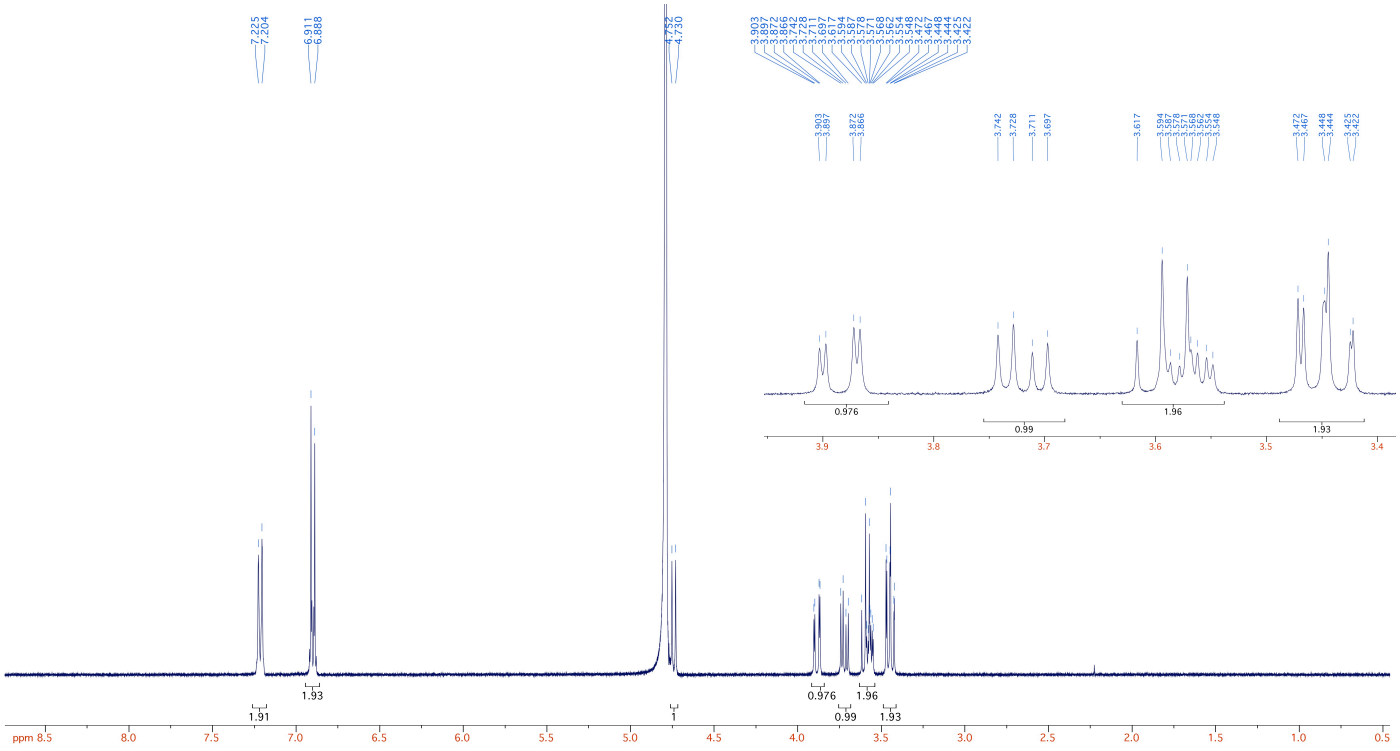
7.225
7.204
6.911
6.888
4.732
4.730
3.903
3.897
3.872
3.866
3.742
3.728
3.711
3.697
3.617
3.594
3.587
3.578
3.571
3.568
3.562
3.554
3.548
3.472
3.467
3.448
3.444
3.425
3.422
0.976
0.99
1.96
1.93
1.91
1.93
1
0.976
0.99
1.96
1.93
ppm 8.5
8.0
7.5
7.0
6.5
6.0
5.5
5.0
4.5
4.0
3.5
3.0
2.5
2.0
1.5
1.0
0.5
3.9
3.8
3.7
3.6
3.5
3.4

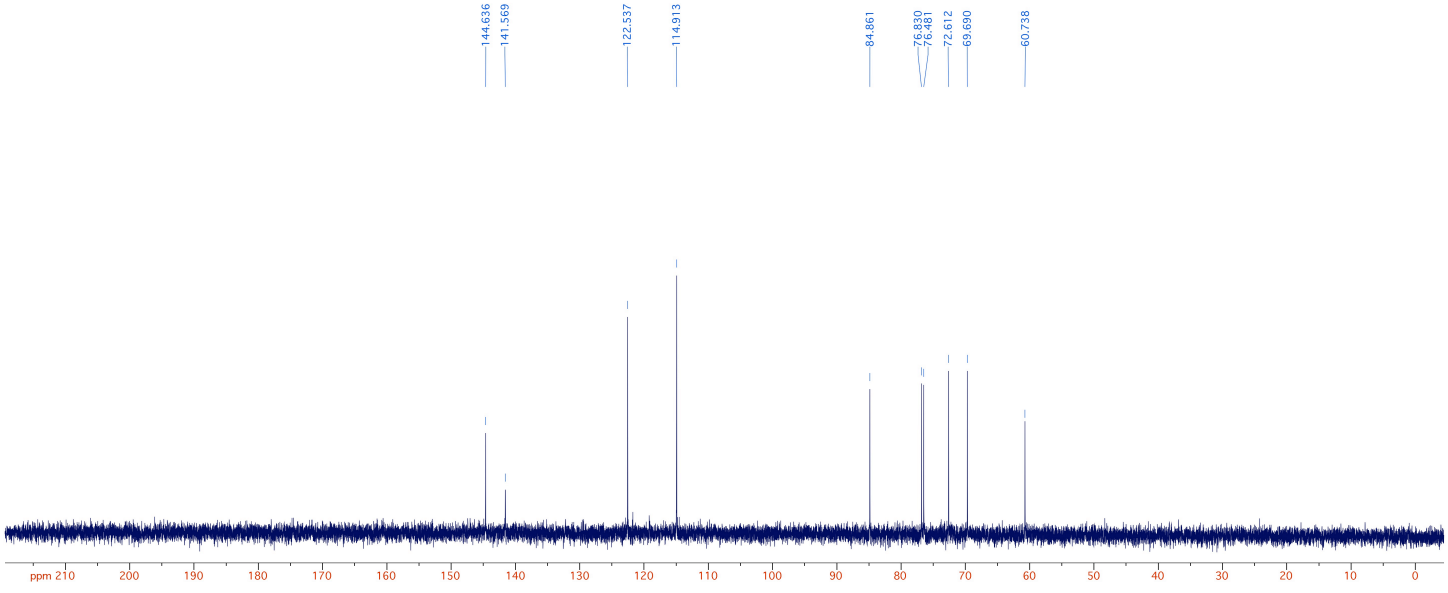
144.636
141.569
122.537
114.913
84.861
76.830
76.481
72.612
69.690
60.738
ppm 210
200
190
180
170
160
150
140
130
120
110
100
90
80
70
60
50
40
30
20
10
0

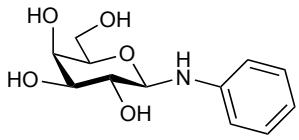
HO
OH
O
H
N
HO
OH

344

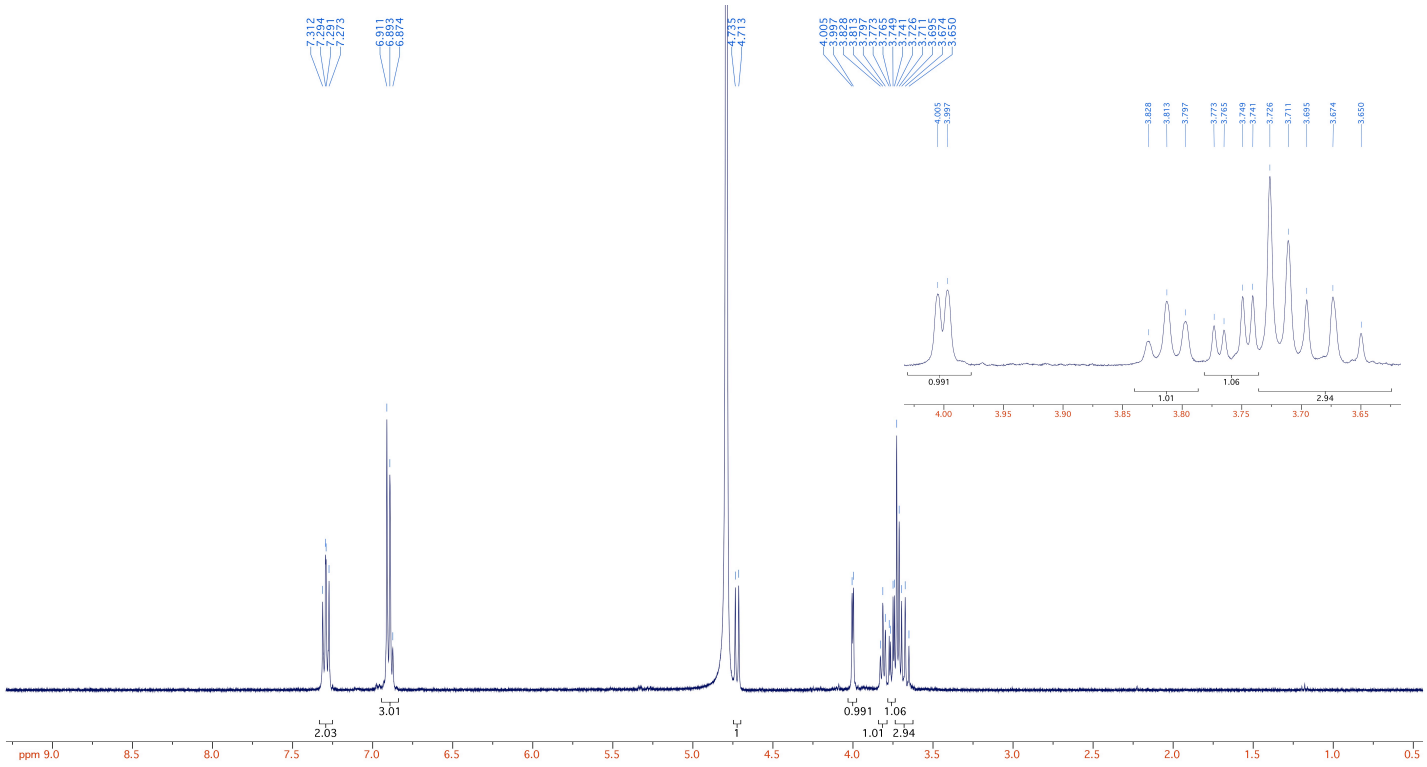
7.312
7.294
7.291
7.273
6.911
6.893
6.874
4.735
4.713
4.005
3.997
3.828
3.813
3.797
3.773
3.765
3.749
3.741
3.726
3.711
3.695
3.674
3.650
2.03
3.01
1
0.991
1.01
1.06
2.94
ppm 9.0
8.5
8.0
7.5
7.0
6.5
6.0
5.5
5.0
4.5
4.0
3.5
3.0
2.5
2.0
1.5
1.0
0.5

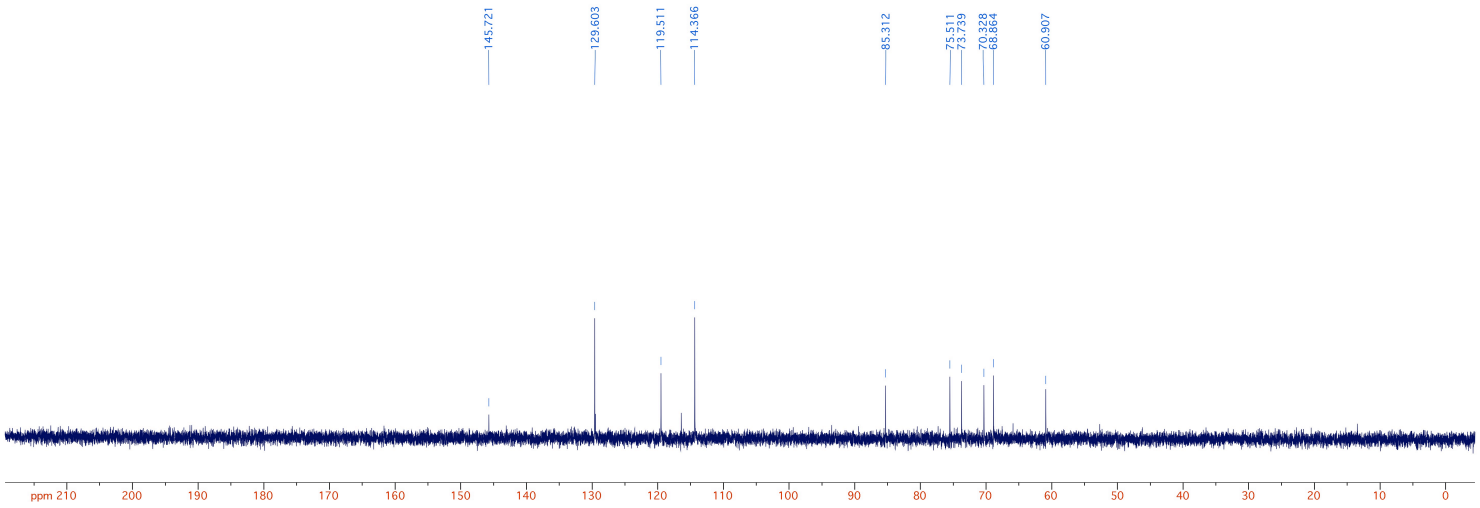
145.721
129.603
119.511
114.366
85.312
75.511
73.739
70.328
68.864
60.907
ppm 210
200
190
180
170
160
150
140
130
120
110
100
90
80
70
60
50
40
30
20
10
0

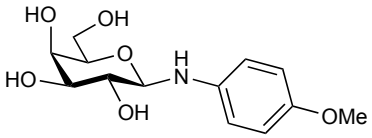
HO
OH
O
H
N
HO
OH
OMe

345

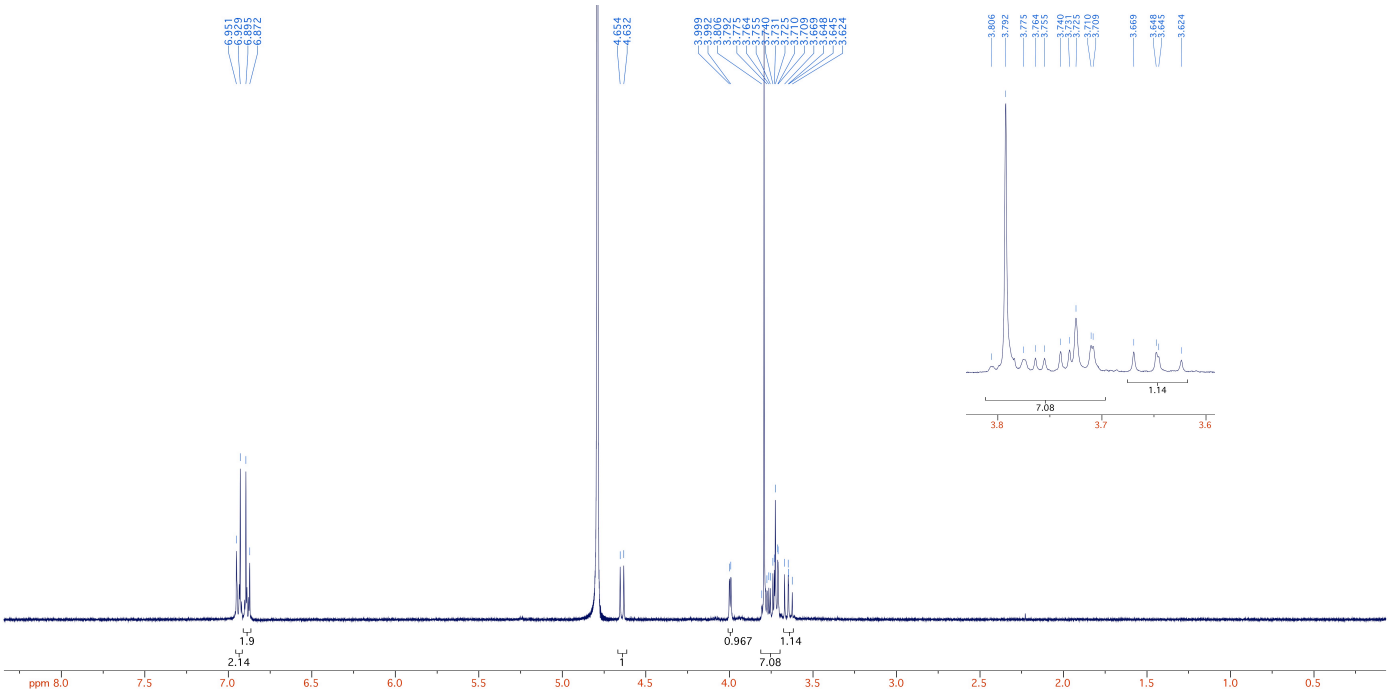
6.951
6.929
6.895
6.872
4.654
4.632
3.999
3.902
3.866
3.792
3.775
3.754
3.740
3.731
3.710
3.709
3.669
3.648
3.645
3.624
3.806
3.792
3.775
3.764
3.755
3.740
3.731
3.721
3.710
3.709
3.669
3.648
3.645
3.624
1.14
7.08
3.8
3.7
3.6
1.9
2.14
1
0.967
7.08
1.14
ppm 8.0
7.5
7.0
6.5
6.0
5.5
5.0
4.5
4.0
3.5
3.0
2.5
2.0
1.5
1.0
0.5

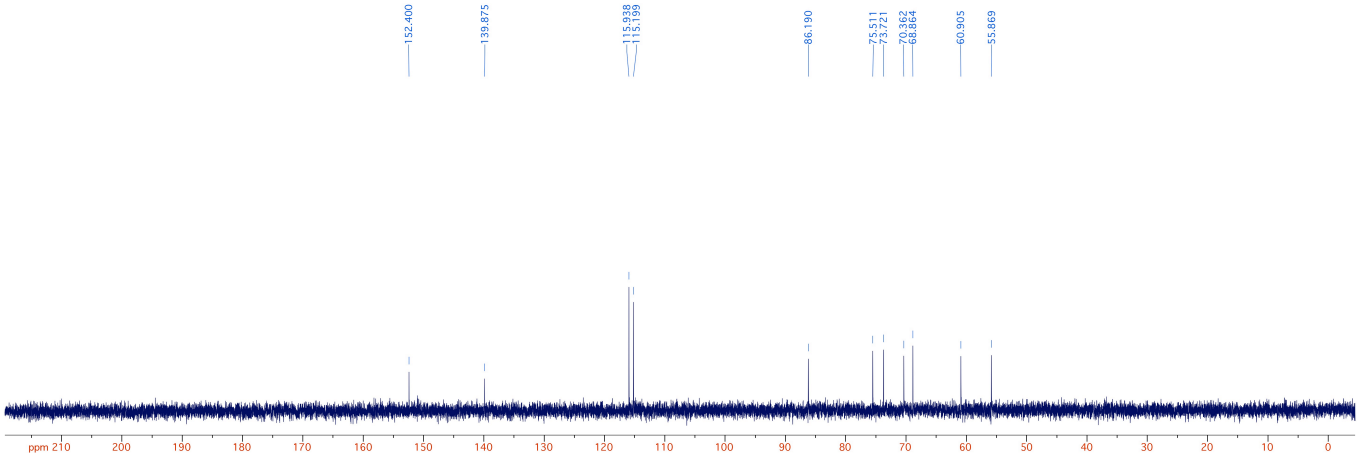
152.400
139.875
115.938
115.199
86.190
75.511
73.721
70.362
68.864
60.905
55.869
ppm 210
200
190
180
170
160
150
140
130
120
110
100
90
80
70
60
50
40
30
20
10
0

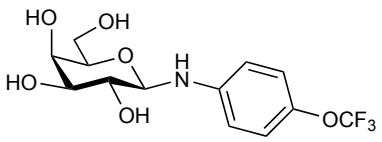
HO
OH
O
H
N
HO
OH
OCF3

346

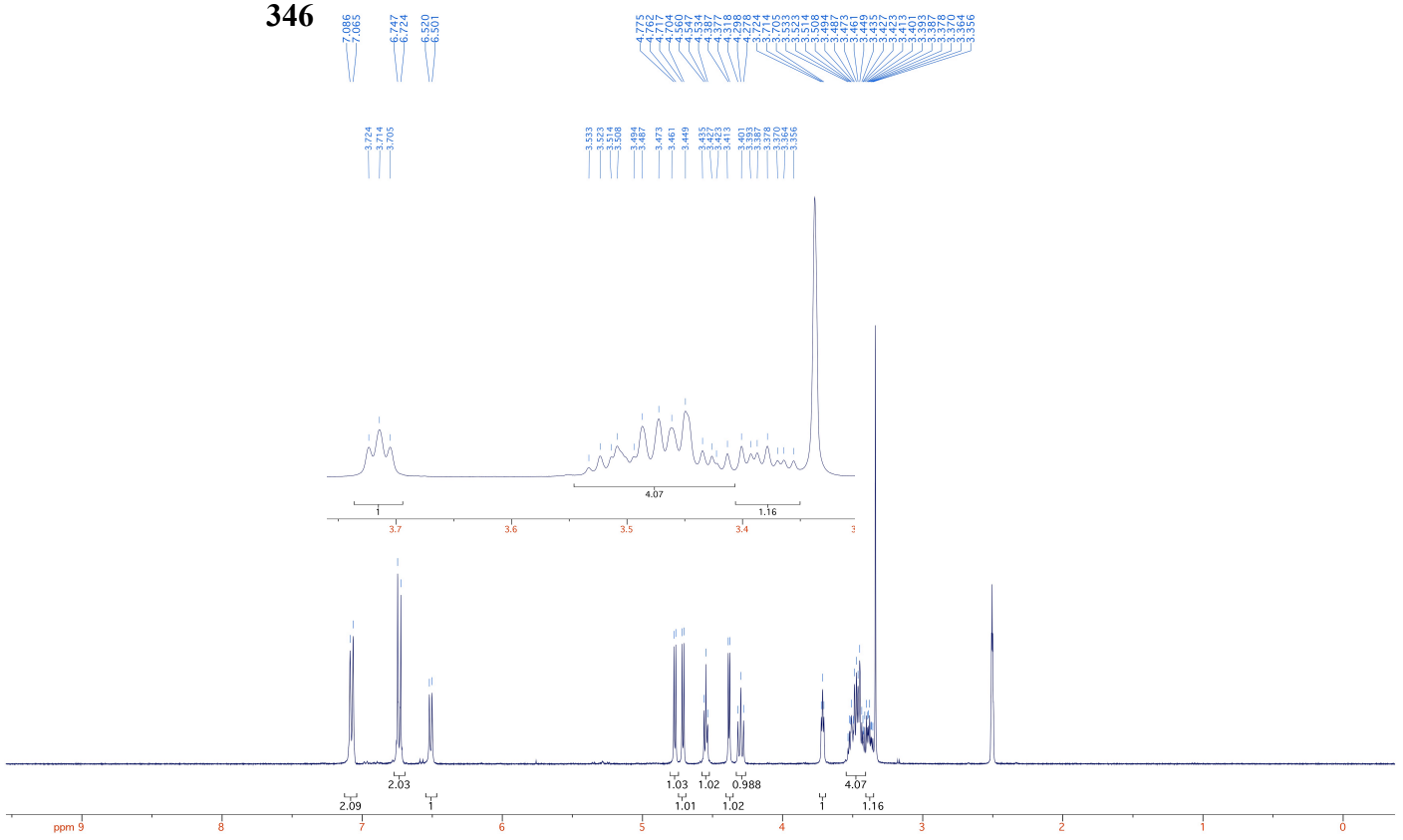
7.086
7.065
6.747
6.724
6.520
6.501
4.775
4.762
4.717
4.704
4.560
4.547
4.534
4.387
4.377
4.318
4.298
4.278
3.724
3.714
3.705
3.533
3.523
3.514
3.508
3.494
3.487
3.473
3.461
3.449
3.435
3.427
3.423
3.413
3.401
3.393
3.387
3.378
3.370
3.364
3.356
4.07
1
1.16
2.09
2.03
1
1.03
1.02
0.988
1.01
1.02
1
4.07
1.16
ppm 9
8
7
6
5
4
3
2
1
0

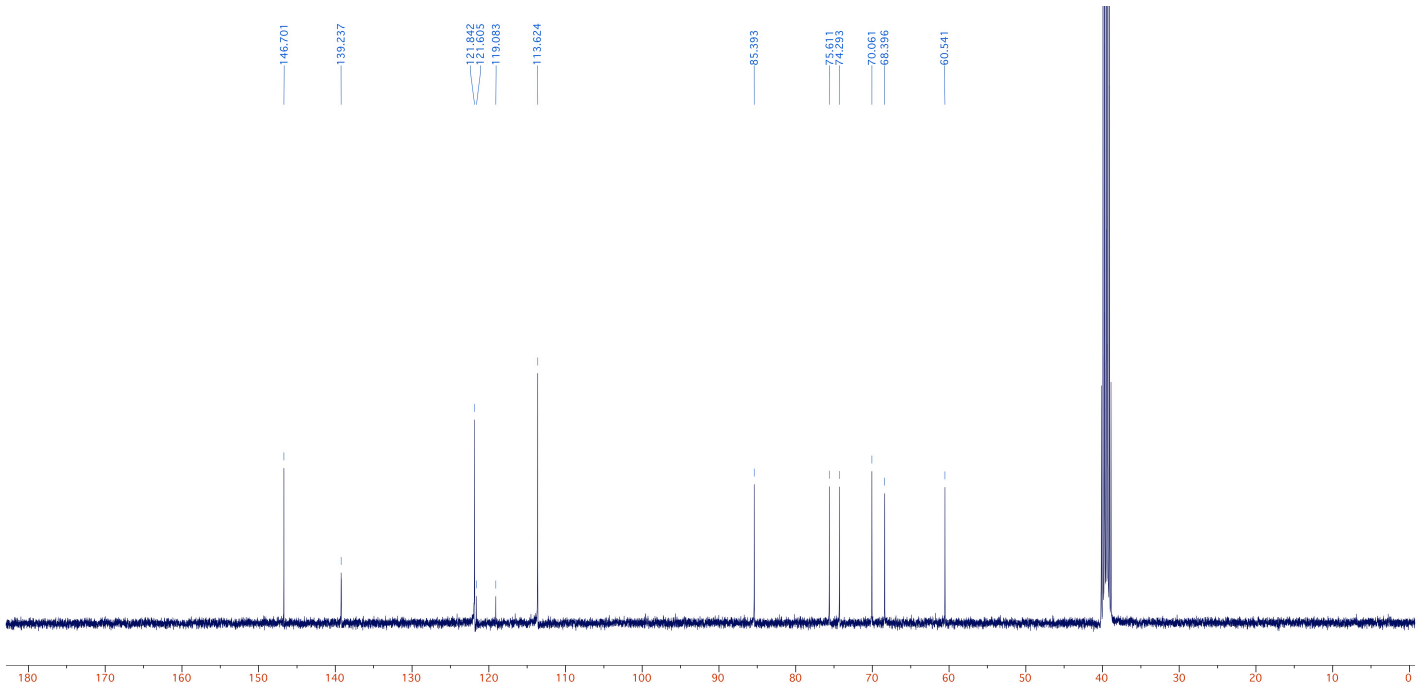
146.701
139.237
121.842
121.605
119.083
113.624
85.393
75.611
74.293
70.061
68.396
60.541
180
170
160
150
140
130
120
110
100
90
80
70
60
50
40
30
20
10
0

3.9 References

(1) Tam, R. Y.; Ferreira, S. S.; Czechura, P.; Chaytor, J. L.; Ben, R. N. *J. Am. Chem. Soc.* **2008**, *130*, 17494–17501.

(2) Chaytor, J. L.; Tokarew, J. M.; Wu, L. K.; Leclère, M.; Tam, R. Y.; Capicciotti, J.; Guolla, L.; von Moos, E.; Findlay, C. S.; Allan, D. S.; Ben, R. N. *Glycobiology* **2012**, *22* (1), 123–133.

(3) Capicciotti, C. J.; Leclere, M.; Perras, F. A.; Bryce, D. L.; Paulin, H.; Harden, J.; Liu, Y.; Ben, R. N. *Chem. Sci.* **2012**, *3*, 1408–1416.

(4) Trant, J. F.; Biggs, R. A.; Capicciotti, C. J.; Ben, R. N. *RSC Adv.* **2013**, *3*, 26005–26009.

(5) Michel, H.; Oesterhelt, D. *Proc. Natl. Acad. Sci. USA* **1980**, *77*, 1283–1285.

(6) Lorber, B.; Bishop, J. B.; DeLucas, L. J. *Biochim. Biophys. Acta.* **1990**, *1023*, 254–265.

(7) Hildreth, J. E. K. *Biochem. J.* **1982**, *207*, 363–366.

(8) Rosevear, P.; VanAken, T.; Baxter, J.; Ferguson-miller, S. *Biochemistry* **1980**, *19*, 4108–4115.

(9) Corma, A.; Iborra, S.; Miquel, S.; Primo, J. *J. Catal.* **1998**, *180*, 218–224.

(10) Capicciotti, C. The Rational Design of Potent Ice Recrystallization Inhibitors for Use as Novel Cryoprotectants, University of Ottawa, 2014.

(11) Czechura, P.; Tam, R. Y.; Dimitrijevic, E.; Murphy, A. V; Ben, R. N. *J. Am. Chem. Soc.* **2008**, *130*, 2928–2929.

(12) Tam, R. Y.; Ferreira, S. S.; Czechura, P.; Chaytor, J. L.; Ben, R. N. *J. Am. Chem. Soc.* **2008**, *130* (51), 17494–17501.

(13) Knight, C. A.; Hallett, J.; Devriess, A. L. *Cryobiology* **1988**, *25*, 55–60.

(14) Jackman, J.; Noestheden, M.; Moffat, D.; Pezacki, J. P.; Findlay, S.; Ben, R. N. *Biochem. Biophys. Commun.* **2007**, *354*, 340–344.

(15) Abraham, S. Development and Implementation of a Kinetic Quantitative Analysis of Novel Small Molecule Ice Recrystallization Inhibitors, University of Ottawa, 2015.

(16) Abraham, S.; Keillor, K.; Capicciotti, C. J.; Perley-Robertson, G. E.; Keillor, J.

W.; Ben, R. N. *Cryst. Growth Des.* **2015**, *15*, 5034–5039.

(17) Elferink, H.; Mensink, R. A.; White, P. B.; Boltje, T. J. *Angew. Chem. Int. Ed.* **2016**, *55*, 1–5.

(18) Boltje, T. J.; Buskas, T.; Boons, G. *Nat. Chem.* **2009**, *1*, 611–622.

(19) Zhu, X.; Schmidt, R. R. *Angew. Chem. Int. Ed.* **2009**, *48*, 1900–1934.

(20) Guo, J.; Ye, X. *Molecules* **2010**, *15*, 7235–7265.

(21) Conchie, J.; Levvy, G. A.; Marsh, C. A. *Adv. Carbohydr. Chem.* **1957**, *12*, 157–187.

(22) Chen, L.; Kong, F. *Tetrahedron Lett.* **2003**, *44*, 3691–3695.

(23) Toshima, K.; Tatsuta, K. *Chem. Rev.* **1993**, *93*, 1503–1531.

(24) Paulsen, B. H. *Chem. Soc. Rev.* **1984**, *13*, 15–45.

(25) Alabugin, I. V; Zeidan, T. A. *J. Am. Chem. Soc.* **2002**, *124*, 3175–3185.

(26) Eliel, E. L.; Giza, C. A. *J. Org. Chem.* **1968**, *33*, 3754–3758.

(27) Eusebio, J.; Cuevas, G. *Tetrahedron* **1992**, *48*, 5019–5087.

(28) Vishveshwara, S.; Rao, V. S. R. *Carbohydr. Res.* **1982**, *104*, 21–32.

(29) Angyal, S. J. *Adv. Carbohydr. Chem. Biochem.* **1984**, *42*, 63–65.

(30) Miljkovic, M. *Carbohydrates: Synthesis, Mechanisms, and Stereoelectronic Effects*; Springer: New York, 2010.

(31) Mitts, E.; Hixon, R. M. *J. Am. Chem. Soc.* **1944**, *66*, 1937–1940.

(32) Hodge, J. E.; Rist, C. E. *J. Am. Chem. Soc.* **1953**, *75*, 316–322.

(33) Erickson, J. G. *J. Am. Chem. Soc.* **1955**, *77*, 2839–2843.

(34) Ojala, C. R.; Ostman, J. M.; Hanson, S. E.; Ojala, H. *Carbohydr. Res.* **2001**, *332*, 415–427.

(35) Sorokin, B. *Chem. Ber.* **1886**, *19*, 513.

(36) Takeda, Y. *Carbohydr. Res.* **1979**, *77*, 9–23.

(37) Dideberg, O.; Lamotte, J.; Dupont, L. *Acta Cryst.* **1980**, *36*, 1500–1503.

(38) Ellis, G. P. *J. Chem. Soc. B.* **1966**, 572–576.

(39) Lemieux, R. U. *Pure Appl. Chem.* **1971**, *25*, 527–548.

(40) Tvaroska, I.; Bleha, T. *Adv. Carbohydr. Chem. Biochem.* **1989**, *47*, 45–123.

(41) Booth, H.; Khedhair, K. A.; Readshaw, S. A. *Tetrahedron* **1987**, *43*, 4699–4723.

(42) Galema, S. A.; Engberts, J. B. F. .; Hoiland, H.; Forland, G. M. *J. Phys. Chem.*

1993, *97*, 6885–6889.

(43) Galema, S. A.; Hoiland, H. *J. Phys. Chem.* **1991**, *95* (22), 5321–5326.

(44) Galema, S. A.; Howard, E.; Engberts, J. B. F. N.; Grigera, J. R. *Carbohydr. Res.* **1994**, *265*, 215–225.

(45) Capicciotti, C. J.; Kurach, J. D. R.; Turner, T. R.; Mancini, R. S.; Acker, J. P.; Ben, R. N. *Sci. Rep.* **2015**, *5*, 9692–9715.

(46) Briard, J. G.; Poisson, J. S.; Turner, T. R.; Capicciotti, C. J.; Acker, J. P.; Ben, R. N. *Sci. Rep.* **2016**, *6*, 23619.

(47) Scott, K. K.; Lecak, J.; Acker, J. P. *Transfus. Med. Rev.* **2005**, *19* (2), 127–142.

(48) Lecak, J.; Scott, K.; Young, C.; Hannon, J.; Acker, J. P. *Transfusion* **2004**, *44* (9), 1306–1313.

(49) Kanias, T.; Acker, J. P. *FEBS J.* **2010**, *277*, 343–356.

(50) Jha, A. K.; Jain, N. *Tetrahedron Lett.* **2013**, *54*, 4738–4741.

(51) Descroix, K.; Wagner, G. K. *Org. Biomol. Chem.* **2011**, *9*, 1855–1863.

Chapter 4: AFGP Disaccharide Analogs as Inhibitors of Ice Recrystallization

4.1 Introduction

Biological antifreezes were first discovered by DeVries and Wohlschlag in 1969 and are classified as either antifreeze proteins (AFPs) or antifreeze glycoproteins (AFGPs).[1,2] These biological antifreezes are found in various insects, plants, and constitute the major protein component in the blood serum of marine teleost fish.[2–5] Each AFGP consists of an alanine-alanine-threonine $(Ala\text{-}Ala\text{-}Thr)_n$ tripeptide repeat with minor sequence variations from one AFGP to the next (**Figure 4.1**).[2,3,6] The secondary hydroxyl group of the threonine residue is glycosylated to a β-D-galactosyl-(1-3)-α-*N*-acetyl-D-galactosamine disaccharide moiety.[1–3,6]

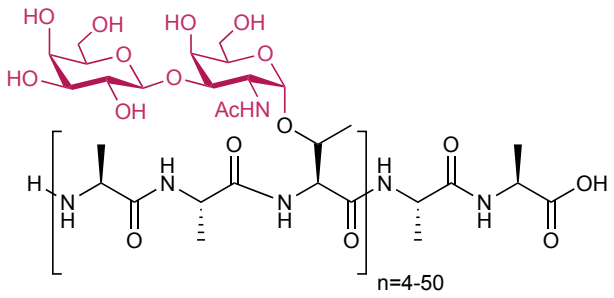

Figure 4.1 Structure of native AFGP-8 consisting of a β-D-galactosyl-(1-3)-α-*N*-acetyl-D-galactosamine disaccharide moiety glycosylated with an $(Ala\text{-}Ala\text{-}Thr)_n$ tripeptide repeat.

AFGPs are divided into eight subclasses depending on their molecular masses, which range from 2.6 kDa (n = 4) to 33.7 kDa (n = 50).[3,6] The presence of AFGPs in the blood serum of marine teleost fish promotes their survival at low temperatures by providing tolerance against freezing. Specifically, AFGPs adsorb to the surface of ice crystals and impede further growth and recrystallization.[3,4,6–10] Due to the antifreeze activity possessed by AFGPs, early work by the Ben laboratory involved the synthesis of *C*-linked AFGP analogs.[11,12] These analogs possessed "custom-tailored" antifreeze activity since they were able to inhibit ice recrystallization without the detrimental effects of thermal hysteresis.[11,12] From these studies, the Ben laboratory demonstrated that the

carbohydrate moiety of these glycoprotein analogs contributes significantly to their antifreeze activity.[13]

Sandra Ferreira (MSc) and Anna Balcerzak (PhD), two graduates of the Ben laboratory, synthesized and assessed AFGP disaccharide analogs **401-403** for their IRI activity (**Figure 4.2**).[14,15]

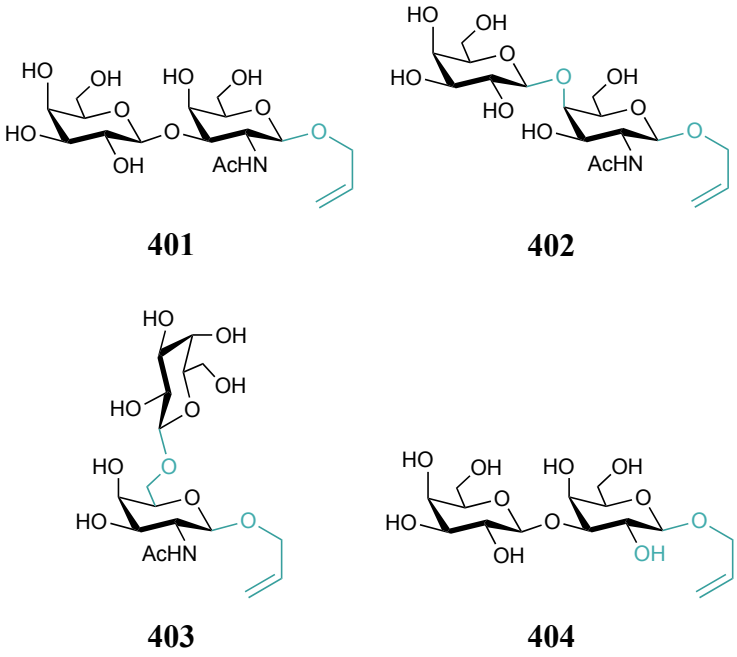

Figure 4.2 Structure of AFGP disaccharide analogs **401-404** previously synthesized by the Ben laboratory and assessed for their IRI activity.

In comparison to native AFGP-8, these analogs possess a β-allyl ether substituent at the C_1 position of the *N*-acetyl-D-galactosamine (GalNAc) moiety in place of the (Ala-Ala-Thr)$_n$ tripeptide repeat. Early work by our laboratory has demonstrated that the IRI activity of β-*C*-allyl-D-glucose is similar to that of β-D-glucose since they both exhibit a % mean grain size (% MGS) of approximately 80 %.[16] As a result, the β-allyl ether substituent was incorporated into derivatives **401-404** since this substituent may only have a small effect on ice recrystallization inhibition. Specifically, disaccharide analogs **401-403** were assessed using the splat-cooling assay to determine the influence of the β-(1,3) glycosidic linkage on IRI activity. When analyzed at 22 mM, the disaccharide

analog **401** possessing the same β-(1,3) glycosidic linkage found in native AFGP-8 was a moderate inhibitor of ice recrystallization exhibiting a % MGS slightly below 70 %.[15,17] The disaccharide analog **402** possessing a β-(1,4) glycosidic linkage was slightly more IRI active than analog **401** exhibiting a % MGS of approximately 50 %. Finally, the disaccharide analog **403** possessing a β-(1,6) glycosidic linkage exhibited IRI activity similar to that of analog **401**.[14,17] Although these analogs are not very effective inhibitors of ice recrystallization, these results suggest that the β-(1,4) glycosidic linkage gives rise to disaccharide analogs exhibiting the greatest IRI activity.[17]

In addition to investigating the influence of the β-(1,3) glycosidic linkage on IRI activity, John Trant (a PhD graduate of the Ben laboratory) synthesized disaccharide analog **404** to elucidate the importance of the C_2 acetamido (NHAc) functional group for IRI activity (**Figure 4.2**).[17,18] The biological antifreezes exhibit two types of antifreeze activity: thermal hysteresis (TH) and ice recrystallization inhibition (IRI).[19] However, our laboratory previously demonstrated that compounds are capable of exhibiting IRI activity without the detrimental effects of TH (i.e. "custom-tailored" antifreeze activity).[11,12] Thus, the structural features present on the disaccharide moiety of native AFGP-8 may only be important for TH but not required for IRI activity. Tachibana and colleagues previously demonstrated that the acetamido (NHAc) functional group at the C_2 position of reducing sugars was an important structural feature for thermal hystersis.[20] However, the importance of this functional group for IRI activity had not been previously investigated. As a result, disaccharide analog **404** was synthesized whereby the C_2 acetamido functional group of analog **401** was replaced with a hydroxyl substituent. When assessed at 22 mM, the IRI activity of disaccharide analog **404** was similar to that of analog **401**, exhibiting a % MGS of approximately 60 %.[17,18] Despite its importance for thermal hysteresis, these results suggest that the acetamido functional group at the C_2 position of disaccharide analogs **401-403** is not an essential structural feature for ice recrystallization inhibition.

While the C_2 acetamido functional group and the glycosidic bond of AFGP disaccharide analogs have been previously investigated for their influence on IRI activity,

a detailed and comprehensive structure-function analysis has yet to be performed. The Ben laboratory has previously identified the *O*-linked aryl glycosides as being an effective class of small molecule inhibitors of ice recrystallization. Thus, important structural features responsible for the IRI activity of *O*-linked aryl glycosides were assessed for their influence on IRI activity when glycosylated to a disaccharide analog of native AFGP-8. As a result, the objectives of this chapter are as follows:

1. The Ben laboratory previously performed an extensive structure-function analysis of *O*-linked aryl glycosides. Conclusions from this study suggest that the *p*-methoxyphenyl (PMP) substituent is an important structural feature that enhances the inhibition of ice recrystallization by *O*-linked aryl glycosides. Thus, the *p*-methoxyphenyl substituent was incorporated into the synthesis of an AFGP disaccharide analog to assess the effect of this analog on IRI activity.

2. While PMP-Glc is one of the most effective inhibitors of ice recrystallization that our laboratory has encountered to date, the PMP-GlcNAc derivative has not yet been investigated. Since this derivative was an intermediate required for disaccharide synthesis, the IRI activity of PMP-GlcNAc was also assessed.

4.2 Synthesis of AFGP Disaccharide Analogs

In contrast to the D-galactose moiety present in native AFGP-8, the disaccharide target **405** consists of a unit of D-glucose (**Figure 4.3**). As previously mentioned, the PMP-Glc derivative was one of the most effective inhibitors of ice recrystallization that the Ben laboratory has encountered to date. As a result, a β-linked *p*-methoxyphenyl (PMP) substituent was employed at the C_1 position of the GalNAc moiety present in analog **405**. Finally, to assess whether the PMP substituent could enhance the IRI activity of AFGP disaccharide analogs, the same β-(1,3) glycosidic linkage found in native AFGP-8 was retained in analog **405**.

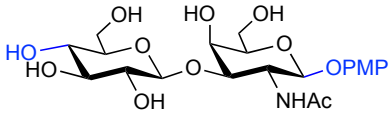

405

Figure 4.3 Structure of the AFGP disaccharide target **405**.

4.2.1 Lewis Acid-mediated Glycosylation of GlcNAc

In an attempt to limit the number of steps required for disaccharide synthesis, this preliminary strategy involved the use of standard glycosylation conditions to install the *p*-methoxyphenyl (PMP) substituent at the C_1 position of GlcNAc intermediates (**Scheme 4.1**). Thus, the AFGP disaccharide analog **405** could be synthesized in 8 steps.

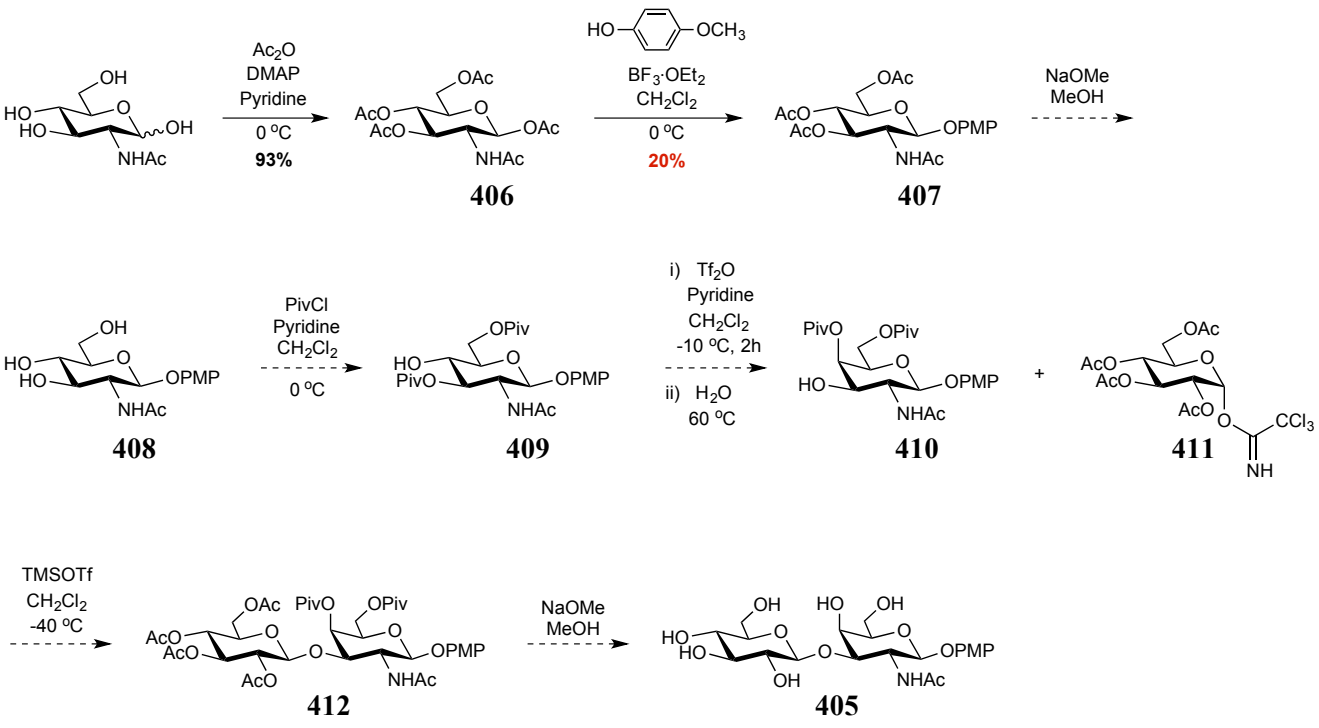

Scheme 4.1 Preliminary strategy for the synthesis of AFGP disaccharide analog **405** via Lewis acid-catalyzed glycosylation of GlcNAc intermediate **406**.

N-acetyl-D-glucosamine (GlcNAc) and *N*-acetyl-D-galactosamine (GalNAc) sugars play a significant role in cell signaling, antifreeze activity, and provide protection against pathogens and physical or chemical damage.[21–24] Unfortunately, GalNAc sugars are quite expensive to obtain commercially and require many protection/deprotection steps to be acquired synthetically. However, Feng *et al.* report a common method for the efficient conversion of GlcNAc derivatives into their corresponding GalNAc derivatives in two steps.[25] As a result, *N*-acetyl-D-glucosamine was used as the starting material for the synthesis of AFGP disaccharide analog **405**. The hydroxyl substituents of GlcNAc were acetate-protected using Ac_2O to afford the acetate-protected intermediate **406** in excellent yield. Using the same methodology first exemplified by the Helferich reaction, glycosylation of the fully acetylated GlcNAc intermediate **406** with *p*-methoxyphenol was attempted using $BF_3{\cdot}OEt_2$ as the Lewis acid catalyst.[26] However, the glycosylation product was only obtained in 20 % yield.

Table 4.1 Optimization of Lewis acid-mediated glycosylation of GlcNAc

Entry	Temperature	Time	Yield
1	rt	24 h	20 %
2	rt	48 h	15 %
3	40 ^{o}C	24 h	20 %
4	40 ^{o}C	48 h	14 %
5	40 ^{o}C	72 h	12 %

Due to low yields obtained early with this strategy, a preliminary optimization was performed whereby the reaction time and temperature were varied (**Table 4.1**). For the purpose of simplification, all optimization trials listed in **Table 4.1** were performed using $BF_3{\cdot}OEt_3$ as the Lewis acid promoter and *p*-methoxyphenol as the corresponding alcohol. In comparison to initial reaction conditions found in Entry 1, extending the reaction time by 24 h resulted in a 5 % decrease in glycosylation yield (Entry 2). Furthermore, increasing the reaction temperature to 40 ^{o}C (i.e. refluxing conditions) and varying the reaction time from 24-72 h failed to exceed a 20 % glycosylation yield (Entries 3-5). Thus, further optimization conditions were attempted including the use of a stronger Lewis acid (TMSOTf), modifying the equivalence of Lewis acid used, and

increasing the reaction temperature (data not shown). Unfortunately, these attempts also failed to increase the glycosylation yield above 20 % and resulted in the formation of multiple side products. However, the low glycosylation yields obtained with GlcNAc intermediates are rationalized by the formation of a resonance-stabilized oxazoline intermediate (**Scheme 4.2**).

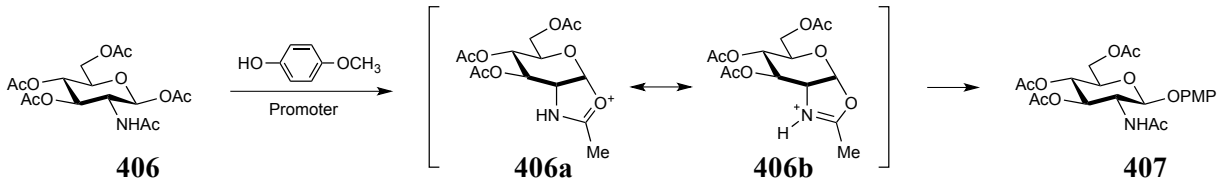

Scheme 4.2 Formation of the resonance-stabilized oxazoline intermediates **406a** and **406b**.

As demonstrated previously with the *O*-linked aryl glycosides, participating protecting groups (such as esters or amides) at the C_2 position of glycosyl donors exert an anchimeric effect favouring the formation of 1,2-*trans* glycosides (**Scheme 4.2**).[27–31] The resulting oxo-carbenium ion can convert to the resonance-stabilized oxazoline intermediates **406a** and **406b** as a 1,2-*cis* fused ring system.[27–32] Compared to the dioxolenium intermediate that forms as a result of C_2 esters, the oxazoline intermediate that forms as a result of C_2 amides is highly stable.[32–34] While both intermediates are stabilized by resonance, the amide nitrogen of the oxazoline intermediate **406b** can better accommodate the positive charge compared to the ester oxygen of the dioxolenium intermediate, thus increasing its stability. Despite the high β-selectivity obtained with oxazoline intermediates upon glycosylation, these intermediates do not exert strong glycosyl donor properties even if subjected to harsh Lewis acid conditions.[32,33] Furthermore, *p*-methoxyphenol is less reactive than primary or secondary alcohols due to conjugation of the aromatic ring, which reduces the nucleophilicity of aryl alcohols. As a result, formation of the resonance-stabilized oxazoline intermediate in conjunction with poor glycosyl donor-alcohol pairing substantiates the low glycosylation yields obtained with Lewis acid-catalyzed glycosylation of GlcNAc derivatives.

4.2.2 Metal Triflate-catalyzed Glycosylation of GalNAc

Jensen and colleagues previously investigated the direct β-selective glycosylation of pivaloyl-protected GlcNAc and GalNAc intermediates.[34–36] Specifically, they hypothesized that the use of metal triflates as Lewis acid catalysts facilitates both the departure of the anomeric leaving group (i.e. the pivaloyl group at C_1) as well as activation of the resonance-stabilized oxazoline intermediate.[34] Thus, glycosylation of GalNAc intermediates was attempted using this methodology.

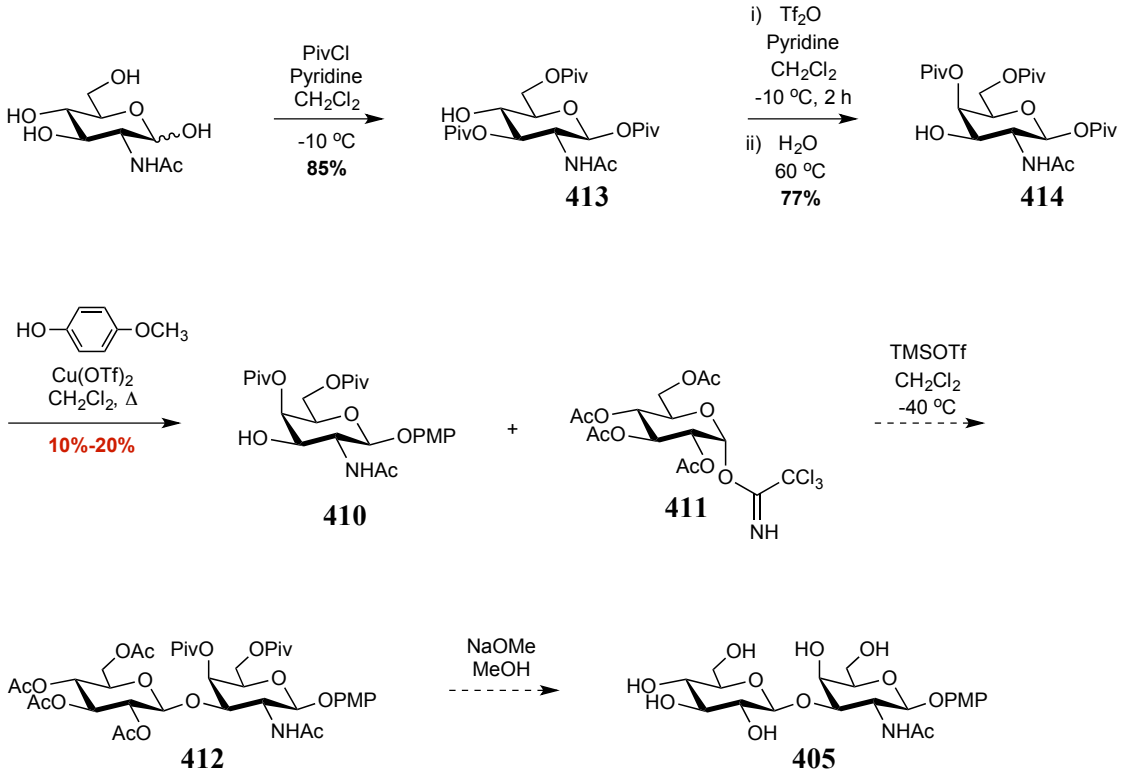

Scheme 4.3 Synthesis of AFGP disaccharide analog **405** via metal triflate-catalyzed glycosylation of GalNAc intermediate **414**.

In comparison with the preliminary strategy, disaccharide synthesis via metal triflate-catalyzed glycosylation of GalNAc intermediate **414** would require only 6 steps (**Scheme 4.3**). The hydroxyl substituents of *N*-acetyl-D-glucosamine were pivaloyl protected in the presence of PivCl, resulting in a mixture of tri- and tetra-pivaloylated products. The tri-pivaloyl-protected intermediate **413** was formed as a major product in 85 % yield. This GlcNAc intermediate was subsequently converted into the

corresponding GalNAc intermediate via a pivaloyl migration from C_3 to C_4.[25] Subsequent addition of water and heat enables an inversion of stereochemistry at the C_4 position resulting in the formation of the GalNAc intermediate **414** in 77 % yield over two steps.

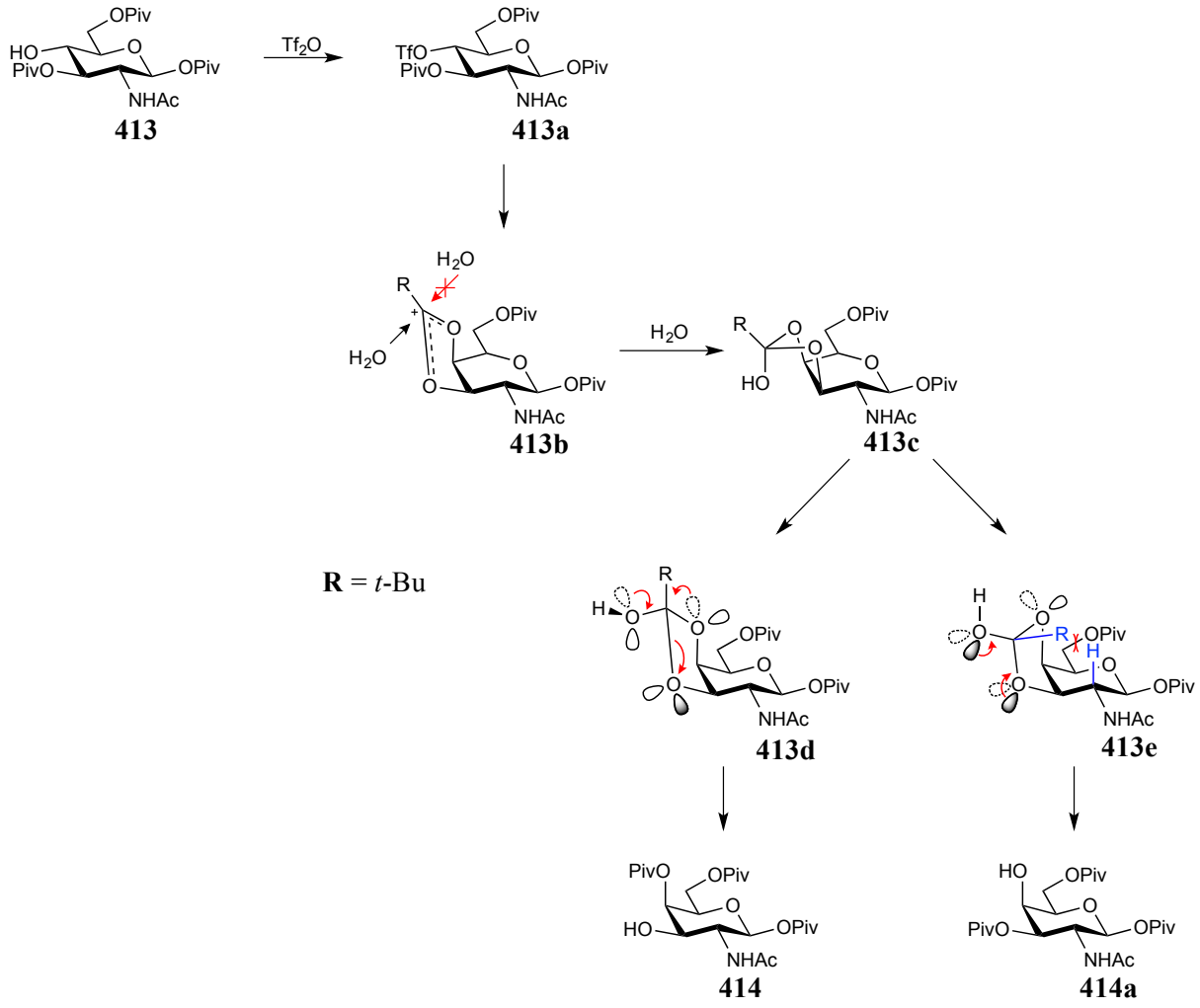

Scheme 4.4 Conversion of GlcNAc intermediate **413** to GalNAc intermediate **414** via cleavage of hemi-orthoester **413d** under stereoelectronic control.

Pivaloyl migration takes place due to cleavage of the hemi-orthoester **413d** under stereoelectronic control as described by Deslongchamps (**Scheme 4.4**).[37] First, the hydroxyl substituent at the C_4 position of intermediate **413** is protected with a triflate upon addition of Tf_2O at -10 ^oC. Anchimeric assistance by the carbonyl oxygen of the pivaloyl substituent at C_3 enables the displacement of the C_4 triflate from the top face,

forming the dioxolenium ion **413b**. To accommodate the planar dioxolenium ion, the pyranose ring of **413b** distorts to a half-chair. Subsequent addition of water under stereoelectronic control must take place from the α-face forming the hemi-orthoester **413c** due to steric hindrance of the incoming water molecule that would otherwise occur from the β-face. The resulting hemi-orthoester **413c** can adopt one of two conformations: **413d** or **413e**, whereby tension in the pyranose ring is released. Conformers **413d** and **413e** are cleaved under primary stereoelectronic control forming the axial ester **414** and the equatorial ester **414a** respectively. Due to steric interactions between the C_2 axial hydrogen and the *tert*-butyl substituent of conformer **413e**, conformer **413d** is favoured. Thus, the GalNAc intermediate **414** is formed as a single product.

Following the conversion of GlcNAc intermediate **413** to its corresponding GalNAc intermediate **414**, metal triflate-catalyzed glycosylation of this intermediate was performed using $Cu(OTf)_2$ as the Lewis acid catalyst (**Scheme 4.3**).[34] However, under reaction conditions identical to those employed by Jensen and colleagues, the glycosylation product **410** was obtained in only 11 % yield. Thus, another preliminary optimization was performed whereby reaction time, temperature, and amount of catalyst were varied (**Table 4.2**).

Table 4.2 Optimization of metal triflate-catalyzed GalNAc glycosylation

Entry	Catalyst Equivalence	Temperature	Time	Yield
1	0.2	40 °C	15 h	11 %
2	0.7	40 °C	36 h	20 %
3	0.03	70 °C	24 h	15 %
4	0.03	70 °C	48 h	10 %

For the purpose of simplification, all optimization trials in **Table 4.2** were performed using $Cu(OTf)_2$ as the metal triflate catalyst and *p*-methoxyphenol as the corresponding alcohol. Compared to the initial reaction conditions found in Entry 1, increasing the reaction time to 36 h resulted in a slight increase in glycosylation yield to 20 % (Entry 2). In addition, modifications to reaction time, temperature, and amount of catalyst resulted in a further decrease in glycosylation yields (Entries 3-4). Thus,

additional optimization attempts were performed whereby a stronger metal triflate ($Bi(OTf)_3$) was used in various amounts (data not shown). Despite these efforts, modifying reaction conditions once again failed to exceed a 20 % glycosylation yield and resulted in the formation of multiple side-products.

In the presence of $Cu(OTf)_2$ or $Bi(OTf)_3$, Jensen and colleagues report glycosylation yields of up to 87 % using the same GalNAc donor **414**.[34] However, these yields were obtained with more electron rich primary and secondary alcohols compared to the electron deficient *p*-methoxyphenol used herein. As previously mentioned, the resonance-stabilized oxazoline intermediate is highly stable and does not exert strong glycosyl donor properties, even if subjected to harsh Lewis acid conditions.[32,33] Despite the high glycosylation yields obtained by Jensen and colleagues, the reduced nucleophilicity of *p*-methoxyphenol compared to that of primary or secondary alcohols results in poor glycosyl donor-alcohol pairing. Once again, this substantiates the low glycosylation yields obtained with this strategy.

4.2.3 GlcNAc Glycosylation via Phase-transfer Catalysis

Thus far, the formation of the stable oxazoline intermediate in conjunction with the reduced nucleophilicity of *p*-methoxyphenol resulted in poor glycosylation yields of GlcNAc and GalNAc intermediates. As a result, a new strategy for the direct β-glycosylation of GlcNAc intermediates was required so as to circumvent the formation of the resonance-stabilized oxazoline intermediate. Phase-transfer catalysis (PTC) has been previously applied to the synthesis of aryl glycosides.[38–40] Roy and Tropper were the first to apply this methodology to the synthesis of *O*-aryl 2-acetamido-2-deoxy-β-D-glucopyranosides.[41,42] In the presence of tetrabutylammonium bromide ($Et_4N^+Br^-$), a β-bromide is formed *in situ* by anomerization of the α-bromide.[43–45] Following conversion to the more stable boat conformation, S_N2 substitution of the β-bromide with an alcohol typically favours the formation of the α-glycoside. However, introducing an aqueous solution of NaOH enables the deprotonation of phenol and reduces competition between the resulting phenoxide and bromide anions for nucleophilic attack at the anomeric center

of intermediate **415** (**Scheme 4.5**). Thus, PTC favours the formation of the β-glycoside (**407)** as opposed to the α-glycoside obtained with *in situ* anomerization.

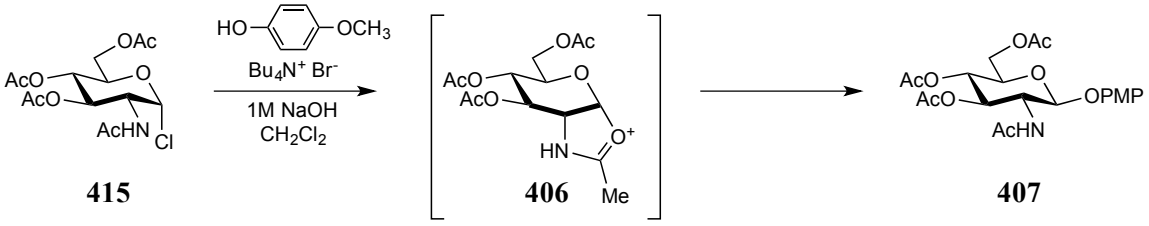

415 **406** **407**

Scheme 4.5 *p*-Methoxyphenol glycosylation of GlcNAc intermediate **415** via phase-transfer catalysis by Roy and Tropper.[41,42]

Roy and Tropper synthesized a variety of aryl GlcNAc derivatives utilizing one equivalent of tetrabutylammonium bromide ($Bu_4N^+Br^-$) in a 1M solution of NaOH.[41,42] They hypothesized that the formation of the resonance-stabilized oxazoline intermediate could be prevented if nucleophilic attack at the anomeric center by the resulting phenoxide occurs faster than that of the catalyst counteranions. Furthermore, they suggest that two equivalents of phenol would reduce competition between phenoxide and the chloride anion that would be released following substitution at the anomeric position. Due to the high glycosylation yields obtained by Roy and Tropper with phase-transfer catalysis, this methodology for the direct β-glycosylation of GlcNAc intermediates was explored (**Scheme 4.6**).

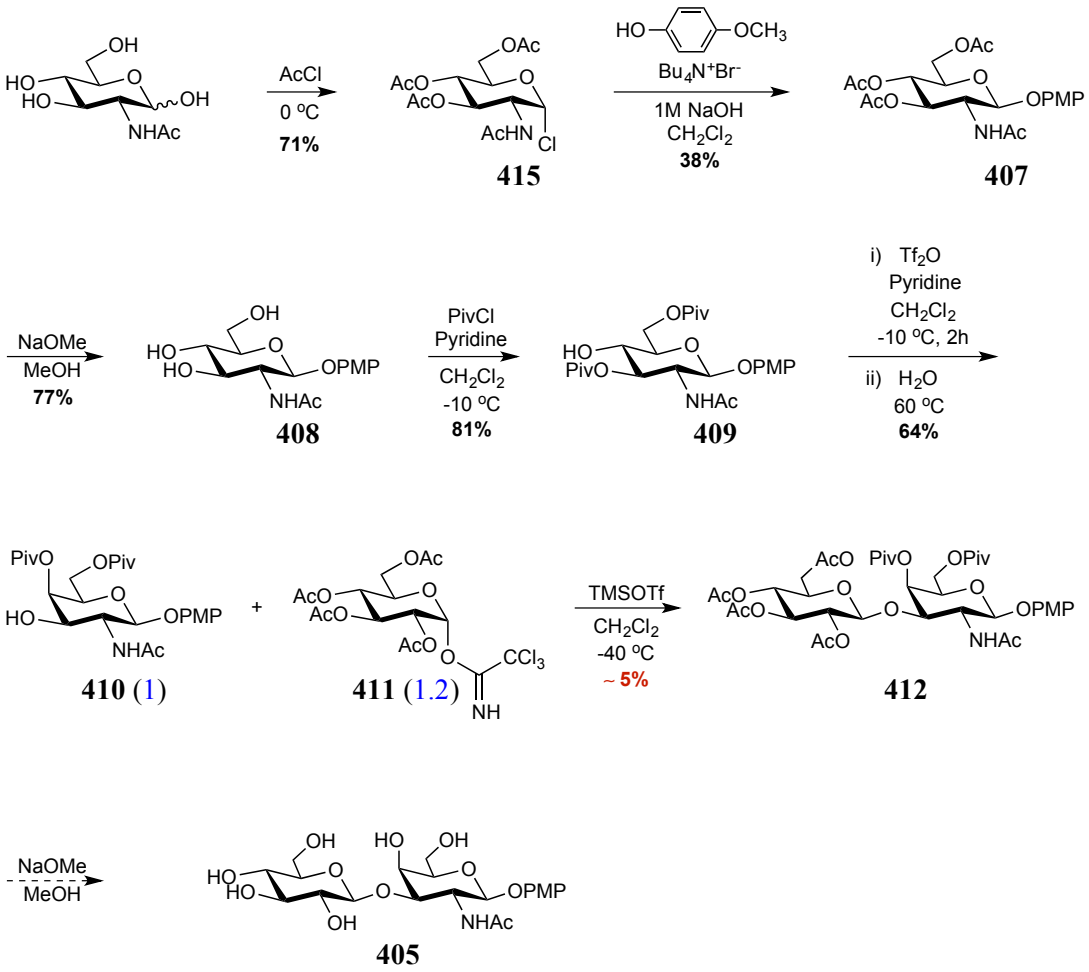

Scheme 4.6 Synthesis of AFGP disaccharide analog **405** via phase-transfer-catalyzed glycosylation of GlcNAc intermediate **415**. Value in brackets indicates the equivalence of glycosyl donor/acceptor used.

Commercially available *N*-acetyl-D-glucosamine was converted in a single step to the acetate-protected glucosyl chloride **415**. Using $Et_3N^+Br^-$ as the phase-transfer catalyst, the PMP-glycosylated intermediate **407** was obtained in 38 % yield. In addition to improved glycosylation yields, PTC did not result in the formation of multiple side products as observed with previous strategies. Thus, disaccharide synthesis was pursued further using this strategy. Following Zemplén deacetylation, the di-pivaloylated intermediate **409** was obtained as a single product in 81 % yield. Once again, a pivaloyl migration from C_3 to C_4 was performed as previously described generating the GalNAc intermediate **410** in high yield. Unfortunately, glycosidation of intermediate **410** with the trichloroacetimidate (TCA) donor **411** resulted in only a 5 % yield of the disaccharide

intermediate **412**. In addition to low glycosylation yields, isolation of intermediate **412** by column chromatography was problematic due to contamination with multiple side-products. However, ^{1}H-NMR analysis of crude side products suggests that the bulky pivaloyl protecting group at the C_4 position of intermediate **410** may not be compatible with the reaction conditions employed. Consequently, the pivaloyl substituents at the C_4 and C_6 positions of intermediate **410** needed to be replaced with new protecting groups that are compatible with carbohydrate glycosidation conditions. However, further synthesis of intermediate **410** was required to proceed. As a result, this opportunity was used to compare glycosylation yields obtained from PTC with those obtained via classical glycosylation of phthalimide-protected amino sugar derivatives.

4.2.4 Synthesis of AFGP Disaccharide Analogs via Glycosylation of Tetrachlorophthalimide-protected Amino Sugar Derivatives

The formation of a resonance-stabilized oxazoline intermediate is one of many challenging features of the acetamido (NHAc) functional group. In addition to exerting weak glycosyl donor properties, GlcNAc and GalNAc intermediates tend to form insoluble powders, which complicate purification by column chromatography. Furthermore, previous strategies for the glycosylation of GlcNAc and GalNAc intermediates resulted in low to moderate yields of glycosylation products (**Schemes 4.1, 4.3, 4.6**). As a result, a new strategy was devised whereby *p*-methoxyphenyl glycosylation of tetrachlorophthalimide (TCP)-protected amino sugars was performed under classical conditions (**Scheme 4.7**). In addition to higher glycosylation yields typically observed, TCP-protected amino sugars can be conveniently converted into their corresponding GlcNAc intermediates. Thus, this strategy was explored.

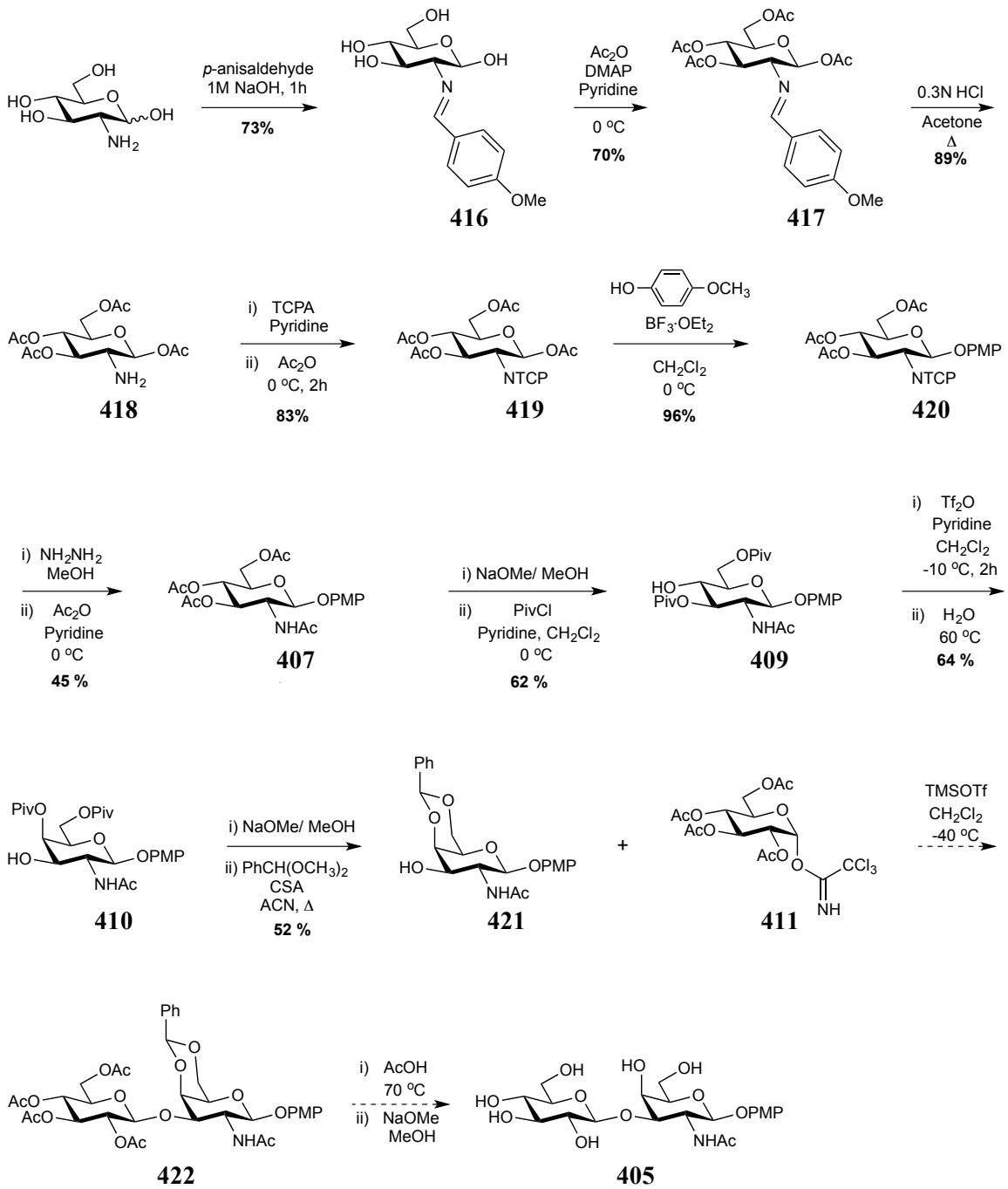

Scheme 4.7 Synthesis of AFGP disaccharide analog **405** via glycosylation of TCP-protected intermediate **419**.

In comparison with previous methods, the current strategy for disaccharide synthesis requires 17 steps. Unfortunately, this strategy requires many protection/deprotection steps since direct acetylation of D-glucosamine would have otherwise resulted in the undesired GlcNAc intermediate. Thus, the 2-amino function of commercially available D-glucosamine was first protected as its *p*-methoxybenzylidene in the presence of *p*-anisaldehyde and a 1 M solution of NaOH to afford intermediate **416** in 73 % yield. Following acetate-protection of the hydroxyl substituents, the 2-amino function was deprotected under acidic conditions to afford the acetate-protected amino sugar **418** in high yield. The 2-amino function of intermediate **418** was subsequently protected with a TCP group in the presence of tetrachlorophthalic anhydride (TCPA) followed by the addition of Ac_2O at 0 ^oC. Despite the high yield of this protection strategy (83 % over two steps), the advantages of using phthalimide protecting groups are typically overshadowed by complicated deprotection strategies.[46,47] As a result, various phthalimides were investigated for their ease of installation and removal. While phthalimide (Phth), dichlorophthalimide (DCPhth), and tetrachlorophthalimide (TCP) protecting groups were all installed onto the 2-amino function with ease, they exert different affinities for deprotection under basic conditions.[46,47] Typically, the base lability of phthalimides increases with increasing number of electron-withdrawing substituents on the aromatic ring.[46,48] Thus, the TCP group was selected to protect the C_2 amino function of intermediate **418** generating intermediate **419** in high yield. Under classical glycosylation conditions, the *p*-methoxyphenyl (PMP) substituent was installed onto the anomeric carbon of intermediate **419** using $BF_3{\cdot}OEt_2$ as the Lewis acid catalyst. Intermediate **420** was obtained as a single product in 96 % yield due to the 1,2-*trans* directing ability of the TCP protecting group at the C_2 position. Following glycosylation, intermediate **420** was converted into the corresponding GlcNAc intermediate **407** via hydrazinolysis in the presence of a methanolic solution of hydrazine hydrate. Subsequent addition of Ac_2O afforded the GlcNAc intermediate **407** in 45 % yield over two steps. As previously stated, pivaloyl protecting groups are not compatible with glycosidation of intermediate **410** to the TCA donor **411** (**Scheme 4.6**). However, the C_3 and C_6 hydroxyl substituents were pivaloyl-protected to enable convenient conversion of GlcNAc intermediate **409** to the corresponding GalNAc intermediate **410**. Once the GalNAc

intermediate was obtained as previously described, the pivaloyl protecting groups were removed under Zemplén conditions. Subsequently, the unprotected hydroxyl substituents at the C_4 and C_6 positions were regioselectively protected with a benzylidene acetal group in the presence of camphorsulfonic acid (CSA) under refluxing conditions forming intermediate **421** in 52 % yield. Unfortunately due to time constraints, the synthesis of the AFGP disaccharide analog **405** was not completed as indicated by the dashed arrows in **Scheme 4.7**. However, prospective efforts would require glycosidation of the glycosyl acceptor **421** to the trichloroacetimidate donor **411** to afford intermediate **422**. It is anticipated that the acetate groups will be removed by Zemplén deacetylation and the benzylidene acetal protecting group under mild acidic conditions to afford the desired disaccharide analog **405**. Once the synthesis of AFGP disaccharide analog **405** is completed, this derivative can be assessed for its IRI activity. Specifically, since the *p*-methoxyphenyl substituent enhanced the IRI activity of *O*-linked aryl glycosides, incorporating this functional group into AFGP disaccharide analogs will determine whether this substituent can also enhance the IRI activity of these analogs.

4.2.5 Summary of PMP Glycosylation Procedures

The major objective of this study was not only to synthesize the AFGP disaccharide analog **405**, but also to compare the efficiency of various GlcNAc and GalNAc glycosylation procedures. Although disaccharide analog **405** was not synthesized, a number of key observations have been made regarding the glycosylation of GlcNAc and GalNAc intermediates that will assist in the synthesis of future AFGP disaccharide analogs. As a result, the efficiency of each GlcNAc and GalNAc glycosylation strategy was assessed. Specifically, the *p*-methoxyphenol glycosylation yield, the number of steps required for each strategy, and the overall yield of the glycosyl acceptor obtained prior to glycosidation with the TCA donor were compared (**Table 4.3**).

Table 4.3 Comparison of various glycosylation strategies for disaccharide synthesis

Method	Number of Steps	PMP Glycosylation Yield	Overall Yield Before Coupling
Lewis acid [$BF_3{\cdot}OEt_2$]	8	20 %	N/A
Metal Triflate [$Cu(OTf)_2$]	6	20 %	13 %
PTC	8	38 %	11 %
$BF_3{\cdot}OEt_2$ with TCP-protected amino sugars	17	96 %	4 %

The lowest glycosylation yields (20 %) of GlcNAc and GalNAc intermediates with *p*-methoxyphenol were obtained using $BF_3{\cdot}OEt_2$ or $Cu(OTf)_2$ as Lewis acid catalysts. In contrast, the glycosylation yield nearly doubled (38 %) when GlcNAc intermediates underwent phase-transfer catalysis. This strategy required roughly the same number of steps as previous strategies (6-8) and resulted in a similar overall yield of the glycosyl acceptor required for glycosidation (13 % vs. 11 %). However, phase-transfer catalysis of GlcNAc intermediates was the most efficient glycosylation strategy due to the increase in glycosylation yield obtained (38 % vs. 20 %). In a final attempt to increase glycosylation yields with *p*-methoxyphenol, the PMP substituent was installed onto a TCP-protected amino sugar derivative that was later converted into the corresponding GlcNAc derivative. Despite a significant improvement in glycosylation yield (96 % vs. 38 %), this strategy required nearly double or triple the amount of reaction steps compared to previous strategies due to an increase in protection/deprotection steps that were required. Thus, the intermediate required for glycosidation to the trichloroacetimidate donor was obtained in only a 4 % overall yield, nearly a third of that obtained with previous methods. As a result, disaccharide synthesis via PMP glycosylation of TCP-protected amino sugars was less efficient than the phase-transfer catalysis procedure despite a significant improvement in *p*-methoxyphenyl glycosylation yields.

4.3 IRI Activity of the PMP-GlcNAc Intermediate

The synthesis AFGP disaccharide analog **405** was not completed and thus could not be tested for its effect on ice recrystallization inhibition. However, the PMP-GlcNAc intermediate **408** encountered in disaccharide synthesis was assessed for its IRI activity using the previously described splat-cooling assay (**Figure 4.5**).

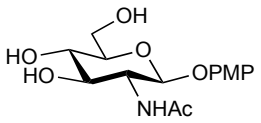

408

Figure 4.4 Structure of intermediate **408** required for the synthesis of AFGP disaccharide analog **405**.

The normalized rate of ice crystal growth in the presence of PMP-Glc **106** (black) and PMP-GlcNAc **408** (red) are found in **Figure 4.6**. The IRI activity of PMP-Glc was previously examined. This derivative remains one of the most effective inhibitors of ice recrystallization encountered by our laboratory since it is capable of achieving full inhibition of ice recrystallization at 44 mM (i.e. V_{norm} = 0 %). In addition, the PMP-Glc derivative exhibits an IC_{50} value of 16.3 ± 1.0 mM, thus also making it an efficacious inhibitor of ice recrystallization.

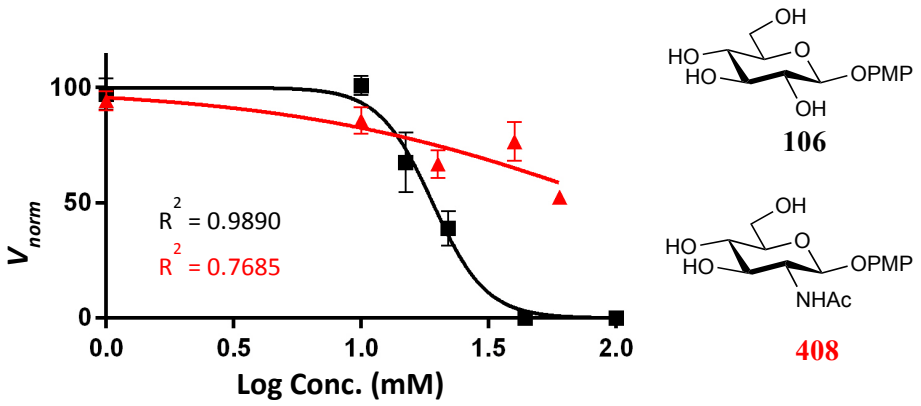

Figure 4.5 Rates of ice crystal growth in the presence of either PMP-GlcNAc (red) or PMP-Glc (black). All rates are normalized to that of a phosphate-buffered saline (PBS) solution (V_{norm}) and plotted against log concentrations (mM). Error bars represent the standard error of the mean (SEM). Equation of fit: y = 100/(1 + 10^((LogIC$_{50}$-x)(Hill slope))).

The PMP-GlcNAc derivative **408** was also assessed for its IRI activity to determine the importance of the C_2 hydroxyl substituent of aryl glycosides for ice recrystallization inhibition. Due to solubility constraints, the PMP-GlcNAc derivative could not be assessed beyond its maximum solubility of 60 mM. However, unlike the corresponding PMP-Glc derivative, the PMP-GlcNAc derivative **408** is only capable of reducing the rate of ice crystal growth approximately by half (V_{norm} = 52.5 %) when assessed at 60 mM. As a result, the PMP-GlcNAc derivative is not as efficient as PMP-Glc at inhibiting ice recrystallization. In addition, due to lack of a characteristic dose-response curve typically exhibited by our inhibitors, the PMP-GlcNAc derivative is not considered an inhibitor of ice recrystallization. These results support previous conclusions of the Ben laboratory suggesting that the acetamido (NHAc) function is not required for IRI activity. While Tachibana and colleagues previously demonstrated the importance of the acetamido function for thermal hysteresis (TH) activity,[20] previous work by John Trant (a PhD graduate of the Ben laboratory) indicates that this acetamido function is not required for IRI activity.[17,18] Similarly, the lack of IRI activity exhibited by the PMP-GlcNAc derivative **408** supports these findings. In addition, replacing the C_2 hydroxyl substituent of aryl glycosides with an acetamido functional group exacerbates the IRI activity formerly exhibited by PMP-Glc. Consequently, these results also demonstrate the

importance of the C_2 hydroxyl group of aryl glycosides for ice recrystallization inhibition.

4.4 Experimental Procedures and Compound Characterizations for Disaccharide Intermediates

Splat-cooling Assay for the Assessment of IRI Activity:

Ice recrystallization inhibition of PMP-Glc and PMP-GlcNAc was assessed at various concentrations in a phosphate-buffered saline solution. A 10 μL droplet of the sample solution was released from a micropipette at a height of approximately 2 meters onto a precooled aluminum block (-80 ^{o}C). The droplet was immediately frozen upon impact and the resulting ice wafer (approximately 20 μm thick and 1 cm wide) was then transferred to a precooled glass cover slip and annealed at -6.4 ^{o}C on a cryostage for 5 minutes. After this time, the cryostage was placed under a microscope and the middle of the ice wafer was photographed using an LMPlanF1 20x/0.40 objective lens.

Dose-response Curves:

Images of ice crystals in the absence of inhibitor (i.e. PBS only) were analyzed in triplicate. In addition, all compounds were assessed in triplicate at a minimum of 5 different concentrations. The area of each individual ice crystal within the field of view was analyzed using ImageJ and corrected for the appropriate magnification factor and objective lens utilized in the splat-cooling assay. The ice crystal areas were "binned" according to their size using an Excel spreadsheet, with the smallest bin occupying ice crystal areas of 0.001 mm^2 and each sequential bin increasing by increments of 0.001 mm^2. From the rate of depletion of ice crystals occupying Bin 1, the initial rates of ice crystal growth were calculated using the following equation:

$$\upsilon_t = \frac{1 - A_t^{rel}}{t}$$

where ν_t is the initial rate at 5 minutes, A_t^{rel} is the relative area of bin 1 at 5 minutes, and t is time. From the initial rates of ice crystal growth, dose-response curves were constructed whereby the normalized rate of ice crystal growth (i.e. initial rate normalized to that of PBS) was plotted against the log concentration. From the dose-response curves, IC_{50} values were calculated, that is the concentration at which our ice recrystallization inhibitors have achieved half of their maximum inhibitory capability.

General Experimental:

All anhydrous reactions were performed in flame-dried or oven-dried glassware under a positive pressure of dry argon. Air sensitive reagents were transferred using oven-dried syringes or cannulae. All flash chromatography was performed with E. Merck silica gel 60 (230-400 mesh). All solution phase reactions were monitored using thin layer chromatography (TLC) with 0.2 mm pre-coated silica gel aluminum plates 60 F254 (E. Merck). Components were visualized with short-wavelength (254 nm) ultra-violet light and/or staining (ceric ammonium molybdate or orcinol/sulphuric acid stain solution). ^{1}H-NMR (300 or 400 MHz) and ^{13}C-NMR (100 MHz) spectra were recorded on a Bruker Avance 300 or Bruker Avance 400 spectrometer. Deuterated chloroform ($CDCl_3$), water (D_2O), or dimethyl sulphoxide ($(CD_3)_2SO$) were used as NMR solvents unless otherwise stated. Chemical shifts are reported in ppm and corrected using the solvent residual peak as an internal standard. Splitting patterns are designated as follows: s, singlet; d, doublet; t, triplet; q, quartet; quint, quintet; m, multiplet; and br, broad. Low resolution mass spectrometry (LRMS) was performed on a Micromass Quatro-LC Electrospray spectrometer with a pump rate of 20 μL/min using electrospray ionization (ESI).

NMR spectra of novel compounds assessed for IRI activity and of intermediate compounds are provided. *N*-acetyl-D-glucosamine and D-glucosamine hydrochloride are commercially available carbohydrates.

1,3,4,6-Tetra-*O*-acetyl-2-acetamido-2-deoxy-β-D-glucopyranoside (406):

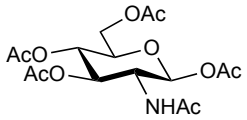

To a mixture of 2.000 g (9.041 mmol) of *N*-acetyl-D-glucosamine, a crystal of DMAP, and 16.0 mL of dry pyridine, 16.0 mL of Ac_2O was added at 0 ^oC and the reaction mixture was gradually warmed to room temperature and stirred overnight. The reaction mixture was diluted with CH_2Cl_2 and washed with saturated NaCl and H_2O, followed by drying over $MgSO_4$. The solution was filtered and all volatiles were removed under vacuum to afford 3.278 g of a white, powdery solid in 93 % yield. **^{1}H-NMR** (400 MHz, $CDCl_3$): δ 6.18 (d, *J* = 3.7 Hz, 1H), 5.56 (d, *J* = 9.0 Hz, 1H), 5.28-5.20 (m, 2H), 4.53-4.47 (m, 1H), 4.26 (dd, *J* = 12.5, 4.1 Hz, 1H), 4.08 (dd, *J* = 12.5, 2.4 Hz, 1H), 4.00 (ddd, *J* = 9.4, 4.1, 2.4 Hz, 1H), 2.21 (s, 3H), 2.10 (s, 3H), 2.07 (s, 3H), 2.06 (s, 3H), 1.95 (s, 3H). **^{13}C-NMR** (100 MHz, $CDCl_3$): δ 171.9, 170.8, 170.0, 169.2, 168.7, 90.9, 70.8, 69.9, 67.6, 61.7, 51.2, 23.2, 21.1, 20.87, 20.83, 20.71. **ESI-MS** *m/z* calcd for $C_{16}H_{23}NO_{10}$ $[M + Na]^+$: 412.12. Found: 411.5.

***p*-Methoxyphenyl 2-acetamido-2-deoxy-3,4,6-tri-*O*-acetyl-β-D-glucopyranoside (407):**

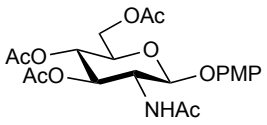

(1)

To a mixture of 0.2933 g (0.7533 mmol) of 1,3,4,6-tetra-*O*-acetyl-2-acetamido-2-deoxy-β-D-glucopyranoside (**406**), 4 Å molecular sieves, 0.1329 g (1.071 mmol) of *p*-methoxyphenol, and 6.0 mL of anhydrous CH_2Cl_2 at 0 ^oC, 1.0 mL (8.103 mmol) of $BF_3{\cdot}OEt_2$ was added. Once gradually warmed to room temperature, the reaction was refluxed overnight. The reaction mixture was diluted with CH_2Cl_2 and quenched with saturated $NaHCO_3$. The organic phase was washed with saturated NaCl and H_2O, followed by drying over $MgSO_4$. The solution was filtered and the crude product was purified by column chromatography (7:3 EtOAc –hexanes) to afford 65.0 mg of a white, powdery solid in 20 % yield.

(2)

To 3.644 g (9.963 mmol) of 2-acetamido-2-deoxy-3,4,6-tri-*O*-acetyl-α-D-glucopyranosyl chloride (**415**), 3.116 g (9.666 mmol) of $Bu_4N^+Br^-$, 3.977 g (32.04 mmol) of *p*-methoxyphenol, and 35 mL of CH_2Cl_2, 35 mL of a 1 M NaOH solution was added and the reaction was stirred vigorously at room temperature for 40 minutes. The reaction mixture was diluted with 90 mL of EtOAc and the organic phase was washed with 1 M NaOH, H_2O, and saturated NaCl followed by drying over $MgSO_4$. The solution was filtered and concentrated under vacuum. The crude product was recrystallized from EtOH to afford 13.44 g of a white, powdery solid in 38 % yield.

(3)

To 0.4957 g (0.7297 mmol) of *p*-methoxyphenyl 3,4,6-tri-*O*-acetyl-2-deoxy-2-(tetrachlorophthalimido)-β-D-glucopyranoside (**420**) suspended in MeOH, 0.14 mL (2.228 mmol) of hydrazine hydrate was added and the reaction was stirred at room

temperature for 2 hours followed by overnight reflux. The reaction was gradually cooled to room temperature, after which 3.0 mL of 5 % HCl was added. After 1 hour, the yellow precipitate was filtered and discarded while the filtrate was concentrated and dried overnight under vacuum. The crude product was dissolved in 2.0 mL of dry pyridine. Once cooled to 0 ^{o}C, 1.0 mL of Ac_2O was added and the reaction was gradually warmed to room temperature and stirred overnight. The reaction mixture was diluted with CH_2Cl_2 and the organic phase was washed with H_2O and saturated NaCl followed by drying over $MgSO_4$. The solution was filtered and concentrated under vacuum. The crude solid was recrystallized from EtOH to afford 0.1507 g of a white, powdery solid in 45 % yield over two steps.

^{1}H-NMR (300 MHZ, $CDCl_3$): δ 6.96 (d, *J* = 9.2 Hz, 2H), 6.82 (d, *J* = 9.2 Hz, 2H), 5.66 (d, *J* = 8.5 Hz, 1H), 5.41 (dd, *J* = 10.5, 9.3 Hz, 1H), 5.17 (d, *J* = 8.2 Hz, 1H), 5.14 (d, *J* = 9.3 Hz, 1H), 4.31 (dd, *J* = 12.2, 5.3 Hz, 1H), 4.17 (dd, *J* = 12.2, 2.5 Hz, 1H), 4.14-4.02 (m, 1H), 3.83 (ddd, *J* = 9.9, 5.3, 2.6 Hz, 1H), 3.79 (s, 3H), 2.10 (s, 3H), 2.08 (s, 3H), 2.06 (s, 3H), 2.00 (s, 3H). **^{13}C-NMR** (100 MHz, $CDCl_3$): δ 171.0, 170.8, 170.4, 169.5, 155.8, 151.2, 118.7, 114.7, 100.3, 72.24, 72.08, 68.7, 62.3, 55.8, 55.1, 23.5, 20.88, 20.85, 20.78. **ESI-MS** *m/z* calcd for $C_{21}H_{27}NO_{10}$ $[M + Na]^+$: 476.15. Found: 476.2.

***p*-Methoxyphenyl 2-acetamido-2-deoxy-β-D-glucopyranoside (408):**

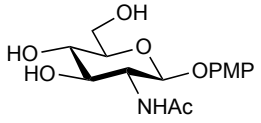

To 3.044 g (6.718 mmol) of *p*-methoxyphenyl 2-acetamido-2-deoxy-3,4,6-tri-*O*-acetyl-β-D-glucopyranoside (**407**) dissolved in MeOH, a 1 M NaOMe/MeOH solution was added dropwise until a pH of approximately 10 was obtained. The reaction was stirred at room temperature until TLC analysis indicated reaction completion. The reaction was neutralized with Amberlite® IR-120 (H+) ion-exchange resin, filtered, and concentrated. The crude solid was recrystallized from MeOH –ether to afford 1.810 g of a

white, powdery solid in 82 % yield. **^{1}H-NMR** (300 MHz, DMSO-d_6): δ 7.79 (d, *J* = 9.0 Hz, 1H), 6.91 (d, *J* = 9.2 Hz, 2H), 6.84 (d, *J* = 9.2 Hz, 2H), 5.06 (d, *J* = 5.1 Hz, 1H), 5.02 (d, *J* = 5.4 Hz, 1H), 4.81 (d, *J* = 8.5 Hz, 1H), 4.59 (t, *J* = 5.8 Hz, 1H), 3.74-3.69 (m, 1H), 3.69 (s, 3H), 3.62 (q, *J* = 9.4 Hz, 1H), 3.47 (m, 1H), 3.41-3.35 (m, 1H), 3.25-3.11 (m, 2H), 1.81 (s, 3H). **^{13}C-NMR** (100 MHz, MeOD): δ 173.9, 156.7, 153.3, 119.1, 115.5, 102.0, 78.2, 75.9, 71.9, 62.6, 57.5, 56.0, 23.0. **ESI-MS** *m/z* calcd for $C_{15}H_{21}NO_7$ $[M + Na]^+$: 350.12. Found: 350.0.

***p*-Methoxyphenyl 2-acetamido-2-deoxy-3,6-di-*O*-pivaloyl-β-D-glucopyranose (409):**

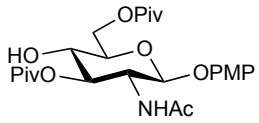

To 1.794 g (5.479 mmol) of *p*-methoxyphenyl 2-acetamido-2-deoxy-β-D-glucopyranoside (**408**), 40 mL of anhydrous CH_2Cl_2 and 20.0 mL of dry pyridine was added and the reaction was stirred overnight. Once cooled to -10 ^{o}C, 1.4 mL (11.37 mmol) of PivCl was added and the reaction was gradually warmed to room temperature and stirred for 48 hours. The reaction mixture was diluted with CH_2Cl_2 and the organic phase was washed with H_2O and saturated NaCl, followed by drying over $MgSO_4$. The solution was filtered and concentrated under vacuum. The crude solid was recrystallized from EtOAc –hexanes to afford 2.256 g of a white, powdery solid in 83 % yield. **^{1}H-NMR** (300 MHz, $CDCl_3$): δ 6.94 (d, *J* = 9.1 Hz, 2H), 6.76 (d, *J* = 9.1 Hz, 2H), 5.20 (t, *J* = 9.8 Hz, 1H), 4.98 (d, *J* = 8.3 Hz, 1H), 4.45 (dd, *J* = 12.0, 2.3 Hz, 1H), 4.32 (dd, *J* = 12.1, 6.1 Hz, 1H), 4.21-4.08 (m, 1H), 3.75 (s, 3H), 3.71 (ddd, *J* = 9.8, 6.1, 2.3 Hz, 1H), 3.57 (t, *J* = 9.4 Hz, 1H), 1.92 (s, 3H), 1.21 (s, 9H), 1.20 (s, 9H). **^{13}C-NMR** (100 MHz, $CDCl_3$): δ 179.9, 179.0, 170.1, 155.4, 151.4, 118.4, 114.4, 100.4, 74.7, 74.3, 69.4, 63.6, 55.6, 54.0, 39.02, 38.89, 27.16, 27.02, 23.1. **ESI-MS** *m/z* calcd for $C_{25}H_{37}NO_9$ $[M + H]^+$: 496.25. Found: 496.2.

***p*-Methoxyphenyl 2-acetamido-2-deoxy-4,6-di-*O*-pivaloyl-β-D-galactopyranose (410):**

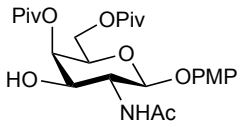

(1)

To 94.5 mg (0.1996 mmol) of 1,4,6-tri-*O*-pivaloyl-2-acetamido-2-deoxy-β-D-galactopyranose (**414**), 78.9 mg (0.6356 mmol) of *p*-methoxyphenol, and 3 mL of anhydrous CH_2Cl_2, 50 mg (0.1382 mmol) of $Cu(OTf)_2$ was added and the reaction was refluxed for 24 hours. The reaction mixture was diluted with CH_2Cl_2 and the organic phase was washed with H_2O and saturated NaCl, followed by drying over $MgSO_4$. The solution was filtered and concentrated under reduced pressure. The crude solid was purified by column chromatography (3:7 acetone –hexanes) to afford 20 % of a white, powdery solid in 20 % yield.

(2)

To 2.189 g (4.417 mmol) of *p*-methoxyphenyl 2-acetamido-2-deoxy-3,6-di-*O*-pivaloyl-β-D-glucopyranose (**409**), 15 mL of anhydrous CH_2Cl_2, and 15 mL of dry pyridine at -10 ^oC, 1 mL (6.096 mmol) of Tf_2O was added and the reaction was gradually warmed to 0 ^oC and stirred for 2 hours. Once TLC analysis indicated reaction completion, 1 mL (55.49 mmol) of H_2O was added and the reaction was heated to 60 ^oC and stirred overnight. The reaction was diluted with CH_2Cl_2 and quenched with saturated $NaHCO_3$. The organic phase was washed with H_2O and saturated NaCl, followed by drying over $MgSO_4$. The solution was filtered and concentrated under reduced pressure. The crude solid was recrystallized from EtOAc –hexanes to afford 1.525 g of a white, powdery solid in 70 % yield.

^{1}H-NMR (400 MHz, $CDCl_3$): δ 6.96 (d, *J* = 9.1 Hz, 2H), 6.78 (d, *J* = 9.1 Hz, 2H), 5.33 (d, *J* = 2.8 Hz, 1H), 5.06 (d, *J* = 8.3 Hz, 1H), 4.16-4.09 (m, 3H), 3.99 (t, *J* = 6.3 Hz, 1H), 3.94-3.88 (m, 1H), 3.75 (s, 3H), 2.05 (s, 3H), 1.25 (s, 9H), 1.18 (s, 9H). **^{13}C-NMR** (100

MHz, $CDCl_3$): δ 178.09, 178.03, 172.7, 155.6, 150.8, 118.1, 114.6, 99.3, 71.7, 71.5, 68.5, 62.4, 55.7, 55.4, 39.3, 38.8, 27.25, 27.13, 23.5. **ESI-MS** *m/z* calcd for $C_{25}H_{37}NO_9$ [M + Na]$^+$: 518.24. Found: 518.0.

2,3,4,6-Tetra-*O*-acetyl-α-D-glucopyranosyl trichloroacetimidate (411):

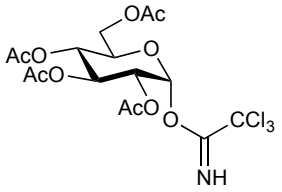

To 5.003 g (12.82 mmol) of 1,2,3,4,6-penta-*O*-acetyl-D-glucopyranose (**325**) in 15 mL of anhydrous THF, 2.2 mL (20.46 mmol) of $BnNH_2$ was added and the reaction was stirred at room temperature for 24 hours. The reaction was diluted with CH_2Cl_2 and the organic phase was washed with 10 % HCl and H_2O, followed by drying over $MgSO_4$. The solution was filtered and concentrated under reduced pressure. The crude oil was purified by column chromatography (1:1 EtOAc –hexanes) to afford 2.674 g of a yellow oil. To a solution of 0.2000g (0.5742 mmol) of 2,3,4,6-tetra-*O*-acetyl-α-D-glucopyranose, 0.4006 g (2.899 mmol) of K_2CO_3, and 5 mL of CH_2Cl_2 at 0 ^oC, 0.6 mL (5.984 mmol) of CCl_3CN was added and the reaction was gradually warmed to room temperature and stirred overnight. The reaction mixture was diluted with CH_2Cl_2 and filtered over Celite. The solution was concentrated under vacuum and the crude product was filtered by column chromatography (4:6 EtOAc –hexanes) to afford 0.1554 g of a colorless oil in 50 % yield over two steps. **^{1}H-NMR** (400 MHz, $CDCl_3$): δ 8.70 (s, 1H), 6.57 (d, *J* = 3.7 Hz, 1H), 5.57 (t, *J* = 9.9 Hz, 1H), 5.19 (t, *J* = 9.9 Hz, 1H), 5.14 (dd, *J* = 10.2, 3.7 Hz, 1H), 4.28 (dd, *J* = 12.3, 4.1 Hz, 1H), 4.22 (ddd, *J* = 10.2, 4.0, 2.1 Hz, 1H), 4.13 (dd, *J* = 12.3, 2.0 Hz, 1H), 2.08 (s, 3H), 2.05 (s, 3H), 2.04 (s, 3H), 2.02 (s, 3H). **^{13}C-NMR** (100 MHz, $CDCl_3$): δ 171.0, 170.44, 170.29, 169.9, 161.3, 93.4, 91.3, 70.47, 70.34, 70.19, 68.3, 61.8, 21.13, 21.13, 21.04, 20.90. All spectra are in accordance with that reported in the literature.[49]

***p*-Methoxyphenyl 2,3,4,6-tetra-*O*-acetyl-β-D-glucopyranosyl-(1→3)-2-acetamido-2-deoxy-4,6-di-*O*-pivaloyl-β-D-galactopyranoside (412):**

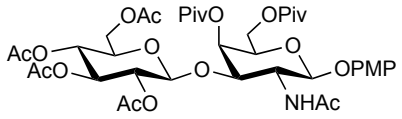

To 49.7 mg (0.1003 mmol) of *p*-methoxyphenyl 2-acetamido-2-deoxy-4,6-di-*O*-pivaloyl-β-D-galactopyranose (**410**) dissolved in 1 mL of anhydrous CH_2Cl_2 at -40 ^oC, 0.03 mL (0.1306 mmol) of TMSOTf was added followed by the dropwise addition of 74 mg (0.1502 mmol) of 2,3,4,6-tetra-*O*-acetyl-α-D-glucopyranosyl trichloroacetimidate (**411**) dissolved in 2 mL of anhydrous CH_2Cl_2 over 1 hour. The reaction was diluted with CH_2Cl_2 and quenched with saturated $NaHCO_3$. The organic phase was washed with H_2O and saturated NaCl, followed by drying over $MgSO_4$. The solution was filtered and concentrated under reduced pressure. The crude solid was purified by column chromatography (1:1 EtOAc –hexanes). Isolation of the product by column chromatography was not possible due to contamination with multiple side products.

1,3,6-Tri-*O*-pivaloyl-2-acetamido-2-deoxy-β-D-glucopyranose (413):

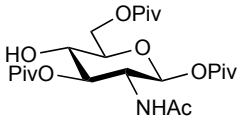

A mixture 1.116 g (5.044 mmol) of *N*-acetyl-D-glucosamine, 20 mL of anhydrous CH_2Cl_2, and 10 mL of dry pyridine was stirred overnight. Once the reaction mixture was cooled to -10 ^oC, 1.9 mL (15.44 mmol) of PivCl was added and the reaction mixture was gradually warmed to room temperature and stirred for 3 days. The reaction mixture was diluted with CH_2Cl_2 and the organic phase was washed with H_2O and saturated NaCl, followed by drying over $MgSO_4$. The solution was filtered and concentrated under reduced pressure. The crude solid was purified by column chromatography (4:6 EtOAc – hexanes) to afford 2.030 g of a white, powdery solid in 85 % yield. **^{1}H-NMR** (400 MHz, $CDCl_3$): δ 5.62 (d, *J* = 9.7 Hz, 1H), 5.57 (d, *J* = 8.8 Hz, 1H), 4.98 (dd, *J* = 10.8, 8.9 Hz,

1H), 4.50 (dd, *J* = 12.3, 4.2 Hz, 1H), 4.32-4.24 (m, 2H), 3.63 (ddd, *J* = 9.8, 4.1, 2.5 Hz, 1H), 3.55 (t, *J* = 9.3 Hz, 1H), 1.87 (s, 3H), 1.23 (s, 9H), 1.20 (s, 9H), 1.18 (s, 9H). **^{13}C-NMR** (100 MHz, $CDCl_3$): δ 180.01, 179.86, 177.5, 170.0, 93.2, 75.5, 74.9, 69.1, 62.9, 52.9, 39.4, 39.4, 39.1, 27.52, 27.35, 27.1, 23.4. **ESI-MS** *m/z* calcd for $C_{23}H_{39}NO_9$ $[M + Na]^+$: 496.25. Found: 496.2. All spectra are in accordance with that reported in the literature.[25]

1,4,6-Tri-*O*-pivaloyl-2-acetamido-2-deoxy-β-D-galactopyranose (414):

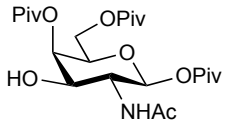

To 0.5758 g (1.222 mmol) of 1,3,6-tri-*O*-pivaloyl-2-acetamido-2-deoxy-β-D-glucopyranose (**413**), 10 mL of anhydrous CH_2Cl_2, and 10 mL of dry pyridine at -10 ^oC, 0.30 mL (1.783 mmol) of Tf_2O was added and the reaction was gradually warmed to 0 ^oC and stirred for 2 hours. Once TLC analysis indicated reaction completion, 2.0 mL (0.1110 mmol) of H_2O was added and the reaction was heated to 60 ^oC and stirred overnight. The reaction mixture was diluted with CH_2Cl_2 and the organic phase was washed with H_2O and saturated NaCl, followed by drying over $MgSO_4$. The solution was filtered and concentrated under reduced pressure. The crude solid was recrystallized from EtOAc – hexanes to afford 0.4463 g of a white, powdery solid in 77 % yield. **^{1}H-NMR** (400 MHz, $CDCl_3$): δ 5.76 (d, *J* = 8.5 Hz, 1H), 5.67 (d, *J* = 8.8 Hz, 1H), 5.33 (d, *J* = 2.6 Hz, 1H), 4.19-4.13 (m, 2H), 4.09 (dd, *J* = 11.2, 6.5 Hz, 1H), 4.00 (t, *J* = 6.7 Hz, 1H), 3.90 (dd, *J* = 10.8, 3.4 Hz, 1H), 2.01 (s, 3H), 1.30 (s, 9H), 1.24 (s, 9H), 1.19 (s, 9H). **^{13}C-NMR** (100 MHz, $CDCl_3$): δ 178.17, 178.07, 177.96, 172.4, 92.8, 72.8, 72.3, 68.2, 61.5, 53.7, 39.5, 39.1, 38.9, 27.4, 27.2, 27.0, 23.3. **ESI-MS** *m/z* calcd for $C_{25}H_{37}NO_9$ $[M + Na]^+$: 496.25. Found: 496.3. All spectra are in accordance with that reported in the literature.[25]

2-Acetamido-2-deoxy-3,4,6-tri-*O*-acetyl-α-D-glucopyranosyl chloride (415):

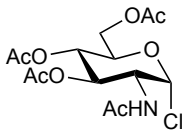

A solution of 5.7093 g (25.81 mmol) of *N*-acetyl-D-glucosamine in 16 mL of freshly distilled AcCl was stirred overnight at room temperature. The reaction mixture was diluted with 65 mL of $CHCl_3$ and the mixture was poured onto ice. The organic phase was washed with H_2O and saturated $NaHCO_3$, followed by drying over $MgSO_4$. The solution was diluted with CH_2Cl_2, filtered, and concentrated under reduced pressure. The crude solid was recrystallized from CH_2Cl_2 –ether to afford 6.672 g of a white, crystalline solid in 71 % yield. **^{1}H-NMR** (300 MHz, $CDCl_3$): δ 6.20 (d, *J* = 8.7 Hz, 1H), 6.12 (d, *J* = 3.7 Hz, 1H), 5.28 (t, *J* = 10.1 Hz, 1H), 5.13 (t, *J* = 9.7 Hz, 1H), 4.48 (ddd, *J* = 10.7, 8.7, 3.7 Hz, 1H), 4.25-4.18 (m, 2H), 4.08-4.03 (m, 1H), 2.02 (s, 3H), 1.97 (s, 3H), 1.97 (s, 3H), 1.92 (s, 3H). **^{13}C-NMR** (100 MHz, $CDCl_3$): δ 171.10, 170.39, 170.19, 169.01, 93.63, 70.73, 69.93, 67.04, 61.06, 53.21, 22.80, 20.53, 20.53, 20.40. **ESI-MS** *m/z* calcd for $C_{14}H_{20}ClNO_8$ $[M + H]^+$: 366.10. Found 366.0.

2-Deoxy-2-(*p*-methoxybenzylidene)amino-β-D-glucosamine (416):

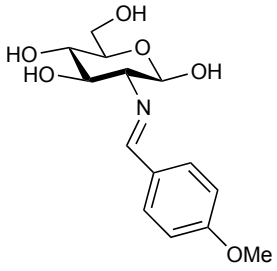

To 20.05 g (95.08 mmol) of D-glucosamine hydrochloride and 92.0 mL (92.00 mmol) of a 1M solution of NaOH at 0 °C, 12.0 mL (98.63 mmol) of *p*-anisaldehyde was added and the reaction was maintained at 0 °C for 1.5 hours. The precipitate was washed with H_2O and 1:1 MeOH –Et_2O and filtered. The white solid was dried overnight under vacuum affording 20.72 g of a white, powdery solid in 73 % yield. **^{1}H-NMR** (300 MHz,

DMSO-d_6): δ 8.11 (s, 1H), 7.68 (d, *J* = 8.9 Hz, 2H), 6.99 (d, *J* = 8.8 Hz, 2H), 6.51 (d, *J* = 6.7 Hz, 1H), 4.90 (d, *J* = 5.2 Hz, 1H), 4.79 (d, *J* = 5.6 Hz, 1H), 4.69 (t, *J* = 7.2 Hz, 1H), 4.53 (t, *J* = 5.8 Hz, 1H), 3.80 (s, 3H), 3.72 (ddd, *J* = 11.6, 5.6, 1.9 Hz, 1H), 3.52-3.38 (m, 2H), 3.27-3.10 (m, 2H), 2.78 (dd, *J* = 9.0, 7.9 Hz, 1H). **^{13}C-NMR** (100 MHz, DMSO-d_6): δ 161.22, 161.04, 129.62, 129.10, 113.90, 95.63, 78.19, 76.86, 74.60, 70.37, 61.28, 55.28. **ESI-MS** *m/z* calcd for $C_{14}H_{19}NO_6$ [M + Na]+: 320.11. Found 320.0. All spectra are in accordance with that reported in the literature.[50]

1,3,4,6-Tetra-*O*-acetyl-2-deoxy-2-(*p*-methoxybenzylidene)amino-β-D-glucosamine (417):

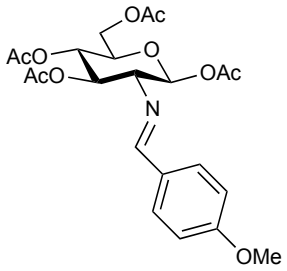

To 17.02 g (57.25 mmol) of 2-deoxy-2-(*p*-methoxybenzylidene)amino-β-D-glucosamine (**416**), 0.1866 g (1.527 mmol) of DMAP, and 90 mL of dry pyridine at 0 ^{o}C, 54 mL of Ac_2O was added and the reaction was gradually warmed to room temperature and stirred overnight. The reaction mixture was poured onto ice and a white precipitate was formed. The precipitate was washed with H_2O and ether and filtered. The white solid was dried overnight under vacuum affording 18.67 g of a white, powdery solid in 70 % yield. **^{1}H-NMR** (400 MHz, $CDCl_3$): δ 8.14 (s, 1H), 7.66 (d, *J* = 8.7 Hz, 2H), 6.91 (d, *J* = 8.9 Hz, 2H), 5.94 (d, *J* = 8.3 Hz, 1H), 5.43 (t, *J* = 9.6 Hz, 1H), 5.13 (t, *J* = 9.8 Hz, 1H), 4.37 (dd, *J* = 12.4, 4.5 Hz, 1H), 4.12 (dd, *J* = 12.4, 2.1 Hz, 1H), 3.96 (ddd, *J* = 10.1, 4.5, 2.1 Hz, 1H), 3.84 (s, 3H), 3.45 (dd, *J* = 9.7, 8.4 Hz, 1H), 2.09 (s, 3H), 2.03 (s, 3H), 2.01 (s, 3H), 1.87 (s, 3H). **^{13}C-NMR** (100 MHz, $CDCl_3$): δ 170.90, 170.11, 169.75, 168.98, 164.48, 162.54, 130.49, 128.54, 114.30, 93.41, 73.50, 73.18, 73.01, 68.30, 62.07, 55.64, 21.04, 20.99, 20.91, 20.74. **ESI-MS** *m/z* calcd for $C_{22}H_{27}NO_{10}$ $[M + Na]^+$: 488.15. Found 488.0. All spectra are in accordance with that reported in the literature.[50]

1,3,4,6-Tetra-*O*-acetyl-2-deoxy-2-acetamido-β-D-glucopyranosyl hydrochloride (418):

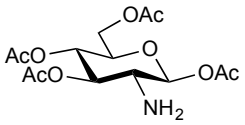

To a refluxing solution of 18.05 g (38.67 mmol) of 1,3,4,6-tetra-*O*-acetyl-2-deoxy-2-(*p*-methoxybenzylidene)amino-β-D-glucosamine (**417**) in 90 mL of acetone, 9.0 mL (45.00 mmol) of HCl was added dropwise until a white precipitate formed (~ 5 min). The reaction was gradually cooled to room temperature and the precipitate was washed with acetone and ether. The precipitate was filtered and dried overnight under vacuum affording 13.30 g of a white, powdery solid in 89 % yield. **^{1}H-NMR** (400 MHz, DMSO-d_6): δ 8.74 (s, br, 2.6 H), 5.90 (d, *J* = 8.7 Hz, 1H), 5.35 (dd, *J* = 10.3, 9.3 Hz, 1H), 4.93 (t, *J* = 9.6 Hz, 1H), 4.19 (dd, *J* = 12.5, 4.4 Hz, 1H), 4.05 (ddd, *J* = 10.1, 4.3, 2.2 Hz, 1H), 3.99 (dd, *J* = 12.4, 2.1 Hz, 1H), 3.56 (dd, *J* = 10.3, 8.7 Hz, 1H), 2.17 (s, 3H), 2.02 (s, 3H), 1.99 (s, 3H), 1.97 (s, 3H). **^{13}C-NMR** (100 MHz, DMSO-d_6): δ 170.20, 170.03, 169.5, 168.9, 90.3, 71.8, 70.6, 68.0, 61.5, 52.4, 21.16, 21.07, 20.72, 20.58. **ESI-MS** *m/z* calcd for $C_{14}H_{22}NO_9$ $[M + H]^+$: 348.13. Found 348.1. All spectra are in accordance with that reported in the literature.[50]

1,3,4,6-Tetra-*O*-acetyl-2-deoxy-2-(tetrachlorophthalimido)-β-D-glucopyranose (419):

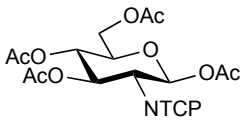

A solution of 13.00 g (33.88 mmol) of 1,3,4,6-tetra-*O*-acetyl-2-deoxy-2-acetamido-β-D-glucopyranosyl hydrochloride (**418**), 11.72 g (41.02 mmol) of TCPA, and 100 mL of dry pyridine was stirred overnight at room temperature. Once cooled to 0 ^oC, 32 mL of Ac_2O was added and the reaction was gradually warmed to room temperature and stirred until TLC analysis indicated reaction completion (~ 2 h). The reaction mixture was co-concentrated with toluene under reduced pressure and the crude solid was

recrystallized from EtOH to afford 17.24 g of a yellow, powdery solid in 83 % yield. **^{1}H-NMR** (400 MHz, $CDCl_3$): δ 6.47 (d, *J* = 8.8 Hz, 1H), 5.79 (dd, *J* = 10.3, 9.1 Hz, 1H), 5.23 (dd, *J* = 10.1, 9.2 Hz, 1H), 4.45 (dd, *J* = 10.3, 8.8 Hz, 1H), 4.36 (dd, *J* = 12.5, 4.5 Hz, 1H), 4.14 (dd, *J* = 12.5, 2.1 Hz, 1H), 3.98 (ddd, *J* = 10.3, 4.4, 2.2 Hz, 1H), 2.11 (s, 3H), 2.04 (s, 3H), 2.03 (s, 3H), 1.90 (s, 3H). **^{13}C-NMR** (100 MHz, $CDCl_3$): δ 170.95, 170.83, 169.7, 169.0, 141.5, 130.8, 127.0, 90.0, 73.0, 71.1, 68.3, 61.8, 54.7, 21.18, 21.08, 20.92, 20.79. **ESI-MS** *m/z* calcd for $C_{22}H_{19}Cl_4NO_{11}$ $[M + Na]^+$: 635.96. Found 636.0.

_p_-Methoxyphenyl 3,4,6-tri-_O_-acetyl-2-deoxy-2-(tetrachlorophthalimido)-β-D-glucopyranoside (420):

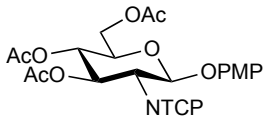

To 3.004 g (4.883 mmol) of 1,3,4,6-tetra-*O*-acetyl-2-deoxy-2-(tetrachlorophthalimido)-β-D-glucopyranose (**419**), 1.235 g (9.948 mmol) of *p*-methoxyphenol, and 10 mL of anhydrous CH_2Cl_2 at 0 °C, 3.0 mL (24.31 mmol) of $BF_3{\cdot}OEt_2$ was added and the reaction was gradually warmed to room temperature and stirred overnight. The reaction mixture was diluted with CH_2Cl_2 and quenched with saturated $NaHCO_3$. The organic phase was washed with H_2O and saturated NaCl, followed by drying over $MgSO_4$. The solution was filtered and concentrated under reduced pressure. The crude oil was recrystallized from EtOH to afford 3.198 g of a yellow, powdery solid in 96 % yield. **^{1}H-NMR** (400 MHz, $CDCl_3$): δ 6.85 (d, *J* = 9.2 Hz, 2H), 6.75 (d, *J* = 9.2 Hz, 2H), 5.84 (d, *J* = 8.5 Hz, 1H), 5.77 (dd, *J* = 10.5, 9.0 Hz, 1H), 5.25 (dd, *J* = 10.1, 9.1 Hz, 1H), 4.56 (dd, *J* = 10.5, 8.5 Hz, 1H), 4.35 (dd, *J* = 12.3, 5.2 Hz, 1H), 4.16 (dd, *J* = 12.3, 2.3 Hz, 1H), 3.92 (ddd, *J* = 10.2, 5.1, 2.4 Hz, 1H), 3.74 (s, 3H), 2.10 (s, 3H), 2.05 (s, 3H), 1.92 (s, 3H). **^{13}C-NMR** (100 MHz, $CDCl_3$): δ 170.74, 170.73, 169.5, 156.0, 150.2, 140.7, 130.2, 127.1, 118.8, 114.6, 97.0, 72.2, 71.0, 68.7, 62.0, 55.8, 55.5, 20.88, 20.75, 20.65. **ESI-MS** *m/z* calcd for $C_{27}H_{23}Cl_4NO_{11}$ $[M + Na]^+$: 699.99. Found 700.0.

***p*-Methoxyphenyl 2-acetamido-2-deoxy-4,6-*O*-benzylidene-β-D-glucopyranose (421):**

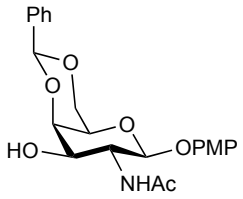

To 1.525 g (3.077 mmol) of *p*-methoxyphenyl 2-acetamido-2-deoxy-4,6-di-*O*-pivaloyl-β-D-galactopyranose (**410**) dissolved in MeOH, a 1 M NaOMe/MeOH solution was added dropwise until a pH of approximately 10 was obtained. The reaction was stirred at room temperature until TLC analysis indicated reaction completion. The reaction was neutralized with Amberlite® IR-120 (H+) ion-exchange resin, filtered, and concentrated. The crude solid was recrystallized from MeOH –ether to afford 0.7530 g of a white, powdery solid in 75 % yield. This product was dissolved in 15 mL of anhydrous acetonitrile. Once dissolved, 28.6 mg (0.1231 mmol) of 10-Camphorsulfonic acid (CSA) and 0.7 mL (4.664 mmol) of benzaldehyde dimethyl acetal was added and the reaction was refluxed for 20 minutes. The reaction was gradually cooled to room temperature and neutralized with Et_3N. The precipitate was filtered and recrystallized from CH_2Cl_2 – hexanes to afford 0.6793 g of a white, powdery solid in 52 % yield over two steps. **^{1}H-NMR** (300 MHz, DMSO-d_6): δ 7.77 (d, *J* = 9.0 Hz, 1H), 7.52-7.47 (m, 2H), 7.41-7.36 (m, 3H), 6.94 (d, *J* = 9.2 Hz, 2H), 6.86 (d, *J* = 9.2 Hz, 2H), 5.62 (s, 1H), 4.98 (dd, *J* = 11.2, 7.4 Hz, 2H), 4.16 (d, *J* = 3.2 Hz, 1H), 4.08 (s, 2H), 4.01-3.92 (m, 1H), 3.79-3.69 (m, 2H), 3.70 (s, 3H), 1.82 (s, 3H). **^{13}C-NMR** (100 MHz, DMSO-d_6): δ 169.7, 154.7, 151.6, 138.7, 128.8, 128.1, 126.5, 118.1, 114.7, 100.4, 99.9, 75.4, 69.5, 68.7, 66.3, 55.6, 52.1, 23.3. **ESI-MS** *m/z* calcd for $C_{22}H_{25}NO_7$ $[M + Na]^+$: 438.15. Found 438.1.

4.5 NMR Spectra of Disaccharide Intermediates

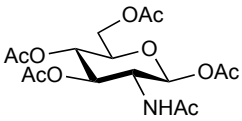

406

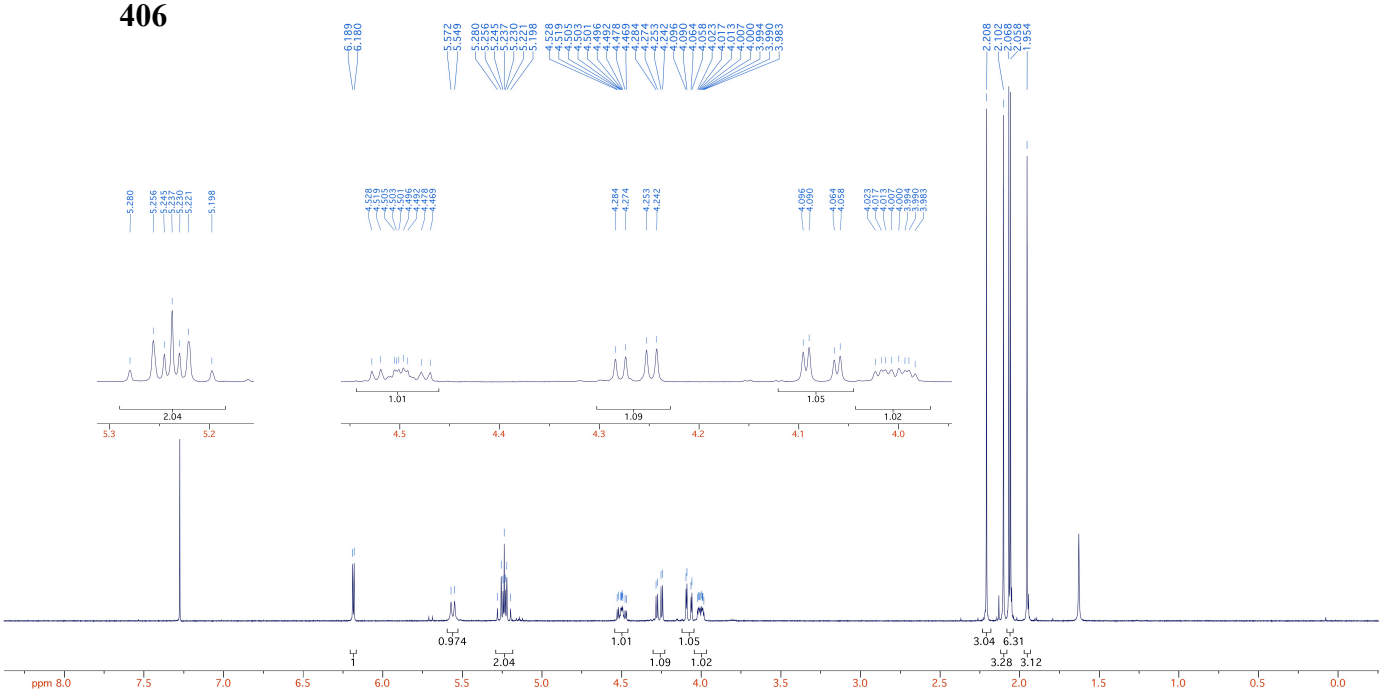

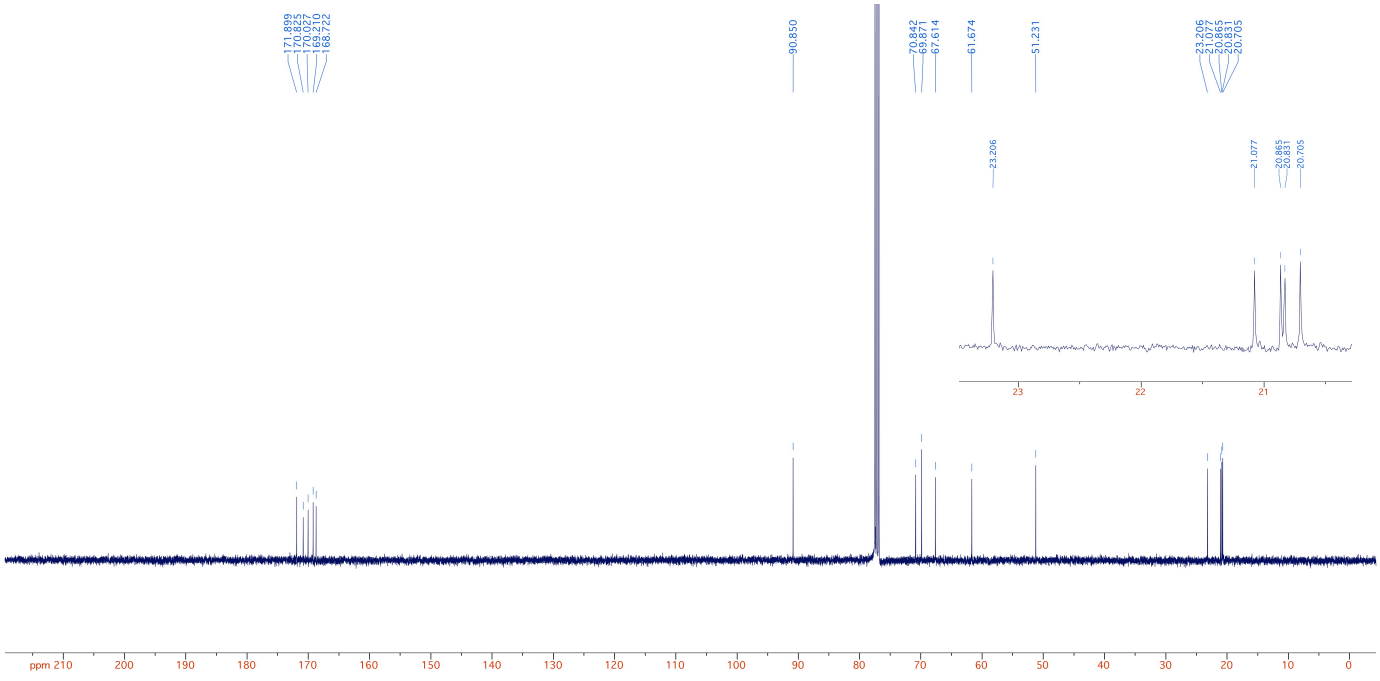

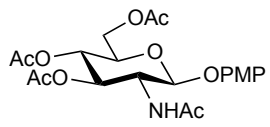

407

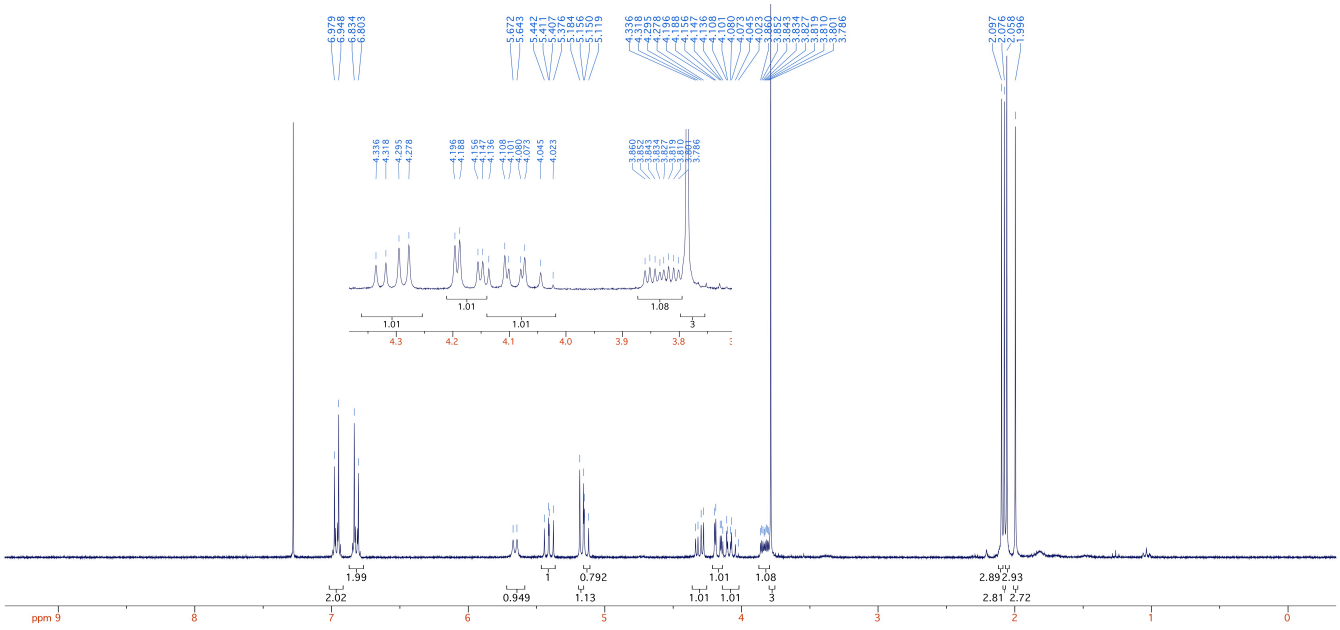

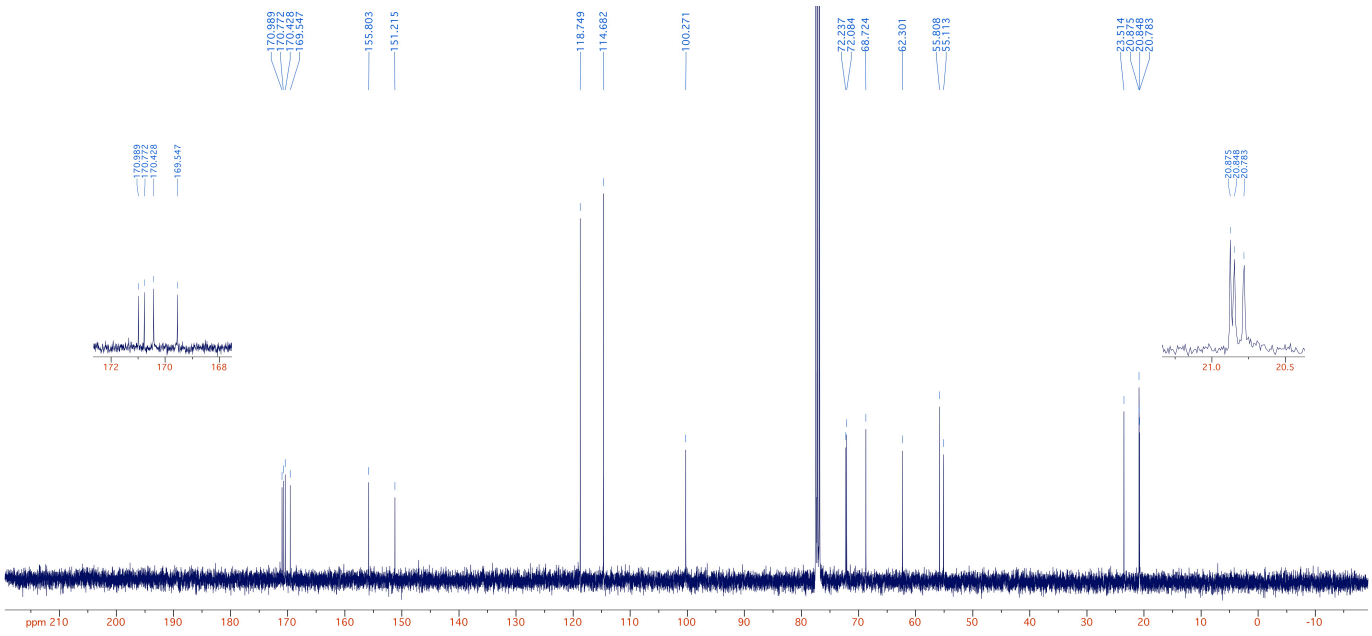

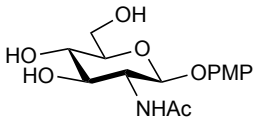

408

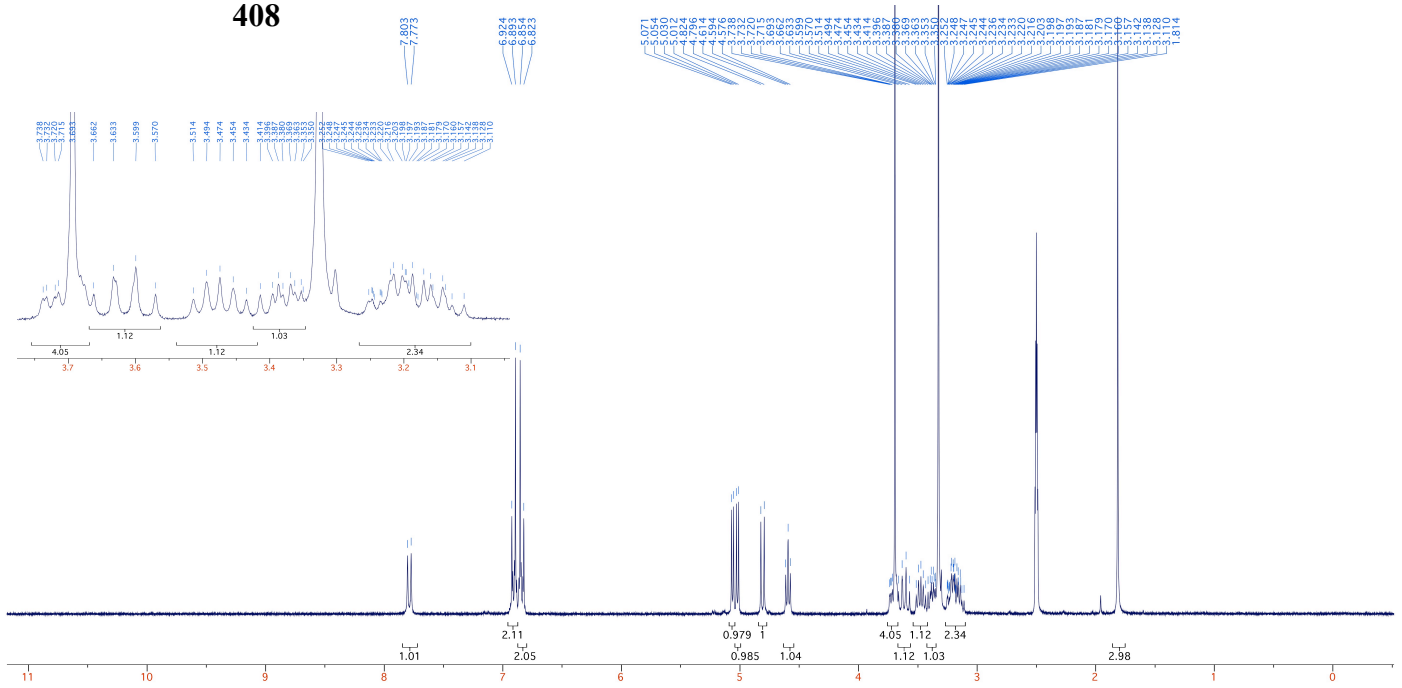

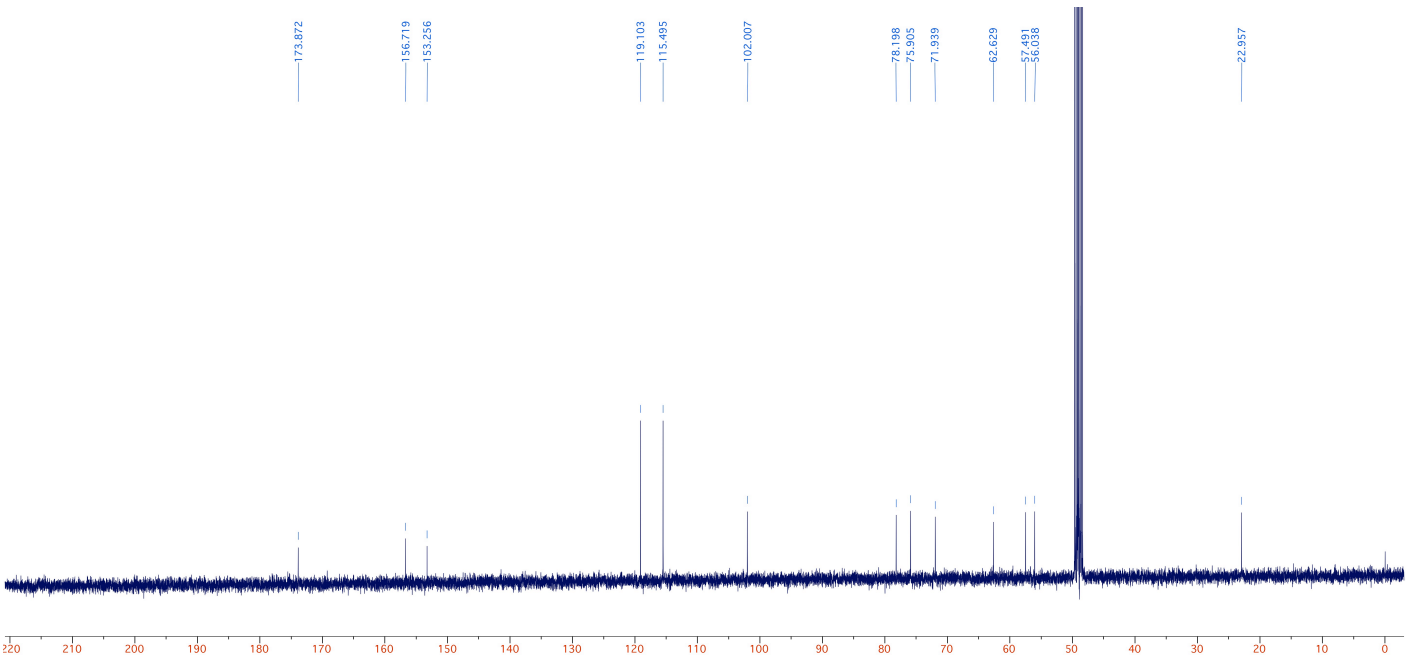

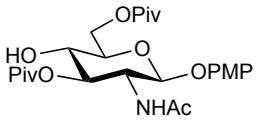

409

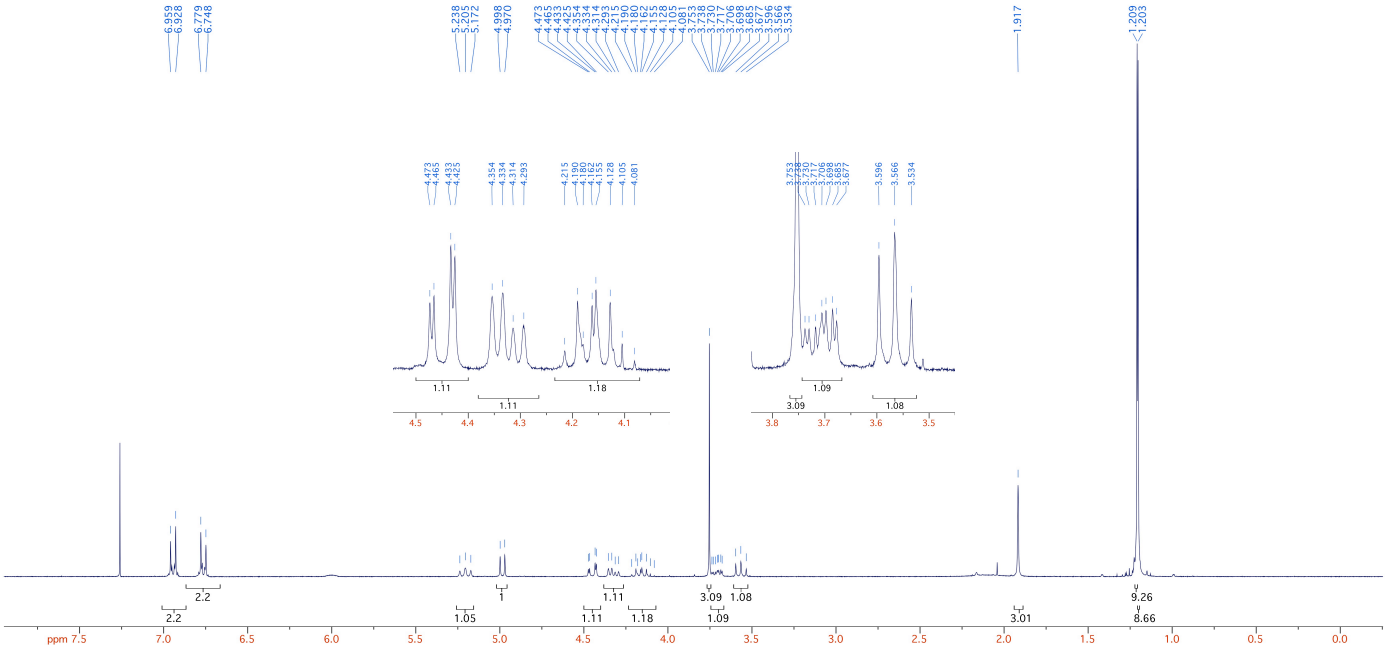

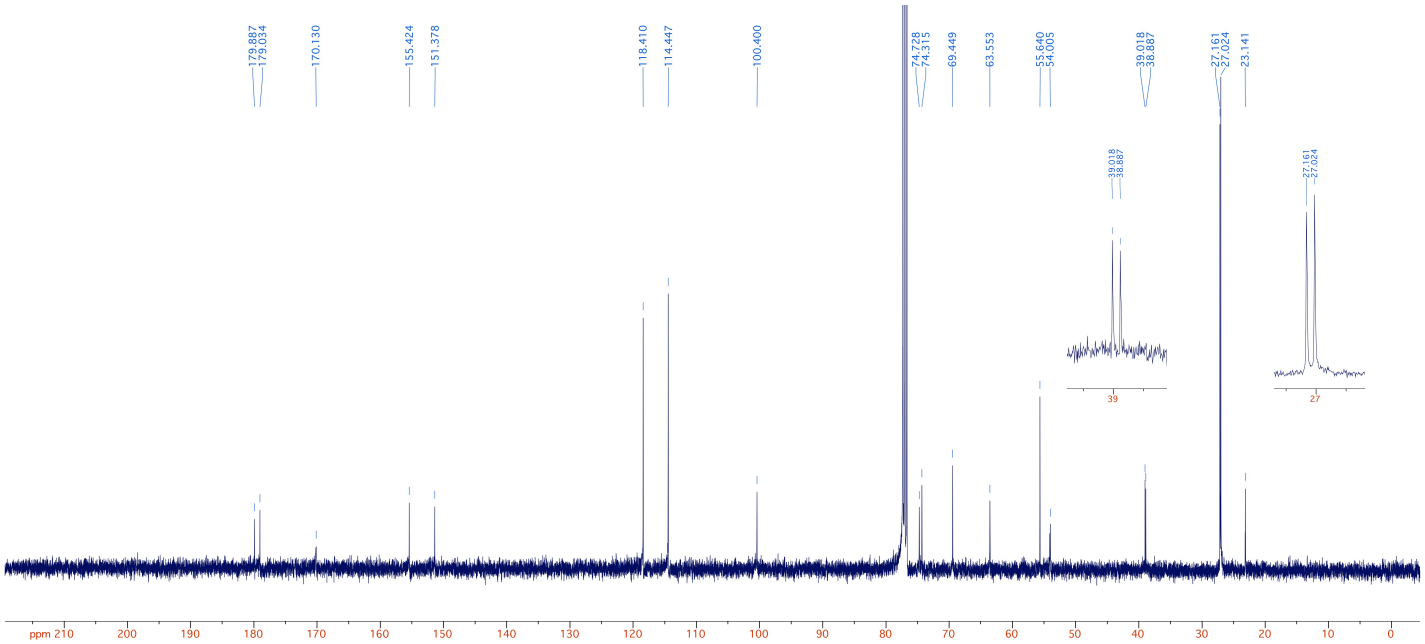

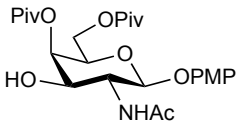

410

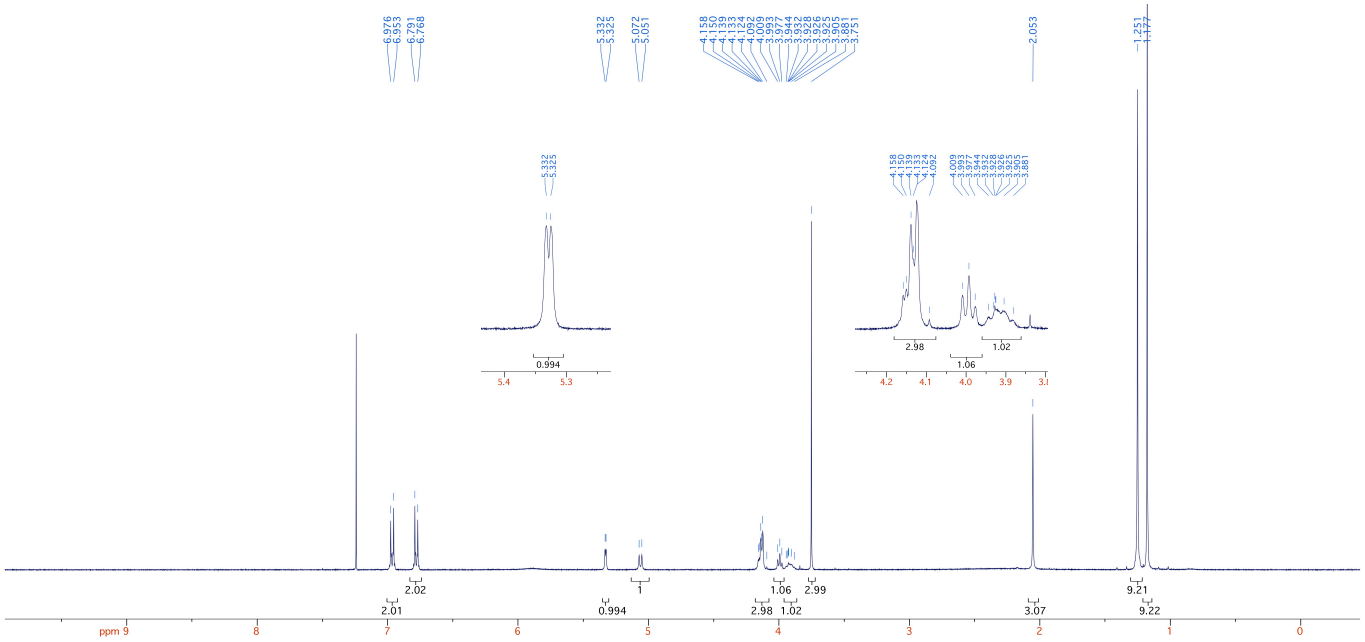

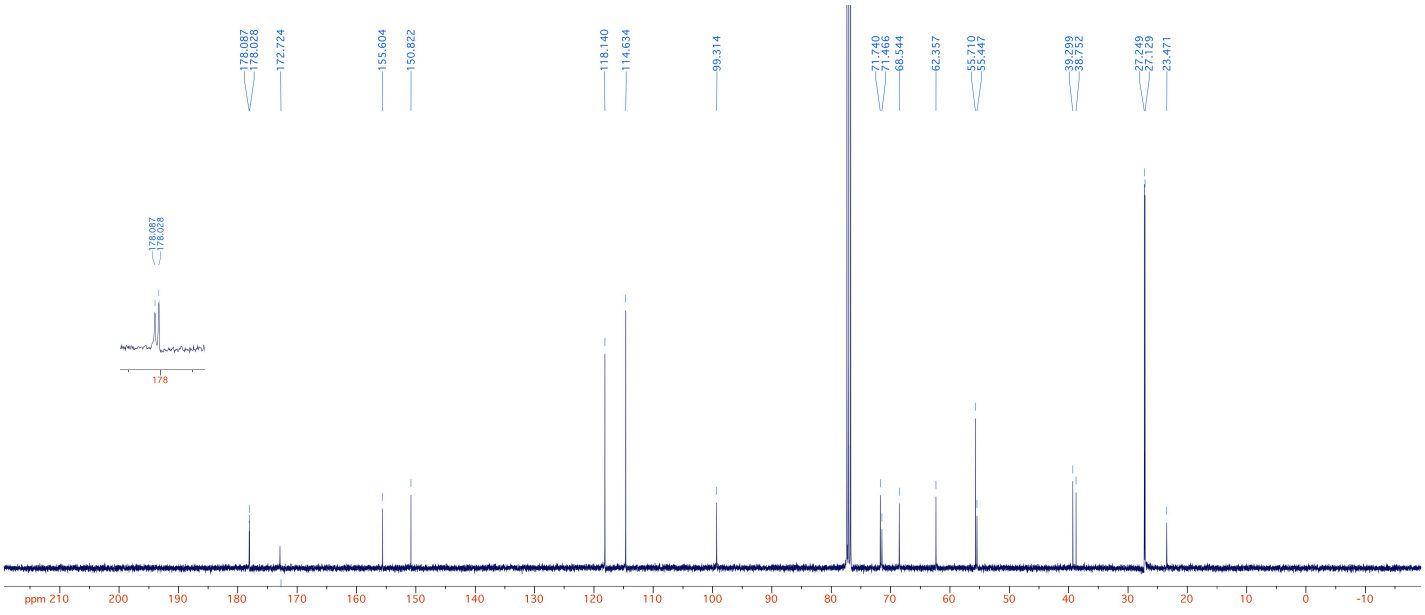

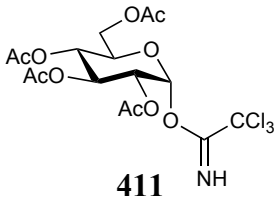
OAc
AcO
AcO
AcO
O
O
CCl3
NH

411

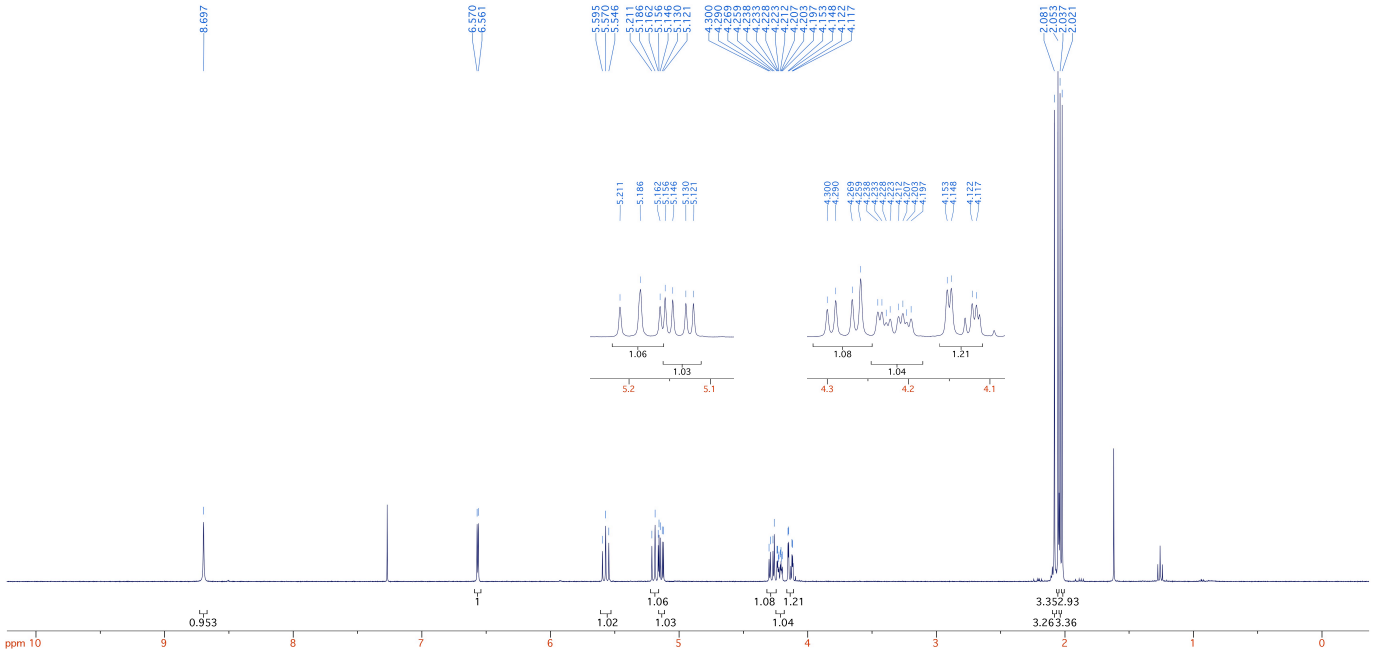
8.697
6.570
6.561
5.595
5.570
5.546
5.211
5.186
5.162
5.156
5.146
5.130
5.121
4.300
4.290
4.269
4.259
4.238
4.233
4.228
4.212
4.207
4.203
4.197
4.153
4.148
4.122
4.117
2.081
2.053
2.037
2.021
1.06
1.03
1.08
1.04
1.21
0.953
1
1.02
1.06
1.03
1.08
1.21
3.352.93
3.263.36
ppm 10
9
8
7
6
5
4
3
2
1
0

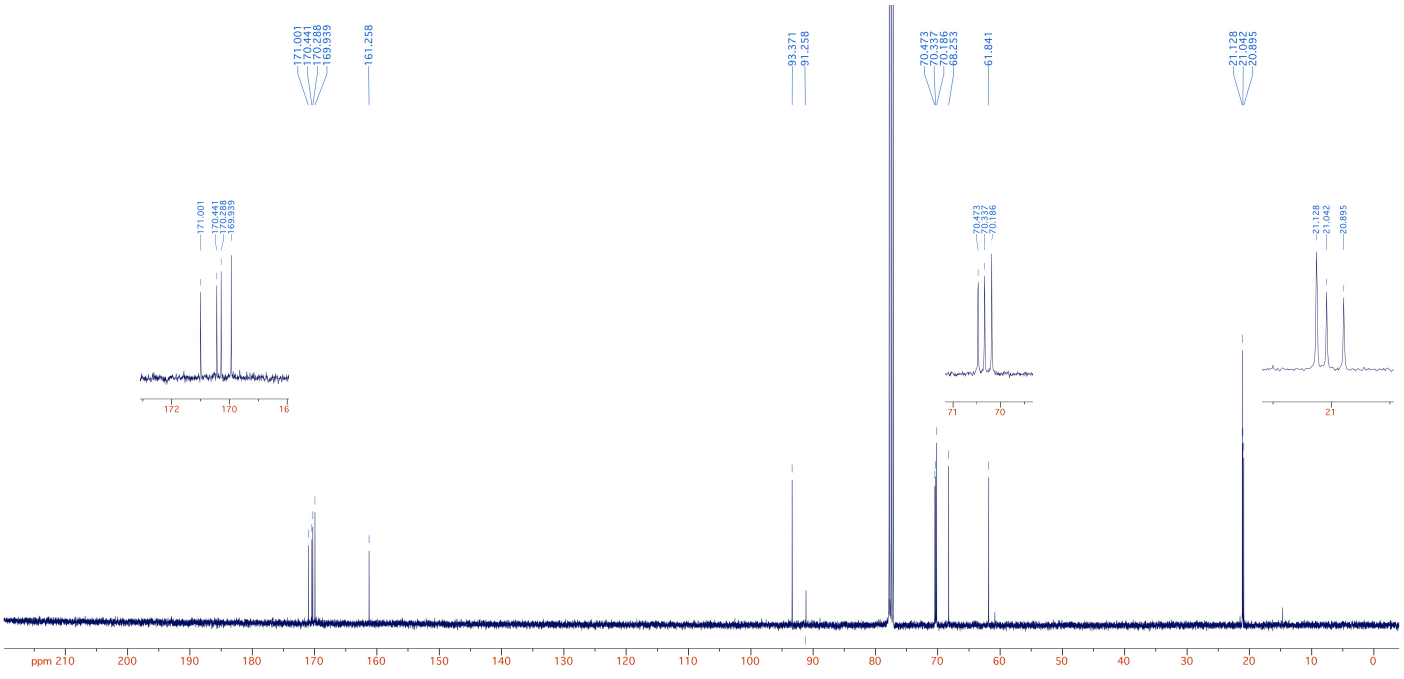
171.001
170.441
170.288
169.939
161.258
93.371
91.258
70.473
70.337
70.186
68.253
61.841
21.128
21.042
20.895
ppm 210
200
190
180
170
160
150
140
130
120
110
100
90
80
70
60
50
40
30
20
10
0

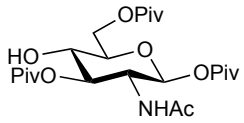

413

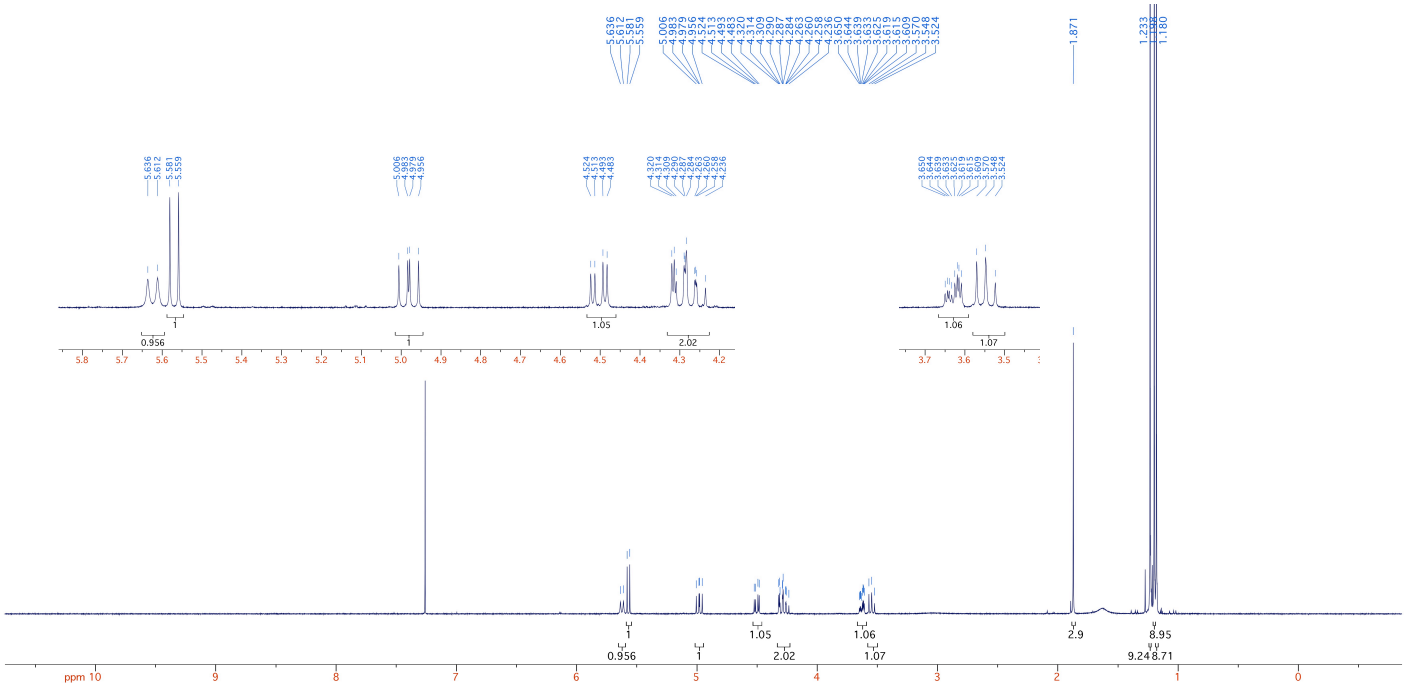

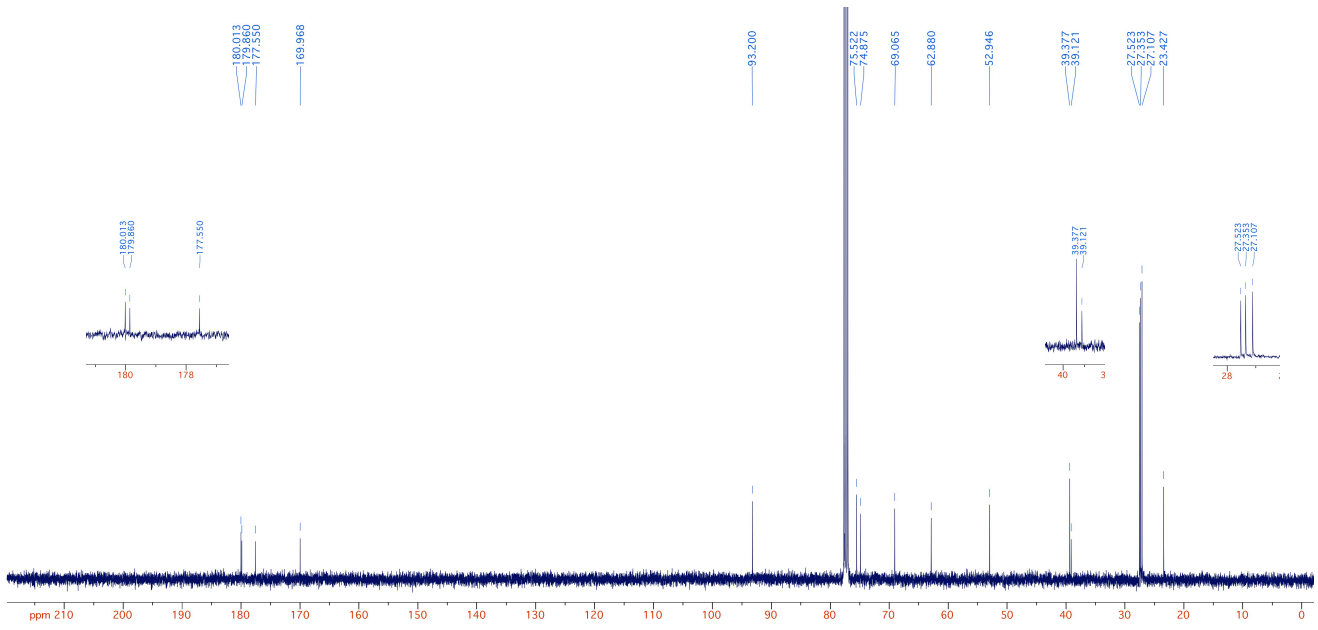

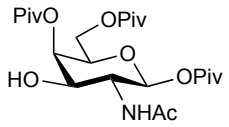

414

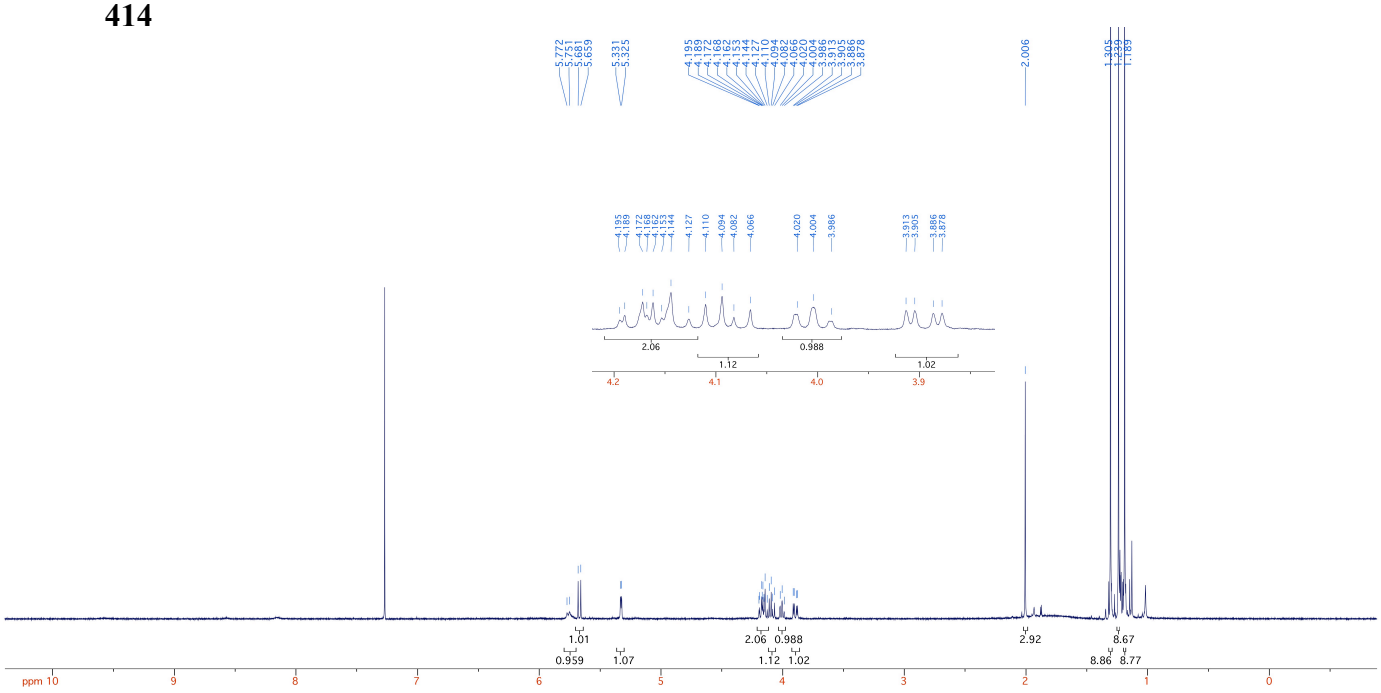

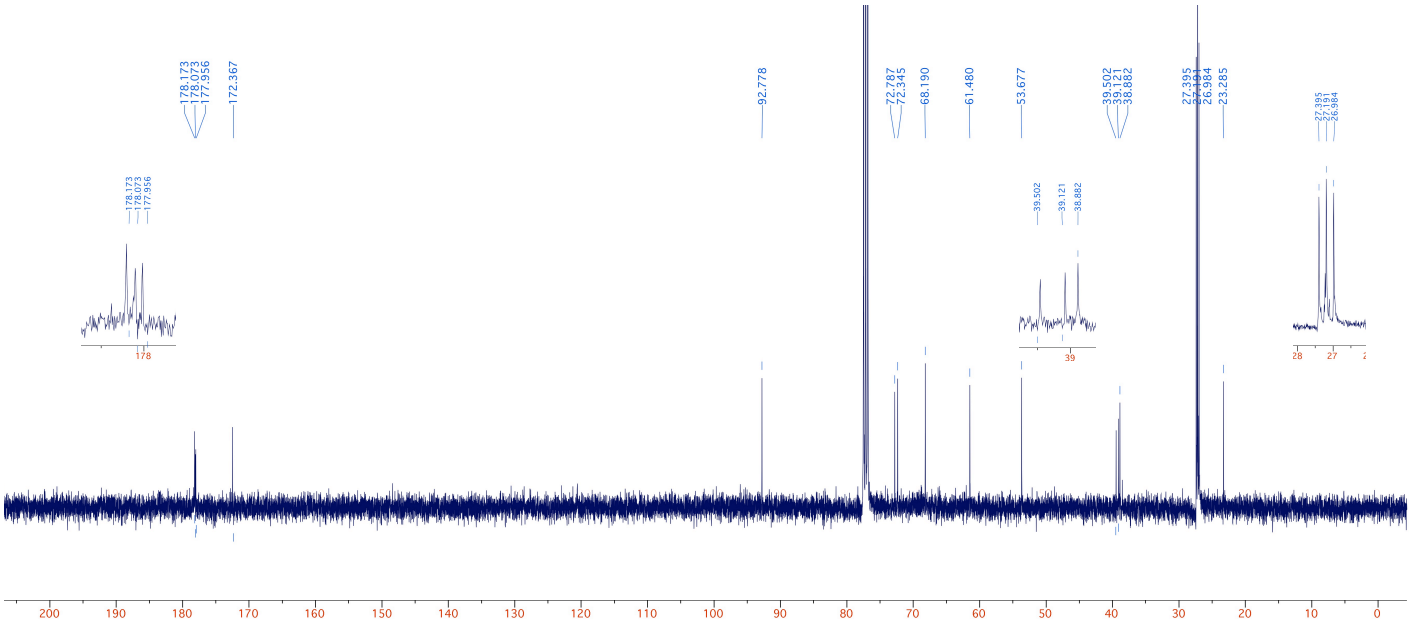

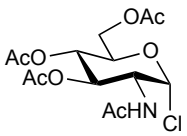
OAc
AcO
AcO
O
AcHN
Cl

415

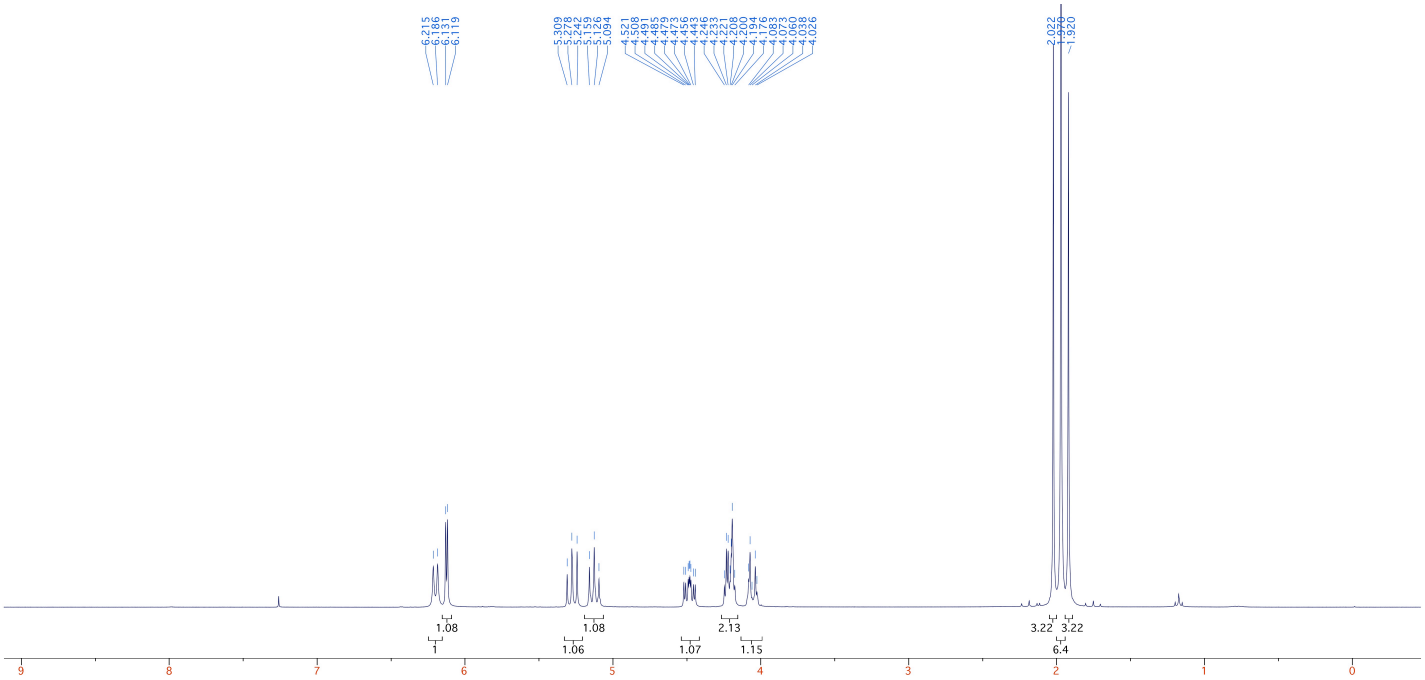
6.215
6.186
6.131
6.119
5.309
5.293
5.242
5.159
5.152
5.094
4.521
4.508
4.491
4.485
4.469
4.473
4.456
4.443
4.426
4.233
4.221
4.208
4.200
4.194
4.176
4.083
4.073
4.060
4.038
4.026
2.022
1.966
1.920
1.08
1.08
2.13
3.22
3.22
1
1.06
1.07
1.15
6.4
9
8
7
6
5
4
3
2
1
0

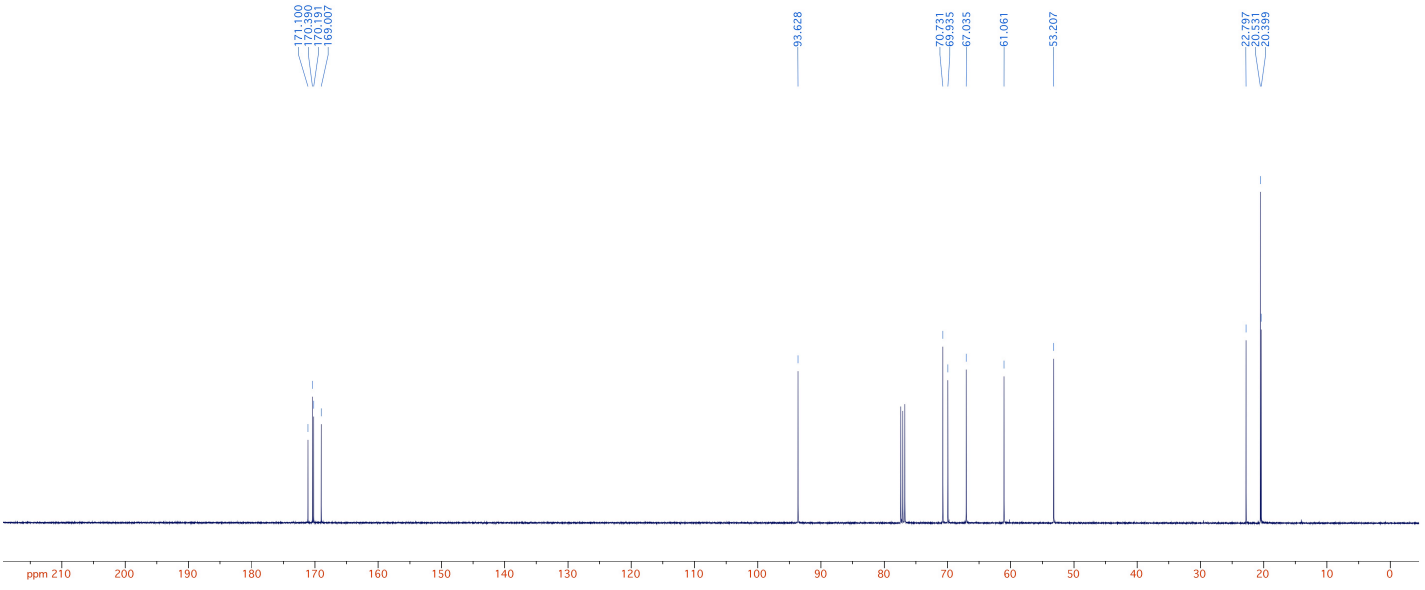
171.100
170.390
170.191
169.007
93.628
70.731
69.935
67.035
61.061
53.207
22.797
20.531
20.399
ppm 210
200
190
180
170
160
150
140
130
120
110
100
90
80
70
60
50
40
30
20
10
0

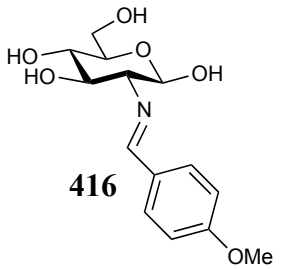

416

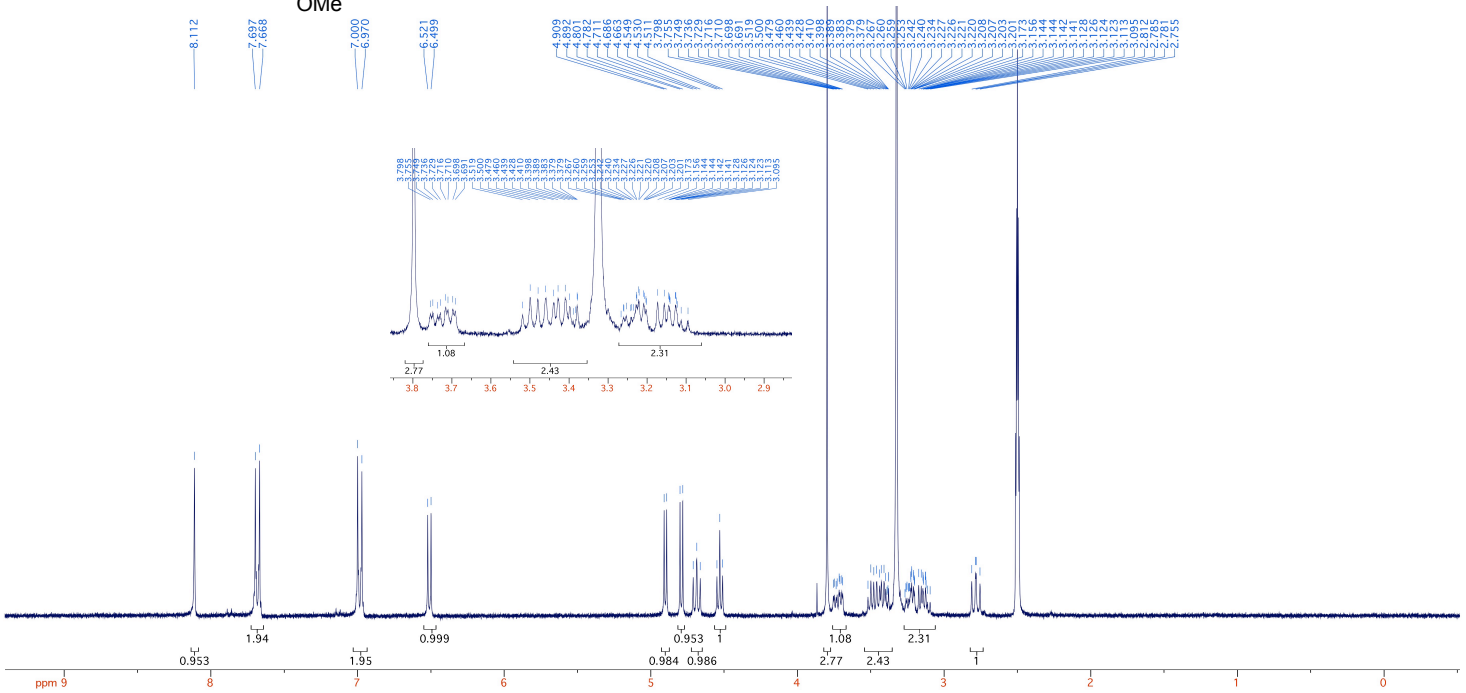

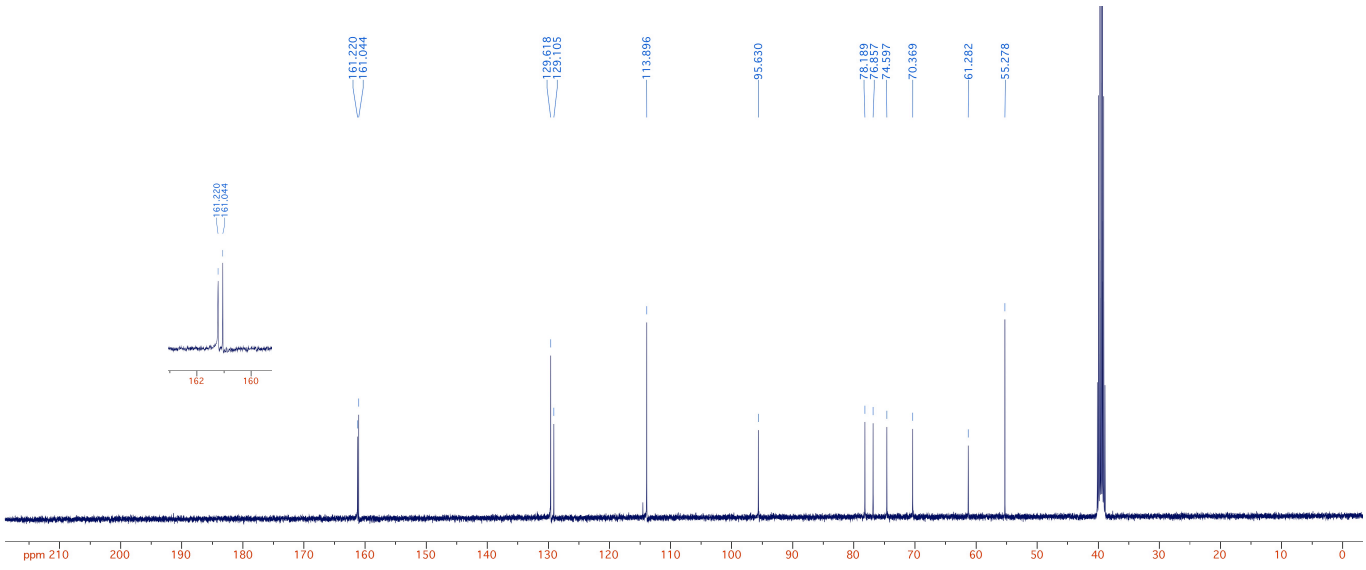

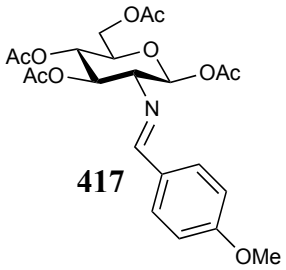

417

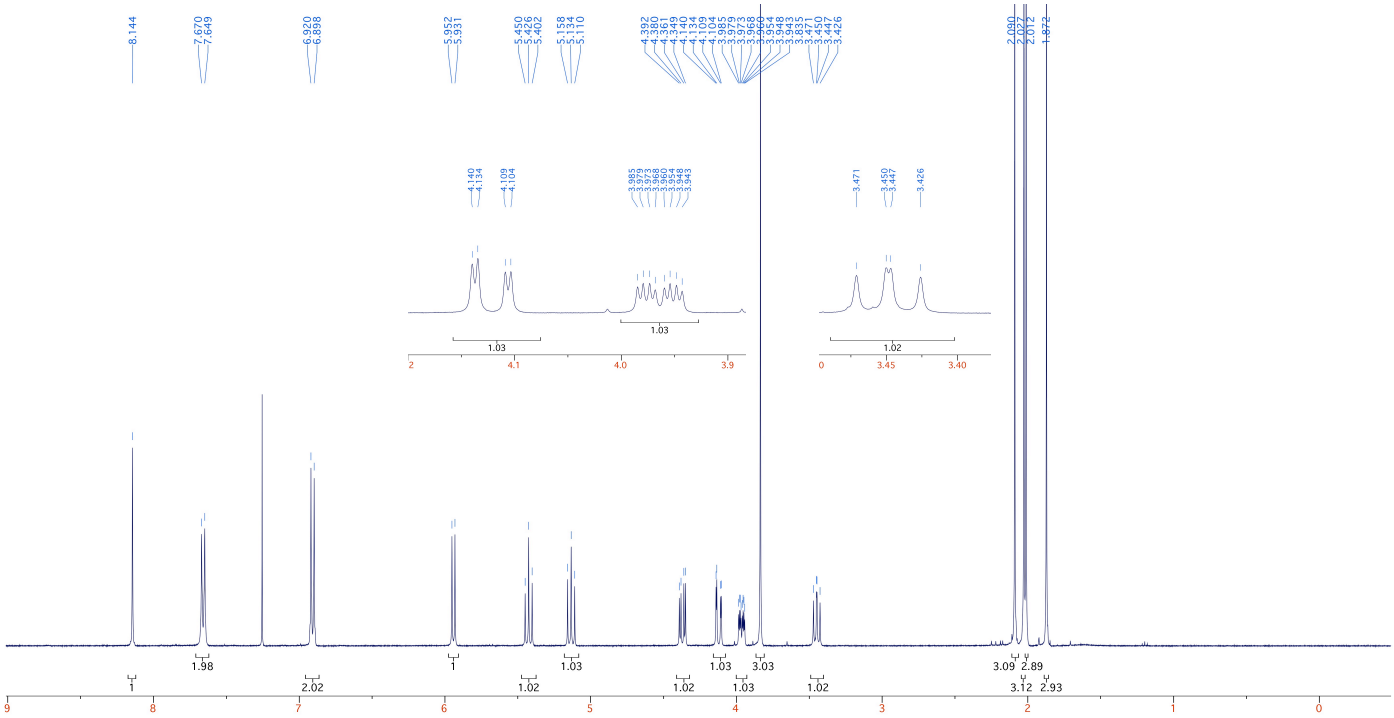

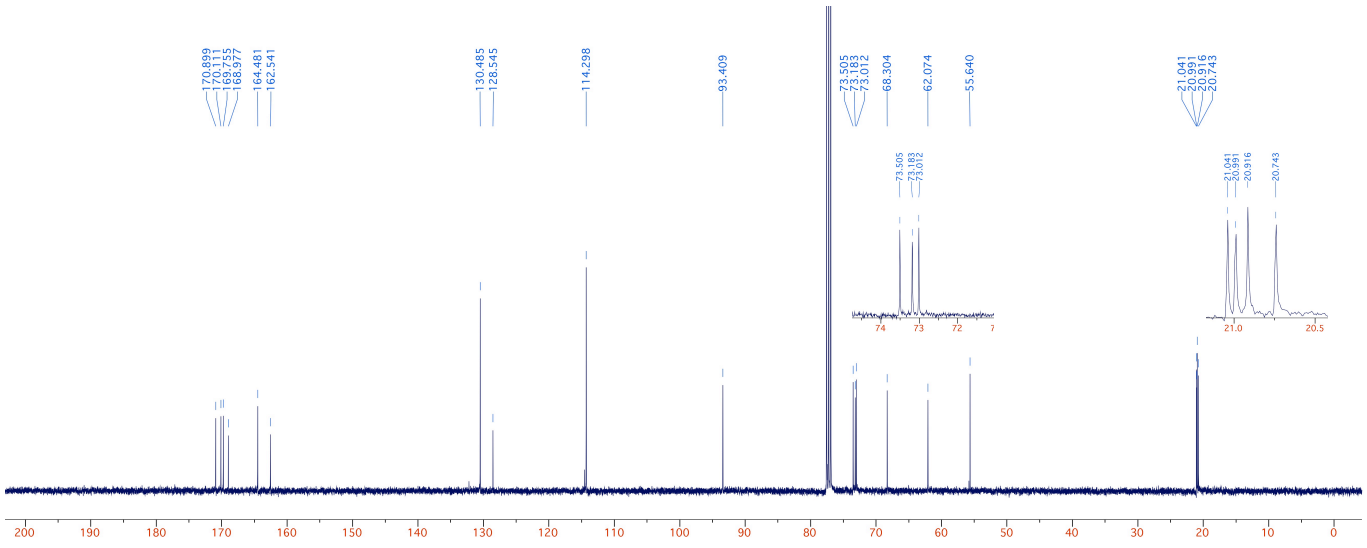

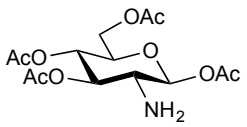

418

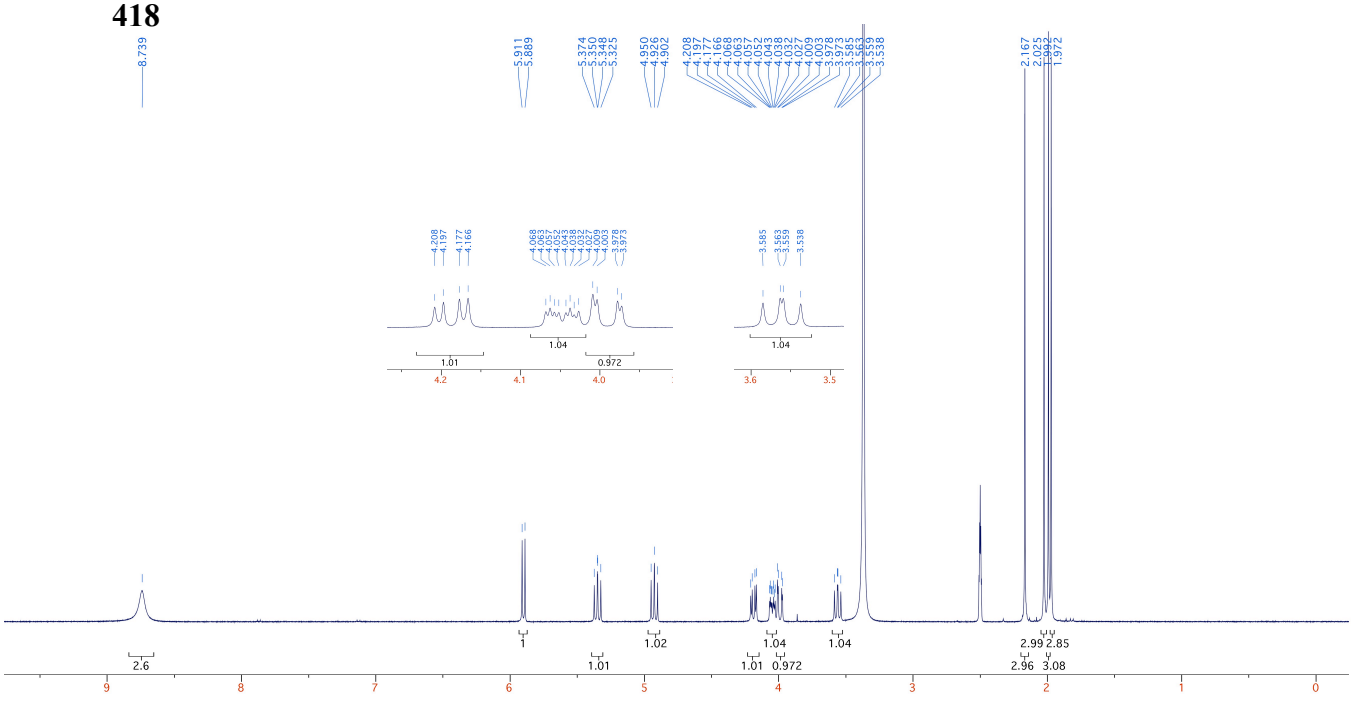

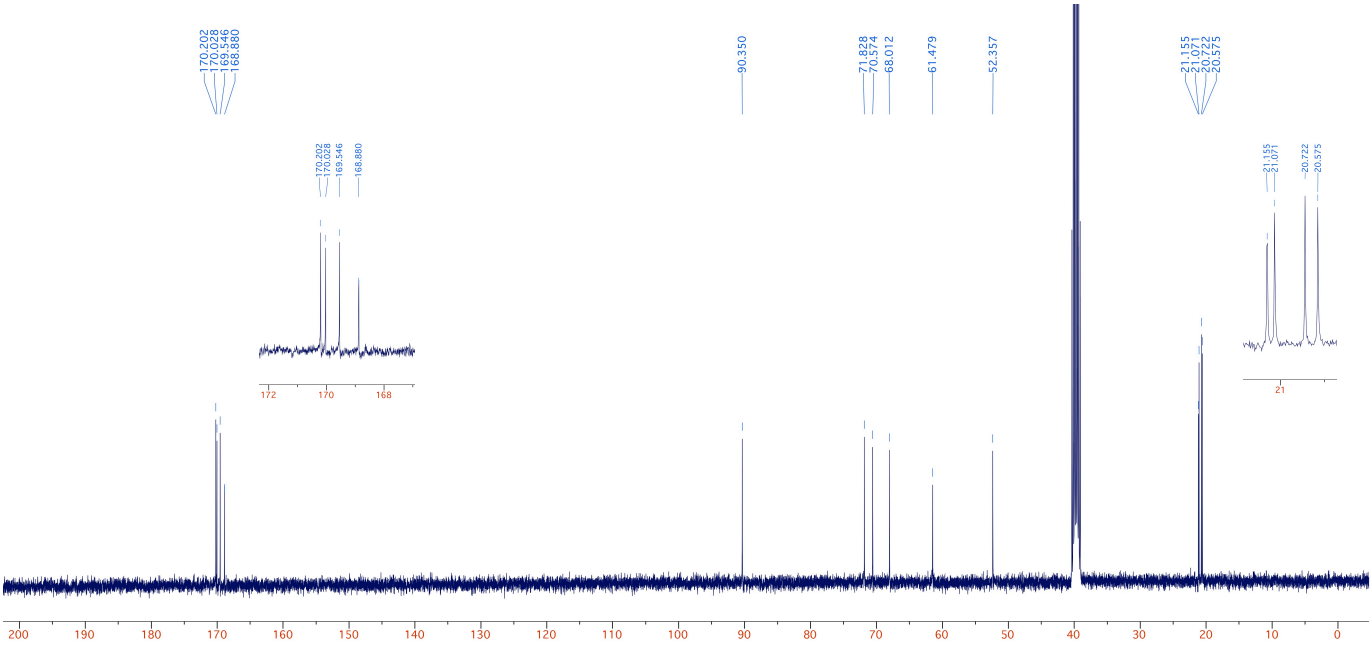

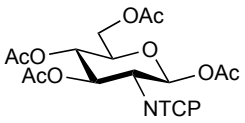

419

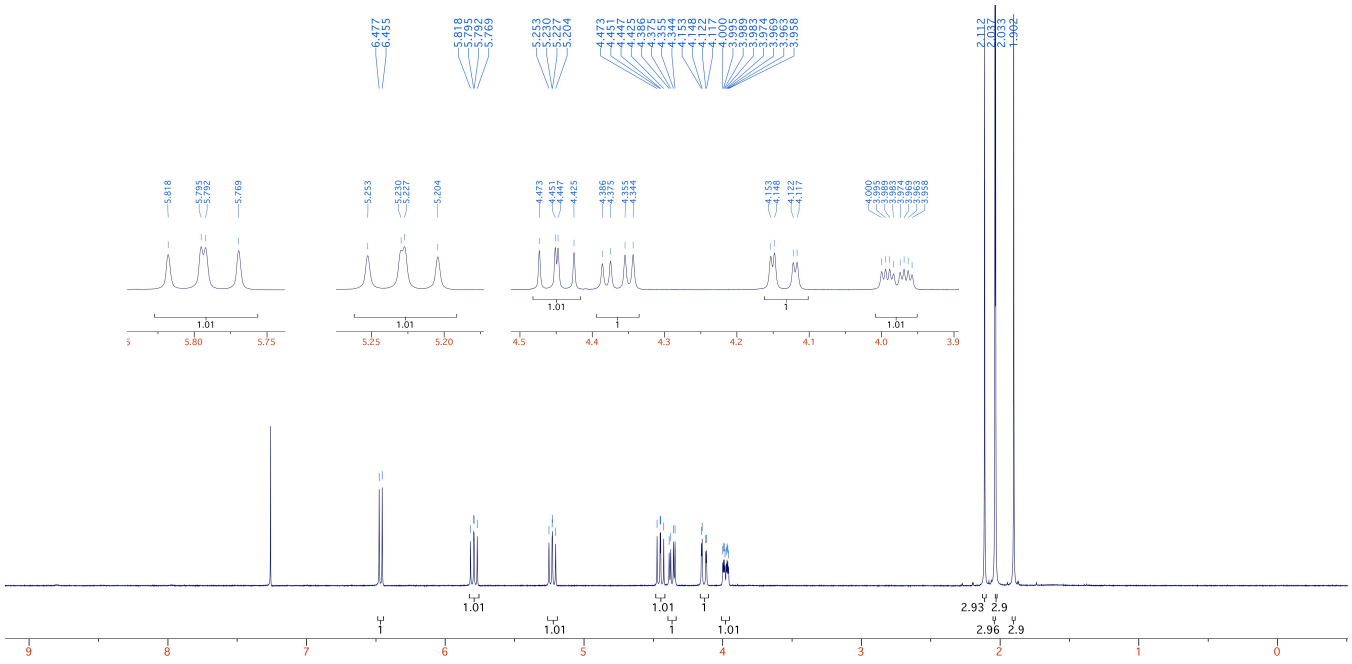

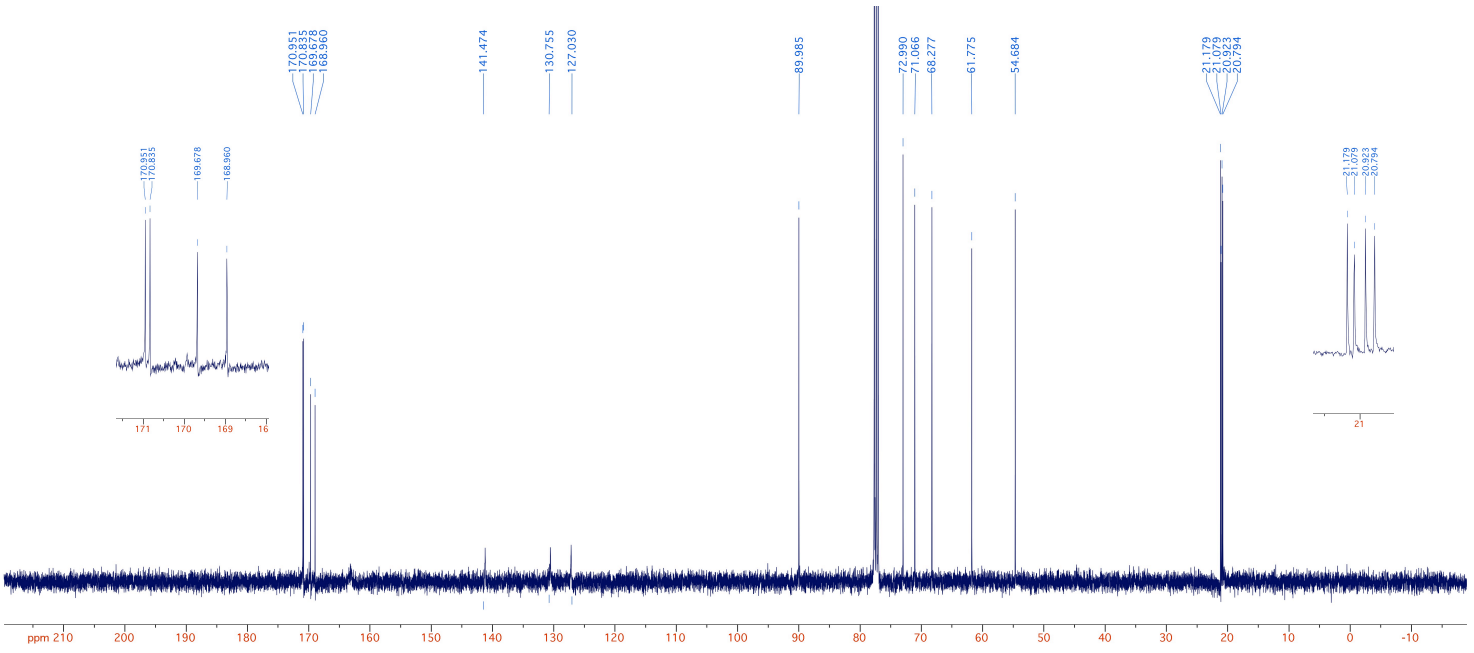

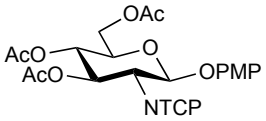
OAc
AcO
O
AcO
OPMP
NTCP

420

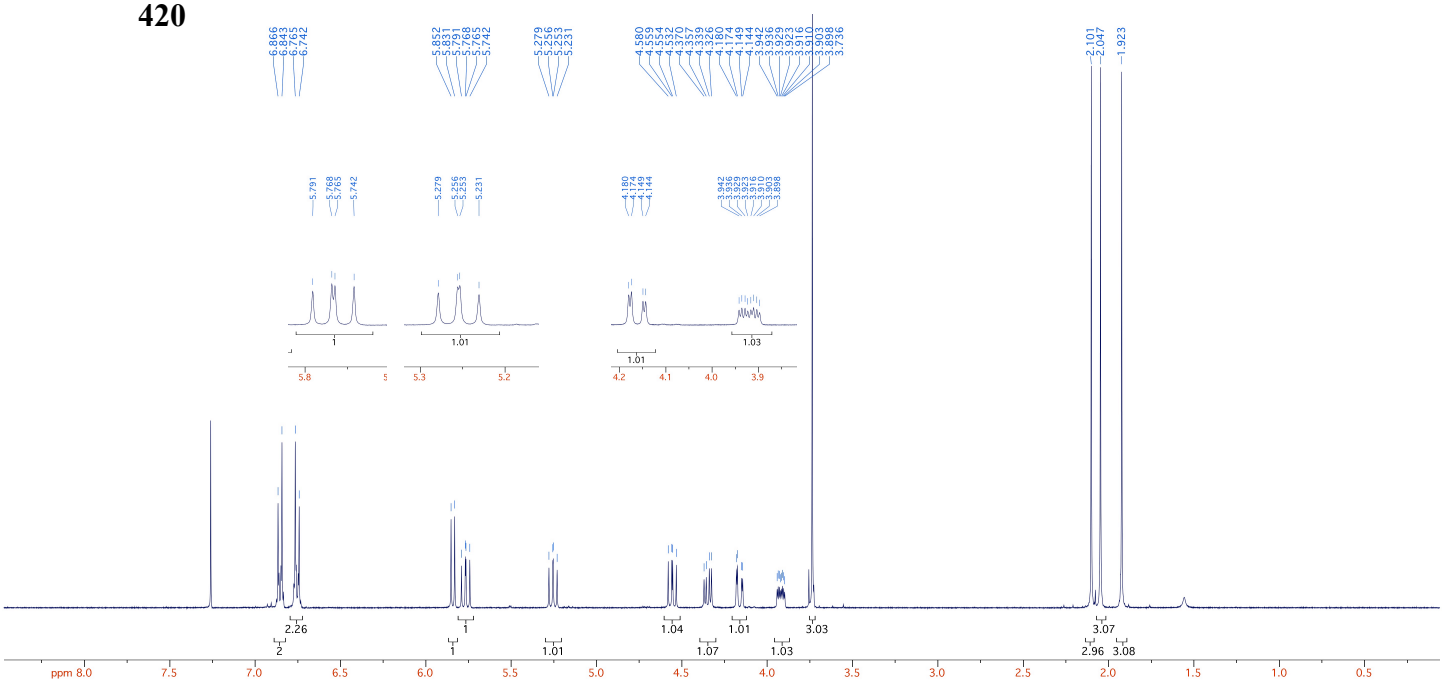
6.866
6.863
6.743
6.740
6.742
5.852
5.831
5.791
5.768
5.765
5.742
5.279
5.256
5.253
5.231
4.580
4.559
4.554
4.532
4.370
4.337
4.326
4.190
4.180
4.154
4.149
4.144
3.942
3.926
3.923
3.911
3.910
3.903
3.898
3.736
2.101
2.047
1.923
2.26
1
1
1.01
1.04
1.01
1.03
3.03
3.07
2.96
3.08
ppm 8.0
7.5
7.0
6.5
6.0
5.5
5.0
4.5
4.0
3.5
3.0
2.5
2.0
1.5
1.0
0.5

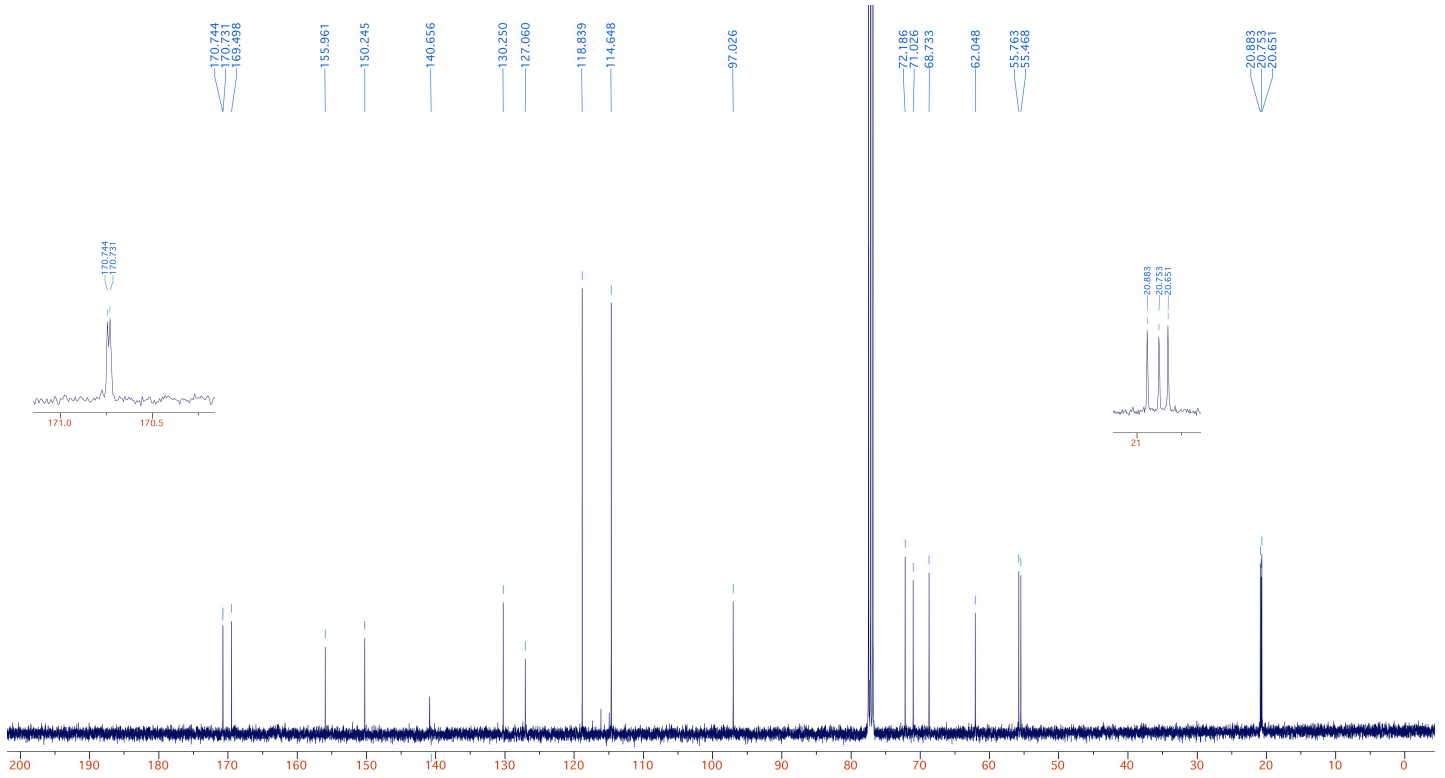
170.744
170.731
169.498
155.961
150.245
140.656
130.250
127.060
118.839
114.648
97.026
72.186
71.026
68.733
62.048
55.763
55.468
20.883
20.753
20.651
200
190
180
170
160
150
140
130
120
110
100
90
80
70
60
50
40
30
20
10
0

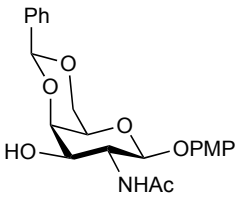
Ph
O
O
O
HO
OPMP
NHAc

421

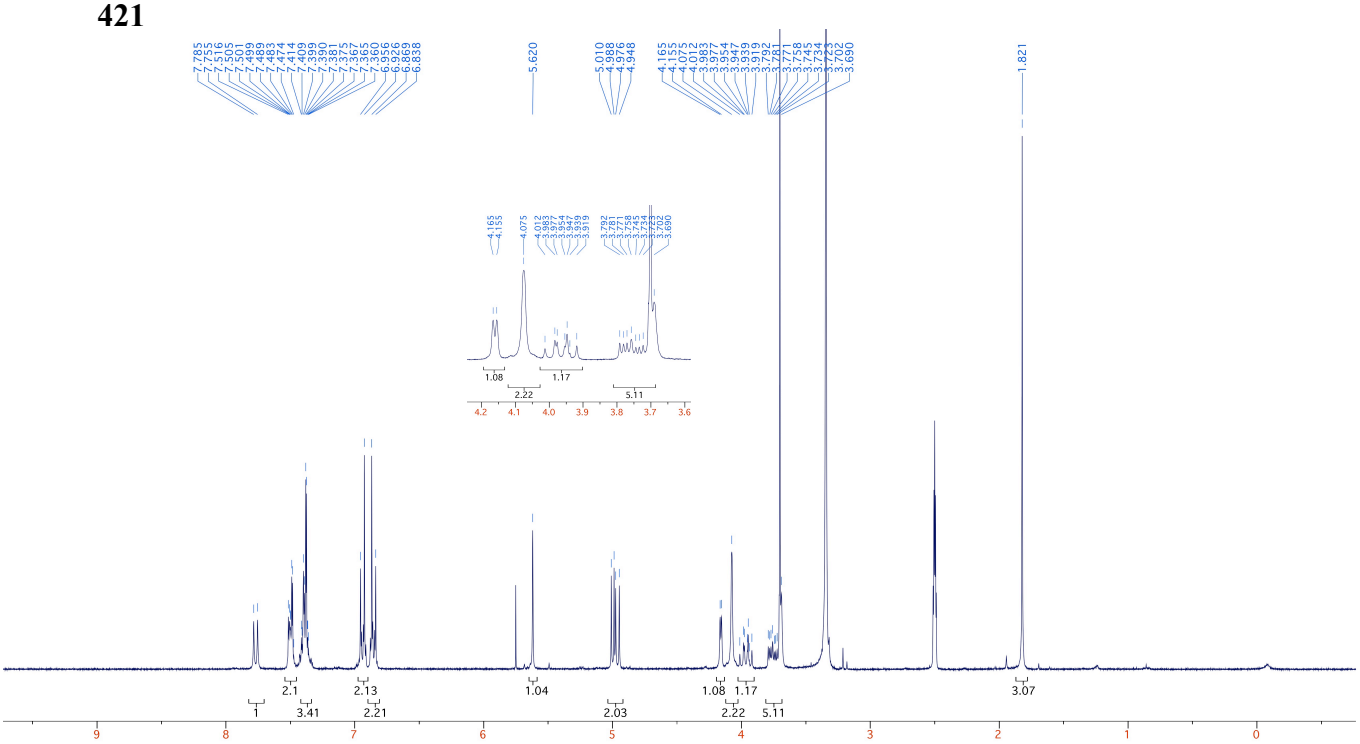
7.785
7.755
7.516
7.505
7.501
7.499
7.489
7.483
7.474
7.414
7.409
7.399
7.390
7.381
7.375
7.367
7.365
7.360
6.956
6.826
6.829
6.838
5.620
5.010
4.988
4.976
4.948
4.165
4.155
4.075
4.012
4.007
3.983
3.977
3.954
3.947
3.939
3.919
3.792
3.781
3.771
3.758
3.745
3.734
3.723
3.702
3.690
1.821
1.08
2.22
1.17
5.11
2.1
3.41
2.13
2.21
1.04
2.03
1.08
1.17
2.22
5.11
3.07

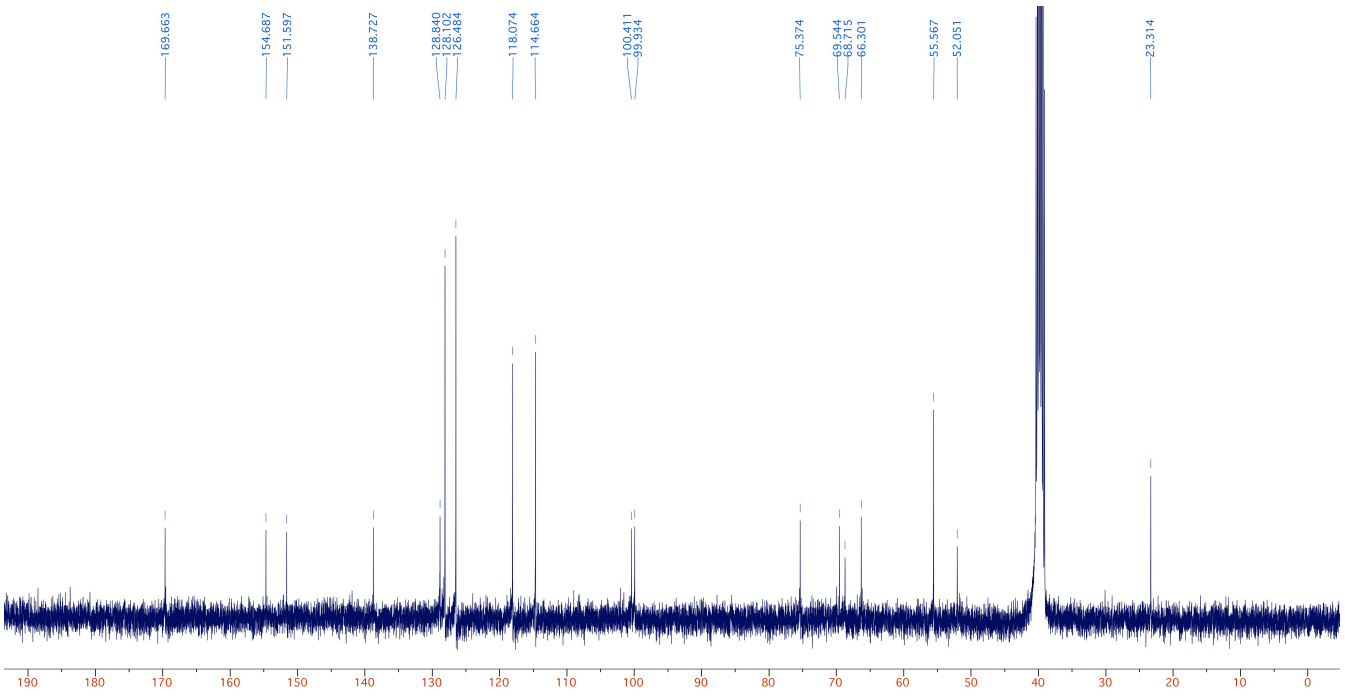
169.663
154.687
151.597
138.727
128.840
128.102
126.484
118.074
114.664
100.411
99.334
75.374
69.544
68.315
66.301
55.567
52.051
23.314

4.6 References

(1) DeVries, A. L.; Komatsu, S. K.; Feeney, R. E. *J. Biol. Chem.* **1970**, *245*, 2901–2908.

(2) DeVries, A. L. *Comp. Biochem. Physiol.* **1982**, *73*, 627–640.

(3) Harding, M. M.; Anderberg, P. I.; Haymet, A. D. J. *Eur. J. Biochem.* **2003**, *270*, 1381–1392.

(4) Gupta, R.; Deswal, R. *J. Biosci.* **2014**, *39*, 931–944.

(5) Bouvet, V.; Ben, R. N. *Cell Biochem. Biophys.* **2003**, *39*, 133–144.

(6) Garner, J.; Harding, M. M. *ChemBioChem.* **2010**, *11*, 2489–2498.

(7) Wu, Y.; Banoub, J.; Goddard, S. V; Kao, M. H.; Fletcher, G. L. *Comp. Biochem. Physiol. Part B* **2001**, *128*, 265–273.

(8) Knight, C. A.; DeVries, A. L.; Oolman, L. D. *Nature* **1984**, *308*, 295–296.

(9) Burcham, T. S.; Osuga, D. T.; Chino, H.; Feeney, R. E. *Anal. Biochem.* **1984**, *139*, 197–204.

(10) Ahlgren, J. A.; Cheng, C.-H. C.; Schrag, J. D.; DeVries, A. L. *J. Exp. Biol.* **1988**, *137*, 549–563.

(11) Eniade, A.; Purushotham, M.; Ben, R. N.; Wang, J. B.; Horwath, K. *Cell Biochem. Biophys.* **2003**, *38*, 115–124.

(12) Liu, S.; Ben, R. N. *Org. Lett.* **2005**, *7*, 2385–2388.

(13) Czechura, P.; Tam, R. Y.; Dimitrijevic, E.; Murphy, A. V; Ben, R. N. *J. Am. Chem. Soc.* **2008**, *130*, 2928–2929.

(14) Balcerzak, A. K. Elucidating the Key Structural Features of Carbohydrates and Surfactants Necessary for Inhibiting Ice Recrystallization, University of Ottawa, 2014.

(15) Ferreira, S. S. Improving the Rational Design of Antifreeze Glycoproteins Through Identification of the Parameters that Influence Ice Recrystallization Inhibition, University of Ottawa, 2014.

(16) Tam, R. Y.; Ferreira, S. S.; Czechura, P.; Chaytor, J. L.; Ben, R. N. *J. Am. Chem. Soc.* **2008**, *130*, 17494–17501.

(17) Balcerzak, A. K.; Ferreira, S. S.; Trant, J. F.; Ben, R. N. *Bioorg. Med. Chem. Lett.*

2012, *22* (4), 1719–1721.

(18) Trant, J. F. Importance of the structural components of C ‐ linked glycopeptides to specific antifreeze activity : from glycopeptides to small molecule inhibitors of ice recrystallization, University of Ottawa, 2012.

(19) Yu, S. O.; Brown, A.; Middleton, A. J.; Tomczak, M. M.; Walker, V. K.; Davies, P. L. *Cryobiology* **2010**, *61*, 327–334.

(20) Tachibana, Y.; Fletcher, G. L.; Fujitani, N.; Tsuda, S.; Monde, K.; Nishimura, S. *Angew. Chem. Int. Ed.* **2004**, *116*, 874–880.

(21) Bond, M. R.; Hanover, J. A. *J. Cell Biol.* **2015**, *208*, 869–880.

(22) Konopka, J. B. *Scientifica (Cairo).* **2012**.

(23) Werz, D. B.; Ranzinger, R.; Herget, S.; Adibekian, A.; von der Lieth, C.-W.; Seeberger, P. H. *ACS Chem. Biol.* **2007**, *2*, 685–691.

(24) Chia, J.; Goh, G.; Bard, F. *Biochim. Biophys. Acta* **2016**, *1860*, 1623–1639.

(25) Feng, J.; Ling, C. *Carbohydr. Res.* **2010**, *345*, 2450–2457.

(26) Conchie, J.; Levvy, G. A.; Marsh, C. A. *Adv. Carbohydr. Chem.* **1957**, *12*, 157–187.

(27) Boltje, T. J.; Buskas, T.; Boons, G. *Nat. Chem.* **2009**, *1*, 611–622.

(28) Guo, J.; Ye, X. *Molecules* **2010**, *15*, 7235–7265.

(29) Chen, L.; Kong, F. *Tetrahedron Lett.* **2003**, *44*, 3691–3695.

(30) Toshima, K.; Tatsuta, K. *Chem. Rev.* **1993**, *93*, 1503–1531.

(31) Paulsen, B. H. *Chem. Soc. Rev.* **1984**, *13*, 15–45.

(32) Demchenko, A. *Handbook of Chemical Glycosylation: Advances in Stereoselectivity and Therapeutic Relevance*; Wiley-VCH Verlag GmbH & Co. KGaA, 2008.

(33) Zhu, X.; Schmidt, R. R. *Angew. Chem. Int. Ed.* **2009**, *48*, 1900–1934.

(34) Rasmussen, M. R.; Marqvorsen, M. H. S.; Kristensen, S. K.; Jensen, H. H. *J. Org. Chem.* **2014**, *79*, 11011–11019.

(35) Christensen, H.; Christiansen, M. S.; Petersen, J.; Jensen, H. H. *Org. Biomol. Chem.* **2008**, *6*, 3276–3283.

(36) Krag, J.; Christiansen, M. S.; Petersen, J. G.; Jensen, H. H. *Carbohydr. Res.* **2010**, *345*, 872–879.

(37) Deslongchamps, P. *Stereoelectronic Effects in Organic Chemistry*; Pergamon Press: Willowdale, Ontario, 1983.

(38) Brewster, K.; Harrison, J. M.; Inch, T. D. *Tetrahedron Lett.* **1979**, *52*, 5051–5054.

(39) Dess, D.; Kleine, H. P.; Weinberg, D. V.; Kaufman, R. J.; Sidhu, R. S. *Synthesis* **1981**, 883–885.

(40) Rothermel, J.; Faillard, H. *Carbohydr. Res.* **1990**, *196*, 29–40.

(41) Roy, R.; Tropper, F. D. *Can. J. Chem.* **1991**, *69*, 817–821.

(42) Roy, R.; Tropper, F. *Synth. Commun.* **1990**, *20*, 2097–2102.

(43) Lemieux, R. U.; Hendriks, K. B.; Stick, R. V; James, K. *J. Am. Chem. Soc.* **1975**, *97*, 4056–4062.

(44) Lemieux, R. U.; Driguez, H. *J. Am. Chem. Soc.* **1975**, *97*, 4063–4069.

(45) Lemieux, U.; Driguez, H. *J. Am. Chem. Soc.* **1975**, *97*, 4069–4075.

(46) Lergenmuller, M.; Ito, Y.; Ogawa, T. *Tetrahedron* **1998**, *54*, 1381–1394.

(47) Debenham, J. S.; Madsen, R.; Roberts, C.; Fraser-Reid, B. *J. Am. Chem. Soc.* **1995**, *117*, 3302–3303.

(48) Castro-Palomino, J. C.; Schmidt, R. R. *Tetrahedron Lett.* **1995**, *36*, 5343–5346.

(49) Andersen, S. M.; Heuckendorff, M.; Jensen, H. H. *Org. Lett.* **2015**, *17*, 944–947.

(50) Silva, D. J.; Wang, H.; Allanson, N. M.; Jain, R. K.; Sofia, M. J. *J. Org. Chem.* **1999**, *64*, 5926–5929.